ParisTech
INSTITUT DES SCIENCES ET TECHNOLOGIES
PARIS INSTITUTE OF TECHNOLOGY

TELECOM ParisTech

2012-ENST-0054

EDITE - ED 130

Doctorat ParisTech

T H è S E

pour obtenir le grade de docteur délivré par

TELECOM ParisTech

Spécialité « Electronique et Communications »

présentée et soutenue publiquement par

Lei Xiao

28/09/2012

Conception de systemes de communication sans fils avec connaissance imparfaite du canal

Directeur de thèse : **Laura Cottatellucci**

Jury

M. Jean-Claude Belfiore, Prof., Wireless Communication, Tél écom Paristech	Président
M. Giorgio Matteo Vitetta, Prof., Information Engineering, Modena University	Rapporteurs
M. Wolfgang Gerstacker, Prof., Telecommunication Laboratory, Erlangen University	Rapporteurs
M. David Gesbert, Prof., Wireless Communication, Eurecom	Examniateurs
M. Gael Scot, Doctor, Satellite Communication Department, CNES	Examniateurs
Mme. Laura Cottatellucci, Prof., Wireless Communication, Eurecom	Directeur de thèse

TELECOM ParisTech
école de l'Institut Télécom - membre de ParisTech

THÈSE

DISSERTATION

In Partial Fulfillment of the Requirements
for the Degree of Doctor of Philosophy
from TELECOM ParisTech

Specialization : Communication and Electronics

Lei Xiao

Design of Wireless Communication System with imperfect Channel State Information

Defense scheduled on the 28th of September 2012 before a committee
composed of :

Reporters	Prof. Giorgio Vitetta, Università di Modena e Reggio Emilia, Italy
	Prof. Wolfgang Gerstacker, Unviversity Erlangen-Nürnberg, Germany
Examiners	Prof. David Gesbert, EURECOM, France
	Prof. Jean-Claude Belfiore, Telecom ParisTech, France
	Dr. Gael Scot, CNES, France
Thesis supervisor	Assistant Prof. Laura Cottatellucci, EURECOM, France

THÈSE

présentée pour obtenir le grade de

Docteur de TELECOM ParisTech

Spécialité : Communication et Electronique

Lei Xiao

Conception de Systèmes de Communication sans Fils avec Connaissance imparfaite du Canal

Thèse prévue le 28 Septembre 2012 devant le jury composé de :

Reporters	Prof. Giorgio Vitetta, Università di Modena e Reggio Emilia, Italy
	Prof. Wolfgang Gerstacker, Unviversity Erlangen-Nürnberg, Germany
Examiners	Prof. David Gesbert, EURECOM, France
	Prof. Jean-Claude Belfiore, Telecom ParisTech, France
	Dr. Gael Scot, CNES, France
Thesis supervisor	Assistant Prof. Laura Cottatellucci, EURECOM, France

Acknowledgements

First of all, I would like to express my deepest and sincerest gratefulness to Prof. Laura Cottatellucci, my advisor of the Ph.D. thesis. Three and half years ago, she offered me the opportunity to become a Ph.D. student. Since then, she has made so much efforts to support me, to motivate me and to guide me. She spent enormous time discussing with me and inspiring me. More importantly, in the past few years, she has delivered to me a great example how to become a qualified and professional researcher and how to behave like a respectable person. Without her extremely kind help, I could never accomplish this thesis.

I would also like to thank my jury members. Thank you so much for spending your precious time reading my thesis, and enable the final defense of my thesis.

I would also like express my appreciation to all of my dear colleges and close friends in Eurecom. I always feel myself extremely lucky to work in a place like Eurecom. It is a big family. People come and leave, but I will always put everyone of you in a very special place in my heart. Especially, I would like to thank my lovely friends, Francesco Negro and Lorenzo Maggi. Thank you for your constant support to help me to overcome so many difficulties. This friendship shall be never forgotten. Additionally, my dear friend Jinhui Chen also helped me a lot when I arrived at Eurecom. She helped me to settle down and provided me so many valuable suggestions that make my life and work much easier. I would also like to express my gratefulness to my officemates, Farukh Munir, Agisilaos Papadogiannis, Fauzi Kaabi, Amara Mustapha, Amelie Gyrard. I feel myself extremely lucky to have the chance to work with these kind and funny people. They filled my life with sunshine.

I could not achieve anything without the very precious support from my family and my friends. My parents and my cousin have always been there for me, no matter when I am high or low. Yizhen Zhang, Yinan Liu, Wei Han, Zihang Feng and Kunlin Yang are my very close friends in France. I will never forget those wonderful gathering and laughters. I would also like to thank Ling Luo, Yi Wang, Tao Sun and Jia Rao. Though we are far apart geographically, but our hearts always bind together. Throughout these years, your kind support and care prove that you are the invaluable treasures in my life.

Finally, I would like to dedicate this work to my uncle in the memory of him.

Abstract

In the first part of the thesis, we focus on the design of a complete satellite communication system adopting adaptive beamforming with mobile satellite terminals. Compared with conventional fixed beamforming, adaptive beamforming can significantly improve the capacity of a satellite system in terms of served satellite terminals (ST) and power efficiency. For the design of an adaptive beamforming system, channel state information (CSI) is critical. Since the propagation delay is too long compared to the coherence time of the channel, the instantaneous CSI is already stale when processed for beamforming. However, some parts of the channel, more specifically, directivity vectors change quite slowly. We utilize this partial knowledge of CSI to design an adaptive beamforming system.

In order to estimate the directivity vectors, we propose an algorithm based on a least square error criterion. Then, based on the estimation of directivity vectors, we propose two heuristics approaches to the design of adaptive beamforming. Additionally, we also propose two approaches, based on directivity estimation for the detection of transmitting terminals and the possible resolution of collisions in the random access channel of the satellite system. Since SDMA system performance depends strongly on the spatial locations of co-existing terminals, we also propose two low complexity algorithms for frequency allocation in a satellite communication system. Finally, we simulate a complete satellite system, including a random access channel and a connection-oriented channel. We analyze the system performance and compare it to conventional fixed beamforming systems.

In the second part of the work, we consider a block fading interfering channel with two transmitter/receiver pairs. We assume that both transmitters have perfect knowledge of direct links but have only statistical knowledge of the interfering links. We study the problem of transmission rate and power allocation in an autonomous and decentralized manner in the absence of perfect CSI. Resource allocation algorithms based on Bayesian games and optimization are proposed.

Dans la première partie de la thèse, on se concentre sur la conception d'un système de communication par satellite complet se basant sur la construction de faisceaux adaptatifs aux terminaux mobiles. Comparé à la construction classique de faisceaux fixes, le système à faisceaux adaptatifs peut considérablement améliorer la capacité du système en termes du nombre de STs desservies et de l'efficacité énergétique. Pour la conception du système à faisceaux adaptatifs, les informations sur l'état de canal (CSI) sont essentielles. Vu que le temps de propagation est trop long par rapport au temps de cohérence du canal, le CSI instantanée est déjà périmé lorsqu'il est reçu pour la construction des faisceaux. Cependant, une partie de l'information du canal, plus particulièrement, les vecteurs de directivité ont une variation assez lente. On utilise cette connaissance partielle du CSI pour concevoir le système à base de faisceaux adaptatifs.

Afin d'estimer les vecteurs de directivité, on propose un algorithme basé sur un critère de minimisation de l'erreur quadratique. Puis, basée sur l'estimation des vecteurs de directivité, on présente deux approches heuristiques pour la conception des faisceaux. En outre, on propose également deux approches qui reposent sur l'estimation de la directivité pour la détection des STs et la résolution possible des collisions sur le canal d'accès aléatoire au satellite. Comme la performance du système SDMA dépend fortement des positions spatiales des STs co-existants, on propose deux algorithmes de faible complexité pour l'attribution des fréquences dans le système de communication par satellite. Enfin, on simule le système satellite complet, comportant un canal d'accès aléatoire et un canal orienté connexion. On analyse les performances du système et le compare à des systèmes classiques avec des faisceaux fixes.

Dans la seconde partie de l'ouvrage, on considère un canal à interférence avec évanouissement par blocs contenant deux paires d'émetteurs/récepteurs. On suppose que les deux émetteurs ont une parfaite connaissance des liens directs mais n'ont qu'une connaissance statistique des liens interférents. On étudie le problème de l'allocation des débits de transmission et des puissances de manière autonome et décentralisée, en l'absence de connaissance parfaite du CSI. Des algorithmes d'allocation des ressources basés sur le jeu bayésien et l'optimisation sont proposés.

Table of Contents

List of Figures

Chapter 1

Contributions

Les futures générations de réseaux de communications sans fil devront accueillir les utilisateurs mobiles avec de hautes exigences en termes de débits de transmission de données. Les techniques adaptatives de traitement du signal jouent un rôle clé dans les systèmes de communication sans fil modernes afin d'améliorer les performances du système. Les émetteurs/récepteurs peuvent s'adapter aux variations de l'environnement. Les techniques adaptatives de traitement du signal peuvent améliorer la capacité du système selon différentes métriques, par exemple, le débit du système et l'efficacité spectrale.

Pour les techniques de génération de faisceaux adaptatifs, la disponibilité des informations complète de l'état du canal (CSI) est essentielle pour améliorer la capacité du système. En général, le CSI peut être obtenu de deux manières. Une première approche consiste à estimer le CSI au niveau du récepteur et retourner l'estimation à l'émetteur. Une seconde suppose la réciprocité du canal et estime le CSI au niveau de l'émetteur.

Dans certains systèmes pratiques, lorsque le délai de transmission est long et que le canal s'estompe très rapidement, le renvoit de l'estimation du CSI instantanée ne peut pas être utilisée vu qu'elle est devenue obsolète. Dans ces cas, une connaissance partielle et/ou statistique du CSI devient bien utile. Dans ces cas, l'obtention d'une connaissance partielle ou statistique sur le CSI permettant d'améliorer les performances du système devient cruciale.

Dans ce travail, nous considérons le problème de la conception du système de communication basé sur des informations partielles ou statistique du CSI.

Ce doccument est structuré en deux parties. Dans la première partie de la thèse, on conçoit un système de communication par satellite complet en adoptant la technique de formation de faisceaux adaptatifs (beamforming). Dans la deuxième partie, on considère un canal à interférence avec évanouis-

sement par blocs contenat deux paires d'émetteurs/récepteurs. Des informations imparfaites sur le canal sont disponibles au niveau de l'émetteur. Les transmetteurs doivent déterminer leur débits et puissance de transmission d'une manière autonome et décentralisée. On étudie le problème d'allocation des ressources par le biais d'une approche de la théorie des jeux.

Dans la Partie I de cette thèse, le système satellitaire est basé sur des faisceaux adaptatifs. A l'opposé des faisceaux statiques classiques, la passerelle peut adapter ses faisceaux aux conditions des terminaux satellitaires (ST) actifs présents dans le système de telle sorte que les ST se retrouvent dans le centre du faisceau les descervant. De cette façon, la capacité du système en termes de ST desservies et d'efficacité de puissance peut être considérablement améliorée.

Comparé aux flux statiques classiques, la construction de faisceaux adaptatifs nécessite la connaissance de l'état des liens entre chaque ST et le satellite. Le système satellitaire présente des particularités : l'une des composantes du canal satellitaire, à savoir les coefficients de propagation s'évanouit rapidement et le délai de propagation est lui aussi beaucoup plus long que le temps de cohérence du canal. Par conséquent, la CSI instantanée est obsolète pour la conception dde faisceaux adaptatifs. Heureusement, le canal satellitaire présente une composante à variation lente, plus précisément, il s'agit des coefficients de directivité qui représente les diagrammes de rayonnement des antennes du satellite vers les différentes positions des utilisateurs. On peut alors exploiter ce genre d'informations partielles du CSI pour aider à la conception du réseau de faisceaux adaptatifs à mettre en place.

On propose un algorithme pour estimer les paramètres des vecteurs de directivité sur la base d'un critère de minimum de l'erreur quadratique moyenne. On montre alors que le problème d'estimation se réduit à un simple problème de détermination des valeurs propres avec contraintes. On appelle l'algorithme estimation paramétrique des moindres carrés (PLSE). L'algorithme proposé ne nécessite pas l'estimation des paramètres de nuisance, ce qui permet une réduction considérable de la complexité.

En se basant sur l'estimation des vecteurs de directivité et la connaissance des statistiques des coefficients de propagation, on propose ici deux approches heuristiques pour concevoir la construction des faisceaux adaptatifs. Les performances de cette technique adaptative sont comparées à celles, plus classique, avec des faisceaux fixes. La méthode proposée montre de nombreux avantages, notamment en termes de probabilité de coupure, d'efficacité de puissance, de rapport signal à interférence plus bruit (SINR). Les résultats numériques montrent que la technique adaptative surpasse celle avec des faisceau fixes dans presque tous les aspects.

En outre, afin de construire un système satellitaire complet, certains problèmes auxiliaires sont également étudiées dans la première partie. Pour résoudre des problèmes de contentions sur le canal d'accès aléatoire pour les ST qui entrent dans le système, on propose deux approches basées sur l'es-

timation des vecteurs de directivité. De cette façon, plusieurs paquets des utilisateurs sur ce canal d'accès aléatoire en collision peuvent être détectés et décodés et par conséquent la technique proposée permet d'augmenter le débit du canal d'accès aléatoire. Ces deux approches sont mises en oeuvre au niveau de la couche physique. Ils peuvent être complémentaires aux protocoles existants conçus pour la couche d'accès multiple (MAC).

Le problème d'attribution des fréquences est également traité dans cette thèse. Dans un système de communication par satellite, il est favorable d'allouer la même bande de fréquence aux STs présentant des canaux décorrélés ou à faibles corrélations. De cette façon, l'interférence dans une bande de fréquence donnée peut être limitée et il est possible d'augmenter le débit du système. Cependant, le problème d'allocation optimale des fréquences présente une complexité NP dur (non polynomiale). Dans cette contribution, on propose deux algorithmes de faible complexité pour l'attribution des fréquences. Nous évaluons les performances des deux approches en les comparant à celles du système avec une allocation opportuniste. Les résultats numériques montrent que les deux algorithmes améliorent la capacité du système satellitaire de manière significative tandis que les complexités restent faibles.

Enfin, et afin d'avoir un aperçu complet de l'ensemble du système satellitaire basée sur la construction de faisceaux adaptatifs et notamment les effets de connaissance incomplète du canal et de l'allocation de bande de fréquence, un simulateur a été conçu pour évaluer les performances du système complet. Le simulateur se compose de deux grandes parties :

1. Un simulateur de canal à accès aléatoire. Il simule les STs qui entrent dans le système. Les contentions sont résolus et la composante lente des canaux des STs sont estimées ;
2. Un simulateur de canal orienté connexion. Il simule à la fois la liaison directe et la liaison inverse. Au niveau de la liaison inverse, il exécute l'estimation des vecteurs de directivité. Au niveau de la liaison descendante, la passerelle effectue les attributions de fréquences et la conception des faisceaux basé sur la connaissance de l'estimée partielle du canal. Les performances du système global sont évaluées en termes de probabilité de coupure et de SINR obtenu.

Dans la deuxième partie de cette contribution, on considère un canal à interférence avec évanouissement par blocs contenat deux paires d'émetteurs/récepteurs. on suppose que la réciprocité du canal n'est pas disponible. Les deux émetteurs ont une parfaite connaissance des liens directs estimés par les récepteurs et diffusés sur le canal retour. Cependant, les liens interférents ne sont pas connus par les émetteurs. Les sources doivent choisir leur puissance de transmission ainsi que le débit délivré d'une manière autonome et décentralisée basée sur la connaissance parfaite des liens directs et seulement une connaissance statistique des liens interférents. En raison du

manque de connaissances sur l'état du canal, des communications fiables ne sont pas garanties et un certain pourcentage d'interruptions peuvent survenir. Ensuite, on étudie les stratégies que les sources devraient adopter pour allouer leurs ressources en l'absence de connaissance parfaite du canal.

Ce problème d'allocation des ressources est abordé avec une approche de la théorie des jeux. L'allocation des ressources est basée sur les fonctions d'utilité considérant les débits réels, et des pénalités pour la consommation d'énergétique. Des algorithmes d'allocation des ressources basé sur les *jeux bayésiens* et l'optimisation sont proposées. Dans le cadre des jeux Bayesiens, on étudie deux cas :

1. allocation de puissance lorsque les débits de transmission sont prédéfinis ;
2. allocation conjointe des puissances et débits.

Pour le premier cas, on montre que l'allocation bayésienne de puissance converge vers un jeu concave. Au contraire, pour l'allocation conjointe des débits et des puissances, le jeu bayésien n'est pas concave. On analyse alors le jeu en se basant sur l'analyse d'un jeu équivalent. L'existence, la multiplicité et la stabilité des équilibres de Nash (NE) sont analysés dans les deux cas. Une attention particulière est consacrée aux régimes asymptotiques où le système est limité respectivement par le bruit et l'interférence.

Chapter 2

Contribution

Next generation of wireless communication networks will accommodate heterogenous users with high requirements of data transmission rate. Adaptive signal processing techniques are widely known as playing a key role in modern wireless communication systems to improve system performance. Transmitters/receivers can adapt to the modification of the channel environment. Adaptive signal processing techniques can improve the capacity of the system in many merits, e.g, system throughput and its spectral efficiency.

In adaptive signalling techniques, the availability of full channel state information (CSI) is critical to improve system capacity [1]. In general, CSI can be obtained in two ways. A first approach consists in estimating the CSI at the receiver and feeding the estimation back to the transmitter. A second one assumes reciprocity of the channel and estimates the CSI at the transmitter.

In some practical systems, when the transmission delay is long and the channel is fading very rapidly, or the feedback channel is not available, the feedback of the estimated instantaneous CSI cannot be utilized because such information is obsolete or unavailable. In these cases, partial/statistical knowledge of CSI is helpful. And obtaining partial or statistical knowledge of CSI and improving the system performance based on this information becomes crucial.

In this contribution, we consider the problem of communication system design based on partial or statistical knowledge of CSI.

This work is structured in two parts. In the first part of the thesis, we design a complete satellite communication system adopting adaptive beamforming with mobile STs. In the second part, we consider a block fading interfering channel with two transmitter/receiver pairs. Imperfect channel

information is available at the transmitter and they have to determine their transmission rate and power in an autonomous and decentralized way. We study the resource allocation probelm via a game theoretical approach.

In Part I of this thesis, a satellite system based on adaptive beamforming is investigated. Differently from conventional static beamformers, a gateway can adapt its beamforming to the active conditions of the satellite terminals (ST) in the system in a way that the STs are almost in the center of a beam. In this way, the capacity of the system in terms of served STs and power efficiency can be significantly improved.

Compared to conventional static multibeams, adaptive beamforming requires the knowledge of the state of the links between each ST and the satellite. Due to the peculiarity of the satellite system, one big challenge is that one component of the satellite channel, i.e, the propagation coefficients, is fast fading, and the propagation delay is much longer that the coherence time. Therefore, the instantaneous CSI is obsolete for the design of adaptive beamforming. Fortunately, the satellite channel exhibits some form of slowing fading components, more specifically, the directivity coefficients which account for the radiation patterns of the satellite antennas to different positions of the users. Then, we exploit this kind of partial knowledge of the CSI to help the design of adaptive beamforming network.

We propose an algorithm to estimate the directivity vector parameters based on a least squares error criterion. We show that the estimation problem reduces to an eigenvalue complementary problem. We dub the proposed algorithm Parametric Least Squares Estimation (PLSE). The proposed algorithm does not require the estimation of nuisance parameters and this enables a considerable complexity reduction.

Based on the estimation of the directivity vectors and the knowledge of the statics of the propagation coefficients, we propose two heuristic approaches to design adaptive beamforming. The performance of the adaptive beamformer is compared with the conventional fixed beamformer in many merits, including outage probability, power efficiency, achieved signal to interference plus noise ratio (SINR). Numerical results show that adaptive beamforming technique outperforms the fixed beamforming in almost every aspect.

Additionally, for the sake of the completeness of the analysis satellite system, some auxiliary problems are also investigated in Part I. We propose two approaches based on the directivity vectors estimation to resolve contentions in the random access channel for the STs entering the system. In this way, the user collisions in the random access channel can be reduced and consequently the throughput of the random access channel increases. These two approaches are implemented at physical layer. They can be complementary to the existing protocols designed for the multiple access layer (MAC).

The frequency allocation is also considered. In a satellite communication system, it is auspicious to allocate the same frequency band to STs

with uncorrelated or low correlated channels. In this way, interference in a given frequency band can be limited and the system throughput is increased. However, the optimal frequency allocation problem is non-deterministic polynomial-time (NP) hard. In this contribution, we propose two low complexity algorithms for frequency allocation. We evaluate the performance of the two approaches by comparing system performance with opportunistic allocation. Numerical results show that the two algorithms improve the capacity of the satellite system significantly while the complexities remain low.

Finally, in order to acquire a comprehensive insight of the whole satellite system based on adaptive beamforming and including the effects of incomplete channel knowledge and frequency band allocation, a simulator is built to evaluate the performance of the complete system. The simulator consists of two major parts :

1) A simulator of random access channel. It simulates new STs entering the system. The contentions are resolved and a slow fading component of the STs are estimated ;

2) A simulator of connection-oriented channel. It simulates both the forward link and reverse link. In the reverse link, it performs the estimation of directivity vectors. In the forward link, the gateway performs frequency allocations and designs the beamformer based on the estimated partial knowledge of CSI. The global system performance is assessed in terms of outage probability and achieved SINR.

In the second part of this contribution, we consider a block fading interfering channel with two transmitter/receiver pairs. We assume that channel reciprocity does not hold. Both transmitters have perfect knowledge of the direct links since the receivers estimate the direct link with the corresponding transmitters and broadcast this information on the feedback channel. However, the interfering links are unknown to the transmitters. The sources have to decide their transmission power and rate in an autonomous and decentralized way based on a perfect knowledge of the direct links and only a statistical knowledge of the interfering links. Due to the lack of knowledge of channel state, reliable communications are not guaranteed and a certain level of outage events may occur. Then, we investigate the strategies that the sources should adopt to allocate their resources in the absence of perfect channel knowledge.

This resource allocation problem is addressed via a game theoretical approach in Part II. The resource allocation is based on utility functions accounting for the real throughput, and some penalties for power consumption. Resource allocation algorithms based on *Bayesian Games* and optimization theory are proposed. In the context of Bayesian game, we investigate two cases : 1) power allocation when transmission rates are predefined ; 2) joint power and rate allocation. For the first case, we show that Bayesian power allocation boils down to a concave game. On the contrary, for joint rate

and power allocation, the Bayesian game is not concave and we analyze the game based on the analysis of an equivalent game. For both cases, the existence, multiplicity and stability of the Nash Equilibriums (NE) are analyzed. Special attention is devoted to the asymptotic high noise regime and the interference limited regime.

Première partie

Satellite System Design with Imperfect Channel State Information

Chapter 3

Notions de base, Problématiques et Motivations

3.1 Introduction

Dans un système satellite (SS) avec des antennes multiples au niveau des satellites, la capacité en termes de nombre de terminaux satellitaires desservis peut être sensiblement améliorée en se basant sur les techniques beamforming (Construction de faisceaux) adaptatifs au lieu des technique beamforming conventionnelles.

Les systèmes satellitaires multidirectionnels actuels se voient leurs directions de transmission construites de telle manière à couvrir des zones géographiques spécifiques. Ceci assure un niveau minimum en termes de qualité de service (QoS) pour toutes les stations se trouvant dans la zone de couverture. Contrairement à cette technique, dans le beamforming adaptatif, la construction des directions est basée à la localisation des terminaux satellitaires (ST) qui de ce fait se retrouvent presque toujours au centre de la direction de transmission. Ceci permet non seulement de minimiser le niveau d'interférence reçu mais aussi de garantir une efficacité énergétique supérieure. Cependant, l'utilisation de cette technique apporte de nouvelles contraintes et problématiques essentiellement reliés à la connaissance préalable du canal de communication entre le SS et les STs appelé "'Channel State Information (CSI)"'.

L'acquisition du CSI et l'implémentation du beamforming adaptatif, ont été étudiés pour les systèmes de communication cellulaires terrestres d'un point de vue des variétés, par exemple, la robustesse face à des connaissances imparfaites du canal, précision requise quant aux retours du CSI. A cause de

la grande différence entre les systèmes terrestres et satellitaires, l'extension des résultats existants n'est pas immédiate. Par ailleurs, l'acquisition des informations canal ainsi que la construction des directions de transmission requiert une investigation sur base ad hoc.

L'un des problèmes majeurs pour les systèmes satellitaire est la validité du CSI instantané. En effet, à cause du long délai de propagation, qui est bien plus grand que celui du temps de cohérence du canal, l'information collectée sur la canal est obsolète au moment de la réception, et ne peut donc pas être utilisée pour la construction des directions de transmission(faisceaux).

L'objectif de ce travail, est la conception complète d'un système satellitaire pour stations mobiles en se basant sur la technique beamforming adaptative. Il a fallu pour cela résoudre quelques problèmes pour l'acquisition d'informations assez fiables sur le canal et de pouvoir l'exploiter pour construire les directions de transmission.

Il est clair que le choix du type d'information d'acquisition sur le canal de transmission dépend des particularités du canal satellitaire et est de toute évidence crucial pour la conception du système.

Le canal du SS peut être modélisé comme la cascade, ou multiplication, de trois composantes :

1. Une composante à variations lente qui est la conséquence de la mobilité du terminal qui est appelée vecteur de directivité entre l'antenne du satellite et celle du terminal.
2. Une composante à variations rapide qui vien de la propagation du signal à travers le canal de transmission.
3. Une composante fixe et connue qui représente la matrice de corrélation au niveau du terminal.

Le vecteur de directivité est l'ensemble des valeurs appliquées aux différentes antennes du satellite pour transmettre dans la direction du terminal désiré. Il permet de focaliser toute l'énergie dans la direction et la position du terminal. Cette composante est relativement indépendante des fréquences utilisées par le satellite mais dépend complètement de la mobilité du terminal.

Les coefficients modélisent le canal de propagation (atmosphérique et shadowing) entre le satellite et les terminaux mobiles. Ces coefficients changent très rapidement et le temps de cohérence du canal est très petit devant le temps de propagation. Dans ce contexte, l'information instantanée du CSI mesurée au niveau des terminaux devient obsolète une fois reçue par le satellite.

La matrice de corrélation quant à elle, prend en considération l'effet de couplage entre les antennes multiples et le couplage entre polarisations.

En considérant la nature et les propriétés du canal satellitaire, on adopte les vecteurs de directivité comme l'information acquise sur l'état du canal afin de construire nos directions de propagation adaptatives.

En plus, on bénéficie, d'une part, de l'insensibilité vis à vis des bandes de fréquences, et de la propriété de réciprocité [1] du canal d'autre part. Ceci nous permet de récupérer les vecteurs de directivité permettant de construire les beams. L'information utilisée pour la transmission dans le sens descendant est basée sur celle acquise dans le sens montant.

En considération des observations précédentes, les systèmes satellitaires présentent deux défis majeurs :

- Le recouvrement des vecteurs de direction en se basant sur les observations est intrinsèquement un problème d'estimation multi-utilisateurs, non linéaire qui n'a pas été traité dans la littérature.
- La conception de transmetteurs/récepteurs non linéaires pour les systèmes MIMO en se basant sur la connaissance statistique du canal est très différente des techniques de conception de beams dans le cas de connaissance parfaite et/ou imparfaite du canal.

En plus de la solution susmentionnée, la conception d'une solution complète de transmission directionnelle adaptative pour les systèmes satellitaires engendre quelques problèmes techniques secondaires :

- Allocation des bandes de fréquence en présence de mobilité.
- Conception d'un canal à accès aléatoire avec résolution des contentions basée sur le multiplexage spatiale. Exploiter les antennes de transmission multiples au niveau du satellite et les estimations à priori des directions.

Dans ce travail, on traite aussi ces problématiques, et propose de nouvelles solutions techniques afin de construire une solution complète pour les systèmes satellitaires mobiles permettant d'améliorer sensiblement leur capacité.

Plus spécifiquement, les antennes multiples au niveau du satellite, permettent l'accès multiple spatiale (SDMA) de manière à ce que plusieurs terminaux mobiles peuvent communiquer avec le satellite en même temps et sur les mêmes bandes de fréquence sous réserve de dispersion assez importante entre les terminaux. Pour cela, il est indispensable de réaliser une allocation optimale des bandes de fréquence entre les terminaux afin d'assurer une séparation spatiale minimale.

La conception de canal à accès aléatoire, est aussi intrinsèquement reliée au problème fondamental de ce travail. En effet, d'un point de vue architectural, une amélioration du nombre de ST servis par un SS nécessite une augmentation similaire de la capacité de traitement des demandes de services sur le canal d'accès. D'un point de vue du traitement du signal, l'acquisition/estimation des vecteurs de directivité permettent l'exploitation de la séparation spatiale des STs afin de résoudre les contentions qui, autrement, seraient traités comme des collisions. On propose aussi des approches basées sur l'estimation des vecteurs de directivité pour améliorer le débit du sys-

1. C'est l'une des propriétés fondamentale qui stipule que le canal reste identique si on inverse le rôle des transmetteurs et récepteurs

tème. En outre, ils sont utiles pour aider à l'attribution des fréquences et la conception de faisceaux pour chaque nouveau ST qui entre dans le système. Il est à noter que ces techniques sont complémentaires aux nombreux protocoles de la couche d'accès multiples (MAC) qui ont récemment été proposés pour augmenter le débit.

Dans ce qui suit, nous présentons un aperçu des thèmes et des résultats figurant dans les différents chapitres de la partie I. Le reste de ce chapitre est consacrée à un examen des concepts fondamentaux utilisés dans ce travail.

Dans le chapitre 3, nous décrivons le modèle du système SS adoptée dans la partie I. Les hypothèses sur le SS sont discutées. Plus de détails sur les canaux directs et réciproques sont donnés. Les trois composantes qui déterminent le canal, c'est à dire, les vecteurs de directivité, les coefficients de propagation, la matrice de corrélation au niveau des récepteurs sont illustrés.

Dans le chapitre 4, nous proposons deux approches heuristiques pour la conception des faisceaux adaptatifs basées sur la connaissance des vecteurs de directivité et la statique des coefficients de propagation. Nous comparons les performances des techniques adaptatives avec une technique classique de beamforming, en considérant différentes métriques : niveau signal à interférence plus bruit (SINR), puissance de transmission requise, et probabilité de coupure de transmission.

Dans le chapitre 5, nous proposons un algorithme pour l'estimation non-linéaire des vecteurs de directivité basé sur un critère de minimisation de l'erreur des moindres carrés. Nous montrons que le problème d'estimation non linéaire peut être réduit à un problème de valeurs propres complémentaires. L'estimation ne nécessite pas l'estimation des coefficients du canal de propagation qui jouent le rôle de paramètres de nuisance. De cette façon, la complexité peut être considérablement réduite. La performance de l'algorithme est également évaluée par des simulations numériques.

Dans le chapitre 6, nous décrivons deux algorithmes pour résoudre les contentions sur le canal d'accès aléatoire. Ces deux algorithmes sont basés sur l'estimation de vecteurs de directivité. Une estimation préliminaire des vecteurs de directivité permet l'exploitation de la séparation spatiale entre les STs afin d'éviter des problèmes de collisions. Les deux algorithmes sont également complémentaires à de nombreux protocoles actuellement proposées pour la résolution des contentions au niveau de la couche MAC.

Dans le chapitre 7, nous proposons deux algorithmes à complexité réduite pour l'attribution des fréquences dans le système SS. Nous comparons les performances du système lorsque les STs se voient attribués différentes porteuses au hasard et quand on leur attribue les porteuses selon ces deux algorithmes. Les résultats numériques montrent que les algorithmes proposés offrent un bon compromis entre la complexité et le débit du système ainsi obtenu.

Au chapitre 8, une description de la structure complète du simulateur SS est faite et une évaluation complète de la performance du système est réa-

lisée. Le système complet comprend les ST mobiles présentant des canaux aléatoires, l'estimation des vecteurs de directivité de l'émetteur, la conception et la formation de faisceau adaptative, attribution des fréquences. Les performances de ce système global sont ainsi évaluées.

3.2 Techniques d'accès multiple et SDMA

Actuellement, quatre principes d'accès multiple sont largement mis en oeuvre dans les systèmes de communication satellitaire fixes et mobiles [2], à savoir :

1. Accès multiple par répartition en fréquence (AMRF) : chaque utilisateur est assigné à une bande de fréquence différente ;
2. Time Division Multiple Access (TDMA) : les utilisateurs peuvent partager la même bande de fréquence, mais chaque utilisateur transmet pendant des intervalles de temps non chevauchants.
3. Access Code Division Multiple Access (CDMA) : une séquence d'étalement différente est affectée à chaque utilisateur. Chaque symbole d'un ST est modulé par une séquence d'étalement et transmis sur la même ressource (fréquence,temps). La séquence d'étalement permet de séparer tous les signaux interférents au niveau du récepteur grâce à l'orthogonalité des séquences d'étalement.
4. Spatial Division Multiple Access (SDMA) : les utilisateurs partagent la même bande de fréquence et transmettent en même temps. Leurs signaux interférents peuvent être séparés grâce à leurs différentes localisations géographiques et la présence d'antennes multiples au niveau du satellite.

Ces méthodes d'accès multiples peuvent être combinées ensemble. Elles ainsi que leurs variantes hybrides sont largement utilisés dans les communications par satellite.

Dans ce travail, nous considérons un système satellitaire basé sur la technologie SDMA. Dans le système SDMA, la diversité géographique des STs est exploitée, et les interférences co-canal entre les STs sont limitées vu la distance les séparant.

La technologie clé permettant de réaliser le SDMA est la présence d'antennes multiples au niveau du satellite. Un traitement approprié, linéaire ou non linéaire des signaux multiple reçus (détection multi-utilisateur) ou transmis (beamforming ou précodage) au niveau de la passerelle permet respectivement d'assurer la séparabilité des signaux d'interférents ou de concentrer l'énergie du signal désiré vers l'emplacement du STs cible.

3.3 Propagation dans le canal de communication par satellite

Pour la transmission et la réception de signaux de communications par satellite, la gamme de fréquences utilisées est généralement de 1 à 30 GHz. A ces fréquences, différentes distorsions sont introduites sur les ondes lors de leur propagation à travers les différentes régions de l'atmosphère.

L'atmosphère peut être divisée en plusieurs régions. La troposphère est la région allant du sol jusqu'à une altitude de 15 km. Dans cette zone, la température tombe en continu, et atteint un niveau aussi bas que -50 ou -60 degrés Celsius. A partir de ce point, la température commence à monter. L'ionosphère est située entre 70 et 1000 km de la surface ; Dans cette région, l'onde radio est affectée par des électrons. Au-delà de l'ionosphère, les signaux peuvent être considérés se propageant dans l'espace libre. La région comprise entre la troposphère et l'ionosphère est dénommé espace intérieur libre. L'espace libre ainsi que l'espace intérieur n'introduisent que des distorsions minimes sur les signaux. Les distorsions les plus importantes sont introduites au niveau de la troposphère et l'ionosphère.

En général, les ondes électromagnétiques sont affectées par plusieurs phénomènes à des degrés divers [3] :

- l'absorption par les gaz atmosphériques
- phénomènes météorologiques (par exemple, la pluie, la glace, nuage, etc...)
- fumée et poussière
- scintillement troposphérique
- rotation de Faraday
- d'atténuation ionosphérique
- scintillement ionosphérique.

Pour les terminaux mobiles par satellite, la propagation est également affectée par des phénomènes supplémentaires :

- réflexions et diffraction des bâtiments
- ombre des arbres et des immeubles de grande hauteur
- décalage de fréquence Doppler.

3.4 Matrice de directivité ces canaux de communication par satellite

Pour les terminaux satellite mobiles, la partie évanouissement dû à la mobilité est modélisée par un vecteur de directivité, un pour chaque ST. Ce vecteur est déterminé par le diagramme de rayonnement des antennes du satellite, dans la direction de la ST correspondante. Un diagramme de rayonnement représente l'énergie, la phase et la polarisation de l'antenne dans des différentes directions de son champ de rayonnement.

Le vecteur de directivité entre les antennes du satellite et une ST est déterminée par deux facteurs :

- La position géographique de la ST, vu que la position de la ST détermine la direction "'relative"' d'une antenne du stellite vers la ST ;
- La fréquence porteuse. Il est intéressant de noter que les effets de la fréquence porteuse sur les vecteurs de directivité sont mineurs. Ils peuvent être négligés dans un système de satellite donnée, par exemple, dans la bande Ka ou la bande Ku. Ceci implique que nous pouvons bénéficier de la réciprocité de la directivité aussi bien pour les systèmes TDD et FDD, et pas seulement en mode TDD, comme c'est le cas pour les communications mobiles terrestres.

3.5 Antennes intelligentes et technologie beamforming

Un système à antennes intelligentes combine des réseaux d'antennes avec des capacités de traitement de signaux afin d'ajuster automatiquement le motif de transmission et/ou réception. L'objectif d'un système à antennes intelligentes est de permettre à chaque ST d'émettre/recevoir des signaux vers/à partir de la passerelle dans une direction particulière minimisant ou annulant les interférences de/vers les autres utilisateurs. En utilisant des antennes intelligentes, la capacité du système peut être augmentée de manière significative.

La technologie de contrôle de la directivité et de les poids de la transmission/réception est une technique de formation de faisceaux appelé beamforming.

Les systèmes à antennes intelligentes sont classés en deux types [4], à savoir :

- Système à faisceaux commuté ;
- Système à faisceaux adaptatifs.

Système à faisceaux commuté

Dans le système à commutation de faisceaux, le satellite est équipé de quelques antennes directionnelles qui pointent vers des directions prédéfinies. La passerelle bascule entre les différentes antennes basées sur l'évaluation du signal reçu, le plus souvent en termes de puissance reçue. Grâce à sa caractéristique de directivité élevée, cette technique améliore les performances du système par rapport à une antenne classique, mais les améliorations sont limitées.

Figure 4.1 montre un système à commutation de faisceaux. Un des problèmes majeurs de ce type de système de commutation est que les faisceaux ne sont pas adaptatifs en fonction les emplacements des STs d'intérêt et, par conséquent, les STs peuvent tomber en dehors du centre des faisceaux principaux correspondants. De ce fait, les STs peuvent recevoir moins d'énergie

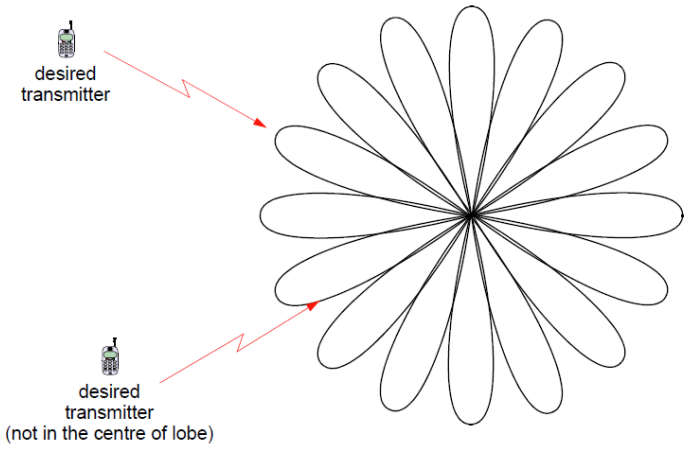

FIGURE 3.1 – Beamforming Commuté : Choix dans un ensemble pré-déterminé de faisceaux

provenant du signal utile et souffrent davantage de l'interférence des autres utilisateurs.

Système à faisceaux adaptatifs

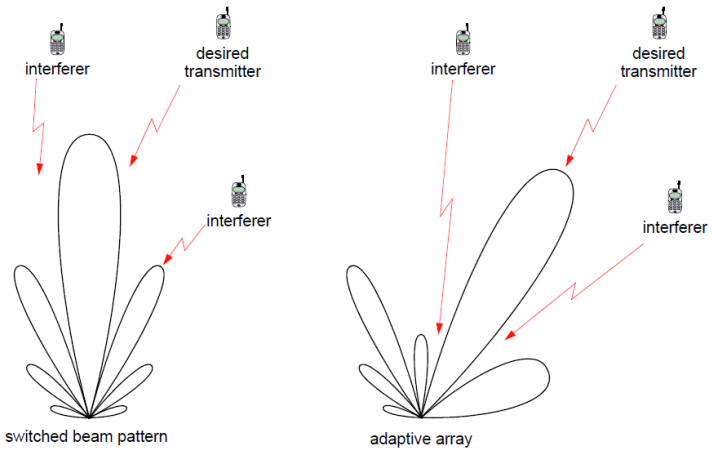

FIGURE 3.2 – Aaisceaux Adaptatifs : Les faisceaux s'adaptent à l'environnement

Dans le système de à faisceaux adaptatifs, la puissance transmise par les faisceaux multiples peut être réglé en temps réel en fonction des changements de l'environnement. La formation de faisceaux permet de régler le diagramme de rayonnement global de plusieurs antennes pour maximiser le gain dans la direction souhaitée et minimiser les interférences provenant d'autres direc-

tions. De cette façon, le rapport signal à interférence plus bruit (SINR) peut être augmentée de manière significative.

Figure 4.2 montre une comparaison entre le système à faisceaux commutés et le système à faisceaux adaptatifs. Dans le système à commutation, le ST d'intérêt peut donc ne pas se trouver dans la direction du lobe principal qui le sert et les STs interférentes ne sont pas dans une direction de rayonnement nulle. Par conséquent, le SINR obtenu à la ST peut être dégradée. Au contraire, dans le système adaptatif, le lobe principal se concentre sur la ST d'intérêt et les STs interférentes sont situées dans un point de rayonnement nul ou presque nul. Par conséquent, le système adaptatif améliore énormément le SINR obtenu par rapport à celui obtenu par un système à commutation.

3.6 Satellites multiples et stratégies de couverture

Dans les systèmes satellitaires actuels, la zone de couverture est habituellement éclairée par des spots de faisceaux fixes. Dans ce cas, les poids du réseau de faisceaux (BFN) au niveau des antennes des satellites sont maintenues constants. Afin de limiter les interférences entre faisceaux adjacents, la réutilisation des fréquences est souvent adoptée. Des faisceaux adjacents utilisent des fréquences différentes.

Figure 4.3 montre un exemple d'un tel système avec un facteur de réutilisation de fréquences de 4. Les zones couvertes par différentes fréquences s'affichent avec des couleurs différentes. Les zones adjacentes utilisent des fréquences différentes. Fréquence 1 est attribuée aux faisceaux 1 et 3. Etant donné que les deux faisceaux sont situés loin les uns des autres, l'interférence co-canal est limitée.

Les faisceaux fixes couvrent une certaine zone et garantissent une qualité minimale de service (QoS) dans une telle zone. Dans ce genre de système, pour un intervalle de temps et de bande de fréquence donnés, une seule ST située dans une certaine zone peut être servie. Si deux ou plusieurs utilisateurs situés dans la même zone de couverture veulent transmettre dans une même tranche horaire, un seul utilisateur peut être servi. En conséquence, lorsque le nombre d'utilisateurs qui demandent une transmission devient élevé, la possibilité d'événements d'interruption devient également élevé. Cette observation limite fortement la capacité d'un tel système à faisceaux fixes.

Dans un projet européen financé par l'Agence spatiale européenne (ESA), un autre système de construction de faisceaux fixes a été proposée pour améliorer la capacité du système [5]. Dans ce système, on évite la réutilisation des fréquences et tous les faisceaux peuvent être desservis par toutes les fréquences disponibles. Les poids de la BFN sont maintenus constants. La différence avec l'ancien système est que, dans ce cas, les faisceaux sont regroupés en groupes de sept et les signaux sont conjointement traitées à la fois

sur la liaison descendante et montante. De cette façon, la passerelle reçoit plusieurs copies de chaqu'un des signaux de STs sur différentes antennes. On applique alors la détection multi-utilisateurs (MUD) pour annuler l'interférence entre STs dans le même cluster. De même pour la liaison directe, les faisceaux fixes sont construits au sein des clusters. Cette approche permet un facteur de réutilisation des fréquences de 1 avec une amélioration considérable de l'efficacité spectrale. Toutefois, les STs à la frontière du cluster souffrent des interférences inter-cluster.

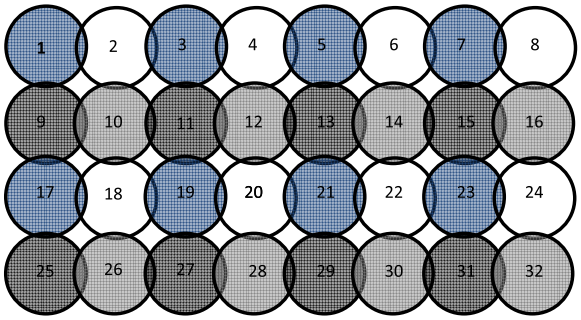

FIGURE 3.3 – Faisceaux fixes pour la couverture satellitaire : réutilisation des fréquences

Le principal inconvénient de ce type de systèmes à faisceaux fixes se trouve dans leur manque de flexibilité. Les faisceaux ne sont pas adaptatifs en fonction de l'emplacement des utilisateurs. Par conséquent, et afin de garantir une qualité de service minimale, plus de puissance est nécessaire à la transmission, ceci induit une réduction conséquente de l'efficacité énergétique.

Grâce à la mise en oeuvre de la gestion adaptative BFN, les poutres peuvent être conçus en fonction des positions tribus ". Leurs lobes principaux se concentrer sur les ST. Chaque faisceau est conçu pour maximiser le gain dans la direction des utilisateurs tandis que l'interférence créée à ST d'autres sont minimisés. Par rapport à la stratégie de formation de faisceau fixe classique, la stratégie de couverture adaptative améliore les performances du système en termes de rendement énergétique et spectral.

En outre, les faisceaux adaptatifs peuvent être conçus pour répondre à la QoS d'un utilisateur donné et on n'a pas besoin de garantir un minimum de qualité de service dans toute une zone de couverture le contenant. La puissance transmise est adaptée aux besoins d'une ST donnée et non pas aveuglément conçue pour répondre à un scénario hypothétique traduisant une situation "'pire des cas"'. Ceci conduit clairement à une amélioration additionnelle de l'efficacité spectrale.

Pour la conception de faisceaux adaptatifs, la connaissance du canal à l'émetteur est un point crucial. Le transmetteur conçoit les faisceaux en fonction de la connaissance qu'il a sur l'état du canal.

Dans cette thèse, on utilise la stratégie de construction de faisceaux adaptatifs pour assurer la couverture satellitaire. Les détails techniques sur la conception des faisceaux adaptatifs sont fournis dans le chapitre 6.

3.7 Attribution des fréquences dans SDMA

Dans la construction classique des faisceaux fixes avec prise en compte de la réutilisation de fréquences, les fréquences sont pré-affecté aux faisceaux et une bande de fréquences est de ce fait, allouée à une ST en fonction de sa position relative par rapport au faisceau de couverture correspondant. Toutefois, cela n'est pas valable pour le système à faisceaux adaptatifs. La réutilisation des fréquences devient un problème NP-difficile. D'un point de vue pratique, il est crucial de réduire la complexité de calcul, tout en garantissant de bonnes performances. Nous étudions le problème de l'attribution des fréquences dans SDMA au chapitre 9.

3.8 Accès aléatoire dans les communications par satellite

Le canal d'accès aléatoire (RACH) est largement utilisé pour l'accès initial de STs dans la SS et pour des transmissions courtes en rafale. À l'heure actuelle, les schémas les plus souvent utilisés pour le canal d'accès aléatoire dans les communications par satellite sont Slotted-Aloha [6] [7] et diversity-Slotted Aloha [8] [9] [10]. Pour les deux régimes, le temps est divisé en slots et une synchronisation est nécessaire. Les STs qui souhaitent communiquer entrent dans le système en transmettant leur demande sur le RACH, au début d'une fenêtre (slot).

Dans le système classique avec construction de faisceau fixe, un faisceau ne peut supporter qu'une seule ST par slot, si plus d'uns ST transmettent sur le même intervalle de temps, une collision se produit et aucune des stations émettrices ne peut être détecté par le système. Lorsque le nombre des STs qui veulent initier une transmission augmente, la probabilité de collisions augmente considérablement. Les STs qui ont subi des collisions doivent répéter leur transmission jusqu'à ce qu'ils soient détectés avec succès. Cela peut conduire à un très grand retard de transmission et à un gaspillage de la bande de fréquence. En outre, le signal de chaque faisceau est indépendamment traité et la diversité spatiale n'est pas exploitée.

Dans ce travail, nous considérons le RACH d'un système satellitaire à faisceaux multiples avec réutilisation de fréquence universel. Nous profitons de la diversité spatiale et de la forte directivité des antennes multiples au niveau du satellite pour résoudre des contentions et effectuer une estimation de canal. En d'autres termes, plusieurs antennes directives fournissent une "signature" unique à chaque ST. Cette dernière est exploitée pour la détection

multi-utilisateur, c'est à dire, la résolution des conflits. Par conséquent, une étape fondamentale de cette technique nécessite l'estimation de la signature unique pour chaque ST.

3.9 Aquisition de l'information partielle du canal de transmission

L'acquisition du CSI est un problème crucial dans la conception des systèmes à faisceaux adaptatifs et dépend fortement des caractéristiques du canal.

L'acquisition conventionnelle du CSI peut être réalisée de différentes manières. La première façon est d'apprendre du retour d'information de la part du récepteur. Le CSI est estimée au niveau du récepteur sur la base des symboles pilotes disponibles *a priori* au niveau du récepteur [11] [12] [13] [14]. L'autre approche se base sur l'hypothèse de la réciprocité du canal, le CSI est estimée au niveau de l'émetteur à l'aide de symboles pilotes qui sont connus a priori par l'émetteur.

Dans un SS, les coefficients de propagation varient très rapidement et le délai de propagation dans le canal satellitaire est très long. De ce fait, l'estimation de la CSI instantanée devient très rapidement obsolète et ne peuvent pas être utilisées pour la conception des faisceaux adaptatifs.

Dans ces cas, d'autres types d'informations, par exemple, l'information sur certaines parties lentement variables dans le canal, peuvent être utilisées à la place du CSI instantané et offre une solution pratique, vu qu'ils changent plus lentement que l'état du canal.

Dans les systèmes de communication, l'information partielle de l'état du canal peut être soit évaluée au niveau de la ST et renvoyée à la passerelle ou estimées au niveau de l'émetteur si la réciprocité du canal est assurée (au moins d'un point de vue statistique). La première approche nécessite des voies de retour et, par conséquent, l'efficacité spectrale diminue. Dans cette contribution, nous supposons que la réciprocité de canal est valable pour les vecteurs de directivité. Par conséquent, on peut estimer les vecteurs de directivité au niveau du satellite, et d'utiliser cette estimation partielle sur le CSI pour concevoir les faisceaux adaptatifs.

L'acquisition de la variation lente du CSI au niveau de la passerelle, dans un système de satellitaire avec des terminaux mobiles (ST) équipés éventuellement de plusieurs antennes de transmission et transmettant avec une polarisation gauche et droite, constitue de nouveaux défis inexplorés comparé aux champs étudié en profondeur de l'estimation des canaux satellitaire afin de réaliser la détection cohérente et le décodage du canal par le récepteur. En supposant que les statistiques des coefficients de propagation sont disponibles au niveau de la passerelle et qu'elles sont décrites par le modèle donné dans [15], l'estimation partielle du CSI se réduit à l'estimation des différentes

composantes lentes, c'est à dire, les vecteurs de directivité. Du point de vue du traitement du signal, ceci qui implique réaliser la tâche difficile d'estimer les paramètres observés à travers les nuisances multiplicatif.

L'estimation des vecteurs de directivité est intrinsèquement *non linéaire*. On considère un modèle paramétrique des canaux où le vecteur paramétrique de la directivité est représenté par une combinaison linéaire de vecteurs de directivité données et connus à l'avance (voir la section 5.1) et où les coefficients de propagation variables jouent le rôle de paramètres de nuisances multiplicatives.

Nous présentons les algorithmes proposés en détail dans le chapitre 7.

Chapter 4

Background, Challenges and Motivations

4.1 Introduction

In a satellite system (SS) with multiple antennas at the satellite, capacity in terms of served ST in the forward link can be sizably enhanced by adopting adaptive beamforming instead of conventional fixed beamforming.

In current multibeam SSs, the beams are designed such that their footprints cover fixed geographical locations and a certain minimum level of quality of service (QoS) is guaranteed to any ST location within the footprint of a beam. On the contrary, in adaptive beamforming, the beamformers are tailored to the ST's locations, which are always almost in the center of the beam, with benefits in terms of both energy consumption and interference avoidance. Compared to systems with fixed multibeams, adaptive beamforming presents new challenges, mainly related to the fact that it requires knowledge of the state of the links between each ST and the satellite.

Acquisition of channel state information (CSI) and adaptive beamforming have been studied in cellular terrestrial communication systems from manifold perspectives, to mention some, robustness w.r.t. imperfect channel knowledge, required level of accuracy in the CSI feedback. Satellite systems with adaptive beamforming differ subsequently from its terrestrial counterpart. The extension of existing results for terrestrial systems is not straightforward, and the acquisition of CSI and beamforming design requires ad hoc investigation.

The key peculiarity of a satellite system is the very long propagation delay of the signal. It is much longer than the coherence time of the system.

Then, feedback of the instantaneous CSI received at the gateway is obsolete for an adaptive beamforming design.

Objective of this work is the complete design of a SS for mobile STs based on adaptive beamforming with focus on the key issues of the acquisition of some kind of information on the state of the channel and design of beamfomer based on such a kind of information.

It is apparent that the choice of the kind of information on the state of the channel to be acquired and used for beamforming depends on the peculiarities of the satellite channel and it is crucial in the design of SS.

The channel of a SS with mobile STs is modeled as a cascade, i.e. analytically as a multiplication, of three components :a) a slow varying component due to the ST's mobility, referred to as directivity vector between a ST and the satellite antennas (SA) ; b) a fast fading component, dubbed propagation component ; c) a fixed and known component, i.e., the correlation matrix at the ST.

The directivity vector consists of the values of the radiation patterns of all SAs, in the direction of a ST. It accounts for the strong directionality of SAs and the ST positions. It is relatively insensitive to frequencies within the range of frequency carriers of a satellite system and its variations depends mainly on the ST's mobility.

The propagation coefficients model the propagation losses (atmospheric and shadowing) between satellite and ST. These propagation coefficients fade very fast and the coherence time of the channel is very short when compared to its propagation delay. Thus, in this context, the instantaneous CSI measured at a ST and fedback is obsolete when received by the gateway.

The correlation matrix of a ST accounts for the coupling effects among multiple antennas and cross polarization.

By considering nature and property of the satellite channel, we adopt the directivity vectors as the kind of information to be acquired on the channel state to design adaptive beamforming.

Additionally, we benefit from the insensitivity of the antenna radiation refer to the carrier frequency within the frequency band of SS and from its property of reciprocity [1] to acquire the directivity vectors for beamforming design in the forward link via observations on the reverse link.

On the light of the previous considerations, the context of SS with adaptive beamforming presents a two-fold main challenge compared to the terrestrial systems : a) the estimation of the directivity vectors based on observations of the gateway is intrinsically a nonlinear, multiuser estimation problem which has not been investigated previously ;b) the design of a multiple input multiple output (MIMO) multiuser nonlinear transceiver based

1. It is a fundamental property of antennas that receiving pattern of an antenna when used for receiving is identical to the far field radiation pattern of the same antennas when used for transmission.

on the statistical knowledge of the channel differs substantially from the existing literature focused on beamforming design with perfect or imperfect (robust beamforming) instantaneous CSI.

Beside the solution of the above mentioned core issues, the design of a comprehensive SS based on adaptive beamforming requires the solutions of the following auxiliary technique problems : a) frequency band allocation in the presence of mobility and b) design of a random access channel with contention resolution based on the spatial multiplexing offered by multiple SAs and initial estimation of directivity vectors. In this work, we investigate also these issues and propose new technical solutions for them in order to build of a comprehensive mobile SS based on adaptive beamforming and to assess the global performance of the system and its capacity enhancement.

More specifically, multiple antennas at the satellite and beamforming enable Space Division Multiple Access (SDMA) such that multiple STs can communicate with the gateway within the same time interval and frequency band under the constraint of a sufficiently wide spatial separation among multiple STs. Therefore, it is of primary relevance an appropriate allocation of the frequency band in order to the STs to guarantee ST separation.

The design of a random access channel is also intrinsically related to the core issues addressed in this work. In fact, from an architectural point of view, an enhancement of the number of STs supported by a SS requires a similar enhancement of the capability to process requests of service in the random access channel. From a signal processing point of view, the acquisition/ estimation of the directivity vectors enable the exploitation of spatial separation of STs to resolve contentions that otherwise would be treated as collisions. Then, we propose approaches based on the estimation of directivity vectors to enhance the throughput of the random access channel. Additionally, they are useful to support frequency allocation and beamforming design for each new ST entering the system. Interestingly, these techniques based on signal processing, are complementary to the numerous protocols at the multiple access layer (MAC) recently proposed to increase the throughput of a random access channel.

In the following, we present an outline of the materials and results contained in the individual chapters of Part I. The rest of this chapter is devoted to a review of the fundamental communication concepts that are utilized in this work.

In Chapter 3, we describe the SS system model adopted in Part I. The assumptions on the SS are discussed. Details on the forward and reverse link channels are provided. Especially, the three components that determine the channel, i.e., the directivity vectors, the propagation coefficients, the correlation matrix at the receivers are illustrated.

In Chapter 4, we propose two heuristics approaches to the design of adaptive beamforming based on the knowledge of the directivity vectors and the statics of the propagation coefficients. We compare the performance

of the adaptive beamforming techniques with a conventional beamforming technique in relevant merits including achieved signal to interference plus noise ratio (SINR) distribution, required transmit power, and transmission outage probability.

In Chapter 5, we propose an algorithm for the nonlinear estimation of the directivity vectors based on a least squares error criterion. We show that the nonlinear estimation problem can be reduced to an eigenvalue complementary problem. The estimation does not require the estimation of the propagation channel coefficients which play the role of nuisance parameters. In such a way, the complexity can be significantly reduced. The performance of the algorithm is also evaluated by numerical simulations.

In Chapter 6, we describe two algorithms to resolve contentions in the random access channel at physical layer. These two algorithms are based on the estimation of directivity vectors. A preliminary estimation of the directivity vectors enables the exploitation of the spatial separation between STs to resolve contentions. The two algorithms are also complementary to numerous protocols currently proposed for contention resolution at MAC layer.

In Chapter 7, we propose two reduced complexity algorithms for frequency allocation in a SS system. We compare the system performance when the STs are allocated into different carriers randomly and when they are allocated by implementing the two algorithms. Numerical results show that the proposed algorithms offer a good tradeoff between complexity and system throughput.

In Chapter 8, we describe the complete structure of the SS simulator and propose a complete assessment of system performance. The complete system includes mobile STs accessing random access channel, estimation of the directivity vectors at the transmitter, adaptive beamforming design and frequency allocation. The performance of this comprehensive system is evaluated.

4.2 Multiple Access Schemes and SDMA

Currently, four principles of multiple access techniques are widely implemented in fixed and mobile satellite communication systems [2], namely :

1. Frequency Division Multiple Access (FDMA) : each user is assigned to a different frequency band ;
2. Time Division Multiple Access (TDMA) : users can share the same frequency band but each user transmits during non overlapping time intervals.
3. Code Division Multiple Access (CDMA) : a different spreading sequence is assigned to each user. Each symbol of a ST is modulated by

a spreading sequence and transmitted over the same frequency band and time interval of the other STs. The spreading sequence enables separation of all the interfering signals at the receiver by multiuser detection.

4. Space Division Multiple Access (SDMA) : users share the same frequency band and transmit at the same time and their interfering signals can be separated thanks to their different spatial locations and multiple antennas of the satellite.

These multiple access methods can be combined together. They and their hybrid schemes are widely used in a satellite communications.

In this work, we consider a satellite system based on SDMA technology. In a SDMA system, the geographic diversity of the STs is exploited, and interference among the co-channel STs is limited because they are far from each other.

The key technology enabling SDMA is the presence of multiple antennas at the satellite. A proper linear or nonlinear processing of the multiple received (multiuser detection) or transmitted signals (beamforming or precoding) at the gateway enable the separability of the interfering signals or the concentration of the energy of the desired signal toward the STs location, respectively.

4.3 Propagation in Satellite Communication Channel

For the transmission and reception of signals in satellite communications, the range of frequencies in use is usually from 1 to 30 GHz. At these frequencies, different distortions on wave propagation are introduced in different regions of the atmosphere.

The atmosphere can be divided into several regions. The troposphere region is from the ground to an altitude of 15 km. Until this point, the temperature falls continuously and it reaches a level as low as -50 or -60 Celsius. Then, after this point, the temperature starts to rise again. The ionosphere is situated between 70 and 1000 km from the ground. In this region, radio waves are influenced by electrons. Beyond the ionosphere, the signals can be considered to transmit in free space. The region between troposphere and ionosphere is referred as inner free space. The free space and the inner free space cause little distortions on the transmit signals, and the most relevant distortions are introduced at the troposphere and ionosphere level.

In general, the electromagnetic waves are affected by several phenomena to a different extent [3] :

- absorption by atmospheric gases,
- meteorological phenomena (e.g., rain, ice, cloud, etc.),

- smoke and dust,
- troposphere scintillation,
- Faraday rotation,
- ionosphere attenuation,
- ionosphere scintillation.

For mobile satellite terminals, propagation is also affected by some additional phenomena :

- reflections and diffraction from buildings,
- shadowing by trees and tall buildings,
- Doppler frequency shift.

4.4 Directivity Matrix in Satellite Communication Channel

For mobile satellite terminals, the fading part due to mobility is modeled by a directivity vector, one for each ST. This vector is determined by the radiation pattern of the antennas at the satellite, in the direction of the corresponding ST. A radiation pattern represents the energy, phase and polarizations of an antenna in different directions of its radiated field.

The directivity vector between antennas at the satellite and a ST is determined by two factors : 1) the geographic position of the ST, since ST's position determines the "relative" direction from an antenna to the ST ; 2)carrier frequency. Interestingly, the effects of the carrier frequency on directivity vectors are minor. They can be neglected in a given satellite system, e.g., in Ka band or Ku band. This implies that we can benefit from directivity reciprocity both in Time and Frequency Division Duplex (TDD/FDD) mode, and not only in TDD mode, as in terrestrial mobile communications.

4.5 Smart Antenna and Beamforming Technology

A smart antenna system combines antenna arrays with the capability of processing signals and adjusting transmission and/or reception pattern automatically. The objective of a smart antenna system is to allow each ST to transmit/receive signals to/from the gateway in a particular direction with low or null interference to/from other users. By utilizing smart antennas, the system capacity can be improved significantly.

The technology to control the directionality and the weights of transmission/reception is called beamforming.

Smart antenna systems are categorized in two types [4], namely,

- switched beamforming system ;
- adaptive beamforming system.

Switched Beamforming System

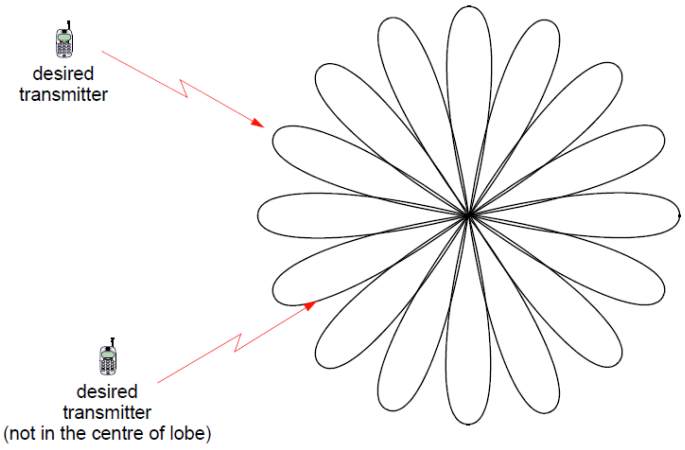

FIGURE 4.1 – Switched Beamforming : predetermined beams to choose from

In the switched beamforming system, the satellite is equipped with some directional antennas which point to some predefined directions. The gateway switches among the different antennas based on received signal assessment, usually in terms of received power. Thanks to its high directivity characteristic, this technique improves system performance compared with a conventional antenna, but the nulling gain is limited.

Figure 4.1 shows a switched beamforming system. A major problem of the switched beamforming system is that the beams are not adaptive to the locations of the STs of interest and thus, the STs may fall outside the center of the main corresponding beams. Due to this fact, the STs may receive less power than the desired one and suffer more from interference from other users.

Adaptive Beamforming System

In the adaptive beamforming system, the power transmitted by multiple beams can be adjusted in real time according to the changes in the environment. The beamformer can adjust the global radiation pattern of multiple antennas to maximize its gain in the desired direction and to minimize the interference from other directions. In such a way, the signal to interference-plus-noise-ratio (SINR) can be increased significantly.

Figure 4.2 shows a comparison between a switched beamforming system and an adaptive beamforming system. In the switched beamforming system, the ST of interest may not fall in the direction of the main lobe which serves it and the interfering STs are not in a null radiation direction. Therefore, the achieved SINR at the ST can be degraded. On the contrary, in the adaptive beamforming system, the main lobe focuses on the ST of interest and the interfering STs are located in a point of null or almost null radiation.

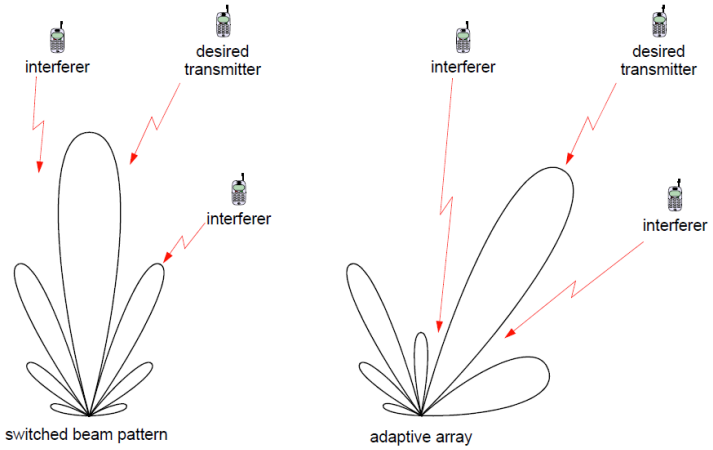

FIGURE 4.2 – Adaptive Beamforming : Adaptive to Environment

Therefore, the adaptive beamforming system improves the system in term of achieved SINR greatly compared to the switched beamforming system.

4.6 Multiple Satellite and Coverage Strategies

In current satellite systems, the coverage area is usually enlightened by fixed beam spots. In this case, the weights of a beamforming network (BFN) at the satellite antennas are kept constant. In order to keep interference from adjacent beams limited, frequency reuse is often adopted. Adjacent beams use different frequencies.

Figure 4.3 shows an example of such a system with a frequency reuse factor equals to 4. Areas covered by different frequencies are shown in different colors. Adjacent areas utilize different frequencies. Frequency 1 is allocated to beam 1 and 3. Since the two beams are located far away from each other, the co-channel interference is limited.

The fixed beams cover a certain area and guarantee a minimum Quality of Service (QoS) in such an area. In this kind of system, in a certain time slot and frequency band, a single ST located in certain area can be served. If two or more users located in the coverage area of the same beams want to transmit at the same time slot, only one user can be served. As a consequence, when the number of users that require transmission is high, the possibility of outage events is also high. This issue strongly limits the capacity of such a fixed beamforming system.

In a European project funded by the European Space Agency (ESA), another fixed beamforming system was proposed to enhance the system capacity [5]. In this system, frequency reuse is avoided and all the beams can be served by all the frequency carriers. The weights of the BFN are kept

constant. Differently from the previous system, in this case, beams are clustered in groups of seven and the signals are jointly processed both in the forward and the reverse link. In this way, the gateway receives multiple copies of each ST's signals from different antennas and multiuser detection (MUD) is performed to cancel interference from other STs in the same cluster. Similarly for the forward link, fixed beamforming is performed within clusters. This approach enables a unit frequency reuse with considerable improvement of the spectral efficiency. However, STs at the border of the cluster suffers from inter-cluster interference.

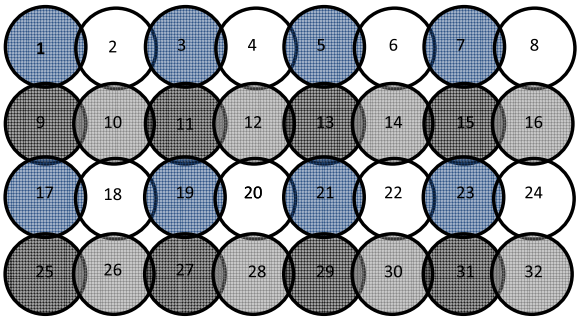

FIGURE 4.3 – Fixed beamformer to cover the satellite area : frequency reuse

The main drawback of these kinds of fixed beamforming systems lies on their lack of flexibility. The beams are not adaptive to the locations of the users. Therefore, in order to guarantee a certain minimum QoS, more transmission power is needed, with consequent reduction of energy efficiency.

Thanks to the implementation of an adaptive BFN, the beams can be designed according to STs' positions. Their main lobes focus on the STs. Each beam is designed to maximize the gain in the direction of the users while the interference affecting other STs is minimized. Compared with conventional fixed beamformer strategy, an adaptive covering strategy improves system performance in terms of spectral and power efficiency.

Additionally, an adaptive beamformer can be designed to meet a given user's QoS and it does not need to guarantee a minimum QoS in a certain coverage area. The transmitted power is tailored to the needs of a given ST and not blindly designed for a hypothetical worst case situation. This determines an additional improvement in spectral efficiency.

For the design of an adaptive beamformer, the knowledge of the CSI at the transmitter is a critical issue. The transmitter has to design the beamformer on the basis of the channel states.

In this contribution, we employe an adaptive beamforming strategy to cover the satellite area. Technical details about adaptive beamforming design are provided in Chapter 6.

4.7 Frequency Allocation in SDMA

In conventional fixed beamforming with frequency reuse, frequencies are preassigned to beams and a frequency band is allocated to a ST depending on its position and the corresponding coverage beam. However, this does not hold for an adaptive beamforming system. Frequency reuse becomes a NP-hard problem with high complexity. From a practical point of view, it is crucial to reduce the computational complexity while achieving good performance. We investigate the problem of frequency allocation in SDMA in Chapter 9.

4.8 Random Access in Satellite Communication

The random access channel (RACH) is widely used for initial access of STs in a SS and short burst transmissions. Currently, the most often adopted schemes for random access channel in satellite communication are Slotted-Aloha [6] [7] and Diversity-Slotted Aloha [8] [9] [10]. For both schemes, time is structured in slots and synchronization is required. STs that desire to communicate enter in the system by transmitting their request on a RACH at the beginning of a slot.

In a conventional fixed beamforming system, a beam can support a single ST per slot ; However, if more than a ST transmit on the same time slot, a collision occurs and none of the transmitting STs can be detected by the system. When the number of STs that want to initiate transmission increases, the possibility of collisions boosts dramatically. The colliding STs have to repeat their transmission until they are successfully detected. This may lead to very large transmission delay and waste of frequency band. Furthermore, the signal from each beam is independently processed and spatial diversity is not exploited.

In this work, we consider the RACH of a multi-beam satellite system with universal frequency reuse. We benefit from the spatial diversity and strong directivity of multiple antennas at a satellite to resolve contentions and perform channel estimation. In other words, multiple directional antennas provide an unique "signature" to each ST that is exploited for multiuser detection, i.e., contention resolution. Therefore, a fundamental step of this technique requires the estimation of the unique signature characterizing each ST.

4.9 Partial Channel State Information Acquisition

CSI acquisition is a crucial problem in the design of adaptive beamforming systems and strongly depends on channel characteristics.

Conventional CSI acquisition can be achieved in different ways. The first way is to learn from the feedback of the receiver. CSI is estimated at the receiver based on the pilot symbols *a priori* available at the receiver [11], [12], [13], [14]. Another approach requires that the assumption of the reciprocity of the channel holds ; In this case, CSI is estimated at the transmitter by using pilot symbols which are a priori known to it.

In a SS, the propagation coefficients vary very rapidly and the propagation delay in the satellite channel is very long. Then, the estimation of the instantaneous CSI becomes obsolete very quickly and cannot be used for the design of adaptive beamforming.

In these cases, other kinds of information, (for example, the information about some slow varying parts of the channel) can be used instead of the instantaneous CSI. This provides a practical solution, since such information changes more slowly than the channel state.

In a communication system, partial CSI can be either estimated at the STs and fed back to the gateway or can be estimated at the gateway if channel reciprocity holds (at least from a statistical point of view). The first approach requires a feedback channel and, therefore, reduces spectral efficiency. In this contribution, we assume that channel reciprocity holds for the directivity vectors. Therefore, we can estimate the directivity vectors at the gateway, and use this estimated partial CSI to design the adaptive beamformer.

The acquisition of slow-varying partial CSI at the gateway, for a satellite system with mobile STs, equipped eventually with multiple antennas and transmitting in left and right polarization, presents completely new challenges compared to the thoroughly studied field of satellite channel estimation finalized to coherent detection and decoding at the receiver side and it is a completely unexplored field. By assuming that the statistics of the propagation coefficients are available at the gateway and follow the model in [15], the partial CSI estimation reduces to the estimation of the slow varying components, i.e, the directivity vectors. From a signal processing perspective, this implies the challenging task of estimating parameters observed through multiplicative nuisance.

The estimation of the directivity vectors is intrinsically *nonlinear*. We consider a parametric model of the channel where the directivity vector is parametrically represented by a linear combination of given known directivity vectors (see in Section 5.1) and the varying propagation coefficients play the role of multiplicative nuisance parameters.

We present the proposed algorithms in detail in Chapter 7.

Chapter 5

Satellite System Model

In this chapter, the system model adopted in Part I is illustrated. The forward and reverse link between the gateway-satellite and the mobile STs are modeled. A model for the propagation components of the channel, a model for the correlation of left and right polarization components and also the directivity matrix of the satellite antennas are discussed.

Two fundamental assumptions of the system model are made throughout the whole Part I : (a) the reciprocity principle holds for the directivity vectors and (b) the directivity vectors are substantially independent of the frequency band. This implies that observations of signals at the gateway received on the random access channel or on a reverse link can be conveniently exploited for the estimation of directivity vectors in the forward link even in the case in which the forward link uses a different frequency band.

We consider an Spatial Division Multiple Access (SDMA) based MIMO mobile satellite system (MSS) with large number of beams and users. The satellite terminals (ST) in this system are mobile phones or laptops of small size and equipped with small antennas. Multi-user detection (MUD) technology is adopted at the STs. We assume that the STs that want to initiate the transmission access to the gateway through a random access channel in a slotted time interval and they are perfectly synchronized. They arrive and leave the system according to a Poisson Process [16]. Furthermore, synchronized transmissions are assumed ; STs start the transmission at the beginning of a time slot and the signals are received synchronously at the gateway. Additionally, during the transmission, all the STs are moving. However, we assume the movements of the STs inside a beam are relatively slow when seen from Geosynchronous (GEO) satellites, Highly Elliptical Orbit (HEO) satellites and Medium Earth Orbit (MEO) [17] [18] satellites.

The satellite is equipped with antennas of very large size in order to compensate for the small antennas size at the STs. The satellite is also equipped with a beamforming network (BFN) whose weights can be updated at high frequency (in the order of some seconds to support adaptive beamforming). Thanks to the large size of antennas available at the satellite, the beamformer has a very strong radiation pattern.

As already mentioned in Section 4.9, the channel of the mobile SS system is modeled as a multiplication of three different components, namely

1. directivity vector between a satellite terminal and the satellite ;
2. propagation component ;
3. correlation matrix at the receiver.

We describe these three components in detail in this chapter.

This chapter is organized as follows : Section 5.1 describes the satellite system model in the forward link ; Section 5.2 illustrates the satellite system model in the reverse link.

5.1 Forward Link

In Part I, we consider a satellite system consisting of a gateway, a bent-pipe satellite equipped with N satellite antennas (SA) and K STs. Each ST is endowed with R antennas. All the antennas transmit in left and right polarizations.

In the forward link, the information bits are encoded at the gateway to generate the channel symbols. Then, the symbols are fed to a beamformer network which modulates the transmission of each symbol on different transmit antennas through weights properly designed. The aim of the beamformer is to generate tailored beams in the direction of the STs as illustrated in Section 4.5. Mathematically, the beamformer is modeled by an $2N \times 2K$ matrix $\boldsymbol{F}$ with complex elements. The dimension $2N$ accounts for the fact that each SA transmits from both left and right polarizations and the dimension $2K$ accounts for two independent streams are transmitted for each ST. Its output, i.e., the linear combinations of all the input streams weighted by the coefficents of the beamforming networks, is transmitted through the downlink channel by the N antennas at the satellite. In an ideal beamforming system, the beamformer signal is linearly amplified and transmitted. However, the nonlinear behavior of the signal processing devices and amplifiers at the satellite induces linear distortions called intermodulation or intermodulation distortions. This intermodulation distortion is modeled as additive noise. The beamformed signal impaired by an additive intermodulation noise is transmitted by the satellite antennas (SA) in left and right polarizations. The transmitted signal is then collected by the antennas of the K STs in both polarizations.

In current satellite systems, the channel for a single carrier can be modeled as flat fading. The discrete-time based received signal at time t is

$$\boldsymbol{y}^f[t] = \boldsymbol{H}^f[t](\boldsymbol{F}\boldsymbol{x}^f[t] + \boldsymbol{e}^f[t]) + \boldsymbol{n}^f[t] \tag{5.1}$$

where $\boldsymbol{H}^f[t]$ denotes the $2KR \times 2N$ transfer matrix of the channel between the STs and the SAs. Dimension $2KR$ accounts for two streams for R receive antennas of all STs, dimension $2N$ accounts for the left and right polarizations of N SAs. $\boldsymbol{F}$ is the $2N \times 2K$ beamformer matrix, $\boldsymbol{x}^f[t]$ is the $2K$ vector of transmitted symbols transmitted, two sequences for each ST ; $\boldsymbol{y}^f[t]$ is the $2KR$-dimensional vector of received signals, and $\boldsymbol{e}^f[t]$ is the $2N$-dimensional vector of intermodulation noise. Finally, $\boldsymbol{n}^f[t]$ is the $2KR$-dimensional vector of zero mean additive Gaussian noise with variance σ_n^2. The noise induced by intermodulation, $\boldsymbol{e}^f[t]$, is related to the total power of the transmitted streams $\boldsymbol{x}^f[t]$. It can be modeled statistically as a white Gaussian noise, i.e. $\boldsymbol{e}_i^f \sim \mathcal{N}(0, \sigma_{ef}^2)$, where

$$\sigma_{ef}^2 = \frac{10^{-\frac{(C/Im)_{moy}}{10}}}{2N} \mathrm{E}\left\{\boldsymbol{x}^f[t]^H \boldsymbol{x}^f[t]\right\}.$$

and $(C/Im)_{moy}$ is the average signal to intermodulation noise ratio. Typically, $(C/Im)_{moy}$ varies in a range of 15-18dB, depending on the quality of the on-board equipments. This means that the power of vector $\boldsymbol{e}^f$ is 15-18dB inferior to the total power of the transmitted vector $\boldsymbol{x}^f$.

In our system, the forward link channel matrix can be written as

$$\boldsymbol{H}^f[t] = \boldsymbol{C}_\alpha^f \boldsymbol{P}^f[t] \boldsymbol{D}^f[t], \tag{5.2}$$

where $\boldsymbol{C}_\alpha^f$ represents the $2KR \times 4KR$ correlation matrix at the receiver, $\boldsymbol{P}^f$ represents the $4KR \times 2K$ propagation matrix between the satellite and the users. $\boldsymbol{D}^f$ represents the $2K \times 2N$ directivity matrix.

Finally, the k-th ST is equipped with a linear multiuser detector $\boldsymbol{M}_k$ to detect the transmitted vector $\boldsymbol{x}_k[t]$ intended for the k-th ST from the received signal $\boldsymbol{y}_k[t]$. A graphical representation of the system model in the forward link is presented in Figure 5.1.

As already stated, the transfer matrix in the forward link can be factorized as $\boldsymbol{H}^f = \boldsymbol{C}_\alpha^f \boldsymbol{P}^f \boldsymbol{D}^f$. In the following, we describe the properties of $\boldsymbol{C}_\alpha^f$, $\boldsymbol{P}^f$ and $\boldsymbol{D}^f$, respectively.

5.1.1 Correlation Matrix at the Receiver

The $2KR \times 4KR$ correlation matrix $\boldsymbol{C}_\alpha^f$ accounts for coupling effects of antennas at the receivers, and for the correlation of the two polarizations. We assume that the correlations of the receiver antennas at a ST are identical

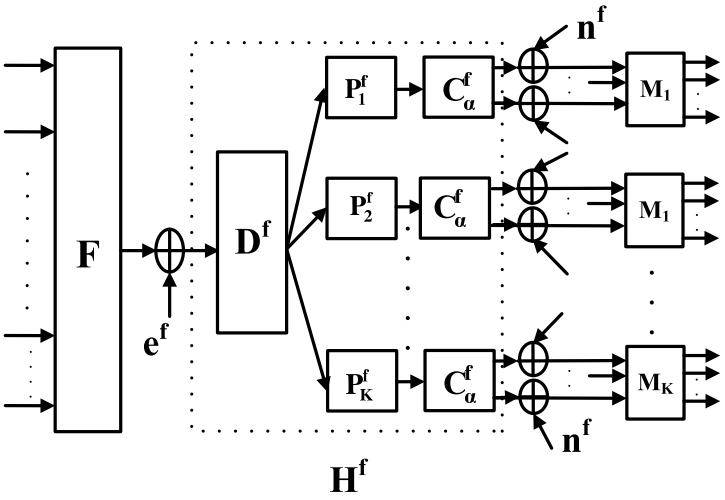

FIGURE 5.1 – Satellite System Model in the Forward Link

and there is no correlation among antennas belonging to different ST. Thus, $\boldsymbol{C}_{\alpha}^{f}$ is a diagonal block matrix, with identical blocks $\boldsymbol{C}_{\alpha ii}$ of size $2R \times 4R$. Furthermore, each line of the correlation matrix $\boldsymbol{C}_{\alpha ii}$ is normalized to have unit norm.

An example for $\boldsymbol{C}_{\alpha ii}$ when $R = 2$ is

$$\boldsymbol{C}_{\alpha ii} = \begin{pmatrix} \sqrt{1-\varepsilon} & b & 0 & 0 & a\sqrt{1-\varepsilon} & ab & ab & a\sqrt{1-\varepsilon} \\ 0 & 0 & b & \sqrt{1-\varepsilon} & a\sqrt{1-\varepsilon} & ab & ab & a\sqrt{1-\varepsilon} \\ a\sqrt{1-\varepsilon} & ab & ab & a\sqrt{1-\varepsilon} & \sqrt{1-\varepsilon} & b & 0 & 0 \\ a\sqrt{1-\varepsilon} & ab & ab & a\sqrt{1-\varepsilon} & 0 & 0 & b & \sqrt{1-\varepsilon} \end{pmatrix}$$

where b represents the isolation between two cross-polarizations of the same antenna ; a accounts for the cross-correlation between two different antennas of the same ST. The coefficients ε, a and b are normalized in a way that each row of $\boldsymbol{C}_{\alpha ii}$ has unit Froboenius norm, i.e.,

$$(1 + 2a^2)\sqrt{1-\varepsilon} + b^2 + 2a^2b^2 = 1.$$

Hence, we can easily obtain

$$\varepsilon = 1 - \frac{1 - b^2 - 2a^2b^2}{1 + 2a^2}.$$

We assume that $\boldsymbol{C}_{\alpha ii}$ is known to the STs and the gateway.

5.1.2 Propagation Matrix

The propagation matrix $\boldsymbol{P}^f$ is a $4KR \times 2K$ block diagonal matrix, with K blocks, and each block is of size $4R \times 2$. The coefficients of the matrix $\boldsymbol{P}_k^f$ represents the propagation losses (atmospheric losses and shadowing) between the satellite antenna and k-th ST. The size 2 of each block accounts for the 2 polarizations.

The matrix $\boldsymbol{P}_k^f$ is structured as

$$\boldsymbol{P}_k = \begin{pmatrix} P_{rr}^{k,(1)} & 0 \\ 0 & P_{rl}^{k,(1)} \\ P_{lr}^{k,(1)} & 0 \\ 0 & P_{ll}^{k,(1)} \\ \vdots & \vdots \\ P_{rr}^{k,(R)} & 0 \\ 0 & P_{rl}^{k,(R)} \\ P_{lr}^{k,(R)} & 0 \\ 0 & P_{ll}^{k,(R)} \end{pmatrix}$$

where $P_{x,y}^{k,(\ell)}$, $\ell = \{1, ..., R\}$, $x, y = \{l, r\}$ denotes the propagation loss on the signal in x polarization received in y polarization at the l-th antenna of the k-th ST.

Each propagation matrix $\boldsymbol{P}_k$ is statistically independent from the others. Several models have been proposed for the propagation matrix of a *mobile* ST equipped with *multiple antennas*. In Part I, when the generation of propagation matrices is necessary for simulations, we adopt the Surrey model [15]. Surrey model is a physical-statistical model of land mobile satellite MIMO radio propagation channel proposed by the Center for Communication Systems Research at the University of Surrey. It provides the empirical statistics of both narrow and wide band satellite MIMO channels. It is validated by the experimental measurements.

Remarks : In this work, *in the reverse link*, the characteristics of the propagation coefficients are not critical for the directivity vectors estimation. On the contrary, in the forward link, in order to design the heuristic beamformer, the statistics of the propagation coefficients are required.

5.1.3 Directivity matrix

The directivity matrix $\boldsymbol{D}^f$ in the forward link provides a mathematical description of the links between the N transmitting antennas at the satellite and the K mobile STs. The size of $\boldsymbol{D}^f$ is $2K \times 2N$.

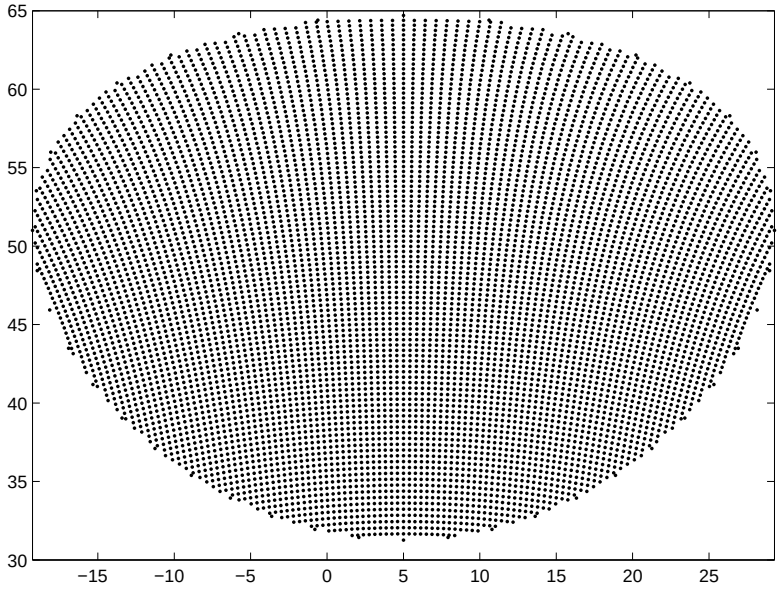

FIGURE 5.2 – Satellite grid in Europa

The directivity matrix is given by

$$\boldsymbol{D}^f = \begin{pmatrix} d^1_{1,rr} & d^1_{1,lr} & \cdots & \cdots \\ d^1_{1,rl} & d^1_{1,ll} & \cdots & \cdots \\ \vdots & \ddots & \ddots & \vdots \\ \cdots & \cdots & d^K_{N,rr} & d^K_{N,lr} \\ \cdots & \cdots & d^K_{N,rl} & d^K_{N,ll}, \end{pmatrix} \tag{5.3}$$

where $d^k_{n,rl}$ represents the directivity of the n-th antenna in left polarization in the direction of the k-th ST in right polarization. The parameter $d^k_{n,rr}$ represents the directivity of the the n-th antenna in right polarization in direction of the k-th ST in right polarization. The elements $d^k_{n,lr}$ and $d^k_{n,ll}$ are defined in a similar way. $d^k_{n,rl}$ and $d^k_{n,lr}$ are the directivity components in cross polarizations and $d^k_{n,rr}$ and $d^k_{n,ll}$ are the directivity components in co-polarization. In general, these coefficients are complex. It is common to assume $d^k_{n,rr} = d^k_{n,ll}$ and $d^k_{n,rl} = d^k_{n,lr}$.

The directivity matrix $\boldsymbol{D}^f$ can be conveniently structured in KN blocks of form

$$\boldsymbol{D}^{f,k}_n = \begin{pmatrix} d^k_{n,rr} & d^k_{n,lr} \\ d^k_{n,rl} & d^k_{n,ll} \end{pmatrix} = \begin{pmatrix} \boldsymbol{d}^{f,k}_{n,r} \\ \boldsymbol{d}^{f,k}_{n,l} \end{pmatrix}, \tag{5.4}$$

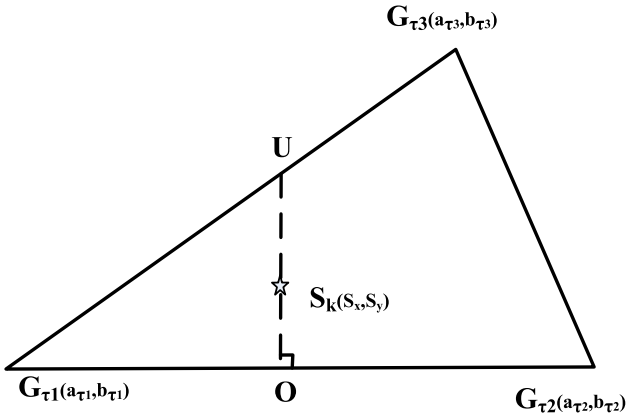

FIGURE 5.3 – Directivity Linear Interpolation

where $\boldsymbol{D}_n^{f,k}$ describes the static part of the channel between the k-th ST and the n-th SA and $\boldsymbol{d}_{n,o}^k = (d_{n,ro}^k, d_{n,lo}^k)$ is the component in o-polarization at antenna n. The block column of size $2 \times 2N$, $\boldsymbol{D}^{f,k} = (\boldsymbol{D}_1^k, \boldsymbol{D}_2^k, \ldots \boldsymbol{D}_N^k)$, represents the directivity coefficients of the k-th ST.

The directivity vector corresponding to a certain ST is determined by two factors : the geographic position of the ST and the carrier frequency. Interestingly, the effects of the carrier frequency on the directivity vectors are minor in the range of frequencies utilized in a satellite system, e.g., in Ka band or Ku band. Then, the variations of the directivity coefficients due to the frequency can be neglected in a given satellite system. This implies that we can benefit from directivity reciprocity both in Time and Frequency Division Duplex (TDD/FDD) mode, and not only in TDD mode, as in terrestrial mobile communications.

Throughout Part I of this thesis, we make the following two realistic assumptions : (a) the directivity vectors of some reference STs in a grid are known at the gateway. The values of realistic directivity vectors for a grid, which covers Europe, have been provided by CNES for the simulations in this thesis. For each grid point, defined by its latitude and longitude, CNES provided a directivity vector consisting of the amplitude and phase of the co-polarization and cross-polarization coefficients for each SA. The grid adopted by CNES is shown in Figure 5.2.

We denote by $\boldsymbol{G}$ the matrix available at the gateway and containing all the directivity vectors of the points in the grid. The transpose of matrix $\boldsymbol{G}$ has a block structure similar to the one of $\boldsymbol{D}^f$ with blocks $\boldsymbol{G}_n^k$ of form (5.4) ; (b) the directivity vector of a ST in an arbitrary position can be determined as a

convex combination of the directivity vectors at some surrounding reference points. More specifically, let us consider the k-th ST with coordinates $S_k \equiv (S_x, S_y)$. Let $\mathcal{T}$ denotes the set of all adjacent triplets τ on the reference grid and let $G_{\tau(i)} \equiv (a_{\tau(i)}, b_{\tau(i)})$, with $i = 1, 2, 3$, be the three nearest and adjacent reference points surrounding ST k. The point S_k can be expressed as convex combination of $G_{\tau(1)}, G_{\tau(2)}$, and $G_{\tau(3)}$, i.e.

$$S_k = \alpha_1^k G_{\tau(1)} + \alpha_2^k G_{\tau(2)} + \alpha_3^k G_{\tau(3)}.$$

The notation shown in Figure 5.3 is adopted, and denoting with $\|AB\|$ the distance between point A and point B, the coefficients α_i^k of the convex combination can be evaluated as

$$\alpha_1^k = \frac{\|G_{\tau(2)}, O\|}{\|G_{\tau(1)}, G_{\tau(2)}\|} \frac{\|S_k, U\|}{\|O, U\|} + \frac{\|G_{\tau(3)}, U\|}{\|G_{\tau(1)}, G_{\tau(3)}\|} \frac{\|S_k, O\|}{\|O, U\|},$$

$$\alpha_2 = \frac{\|G_{\tau(1)}, O\|}{\|G_{\tau(1)}, G_{\tau(2)}\|} \frac{\|S_k, U\|}{\|O, U\|},$$

$$\alpha_3 = \frac{\|G_{\tau(1)}, U\|}{\|G_{\tau(1)}, G_{\tau(3)}\|} \frac{\|S_k, O\|}{\|O, U\|}.$$

It is straightforward to verify that $0 \leq \alpha_i^k \leq 1$, for $i = \{1, 2, 3\}$, and $\sum_{i=1}^{3} \alpha_i^k = 1$. If $\boldsymbol{G}^{\tau(i)}$ denotes the $\tau(i)$ block column of $\boldsymbol{G}$ corresponding to point $G_{\tau(i)}$, then, the directivity column block $\boldsymbol{D}^{f,k}$ of k-th ST is given by the convex combination of the directivity row vectors with identical coefficients

$$\boldsymbol{D}^{f,k} = \alpha_1^k \boldsymbol{G}^{\tau(1)^T} + \alpha_2^k \boldsymbol{G}^{\tau(2)^T} + \alpha_3^k \boldsymbol{G}^{\tau(3)^T}. \tag{5.5}$$

Remark In Figure 5.3, we assume that $G_{\tau(1)}, G_{\tau(2)}$ is the longest edge of the triangle. Then, point O is the projection of S_k on this edge. This ensures that the O point is not external to the edge of the triangle. Point U lies on the same line as S_k and O, and belongs to another edge of the triangle.

5.2 Reverse Link

Figure 5.4 shows the satellite system model in the reverse link.

In Part I of the thesis, we are interested in the transmission in the reverse link only for the estimation of the directivity coefficients in the forward link. Therefore, we focus on modeling the transmission of training sequences again.

In the reverse link, the received signal at the gateway at time t is given by

$$\boldsymbol{y}^{re}[t] = \boldsymbol{S}\left(\boldsymbol{D}^{re}[t]\boldsymbol{P}^{re}[t]\boldsymbol{C}_{\alpha}^{re}\boldsymbol{x}^{re}[t] + \boldsymbol{e}^{re}[t]\right) + \boldsymbol{n}^{re}[t] \tag{5.6}$$

where $\boldsymbol{S}$ is the matrix describing the beamforming network in the reverse link. It has $2N$ columns and a number of rows depending on the number of

signals forwarded to the gateway. The column vector $\boldsymbol{y}^{re}[t]$ is the vector of received signals whose size depends on the number of signals forwarded from the satellite to the gateway (BFN design) ; $\boldsymbol{D}^{re}[t]$ is the directivity matrix in the reverse link of size $2N \times 2K$; $\boldsymbol{P}^{re}[t]$ is the $2K \times 4RK$ propagation matrix in the reverse link ; $\boldsymbol{C}_{\alpha}^{re}$ is the $4RK \times 2RK$ correlation matrix at the ST ; $\boldsymbol{x}^{re}[t]$ is the $2RK$ vector of transmitted signals, the dimension $2RK$ accounts for two sequences transmitted to R receiving antennas of K STs ; and $\boldsymbol{e}^{re}[t]$ and $\boldsymbol{n}^{re}[t]$ are the vectors of intermodulation noise introduced at the satellite and the thermal noise introduced at the gateway, respectively. Both noises are modeled as white Gaussian with variances $\sigma_{e^{re}}^2$ and σ_n^2, respectively. The noise induced by intermodulation, $\boldsymbol{e}^{re}$, is related to the total power of the streams received at the satellite, $\boldsymbol{r}[t] = \boldsymbol{D}^{re}[t]\boldsymbol{P}^{re}[t]\boldsymbol{C}_{\alpha}^{re}\boldsymbol{x}^{re}[t]$. It can be modeled statistically as a white Gaussian noise, i.e., each component $e_i^{re} \sim \mathcal{N}(0, \sigma_{e^{re}}^2)$, where

$$\sigma_{e^{re}}^2 = \frac{10^{-\frac{(C/Im)_{moy}}{10}}}{2N} \mathrm{E}\{\boldsymbol{r}[t]^H \boldsymbol{r}[t]\}.$$

The vector $\boldsymbol{x}^{re}[t]$ of transmitted signals at time t consists of symbols line from each of the $2RK$ training sequences transmitted synchronously by the K STs. It is obtained by stacking together the K vectors $\boldsymbol{x}_k^{re}[t]$ transmitted by each of the ST and of size $2R$.

Let $\boldsymbol{x}_k^{re}[t]$ be the $2R$-dimensional vector of symbols transmitted in left and right polarization by the R antennas of ST k. Then, the vector $\boldsymbol{x}^{re}[t]$ of transmitted signals is obtained by stacking together the K vectors $\boldsymbol{x}_k^{re}[t]$, i.e.,

$$\boldsymbol{x}^{re}[t] = \left(\boldsymbol{x}^{re}[t]_1^T, \boldsymbol{x}^{re}[t]_2^T, ..., \boldsymbol{x}^{re}[t]_K^T\right)^T. \tag{5.7}$$

The propagation matrix $\boldsymbol{P}^{re}[t]$ and the correlation matrix $\boldsymbol{C}_{\alpha}^{re}$ are block diagonal matrices with K blocks $\boldsymbol{P}_k^{re}[t]$ and $\boldsymbol{C}_{\alpha,k}^{re}$ of size $2 \times 2R$ and $4R \times 2R$, respectively. Furthermore, correlation matrix $\boldsymbol{C}_{\alpha}^{re}$ equals to the transpose matrix of the correlation matrix in the forward link, i.e,

$$\boldsymbol{C}_{\alpha}^{re} = \boldsymbol{C}_{\alpha}^{f\,T}.$$

The blocks $\boldsymbol{C}_{\alpha,k}^{re}$ are identical for all the STs, account for the coupling effects at the transmitters, and are known to the STs and the gateway.

The directivity matrix $\boldsymbol{D}^{re}$ in the reverse link equals to the transpose matrix of $\boldsymbol{D}^{f}$, and it can conveniently be structured in NK blocks of form

$$\boldsymbol{D}_n^{re,k} = \begin{pmatrix} d_{n,rr}^k & d_{n,rl}^k \\ d_{n,lr}^k & d_{n,ll}^k \end{pmatrix} = \begin{pmatrix} \boldsymbol{d}_{n,r}^{re,k} \\ \boldsymbol{d}_{n,l}^{re,k} \end{pmatrix}. \tag{5.8}$$

The block column of size $2N \times 2$, $\boldsymbol{D}^{re,k} = (\boldsymbol{D}_1^{re,kT}, \boldsymbol{D}_2^{re,kT}, \ldots \boldsymbol{D}_N^{re,kT})^T$, represents the directivity coefficients of the k-th ST in reverse link.

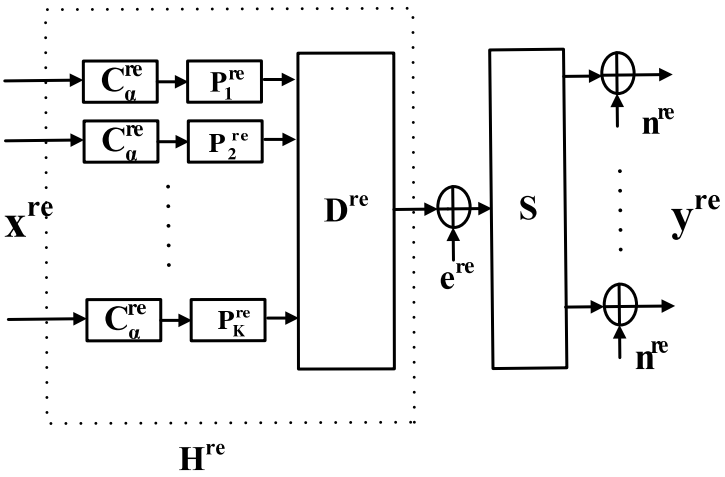

FIGURE 5.4 – Satellite System Model in the Reverse Link

Similar as (5.5), $\boldsymbol{D}^{re,k}$ can be written as a convex combination of column vectors with coefficients

$$\boldsymbol{D}^{re,k} = \alpha_1^k \boldsymbol{G}^{\tau(1)} + \alpha_2^k \boldsymbol{G}^{\tau(2)} + \alpha_3^k \boldsymbol{G}^{\tau(3)} \tag{5.9}$$

where $0 \leq \alpha_i^k \leq 1$, and $\sum \alpha_i^k = 1$.

In this work, we assume that the beamforming matrix $\boldsymbol{S}$ is a $2N \times 2N$ identity matrix. This choice has the twofold advantage of (i) not making any compression of the information signals at the satellite antenna to transfer them to the gateway, (ii) keeping white the intermodulation noise. The system model (5.6) reduces then to

$$\begin{aligned} \boldsymbol{y}^{re}[t] &= \boldsymbol{D}^{re}[t]\boldsymbol{P}^{re}[t]\boldsymbol{C}_\alpha^{re}\boldsymbol{x}^{re}[t] + \boldsymbol{e}^{re}[t] + \boldsymbol{n}^{re}[t] \\ &= \boldsymbol{D}^{re}[t]\boldsymbol{P}^{re}[t]\boldsymbol{C}_\alpha^{re}\boldsymbol{x}^{re}[t] + \boldsymbol{z}[t] \end{aligned} \tag{5.10}$$

where $\boldsymbol{z}[t]$ is the white additive Gaussian noise with variance $\sigma_z^2 = \sigma_{e^{re}}^2 + \sigma_n^2$.

When we focus on the signal received at the gateway from the n-th SA in o-polarization, with $o \in \{l, r\}$, at time instant t, the model 5.10 reduces to

$$y_{n,x}^{re}[t] = \boldsymbol{d}_{n,o}^{re}[t]\boldsymbol{P}^{re}[t]\boldsymbol{C}_\alpha^{re}\boldsymbol{x}^{re}[t] + z_{n,o}[t]. \tag{5.11}$$

Chapter 6

Adaptive Beamforming Design based on limited Channel State Information

In this chapter, we focus on describing the design of an adaptive beamforming based on limited channel state information.

As already described in Chapter 5, the satellite channel is modeled as a cascade of three components including : directivity vectors, propagation coefficients and correlation matrix at the receiver. Since the propagation matrix is fast fading and the feedback information requires a long transmission time in a satellite communication, the feedback of the instantaneous estimation will be stale when received. Therefore, in this work, we propose several heuristic approaches to the design of a linear beamformer based on the use of the directivity components estimated at the transmitter and the statistics of the propagation fast fading components.

This chapter is structured as follows : Section 6.1 reviews the state of art on beamforming design and beamforming design based on limited CSI. Section 6.2 introduces two practical BFN design approaches. Section 6.3 describes a conventional fixed beamforming network as a benchmark for the adaptive beamformer. Section 6.4 evaluates the BFN design approaches with numerical simulations. The results are also compared with the benchmark system.

In this chapter, we only consider the satellite system in the forward link, therefore, for the sake of simplicity, we remove the superscript of $\{\cdot\}^f$. We replace in this chapter $\boldsymbol{y}^f$, $\boldsymbol{x}^f$, $\boldsymbol{D}^f$, $\boldsymbol{P}^f$ and $\boldsymbol{C}_\alpha^f$ by $\boldsymbol{y}$, $\boldsymbol{x}$, $\boldsymbol{D}$, $\boldsymbol{P}$ and $\boldsymbol{C}_\alpha$, respectively.

6.1 State of the Art

In order to support transmission in broadcast wireless systems endowed multiple transmit antennas, the information streams intended for different STs are modulated by different beamformers at the transmitter. Based on channel state information, beamformers can be jointly designed for all the STs. Many work have been devoted to study the design of beamformer. In general, precoding design algorithms can be categorized into two different types : linear precoding or beamforming and nonlinear precoding.

Nonlinear precoding approaches are based on the Dirty Paper Coding (DPC) [19] [20] approach which achieves the channel capacity. Tomlinson-Harashima precoding [21] [22] is regarded as a practical low-complexity implementations of the optimal DPC. It achieves good performance in terrestrial MIMO link, affected by independent Rayleigh fading [5]. However, in practice, nonlinear precoding approaches are unfeasible to implement because they have very high complexity.

Among the linear precoding approaches, Zero Forcing (ZF) [23] and Minimum Mean Squared Error (minimum mean squared error) beamforming are the most well known.

In the case of broadcast channels with receivers equipped with a single antenna and full CSI at the transmitter, the design of an optimum linear beamformer satisfying total power constraint is well known and understood. Iterative schemes based on the dual relation between the broadcast channel and the multiple access channel for designing such beamformer are proposed in [24] [25] [26] [27] [28] [29].

The same problem, when the receivers are equipped with multiple antennas and CSI is available both at the transmitter and the receiver, is more complex. Possible algorithms for linear beamforming design are proposed in [25]. They are also based on the property of duality .

Nevertheless, as already mentioned, in practical communication systems, perfect CSI in many cases is not available at the transmitter. Therefore, beamforming design with imperfect CSI is an interesting research topic in practical systems. Beamforming based on imperfect CSI is often referred to as robust beamforming. In the case of a broadcast channel with multiple users equipped with a single antenna (MISO), robust beamforming design aiming to minimize the worst case mean-square-error (MSE) is studied in [30]. In [31] [28], the authors consider the problem to minimize transmission power with the constraint of guaranteing quality of service (QoS) in MISO channel in the worst case.

When both transmitter and receivers are equipped with multiple antennas (MIMO), robust linear beamformers against channel uncertainty are investigated in [32]. Unfortunately, the duality property does not hold for a broadcast channel with full CSI only available at the receiver [33] and the channel capacity of the system is unknown. Some initial results are presen-

ted in [33]. Similarly, no algorithm for an optimal beamforming design is available in literature at the best of the authors' knowledge.

The case that CSI at the transmitter has an uncertainty error is also studied. In [34], the authors consider a scenario where the CSI at the transmitter has an uncertainty error bounded by an ellipsoidal region. They propose a robust joint transceiver beamformer to minimize the transmit power while guaranteeing the QoS in term of signal to noise-interference ratio (SINR).

6.2 Adaptive BFN based on limited channel state information

We assume that only partial knowledge of the channel is available at the transmitter side. The transmitter has knowledge only of the directivity matrix and the statistics of the propagation matrix. Thus, we design the beamformer based solely on the directivity matrix $\boldsymbol{D}$ and the statistics of $\boldsymbol{C}_\alpha \boldsymbol{P}$ but not on the exact realizations. More specifically, the statistics of the matrix $\boldsymbol{C}_\alpha \boldsymbol{P}$ are used to determine a deterministic channel. The average signal to noise and interference ratio (SINR) at the output of the deterministic channel is utilized in the design of the beamformer matrix constrained to a target SINRs. The beamforming design takes also into account the different sources of noise introduced in different points of the system (intermodulation noise and thermal noise) as an unique additive noise, eventually colored.

6.2.1 Approach A

In this approach, referred in the following as approach A, we make use of the linear beamforming method designed for broadcast channels with single receive antenna and full CSI at the transmitter and the receivers.

Approximation via a Deterministic Channel

The deterministic channel is illustrated in Figure 6.1 and is obtained from the following considerations and approximations :

- The white Gaussian intermodulation noise $\boldsymbol{e} \sim \mathcal{CN}(\boldsymbol{0}, \sigma_e^2 \boldsymbol{I})$ introduced in the satellite can be equivalently modeled as an additive noise $\widetilde{\boldsymbol{e}}_k(t)$ at the receiver k. At a given time instant t such a noise is Gaussian with covariance matrix $\boldsymbol{C}_{\widetilde{\boldsymbol{e}}_k(t)}$ depending on the realization of the propagation matrix. Namely, $\boldsymbol{C}_{\widetilde{\boldsymbol{e}}(t)} = \sigma_e^2 \boldsymbol{C}_{\alpha,kk} \boldsymbol{P}_k \boldsymbol{D}_k \boldsymbol{D}_k^H \boldsymbol{P}_k^H \boldsymbol{C}_{\alpha,kk}^H$. When considered over time, we approximate the distribution of the equivalent noise by a Gaussian distribution with covariance matrix $\boldsymbol{C}_{\widetilde{\boldsymbol{e}}_k} = \sigma_e^2 \mathbb{E}\{\boldsymbol{C}_{\alpha,kk} \boldsymbol{P}_k \boldsymbol{D}_k \boldsymbol{D}_k^H \boldsymbol{P}_k^H \boldsymbol{C}_{\alpha,kk}^H .\}$
  The equivalent noise at the receiver is then modeled as an additive colored noise $\boldsymbol{z}_k$ with zero mean and covariance matrix $\boldsymbol{C}_{\boldsymbol{z}_k} = \sigma_n^2 \boldsymbol{I} + \boldsymbol{C}_{\widetilde{\boldsymbol{e}}_k}$.

- The cascade of the propagation matrix $\boldsymbol{P}_k$, the correlation matrix $\boldsymbol{C}_{\alpha,kk}$, and the additive noise yields to a system model

$$\boldsymbol{r}_k = \boldsymbol{C}_{\alpha,kk}\boldsymbol{P}_k\boldsymbol{x}_{c,k} + \boldsymbol{z}_k \tag{6.1}$$

where $\boldsymbol{x}_{c,k}$ is the input to the cascade. This model is equivalent, in terms of SINR to the model,

$$\overline{\boldsymbol{r}}_k = \boldsymbol{\Lambda}_k^{-1/2}\boldsymbol{U}_k\boldsymbol{C}_{\alpha,kk}\boldsymbol{P}_k\boldsymbol{x}_{c,k} + \boldsymbol{w}_k \tag{6.2}$$

where $\boldsymbol{w}_k$ is an additive white Gaussian noise with covariance matrix $\boldsymbol{I}$ and $\boldsymbol{\Lambda}_k$ and $\boldsymbol{U}_k$ are obtained from the eigenvalue decomposition of $\boldsymbol{C}_{\boldsymbol{z}_k}$, i.e. $\boldsymbol{C}_{\boldsymbol{z}_k} = \boldsymbol{U}_k^H\boldsymbol{\Lambda}_k\boldsymbol{U}_k$. The system model in (6.2) can be rewritten as

$$\widetilde{\boldsymbol{r}}_k = \sqrt{\frac{\kappa_k}{2}}\widetilde{\boldsymbol{C}}_{\alpha,kk}\widetilde{\boldsymbol{P}}_k\boldsymbol{x}_{c,k} + \boldsymbol{w}_k \tag{6.3}$$

where

$$\kappa_k = \mathrm{tr}\left(\frac{\mathbb{E}(\boldsymbol{P}_k\boldsymbol{C}_{\alpha_{kk}}\boldsymbol{C}_{\alpha_{kk}}^H\boldsymbol{P}_k^H)\boldsymbol{C}_{\boldsymbol{z}_k}^{-1}}{2}\right), \tag{6.4}$$

$\widetilde{\boldsymbol{C}}_{\alpha,kk} = \boldsymbol{\Lambda}_k^{-1/2}\boldsymbol{U}_k\boldsymbol{C}_{\alpha,kk}$, and $\widetilde{\boldsymbol{P}}_k = \frac{\boldsymbol{P}}{\sqrt{\kappa_k}}$ such that $\mathbb{E}\{\widetilde{\boldsymbol{C}}_{\alpha,kk}\widetilde{\boldsymbol{P}}_k\widetilde{\boldsymbol{P}}_k^H\widetilde{\boldsymbol{C}}_{\alpha,kk}^H\} = 4R$ and κ_k represents the SNR over all antennas and polarizations.

- In the design of the beamforming network we account for the random attenuation introduced by the cascade described in the previous item via the constant factor κ_k and we neglect the effects of the randomness in the matrix $\widetilde{\boldsymbol{P}}_k$ and the effects of the normalized correlation matrix $\widetilde{\boldsymbol{C}}_{\alpha,kk}$. We assume that the receiver of ST k, which has knowledge of the transmission channel between the satellite and its receive antennas, is able to compensate for the neglected local effects of the fading. The deterministic system utilized for the beamforming design is shown in Figure 6.1. In Figure 6.1, $\widetilde{\boldsymbol{D}} = \boldsymbol{K}\boldsymbol{D}$, where $\boldsymbol{K} = \mathrm{diag}(\boldsymbol{\kappa} \otimes (1,1))$ and $\boldsymbol{\kappa} = (\kappa_1, \kappa_2, \ldots, \kappa_K)$.

Beamforming Algorithm

In the following we specialize the design of beamformers in [24] to the forward link model

$$\widetilde{\boldsymbol{y}} = \widetilde{\boldsymbol{D}}\boldsymbol{F}\boldsymbol{Q}^{1/2}\boldsymbol{x} + \boldsymbol{w} \tag{6.5}$$

where $\widetilde{\boldsymbol{y}}$ is the $2K$-dimensional vector of received signals, $\boldsymbol{Q}$ is the $2K \times 2K$ diagonal matrix of the power level for the transmit signals, $\boldsymbol{x}$ is the transmitted signal vector such that $\mathbb{E}(\boldsymbol{x}\boldsymbol{x}^H) = \boldsymbol{I}$, $\boldsymbol{F}$ is the beamforming matrix normalized in a way that $\mathrm{diag}(\boldsymbol{F}^H\boldsymbol{F}) = \boldsymbol{I}$, and $\boldsymbol{w}$ is the additive white Gaussian noise with unit variance. The corresponding dual reverse link model is

$$\widetilde{\boldsymbol{y}}^{(\mathrm{ul})} = \widetilde{\boldsymbol{D}}^H\boldsymbol{\mathcal{P}}^{1/2}\boldsymbol{x}^{(\mathrm{ul})} + \boldsymbol{w}^{(\mathrm{ul})} \tag{6.6}$$

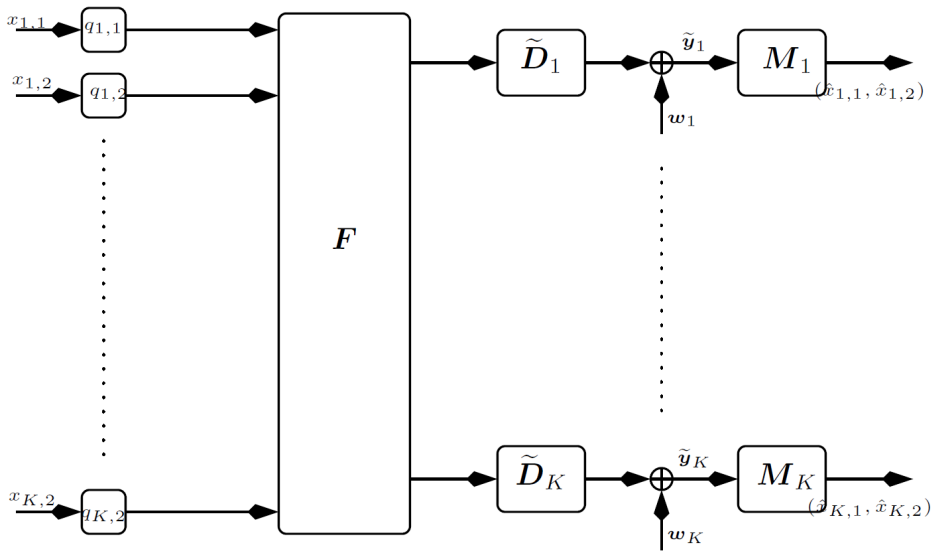

FIGURE 6.1 – System model adopted for Approach A

where $\boldsymbol{\mathcal{P}}$ is the $2K \times 2K$ diagonal matrix of the power levels for the transmit signals, $\boldsymbol{x}^{(\mathrm{ul})}$ is the transmit signal with unit covariance,and $\boldsymbol{w}^{(\mathrm{ul})}$ is the white additive Gaussian noise with unit variance.

If $\boldsymbol{F}^H$ is any multiuser detector for the reverse link, i.e.

$$\hat{\boldsymbol{x}}^{(\mathrm{ul})} = \boldsymbol{F}^H \boldsymbol{y}^{(\mathrm{ul})}, \tag{6.7}$$

with rows normalized to one, the signal to interference plus noise ratio SINR_k of the k-th ST is given by

$$\mathrm{SINR}_k = \frac{p_k |(\boldsymbol{F}^H \widetilde{\boldsymbol{D}})_{kk}|^2}{1 + \sum_{j \neq k} p_j |(\boldsymbol{F}^H \widetilde{\boldsymbol{D}})_{kj}|^2}. \tag{6.8}$$

We define the vector $\boldsymbol{a}$ with the k-th component

$$a_k = \frac{\mathrm{SINR}_k}{(1 + \mathrm{SINR}_k)|(\boldsymbol{F}^H \widetilde{\boldsymbol{D}})_{kk}|^2} \tag{6.9}$$

where vector $\boldsymbol{p} = \mathrm{diag}(\boldsymbol{\mathcal{P}})$ can be expressed as

$$(\boldsymbol{I} - \mathrm{diag}(a_1, a_2, \ldots a_{2K}) \boldsymbol{\Omega}^T) \boldsymbol{p} = \boldsymbol{a}. \tag{6.10}$$

and $\boldsymbol{\Omega}$ is a square matrix with (k, j) components equal to $\left|(\widetilde{\boldsymbol{D}}\boldsymbol{F})_{kj}\right|^2$. It is possible to show that a positive solution to (6.10) exists if and only if the

Perron-Frobenius eigenvalue of the matrix $\text{diag}(a_1, ...a_{2K})\boldsymbol{\Omega}^T$ is less than 1, [24]. Similarly, for the dual channel we can consider the linear beamforming $\boldsymbol{F}$. The SINR at the k-th receiver can be written as

$$\text{SINR}_k = \frac{q_k \left|(\widetilde{\boldsymbol{D}}\boldsymbol{F})_{kk}\right|^2}{1 + \sum_{j \neq k} q_j \left|(\widetilde{\boldsymbol{D}}\boldsymbol{F})_{kj}\right|^2} \tag{6.11}$$

and we can define a variable b_k as

$$b_k = \frac{\text{SINR}_k}{(1 + \text{SINR}_k)\left|(\widetilde{\boldsymbol{D}}\boldsymbol{F})_{kk}\right|^2}. \tag{6.12}$$

Then, the vector $\boldsymbol{q} = diag(\boldsymbol{Q})$ of the powers of the encoded transmitted information can be expressed as

$$(\boldsymbol{I} - \text{diag}(b_1, b_2, ..., b_{2K})\boldsymbol{\Omega})\, \boldsymbol{q} = \boldsymbol{b} \tag{6.13}$$

This equation admits a positive solution $\boldsymbol{q}$ if and only if the matrix $\text{diag}(b_1, ...b_{2K})\boldsymbol{\Omega}$ has the Perron-Frobenius eigenvalue lower than 1. Since the matrices $\text{diag}(a_1, ...a_{2K})\boldsymbol{\Omega}^T$ and $\text{diag}(b_1, ...b_{2K})\boldsymbol{\Omega}$ have the same spectral radius, if there exists a vector $\boldsymbol{p}$ with nonnegative components achieving a target SINR vector, then, there exists also a vector $\boldsymbol{q}$ for the same target SINR vector. It is worth noticing that these considerations hold for any linear detectors $\boldsymbol{F}^H$ and any linear beamformer $\boldsymbol{F}$.
We are interested in designing a linear beamformer in a way that the transmitted vector $\boldsymbol{Q}^{1/2}\boldsymbol{x}$ satisfies the constraints

$$\mathbb{E}\left\{\left\|\boldsymbol{x}^H\boldsymbol{Q}\boldsymbol{x}\right\|\right\} = \text{trace}(\boldsymbol{Q}) \leq P_{\max}$$

and it satisfies some minimum requirements on the SINRs at the receivers.

Denote the target SINRs as $(\chi_1, ..., \chi_{2K})$, so that $\text{SINR}_k \geq \chi_k$ and (6.9) implying that

$$a_k \leq \frac{\chi_k}{(1 + \chi_k)\boldsymbol{\Omega}_{kk}}. \tag{6.14}$$

Consequently, the SINR for the forward link satisfies the inequality

$$[\boldsymbol{I} - \text{diag}(\boldsymbol{a})\boldsymbol{\Omega}]\, \boldsymbol{q} \geq \boldsymbol{\chi} \tag{6.15}$$

while for its dual reverse link, it satisfies

$$\left[\boldsymbol{I} - \text{diag}(\boldsymbol{a})\boldsymbol{\Omega}^T\right] \boldsymbol{p} \geq \boldsymbol{a}. \tag{6.16}$$

The conditions for the feasibility [1] of this problem are summarized in the following theorem.

1. Definition of feasibility in this context : When SNR $\to \infty$, i.e. when $P_{\max} \to +\infty$, we say the system is feasible if the above power allocation equations have solutions, $\boldsymbol{q}^* \geq 0$ and $\boldsymbol{p}^* \geq 0$.

Theorem 1. *[26] The feasibility of the target SINR vector $\boldsymbol{\chi}$ is achieved for both reverse link and forward link with linear processing matrices $\boldsymbol{F}^H$ and $\boldsymbol{F}$, respectively, if and only if the non-negative matrix $diag(\boldsymbol{a})\boldsymbol{\Omega}$ has Perron-Frobenius eigenvalue $\rho(diag(\boldsymbol{b})\boldsymbol{\Omega}) < 1$. In this case, the allocation equations are given by*

$$\boldsymbol{q}^* = [\boldsymbol{I} - diag(\boldsymbol{a})\boldsymbol{\Omega}]^{-1}\boldsymbol{a} \tag{6.17}$$

and

$$\boldsymbol{p}^* = \left[\boldsymbol{I} - diag(\boldsymbol{a})\boldsymbol{\Omega}^T\right]^{-1}\boldsymbol{a}. \tag{6.18}$$

The solutions $\boldsymbol{q}^*$ and $\boldsymbol{p}^*$ are the componentwise minimal powers that achieve the target SINR, $\boldsymbol{\chi}$ with equality, and $\sum_k \boldsymbol{q}_k^* = \sum_k \boldsymbol{p}_k^*$.

From the previous results follows that, for a given sum-power constraint $\mathrm{Q} \leq P_{\max}$, a target SINR vector $\boldsymbol{\chi}$ is feasible if and only if :

- $\rho(\mathrm{diag}(\boldsymbol{a})\boldsymbol{\Omega}) < 1$,
- The sum of the componentwise minimum power vector $\boldsymbol{q}^*$ satisfies

$$\sum_k q_k^* = \mathbf{1}^T [\boldsymbol{I} - \mathrm{diag}(\boldsymbol{a})\boldsymbol{\Omega}]^{-1}\boldsymbol{a} \leq P_{\max}. \tag{6.19}$$

The duality approach yields a solution of the classical beamforming problem

$$\begin{aligned} &\min_{\boldsymbol{F},\boldsymbol{q}} \textstyle\sum_k \boldsymbol{q}_k \\ &\text{subject to } \mathrm{SINR}_k \geq \boldsymbol{\chi}_k, \quad k = 1, ..., 2K. \end{aligned} \tag{6.20}$$

For any set of transmit power $\boldsymbol{p}$, it is well known that the MMSE filter maximizing the SINRs for each ST is given by

$$\boldsymbol{F} = \left[\boldsymbol{I} + \widetilde{\boldsymbol{D}}^H \mathrm{diag}(\boldsymbol{p})\widetilde{\boldsymbol{D}}\right]^{-1} \widetilde{\boldsymbol{D}}^H \mathrm{diag}(\boldsymbol{X}') \tag{6.21}$$

where $\boldsymbol{X}'$ is a diagonal matrix with positive diagonal elements.

The SINR performance of a detector is invariant to right multiplication of any diagonal matrix with non-zero diagonal elements. Hence, we assume that diagonal matrix $\boldsymbol{X}'$ normalizes the $\boldsymbol{F}$ in a way that $\left[\boldsymbol{F}^H\boldsymbol{F}\right]_{kk} = 1$ for all k. The reverse link SINR of the k-th ST with the MMSE detector can be written as

$$\mathrm{SINR}_k = p_k \widetilde{\boldsymbol{d}}_k \boldsymbol{\Sigma}_i^{-1} \widetilde{\boldsymbol{d}}_k^H \tag{6.22}$$

where

$$\boldsymbol{\Sigma}_k \triangleq \boldsymbol{I} + \sum_{j \neq k} p_j \widetilde{\boldsymbol{d}}_j^H \widetilde{\boldsymbol{d}}_j \tag{6.23}$$

is the interference plus the noise covariance matrix at the ST k.

The dual reverse link precoding problem can be formulated as

$$\begin{aligned} &\min_{\boldsymbol{F},\boldsymbol{q}} \sum_k q_k \\ &\text{subject to } \mathrm{SINR}_k \geq \chi_k, \quad k = 1, ..., 2K \end{aligned} \tag{6.24}$$

The above problem can be rewritten as

$$\begin{aligned} &\min_{\boldsymbol{F},\boldsymbol{p}} \sum_k p_k \\ &\text{subject to } \quad p_k \widetilde{\boldsymbol{d}}_k \boldsymbol{\Sigma}_k^{-1} \widetilde{\boldsymbol{d}}_k^H \geq \chi_k \end{aligned} \tag{6.25}$$

This problem is a *standard power control* problem studied already in [35]. Therefore, if the problem is feasible, its solution is provided by the following iterative power control algorithm.

Standard form of power control algorithm is available in Algorithm 1 :

1 Determine the vector $\boldsymbol{p}^*$ by the fixed point equation

$$p_k^{(l)} = \frac{\chi_k}{\widetilde{\boldsymbol{d}}_k [\boldsymbol{I} + \sum_{j \neq k} p_j^{(l-1)} \widetilde{\boldsymbol{d}}_k^H \widetilde{\boldsymbol{d}}_k]^{-1} \widetilde{\boldsymbol{d}}_k^H} \tag{6.26}$$

for $l = 1, 2, ...,$ with initial condition $\boldsymbol{p}^{(0)} = \boldsymbol{0}$, and $\lim_{l \to \infty} \boldsymbol{p}^{(l)} = \boldsymbol{p}^*$.

2 Determine the beamforming matrix

$$\boldsymbol{F}^* = \left[\boldsymbol{I} + \widetilde{\boldsymbol{D}}^H \mathrm{diag}(\boldsymbol{p}^*) \widetilde{\boldsymbol{D}} \right]^{-1} \widetilde{\boldsymbol{D}}^H \mathrm{diag}(\boldsymbol{X}'). \tag{6.27}$$

3 Determine the vector $\boldsymbol{q}^*$ by applying (6.13).

Algorithm 1: Standard form of Power Control Algorithm for Adaptive Beamforming design

Remarks on the beamforming design :

- In [26], a theory has been developed to check the feasibility of this problem.
  1. When the sequence $\sum_{k=1}^{2K} p_k^{(l)}$ diverges, the problem is not feasible.
  2. If $\mathrm{rank}(\widetilde{\boldsymbol{D}}) = 2K$, the problem is always feasible.
  3. In all the other cases, the feasibility must be always tested. It can be tested by iterating and checking if the sum power is above a maximum threshold.
- In the context of a satellite system the previous algorithm need be iterated several times because the noise variance depends on the power allocated by the beamforming. Before the beamformer design, no

knowledge of the total power assigned to all STs is available at the satellite gateway. Then, the covariance of the intermodulation noise σ_e^2 is also unavailable. To circumvent this problem, the beamformer is designed by assuming that there is no intermodulation noise in the system. Once this beamformer is designed based on this assumption, the total power assigned for such beamformer can be used as initial estimation of the intermodulation covariance matrix. By iterating the proposed algorithm adopting the previous estimation of the intermodulation noise covariance matrix we converge to the desired linear beamformer.

Remarks on Approach A

- The equivalent system is determined in a heuristic way.
- The beamforming network is designed in such a way that the presence of multiple antennas at the receiver is ignored. More specifically, there exists a "virtual destination" associated to the left polarization and a "virtual destination" associated to the right polarization for each ST. These virtual destinations are considered as independent and the beamformer is designed to concentrate one information flow on the left polarization and the other information flow on the left polarization. The exploitation of the possibilities offered by multiple antennas is performed by a subsequent multiuser detector which knows the exact channel realization and it is not limited by a statistical knowledge of the channel.

6.2.2 Approach B

Approach B relies on similar assumptions as Approach A :

- The channel between the satellite and the receiver of an information stream is approximated by a deterministic channel between the satellite and a single receive antenna, ignoring the presence of eventual multiple antennas and other information flows intended for the same receiver.
- The beamforming approach is the same as in Approach A assuming a single antenna at the intended receiver.

Approximation via a Deterministic Channel

Let $\boldsymbol{R}_k = \boldsymbol{C}_{\alpha,kk}\boldsymbol{P}_k$ be the fading part of the channel for the k-th ST and $\boldsymbol{D}_k$ the block row of the directivity matrix $\boldsymbol{D}$ corresponding to the k-th ST and consisting of rows $2k-1$ and $2k$. The cascade of the channel for the k-th ST can be equivalently described by the cascade of the directivity matrix $\boldsymbol{D}_k$, a bank of multipliers with a multiplier for each information flow, a bank of adders of Gaussian noises, in general, a matrix $\widetilde{\boldsymbol{R}}_k$, whose columns have unit Froboenius norms and accounts for the randomness of the matrix $\boldsymbol{R}_k$.

We denote by $\boldsymbol{g}_k = (g_{k,1}, g_{k,2})$ the square of the multiplier vector for the two information flows of the k-th ST. Figure 6.2 shows the proposed cascade.

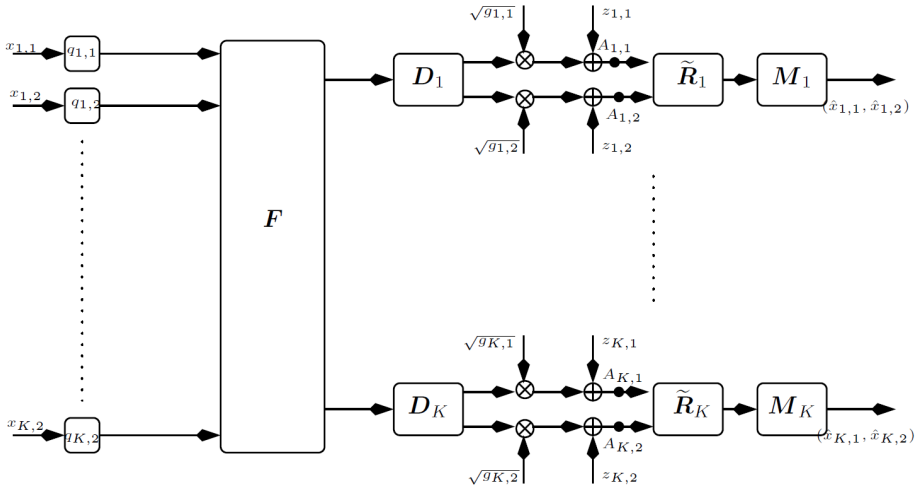

FIGURE 6.2 – System model adopted for Approach B

In the following we detail the characteristics of the different components.

Let $\boldsymbol{r}_{k,1}$ and $\boldsymbol{r}_{k,2}$ be the columns of the the matrix $\boldsymbol{R}_k$ and let $g_{k,1} = \frac{\boldsymbol{r}_{k,1}^H \boldsymbol{r}_{k,1}}{2}$ and $g_{k,2} = \frac{\boldsymbol{r}_{k,2}^H \boldsymbol{r}_{k,2}}{2}$. Then, it is possible to express $\boldsymbol{R}_k$ as the product

$$\boldsymbol{R}_k = \widetilde{\boldsymbol{R}}_k \sqrt{\boldsymbol{G}_k}$$

with $\boldsymbol{G}_k = \begin{pmatrix} g_{k,1} & 0 \\ 0 & g_{k,1} \end{pmatrix}$. Note that on the average the columns of the matrix $\widetilde{\boldsymbol{R}}_k$ have Froboenius norm equal to 2 and trace $\left(\widetilde{\boldsymbol{R}}_k^H \widetilde{\boldsymbol{R}}_k\right) = 2R$. The noise $\boldsymbol{z}_k = (z_{k,1}, z_{k,2})^T$ is obtained as the sum of the equivalent intermodulation noise and the equivalent thermal noise both at the output of the multipliers $\sqrt{\boldsymbol{g}_k} = (\sqrt{g_{k,1}}, \sqrt{g_{k,2}})^T$. The equivalent intermodulation noise $\widetilde{\boldsymbol{e}}_k$ at the output of the multipliers is zero mean Gaussian with covariance matrix $\boldsymbol{C}_{\widetilde{\boldsymbol{e}}_k} = \sigma_e^2 \sqrt{\boldsymbol{G}_k} \boldsymbol{D}_k \boldsymbol{D}_k^H \sqrt{\boldsymbol{G}_k}$. The thermal noise at the output of the multipliers is approximated by Gaussian additive noise with covariance matrix

$$\begin{aligned} \boldsymbol{C}_{\widetilde{n}_k} &= \sigma_n^2 \mathbb{E}\{(\widetilde{\boldsymbol{R}}_k^H \widetilde{\boldsymbol{R}}_k)^{-1}\} \\ &= \sigma_n^2 \sqrt{\boldsymbol{G}_k} \mathbb{E}\{(\boldsymbol{R}_k^H \boldsymbol{R}_k)^{-1}\} \sqrt{\boldsymbol{G}_k}. \end{aligned}$$

Then, the equivalent noise $\boldsymbol{z}_k$ has covariance matrix

$$\begin{aligned}\boldsymbol{C}_{\boldsymbol{z}_k} &= \boldsymbol{C}_{\widetilde{e}_k} + \boldsymbol{C}_{\widetilde{n}_k} \\ &= \sigma_e^2 \sqrt{\boldsymbol{G}_k} \boldsymbol{D}_k \boldsymbol{D}_k^H \sqrt{\boldsymbol{G}_k} + \sigma_n^2 \sqrt{\boldsymbol{G}_k} \mathbb{E}\{(\boldsymbol{R}_k^H \boldsymbol{R}_k)^{-1}\} \sqrt{\boldsymbol{G}_k}. \end{aligned} \tag{6.28}$$

Beamforming Matrix

The beamformer is designed considering the system from the gateway to the points $A_{k,1}$ and $A_{k,2}$, in Figure 6.2. The points $A_{k,1}$ and $A_{k,2}$ can be regarded as the virtual destinations for x_{2k-1} and x_{2k}, the information streams intended for the k-th ST, respectively. The same algorithm adopted for Approach A is adopted here. In this case the matrix $\widetilde{\boldsymbol{D}}$ is defined in a way that the block row $\widetilde{\boldsymbol{D}}_k$, consisting of the rows $2k-1$ and $2k$, satisfies the relation

$$\widetilde{\boldsymbol{D}}_k = \boldsymbol{\Lambda}_k^{-1/2} \boldsymbol{U}_k^H \sqrt{\boldsymbol{G}_k} \boldsymbol{D}_k \tag{6.29}$$

where $\boldsymbol{D}_k$ is the block row of matrix $\boldsymbol{D}$ consisting of the rows $2k-1$ and $2k$ and $\boldsymbol{U}_k$ and $\boldsymbol{\Lambda}_k$ are obtained from the eigenvalue decomposition of the noise covariance matrix

$$\boldsymbol{C}_{\boldsymbol{z}_k} = \boldsymbol{U}_k \boldsymbol{\Lambda}_k \boldsymbol{U}_k^H.$$

Thanks to definition (6.29), the matrix $\widetilde{\boldsymbol{D}}_k$ accounts also for the colored noise, since the algorithm described in Section 6.2.1 is formulated for systems with additive white Gaussian noise and unit variance.

Note that this kind of approach suffers from the same limitations as Approach A (see "Remarks on Approach A" in Section 6.2.1).

6.3 A Benchmark for Adaptive Beamforming : Conventional Beamforming

In order to assess the performance improvements of the proposed adaptive beamforming, we use the *conventional beamformer* as a benchmark. In the conventional fixed beamformer, the weights of a BFN at the satellite antennas are kept constant and the BFN is designed to serve the coverage area of the satellite. In order to keep limited interference from adjacent beams, frequently reuse is adopted. For implementation issue in our simulations, a coloring map 4 is assumed, i.e. 4 different frequency bands are used for 4 adjacent beams. For numerical simulations, we adopt a beamformer covering the region, $([-10, 40], [-10, 60], [20, 40], [20, 60])$ denoted in longitude and latitude in Figure 6.3 and 100 "almost non-overlapping" beams are supported by the same carrier. The BFN is designed applying the same approach we adopted to design adaptive beamformers but the centers of beams are assigned in given fixed positions independent of the positions of the STs. For example, the 100 points denoted by ■ in Figure 6.3 are selected for designing

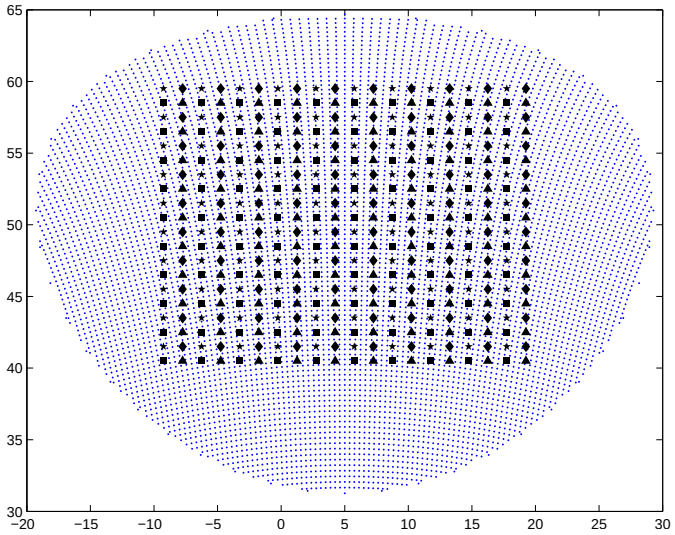

FIGURE 6.3 – Points selected for designing beamformers in different carrier

the beamforming matrix of carrier 1. As for the adaptive beamforming, we determine the beamforming matrix for such directivity matrix in order to achieve a target SINR. Each of the obtained beams points at the positions in the set of Figure 6.3. Similarly, ▲, ★, ♦ denote the points selected for the designing of the beamformer to transmit on carrier 2, 3 and 4 respectively. All these points are uniformly distributed on the map. The distance between adjacent points are equal in latitude and longitude.

Since the generated beams remain constant regardless of the positions of the STs in the system, the weakest SINR achieved in the coverage area of a specific beam should satisfy a certain actual target SINR. We iterate between an adjusted target SINR for the beamforming design and the compensation of the minimal SINR in the area of coverage of each beam to determine the beamforming matrix satisfying the requirements of a guaranteed SINR in all the locations covered by the beams.

Each ST receives information from the stronger beam that points to it. One beam can serve a single ST at one time. Additionally, each ST designs its own multi-stream detector according to the acquired knowledge about the communication channel.

In the following, we summarize the algorithm to allocate STs to beams. We assume that the STs are sequentially inserted in the system in Algorithm 2.

```
for k = 1, ..., K do
    Find the strongest beam n serving ST k by detecting the nearest
    point on the grid adopted to design the beamformer
    if this beam is already utilized by another ST
    then
        ST k is excluded from the system.
        else
            Beam n is allocated to ST k, and the corresponding carrier
            assigned to ST k.
        end
    end
end
```

Algorithm 2: Algorithm to allocate STs to beams in a Conventional Beamforming System

6.4 Numerical Simulations

In this section, we analyze the performance of the proposed algorithms by numerical simulations. We analyze the system performance for both cases where the satellite STs are in fix positions (static ST) and move within the coverage area.

In this chapter, we do not perform carrier allocation. We focus on a system with a single frequency band. Furthermore, we assume in this section that the satellite has the perfect knowledge of the actual directivity matrix, and the beamforming matrix is designed on this actual directivity matrix. Therefore, the impact of the estimation error of directivity vectors is not taken into account in this section. We also compare the performance of a system based on a fixed beamforming with frequency reuse 4.

If it is not differently stated, throughout this section we make the following assumptions : 1) all the simulations are performed for satellite STs equipped with two antennas and receiving two independent information streams ; 2) the correlation coefficients are set to be $a = -15\text{dB}$ and $b = -22\text{dB}$; 3) the positions of the STs are generated randomly and uniformly in the region $([-10, 40], [-10, 60], [20, 40], [20, 60])$ in Figure 5.2 ; 4) the results shown in this section are obtained by averaging over 100 independent random generations of the STs over the satellite coverage area.

6.4.1 Simulation Results for Static Satellite Terminals

First, we illustrate the performance of a satellite system with static STs. We assume that a single carrier is available. These assumptions imply that this system cannot exploit opportunistically ST diversity by proper frequency allocation. The performance of this system is susceptible of significant im-

provements.

We compare the performance of the two proposed different approaches, namely approach A and approach B. In our simulations, the thermal noise at the receiver is Gaussian distributed with covariance $\sigma_n^2 = -20$dBW. The number of STs K is either 50 or 100.

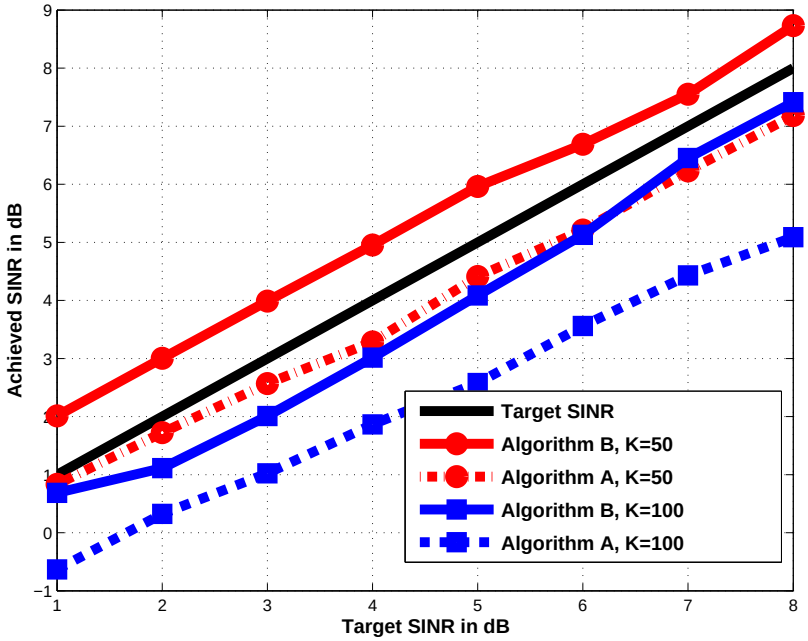

FIGURE 6.4 – The achieved SINR versus target SINR when STs have perfect CSI for Algorithm A and B. System setting : $K = 50$ or 100, $\sigma_n^2 = -20$dBW, CIM$= -15$dB

Figure 6.4 compares the achieved SINR by implementing algorithm A and B under the assumption that the receivers have perfect knowledge of the channel. As the number of STs increases, the achieved SINR decreases. This is due to the additional interference in the system. Let us first observe that for both algorithms, there exists a gap between the target SINR and the achieved SINR. This is due to the heuristic approach employed to adapt an algorithm for beamforming design in a system with complete channel state information at a transmitter to a system with only statistical knowledge of the channel at the transmitter. Note that exist no algorithm available in literature for the design of a beamformer in a system with statistical knowledge of the channel at the transmitter and complete knowledge of the channel at the receiver. There is a long lasting open problem in communication theory of relevant practical interest. For the application of these heuristic algorithms in practical systems, it is relevant to note that this gap remains constant to over the full range of SINR and depends only on the number of STs in

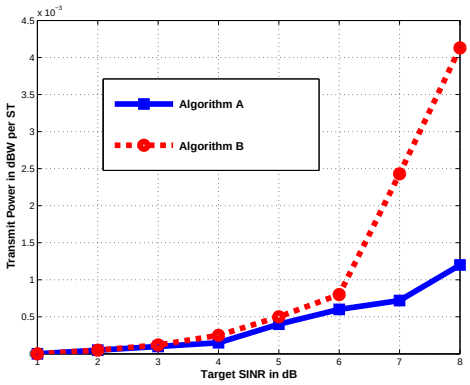

FIGURE 6.5 – The transmit power versus target SINR for Algorithm A and B. System settings : $K = 50$, $\sigma_n^2 = -20$dBW, CIM= -15dB

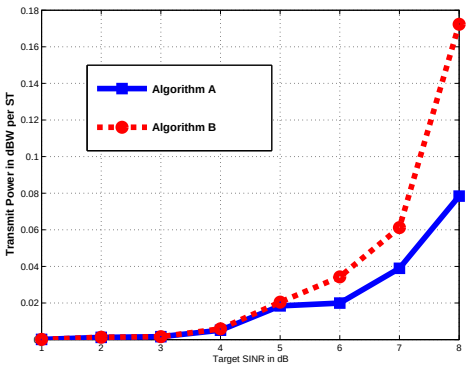

FIGURE 6.6 – The transmit power versus target SINR for Algorithm A and B. System settings : $K = 100$, $\sigma_n^2 = -20$dBW, CIM= -15dB

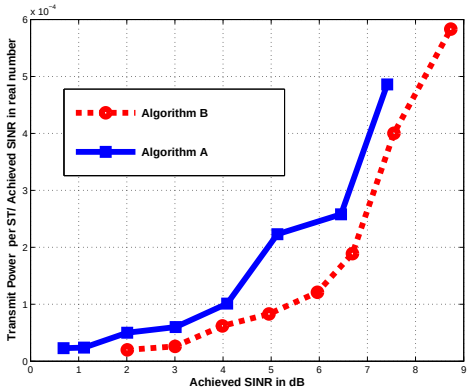

FIGURE 6.7 – Power/achieved SINR versus achieved SINR for Algorithm A and B. System settings : $K = 50$, $\sigma_n^2 = -20$dBW, CIM= -15dB

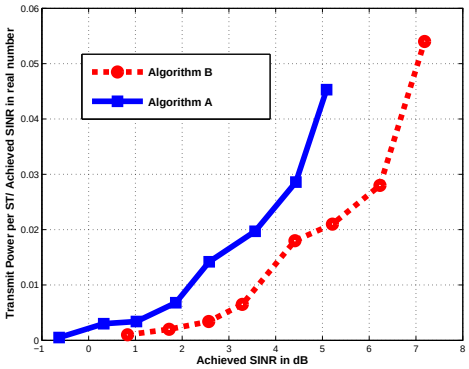

FIGURE 6.8 – Power/achieved SINR versus achieved SINR for Algorithm A and B. System settings : $K = 100$, $\sigma_n^2 = -20$dBW, CIM= -15dB

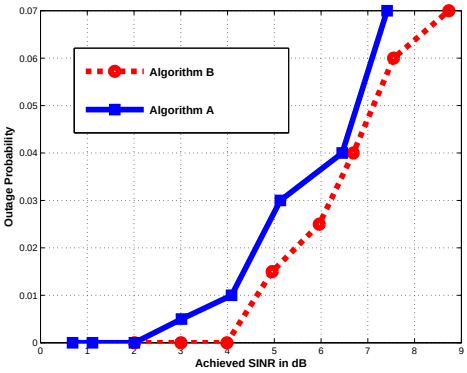

FIGURE 6.9 – The outage probability versus achieved SINR for Algorithm A and B. System settings : $K = 50$, $\sigma_n^2 = -20$dBW, CIM= -15dB

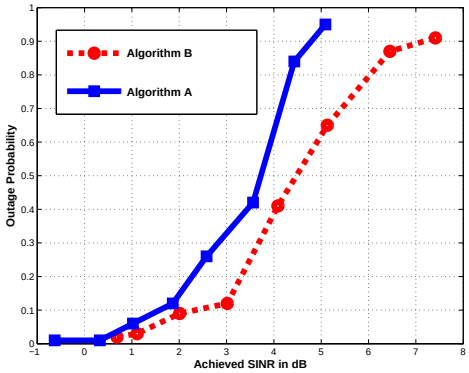

FIGURE 6.10 – The outage probability versus achieved SINR for Algorithm A and B. System settings : $K = 100$, $\sigma_n^2 = -20$dBW, CIM= -15dB

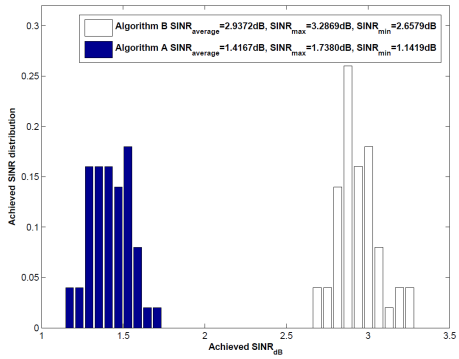

FIGURE 6.11 – The achieved SINR distribution for Algorithm A and B. System settings : $K = 50$, and SINR target is 2dB, $\sigma_n^2 = -20$dBW, CIM= -15dB

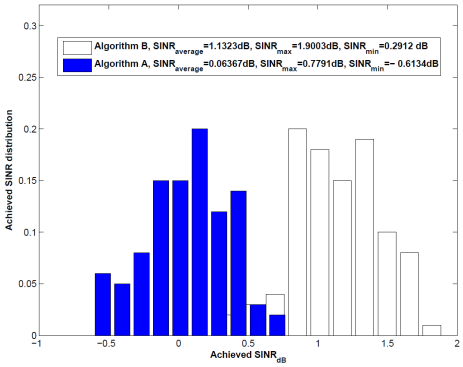

FIGURE 6.12 – The achieved SINR distribution for Algorithm A and B. System settings : $K = 100$, and SINR target is 2dB, $\sigma_n^2 = -20$dBW, CIM= -15dB

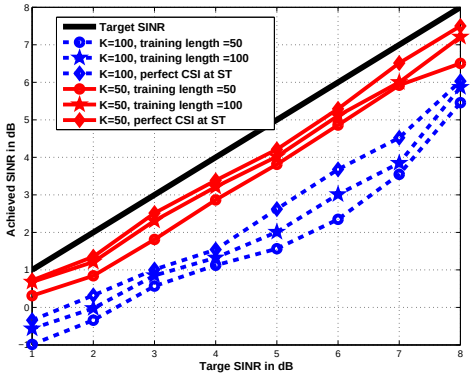

FIGURE 6.13 – The achieved SINR versus target SINR for Algorithm A by different training length. System settings : $\sigma_n^2 = -20$dBW, CIM= -15dB

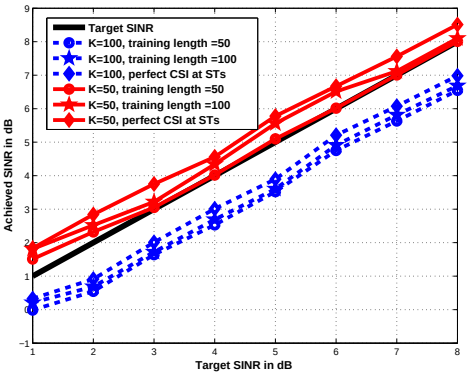

FIGURE 6.14 – The achieved SINR versus target SINR for Algorithm B by different training length. System settings : $\sigma_n^2 = -20$dBW, CIM= -15dB

the system. Thus, in practice, we may simply adjust the target SINR for the beamforming designing.

A comparison of the performance provided by algorithm A and algorithm B shows that algorithm B gains approximately 1dB compared to algorithm A. Thus, it becomes interesting to compare the two algorithms in term of total transmit power. Figure 6.5 and 6.6 show the total transmit power when $K = 50$ and $K = 100$, respectively. Algorithm A always requires less power than Algorithm B as justified by the lower achieved SINR. When the target SINR increases, the required transmit power also increases. Moreover when the SINR target is larger than 5dB, the transmit power increases dramatically.

In order to make a fair comparison between the two algorithms, we adopt as efficiency metric the ratio between the total transmit power and the achieved SINR. Figure 6.7 and 6.8 show the efficiency of the two algorithms as a function of the achieved SINR. In the achievable SINR range, algorithm B is more efficient since it requires less power than Algorithm B to achieve the same SINR.

An additional performance metric of interest is the outage probability. We say that an event of outage occurs in the system if the total transmit power necessary to achieve a certain average SINR for a given spatial allocation of the STs exceed the total available transmit power. Figure 6.9 and 6.10 show the outage probability when there are 50 and 100 active STs in the system, respectively. As expected, when the target SINR increases, more outage events occur.

For $K = 50$, even when the achieved SINR is as high as 7dB, the outage probability is still relatively low for both algorithms. On the contrary, for $K = 100$, when the achieved SINR is around 6dB, the outage probability

for both algorithms is almost as big as 1, i.e., the system cannot serve 100 STs having such QoS requirements without carrier allocation. Figure 6.9 and 6.10 show that both algorithms have similar performance in terms of outage probability. However, when for high number of STs and high QoS requirements, Algorithm B outperforms Algorithm A.

As already observed, the heuristic characteristic of the proposed algorithms do not enable to obtain an average SINR at the output of the receiver exactly equal to the target SINR. Figure 6.4 plots the achieved SINR average over all receive STs. Then, it is interesting to get insights about the distribution of the achieved SINR around an average value. Figure 6.11 and 6.12 show the histogram of the achieved SINR when SINR target is 2dB for $K = 50$ and $K = 100$. Figure 6.11 shows that when $K = 50$, the achieved SINR for all the STs falls in the range of ± 0.5dB from the average achieved SINR for both algorithms. Moreover, the achieved SINR of more than 75% STs is in the range of ± 0.2dB from the average for both algorithms. Figure 6.12 shows that when $K = 100$, Algorithm B ensures the achieved SINR of approximately 90% STs falls in the range of ± 0.5dB from the average, while Algorithm A ensures the achieved SINR of approximately 85% STs falls in the range of ± 0.5dB from the average.

All the previous presented simulation results are obtained under the assumption of perfect channel state information at the STs (receiver side). In a real system, the channel state information is imperfect at the receiver due to the intrinsic error affecting the channel estimation. In a satellite system, channel estimation is based on training sequences (pilot-aided channel estimation) and the estimation error decreases by increasing the channel training length. In order to evaluate the impact of the channel estimation errors on system performance and determine a training sequence length with acceptable performance degradation for transmission in the forward link, we investigate the system performance as a function of the training length of the receiver.

Improvements on channel estimation are possible by removing the constraint of linear channel estimation and multiuser detection and adopting a turbo decoder which iteratively performs channel estimation, multiuser detection and single user soft decoding. This technique improves the performance at each step by exploiting the extrinsic information on the transmit date acquired at the previous iteration. However, this nonlinear approach leads to a considerable increase of the complexity at the STs.

Figure 6.13 and 6.14 illustrate the achieved SINR of algorithms A and B with different training lengths. Figure 6.13 shows that for both $K = 50$ and $K = 100$, when the training sequence has length 100, the system achieves almost the same performance as that receivers with perfect channel information. For a system adopting algorithm B, a similar behavior occurs. In Algorithm A, if the training sequence has training length equals to 50, the achieved SINR is approximately 0.5dB inferior compared to perfect CSI

at the receivers.

6.4.2 Simulation Results for Static Satellite Terminals with Different Levels of Noise

In the previous subsection, we showed some simulation results refering to a scenario in which the thermal noise at the receiver is Gaussian distributed with covariance $\sigma_n^2 = -20$dBW and the ratio between the transmit power and the intermodulation noise induced on board is CIM= -15dB. We are also interested in system performance for other values of σ_n^2 and CIM. In this section, we show some simulation results for different level of thermal noise and intermodulation noise. Namely, we consider the case when $\sigma_n^2 = -10$dBW and CIM= -18dB and the case when $\sigma_n^2 = -10$dBW and CIM= -15dB.

Figure 6.15 compares the achieved SINR of different levels of intermodulation noise and thermal noise. It shows that, for the same target SINR with same level of intermodulation noise, the achieved SINR decreases as the thermal noise increases. Figure 6.16 compares the transmit power for different levels of thermal noise and intermodulation noise. It shows that the transmit power increases when thermal noise or intermodulation noise increases. Figure 6.17 compares the efficiency defined as the ratio between the transmit power per ST and achieved SINR for different levels of thermal noise and intermodulation noise. The efficiency of the system increases as the intermodulation noise and thermal noise decreases. It is also interesting to investigate the impact of the noises on the outage probability. Figure 6.18 shows the outage probability of the system with different levels of thermal noise and intermodulation noise. The outage probability is much more sensitive to the intermodulation noise level. It can be seen from the plot that, when CIM= -15dB, with different levels of thermal noise, the outage probability of the system is almost the same. However, for lower level of intermodulation noise, namely, CIM= -18dB, the system presents significantly less outage events than the other two cases.

6.4.3 Simulation Results for Mobile Satellite Terminals

In this subsection, we illustrate some performance results assuming that the terminals are moving in the coverage area of the satellite. We focus only on Approach B.

We assume that each terminal is moving inside the map at a random generated speed and in a random generated direction. We also assume that a single carrier is available and the locations of the terminals are randomly generated. As already mentioned, this assumption implies that this system cannot allocate opportunistically the terminals on different carriers and exploits user diversity.

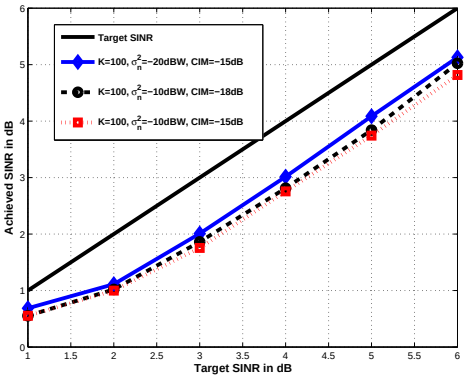

FIGURE 6.15 – The achieved SINR versus target SINR for Algorithm B for different levels of noise and intermodulation noise. System settings : $K = 100$

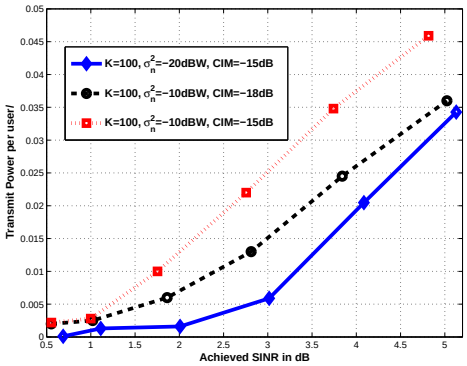

FIGURE 6.16 – The transmit power versus achieved SINR for Algorithm B for different levels of noise and intermodulation noise. System settings : $K = 100$

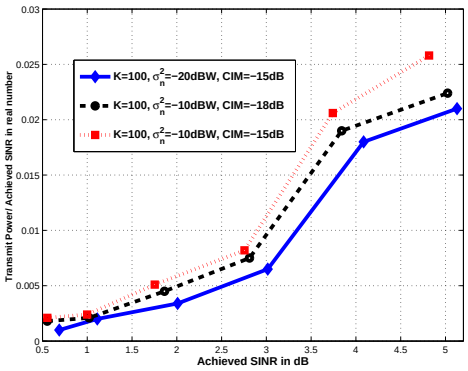

FIGURE 6.17 – The transmit power per achieved SINR versus achieved SINR for Algorithm B for different levels of noise and intermodulation noise. System settings : $K = 100$

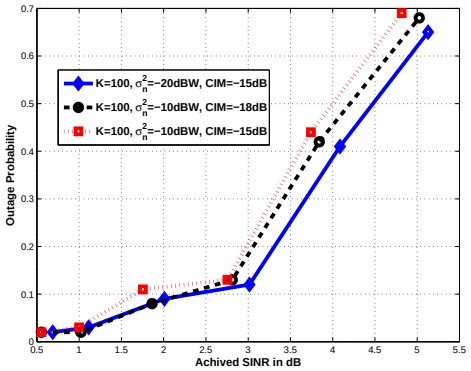

FIGURE 6.18 – The outage probability versus achieved SINR for Algorithm B for different levels of noise and intermodulation noise. System settings : $K = 100$

STs are constantly moving. Thus, the directivity matrix of the STs varies because of the movement of the mobile terminals. However, the system updates the positions of the satellite terminals and compute again the beamforming matrix with a period equal to one minute. Thus, the beamforming matrix remains constant for one minute. Moreover, we assume that the mobile terminals are capable of designing their own multiuser detectors instantaneously. In this subsection, we analyze the robustness of the beamformer to mobility and the system performance degradation due to the delay in updating the beamformer.

In our simulation, the thermal noise at the receiver is Gaussian distributed with covariance $\sigma_n^2 = -20$dBW. We assume that the ratio between the total transmit power and the intermodulation noise induced on board is CIM$= -15$dB. The number of STs K is 100. The terminals are generated randomly in the whole area on the map in Figure 5.2. The speed of each terminal is uniformly distributed in the range from 80km/h and 140km/h. The moving direction of each terminal is uniformly distributed between 0 and 2π. However, if a terminal goes out of the map, we generate another direction to ensure it remains in the map during the simulation time.

Figure 6.19 compares the SINR in different time slots achieved by implementing algorithm B under the assumption that the receivers have perfect knowledge of the channel. From Figure 6.19, it can be interpreted that the degradation of the achieved SINR is less than 0.1dB when the beamformer remains constant for one minute. This degradation is still acceptable.

Figure 6.20 compares the achieved SINR with different training lengths keeping the beamforming matrix constant for 60 seconds. When $K = 100$, the achieved SINR with training sequences of length 100 and moving terminals is approximately 0.4dB lower than the achieved SINR with perfect CSI. Figure 6.21 shows the efficiency metric as already defined in the previous subsection when $K = 100$, the beamformer is updated every 60 seconds, and the STs have perfect knowledge of the CSI.

6.4.4 Simulation Results for Adaptive Beamforming versus Conventional Beamforming

In this subsection, we compare the performance offered by adaptive beamforming and conventional beamforming. We assume that 4 orthogonal carriers are available in the system. In the adaptive beamformer, the STs are assigned to the carriers by random allocation. For the conventional beamformer strategy, the beams are fixed and cover constantly the same area and adjacent beams use different carriers for interference mitigation purposes. Each terminal receives information from the stronger beam that points to it. One beam can serve only a single terminal at a time. Both schemes aim to ensure that the lowest achieved SINR satisfies a certain given target. Additionally, each terminal design its own multi-stream detector on the basis of to

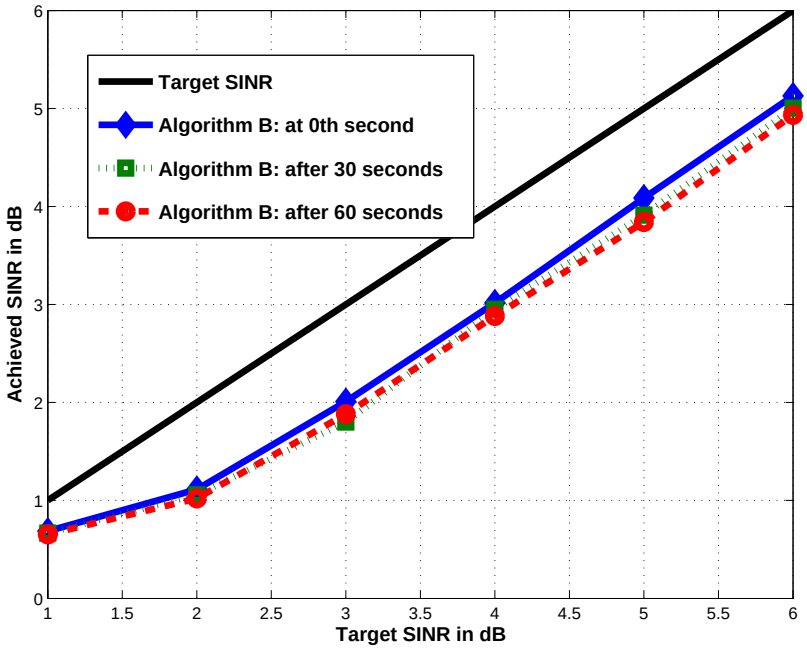

FIGURE 6.19 – The SINR achieved by algorithm B versus target SINR with mobile STs and perfect CSI at receiver. System settings : $K = 100$,$\sigma_n^2 = -20$dBW, CIM=-15dB

the acquired knowledge of the channel. In our simulations, the thermal noise at the receiver is Gaussian distributed with covariance $\sigma_n^2 = -10$dBW. We assume that the ratio between the total transmit power and intermodulation noise induced on bard is CIM= -15dB.

The simulation in this subsection are performed for varies number of STs K, namely, $K = 80, 180, 280$ and 380. We assume that the maximal available power for the conventional beam is 15dBW, while the maximal power for the adaptive beamformer is the actual power required by the conventional beamformer. Both schemes ensure that the lowest achieved SINR among all the STs attains a given target. The simulation result is achieved by averaging over 25 independent random allocations of the STs in the given region.

Figure 6.22 shows the outage probability for the two different schemes. For the conventional beamforming, the outage probability is not correlated to the target SINR. Once the constant beamformer for a given target SINR is obtained, the outage probability is determined by the geographic distribution of the STs since one beam can only serve one ST at a time. For the conventional beamformer, when $K = 80$, the outage probability is approximately 10% while when $K = 280$ and $K = 380$, the outage probability increases to nearly 28% and 35%. For the adaptive beamforming strategy, the outage probability depends on the target SINR. When $K = 280$ and

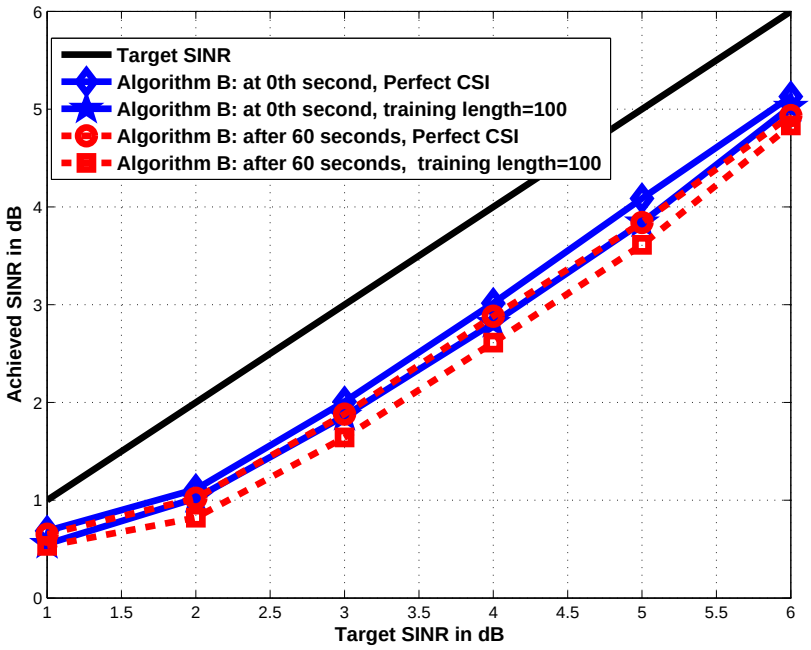

FIGURE 6.20 – The SINR achieved by algorithm B versus target SINR with mobile STs and varying levels of accuracy on the knowledge of the CSI at the STs and the gateway. System setting : $K = 100$, $\sigma_n^2 = -20$dBW, CIM$=-15$dB

the target SINRs are 1dB and 2dB, the outage probability is about 3%, much lower than the outage probability for the conventional beamforming. However, when the number of STs increases to 380, the outage probability increase dramatically. When the target SINR is 2dB, the outage probability of the system is 50%. This dramatic increase is due to the fact that, if there are many users in the system, the level of interference between the users is high. More power would be required compared to the conventional beamformer to mitigate the interference and to ensure that the lowest SINR attains the target SINR. Therefore, outage events occur. It is also worth noticing that, when the target SINR is 3dB, the outage probability of the adaptive beamforming is lower than that for the case when the target SINR is 2dB. This is due to the fact that the required transmit power for the conventional beamforming is much higher when target SINR is 3dB compared to the case when target SINR is 2dB. Thus, much more power is available for the adaptive beamforming when the target is 3dB compared to 2dB, and the outage probability is lower.

Figure 6.23 shows the transmit power per user of the adaptive beamforming with different numbers of users. It shows that the power required for transmission increases as the number of users gets larger. Moreover, for

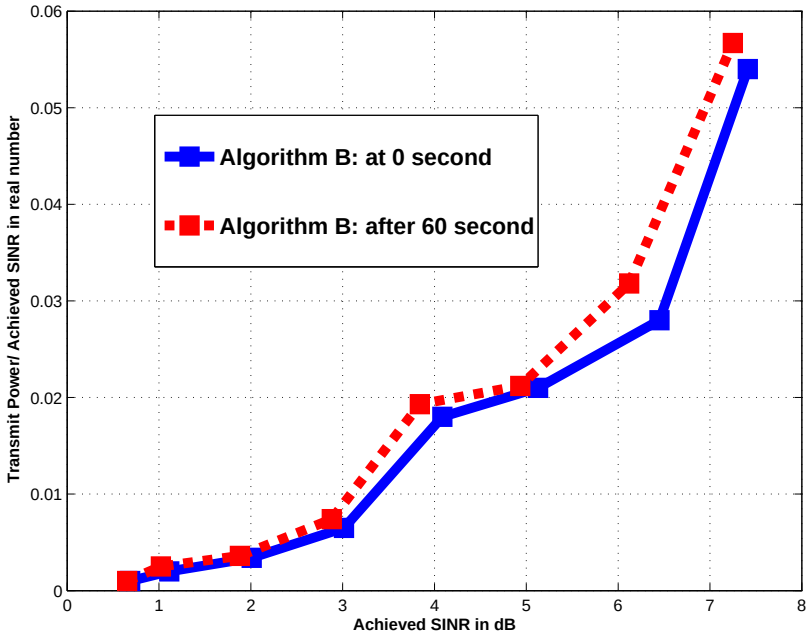

FIGURE 6.21 – Power/achieved SINR versus achieved SINR in one minute with perfect CSI at ST. System settings : $K = 100$, $\sigma_n^2 = -20$dBW, CIM=-15dB

the same level of achieved SINR, the transmit power required is significantly larger with $K = 380$ compared to $K = 280$. Figure 6.24 shows the efficiency metric, i.e, ratio between the power per user needed to achieve a certain average SINR and such average achieved SINR with different numbers of users. It shows that the above mentioned ratio increases as the number of users increases or the achieved SINR increases. Figure 6.25 shows the efficiency metric of adaptive beamforming and conventional beamforming when $K = 280$. Note that the average achieved SINR of conventional beamforming is much higher than the one for adaptive beamforming since a conventional beamformer is not optimized to minimize the transmit power.

Figures 6.26 and 6.27 show the histogram of the achieved SINR when the target SINR is 1dB for both adaptive beamforming and conventional beamforming with $K = 280$ and $K = 380$, respectively. Both figures show that conventional beamforming achieves higher SINR than adaptive beamforming strategy. When $K = 280$, the average achieved SINR of conventional beamformer is 4.2dB higher than the target SINR while the average achieved SINR of adaptive beamformer is only 0.86dB higher than the target. Thus, the adaptive beamforming strategy is more efficient as expected since the beam is tailored on the ST's positions. Moreover, the distribution of achieved SINR of the conventional beamformer is much sparser compared to the

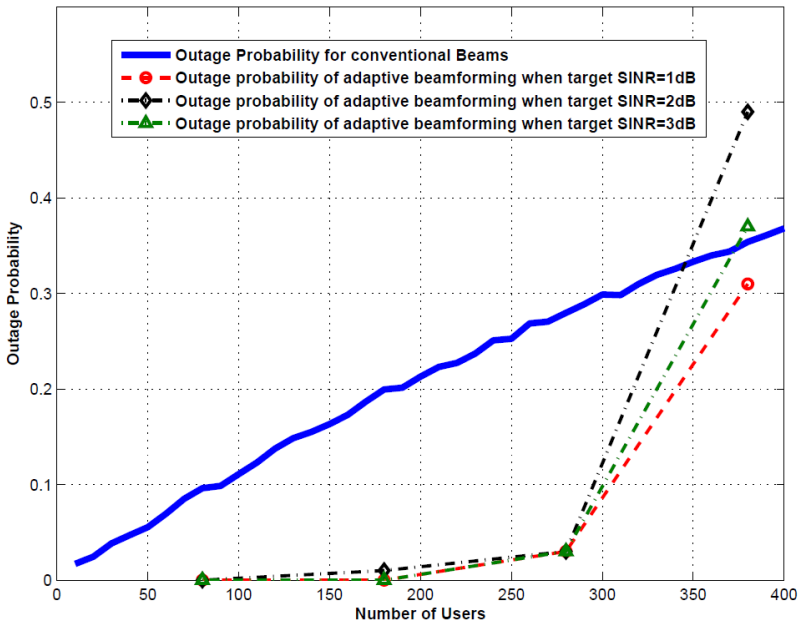

FIGURE 6.22 – Outage probability versus number of STs for adaptive and fixed beamforming design schemes. System settings : Maximal available power for conventional beamformer is 15dBW, $\sigma_n^2 = -10$dBW, CIM=-15dB

adaptive beamformer with adaptive beamformer. When $K = 380$, the support of the achieved SINR histogram is about 9dB, while, for the adaptive beamforming, the same support is about 2.7dB.

Figure 6.28 and Fig 6.29 show the histogram of the achieved SINR of both adaptive and conventional beamforming when the target SINR is 2dB and 3dB with $K = 280$, respectively. For all levels of target SINR, the adaptive beamforming is more efficient than the conventional beamforming. Moreover, the distribution of achieved SINR of the conventional beamformer is sparser compared to the adaptive beamformer with resource allocation for all different levels of target SINRs.

Figure 6.30 shows the histogram of the achieved SINR for both adaptive beamforming and conventional beamforming with $K = 380$ when the target SINR is 3dB. The range of the achieved SINR for the conventional beamforming is approximately 13dB large while for the corresponding range for the adaptive beamforming is only 3.5dB. Also, it is worthy noticing the lowest achieved SINR for the conventional beamforming is 0.8dB, which is 2.2dB lower than the target SINR. Since the number of STs in the system is large, the interference between users is high, thus some STs achieve much lower SINR compared to the target SINR. However, the difference between the target SINR and the lowest achieved SINR is not big for the adaptive beamforming.

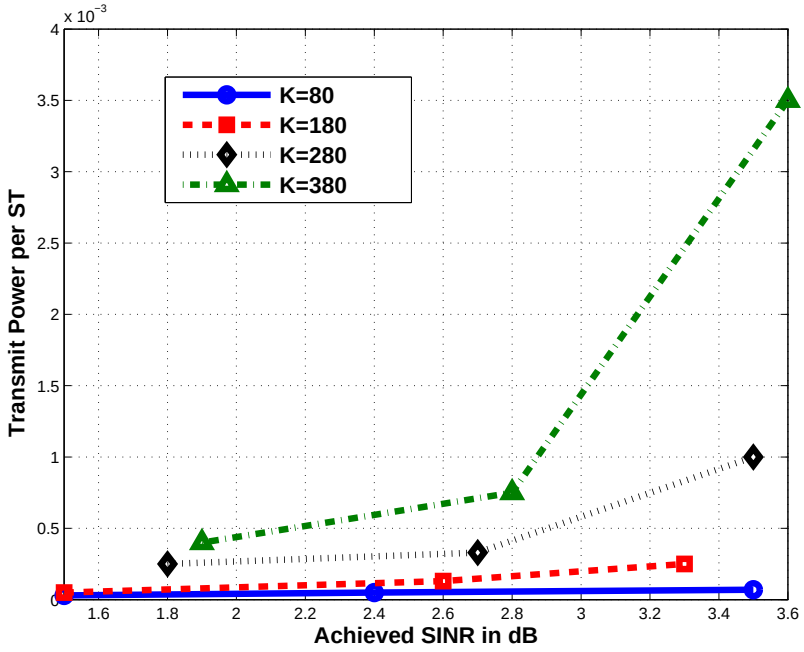

FIGURE 6.23 – Transmit power per user versus achieved SINR of adaptive beamforming. System settings : $\sigma_n^2 = -10$dBW, CIM=-15dB

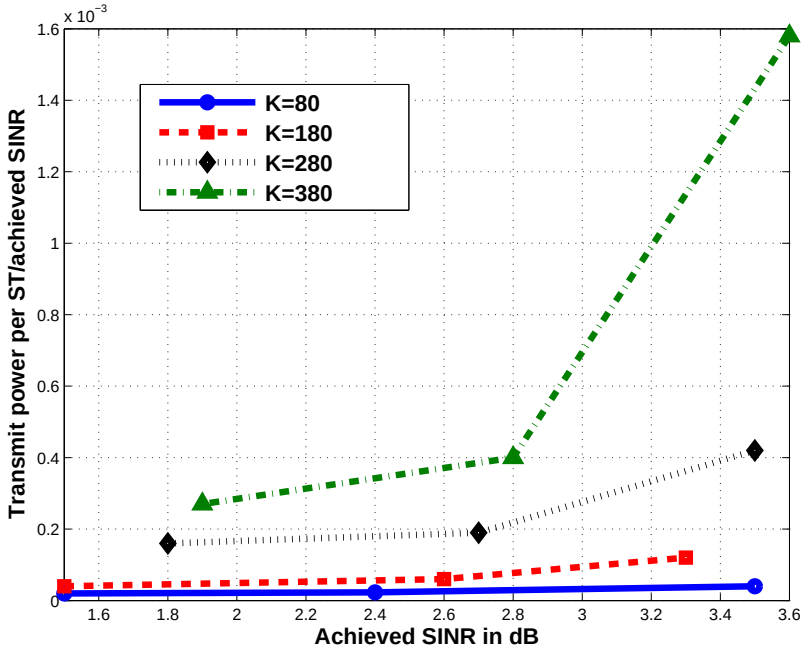

FIGURE 6.24 – Transmit power per user/ achieved SINR versus achieved SINR for an adaptive beamforming. System settings : $\sigma_n^2 = -10$dBW, CIM=-15dB

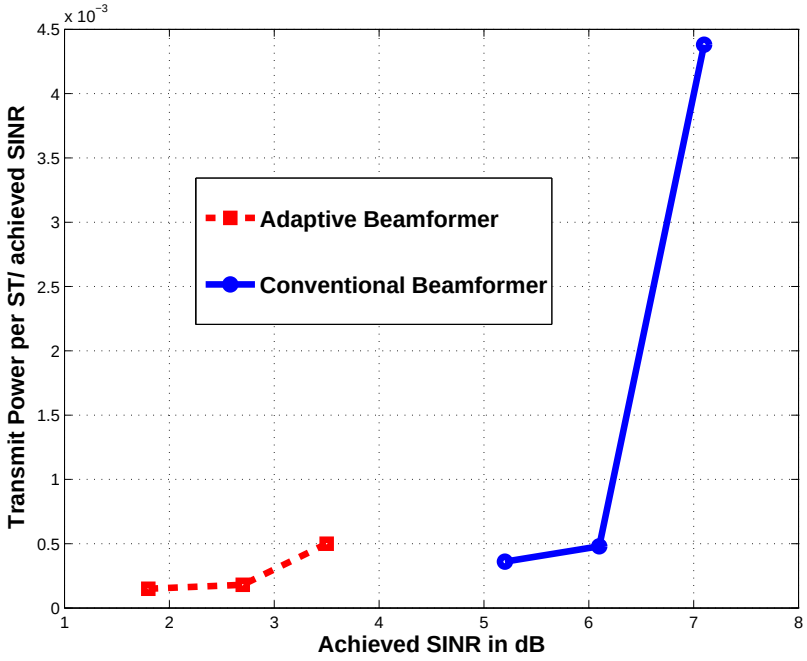

FIGURE 6.25 – Transmit power per user/ achieved SINR versus achieved SINR of adaptive and conventional beamforming, system settings : $K = 280$, $\sigma_n^2 = -10$dBW, CIM=-15dB

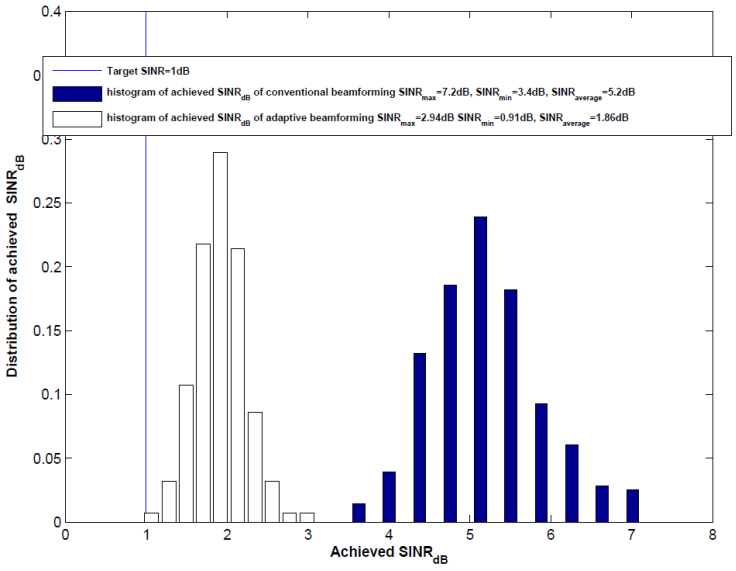

FIGURE 6.26 – Distribution of achieved SINR for adaptive beamforming and conventional beamforming. System settings : $K = 280$, target SINR=1dB, $\sigma_n^2 = -10$dBW, CIM=-15dB

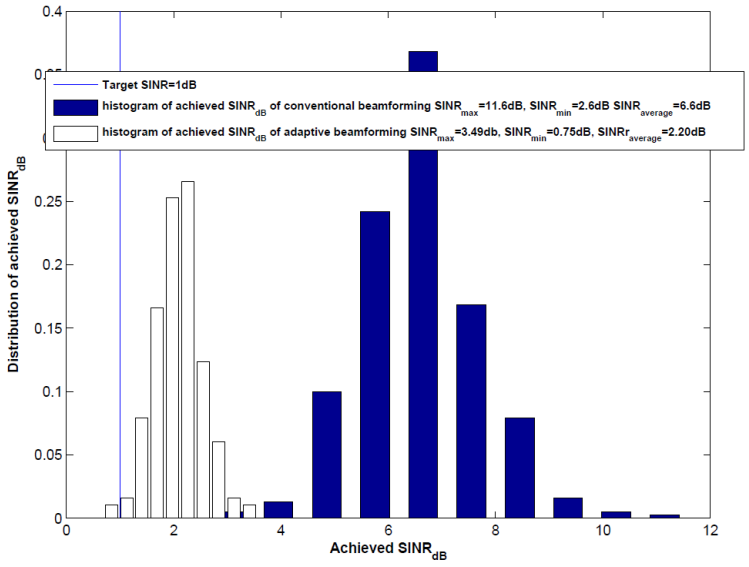

FIGURE 6.27 – Distribution of achieved SINR for adaptive beamforming and conventional beamforming. System settings : $K = 380$, target SINR=1dB, $\sigma_n^2 = -10$dBW, CIM=-15dB

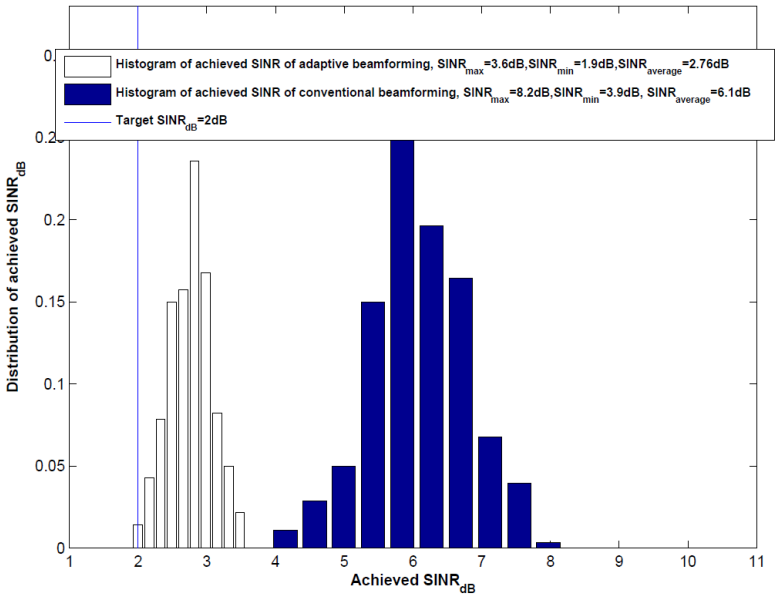

FIGURE 6.28 – Distribution of achieved SINR for adaptive beamforming and conventional beamforming. System settings : $K = 280$, target SINR=2dB, $\sigma_n^2 = -10$dBW, CIM=-15dB

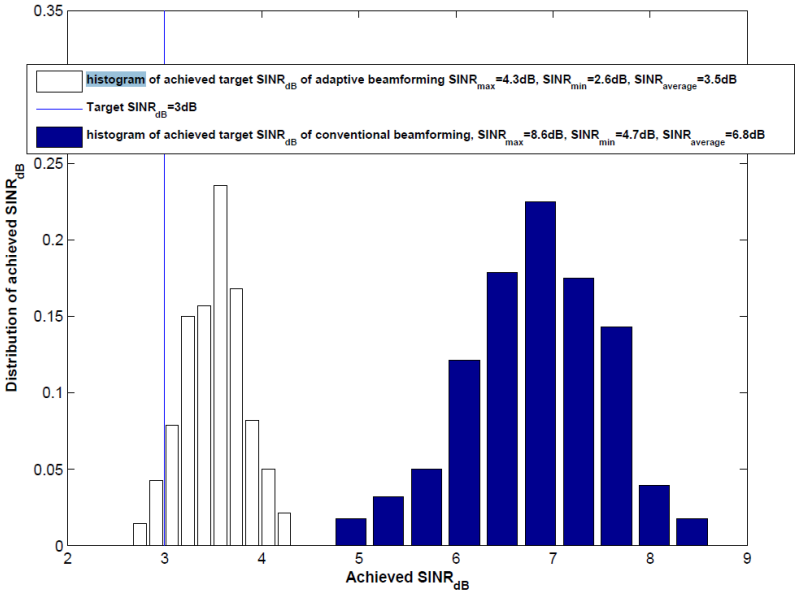

FIGURE 6.29 – Distribution of achieved SINR for adaptive beamforming and conventional beamforming. System settings : $K = 280$, target SINR=3dB, $\sigma_n^2 = -10$dBW, CIM=-15dB

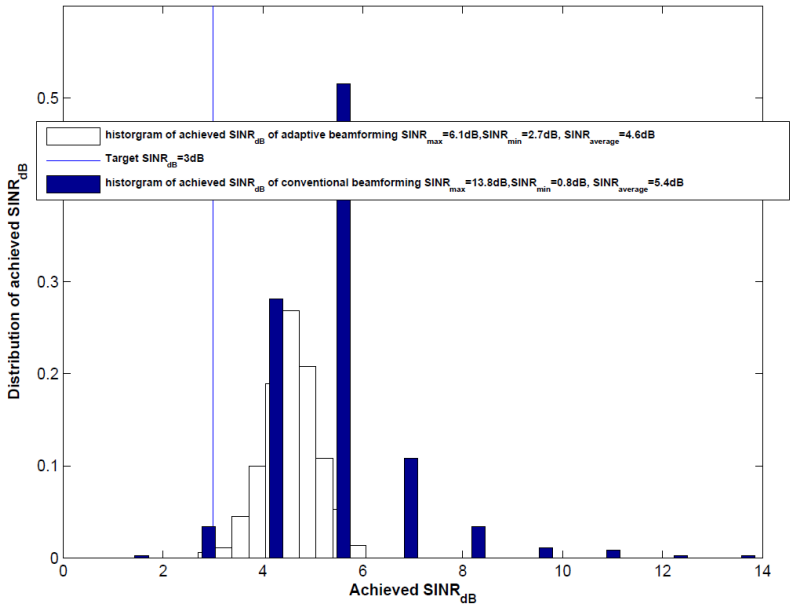

FIGURE 6.30 – Distribution of achieved SINR for adaptive beamforming and conventional beamforming. System settings : $K = 380$, target SINR=3dB, $\sigma_n^2 = -10$dBW, CIM=-15dB

6.5 Conclusions

The analysis carried out in the previous sections shows that adaptive beamforming is an excellent candidate for next generation satellite systems. In fact, when compared to conventional beamformers, it provides a very high gain in capacity, i.e. intended here as the number of STs that can be supported by the system with a given guaranteed QoS.

Additionally, the adaptive beamformer reduces the variance of the achieved SINR and facilitates the design of efficient beamformers that effectively expolit the available power.

A critical aspect in this study was the impact of the imperfect or incomplete knowledge of the channel at the satellite/gateway for the beamforming design and at the STs' because of the multi-stream detector design. Our analysis shows that an imperfect CSI at the STs determines an acceptable performance loss. This loss can be made arbitrarily small at the cost of longer training sequences and thus, reduced spectral efficiency. In this respect, significant improvements could be achieved by adopting nonlinear receivers with higher complexity performing jointly channel estimation, multi-stream detection and decoding.

More critical appeared the incomplete channel knowledge at the transmitter due to only statistical knowledge of the propagation matrix at the gateway. This determines fluctuations of the SINR at the STs. Such fluctuations could be reduced by (i) optimum or quasi optimum beamforming design for broadcast systems with statistical CSI and the transmitter; (ii) exploring the possibility to exploit the temporal correlation of the channel; (iii) new transmission techniques exploiting stale CSI.

The robustness of the system against mismatches between the actual directivity matrix and the directivity matrix used for beamforming has also been object of analysis. We investigated the effects of the mismatch when it is due to ST's mobility and the ST's positions are updated each second. Simulations show that the satellite system can support high speed mobility.

The effects of intermodulation noise and thermal noise have been also object of investigation. Numerical results show that intermodulation noise has a major impact on the outage probability and thus on the system capacity while thermal noise plays a minor role. Therefore, high quality of the satellite equipment is crucial to improve system capacity compared to the quality of STs.

Chapter 7

Parametric Least Squares Estimation for Nonlinear Satellite Channels

A key assumption that has driven the design of the adaptive beamforming in this work and has also a relevant impact in the design of the algorithms for the satellite partial CSI acquisition in the reverse link is the following : The propagation matrix is fast fading and its coherent time is too short compared to the propagation time of the channel. Any feedback information to the gateway about the propagation matrix should be considered stale. Therefore, only statistical knowledge of the of the propagation matrix at the gateway can be assumed for beamforming design.

The estimation and feedback of the channel transfer matrix is not sufficient for the design of adaptive beamforming since this depends on the instantaneous realizations of the fading propagation coefficients. When the estimation of the full (or instantaneous) CSI is not feasible since the propagation delay is very long and the instantaneous fed back CSI measurement becomes obsolete, slow varying components of the channel matrix could be used to provide a partial knowledge of the CSI instead of the instantaneous CSI. This is a practical alternative when the acquisition of the instantaneous CSI is not feasible.

The acquisition of the partial slow-varying CSI at the gateway, for a satellite system with mobile STs equipped eventually with multiple antennas and transmitting in left and right polarization, presents completely new challenges compared to the thoroughly studied satellite channel estimation techniques finalized to the coherent detection and decoding of the channel

at the receiver side. This is a completely unexplored field.

As discussed in Chapter 5, the directivity vectors are a multiplicative components of the channel that fade slowly even compared to the propagation delay of a satellite system when the STs move with a reasonably high speed, e.g. 140km/h. Then, in this chapter, we focus on the estimation of the directivity vector component at the gateway based on the observation in the reverse link. From a signal processing perspective, this implies the challenging task of estimating parameters observed through multiplicative nuisance.

The estimation of the directivity vectors is intrinsically nonlinear. We consider a parametric model of the channels where the directivity vector is parametrically represented by a linear combination of given known directivity vectors and the varying propagation coefficients play the role of multiplicative nuisance parameters.

In this chapter, we propose an algorithm to estimate the directivity vector parameters based on a least squares criterion. We show that the estimation problem reduces to an eigenvalue complementary problem. We dub the proposed algorithm Parametric Least Squares Estimation (PLSE). The proposed algorithm does not require the estimation of nuisance parameters and this enables a considerable complexity reduction.

This chapter is organized as follows : Section 7.1 describes the estimation problem and the PLSE algorithm ; Section 7.2 illustrates the application of the PLSE algorithm to a data transmission channel ; In Section 7.3, the performance of the proposed estimation algorithm is assessed through numerical simulations. In Section 7.4, we give some conclusions.

7.1 Parametric Least Squares Algorithm for Directivity Matrix Estimation

7.1.1 System Model

As shown in Section 5.2, the system model in the reverse link can be written as

$$\boldsymbol{y}^{re}[t] = \boldsymbol{D}^{re}[t]\boldsymbol{P}^{re}[t]\boldsymbol{C}_{\alpha}^{re}\boldsymbol{x}^{re}[t] + \boldsymbol{z}[t], \tag{7.1}$$

where the column vector $\boldsymbol{y}^{re}[t]$ represents the $2N$-dimensional vector of received signals ; $\boldsymbol{D}^{re}[t]$ is the directivity matrix in the reverse link of size $2N \times 2K$; $\boldsymbol{P}^{re}[t]$ is the $2K \times 4RK$ propagation matrix in the reverse link ; $\boldsymbol{C}_{\alpha}^{re}$ is the $4RK \times 2RK$ correlation matrix at the STs ; $\boldsymbol{x}^{re}[t]$ is the $2RK$ vector of transmitted signals from all the STs ; $\boldsymbol{z}[t]$ is the white additive Gaussian noise with variance given by sum of the variance of intermodulation noise and thermal noise at the gateway.

In this chapter, we consider the satellite system only in the reverse link. Therefore, for the sake of simplicity, we remove the superscript $(\cdot)^{re}$. We replace in this chapter $\boldsymbol{y}^{re}$, $\boldsymbol{x}^{re}$, $\boldsymbol{D}^{re}$, $\boldsymbol{P}^{re}$ and $\boldsymbol{C}_{\alpha}^{re}$ by $\boldsymbol{y}$, $\boldsymbol{x}$, $\boldsymbol{D}$, $\boldsymbol{P}$ and $\boldsymbol{C}_{\alpha}$, respectively.

To further simplify the notation, we also introduce the short notation

$$\boldsymbol{P}_k^{(c)}[t] = \boldsymbol{P}_k[t]\boldsymbol{C}_{\alpha,k}$$

In this chapter, we assume that the leakage signal from left or right polarization to the corresponding cross-polarization is negligible, i.e. $b = 0$, and the transmit antennas are uncorrelated, i.e. $a = 0$. Then, $\boldsymbol{P}_k^{(c)}$ boils down to the simple structure

$$\boldsymbol{P}_k^{(c)}[t] = \begin{pmatrix} P_{k,r}^{(1)}[t] & 0 & \cdots & P_{k,r}^{(R)}[t] & 0 \\ 0 & P_{k,l}^{(1)}[t] & \cdots & 0 & P_{k,l}^{(R)}[t] \end{pmatrix},$$

where $P_{k,o}^{(\ell)}[t]$, with $o \in \{r, l\}$, denotes the fast fading coefficients affecting the link between the satellite and ℓ-th antenna at k-th ST in o polarization [1].

It is worth noting that this fading component is due to the local perturbation of the signals around the ST. Due to the very large distance between the SAs and a ST, and propagation in deep space, the same fast fading components affects the signals from all SAs to a single antenna in a certain polarization.

We make the realistic assumption that the variations of the directivity vectors due to ST movements are negligible in the time interval when the channel is measured for estimation. Thus, we assume that the directivity vectors are constant in our system model and we drop the time index in the matrix $\boldsymbol{D}[t]$.

As already shown in (5.8), the directivity matrix $\boldsymbol{D}$ can conveniently be structured in KN blocks with each block column of size $2N \times 2$, $\boldsymbol{D}^k = (\boldsymbol{D}_1^{kT}, \boldsymbol{D}_2^{kT}, \ldots, \boldsymbol{D}_N^{kT})^T$ represents the directivity coefficients of the k-th ST.

$$\boldsymbol{D}_n^k = \begin{pmatrix} d_{n,rr}^k & d_{n,rl}^k \\ d_{n,lr}^k & d_{n,ll}^k \end{pmatrix} = \begin{pmatrix} \boldsymbol{d}_{n,r}^k \\ \boldsymbol{d}_{n,l}^k \end{pmatrix},$$

In Section 5.2, we have also shown that the directivity column block $\boldsymbol{D}^k$ of the k-th ST is given by convex combination of the directivity column vectors with identical coefficients

$$\boldsymbol{D}^k = \alpha_1^k \boldsymbol{G}^{\tau(1)} + \alpha_2^k \boldsymbol{G}^{\tau(2)} + \alpha_3^k \boldsymbol{G}^{\tau(3)} \tag{7.2}$$

where $0 \leq \alpha_i^k \leq 1$, $\sum \alpha_i^k = 1$. Here, $\boldsymbol{G}$ denotes the matrix available at the gateway and containing all the directivity vectors of the points in the grid

1. The impact of the assumption that the leaking signal from left or right polarization to the corresponding cross-polarization is negligible is evaluated in Section 7.3.

in Figure 5.2 and $\boldsymbol{G}^{\tau(i)}$, $i = \{1, 2, 3\}$ denotes the $\tau(i)$ block column of $\boldsymbol{G}$ corresponding to point $G_{\tau(i)}$, a point of a triplet surrounding the k-th ST.

Then, the system model (7.1) reduces to

$$\boldsymbol{y}[t] = \boldsymbol{D}\boldsymbol{P}^{(c)}[t]\boldsymbol{x}[t] + \boldsymbol{z}[t] \tag{7.3}$$

The estimation of the directivity matrix $\boldsymbol{D}$ is based on the synchronous transmissions of pilot sequences by all active STs. The k-th ST transmits $2R$ pilot sequences of length L, one for each antenna and polarization. They are known to the gateway and differ from each other and from the pilot sequences assigned to other STs. The pilot sequences are transmitted during a time slot not longer than the coherence time of the channel. Thus, in a time slot, the propagation matrix is constant and we denote the constant values in the q-th time slot as $\boldsymbol{P}_k^{(c)}(q)$ and $\boldsymbol{P}^{(c)}(q)$. Observations over Q different time slots are used for the estimation. In general, the time slots are nonconsecutive and such that the corresponding propagation channels can be considered statistically independent. However, these Q time slots are sufficiently close such that the directivity matrix can be considered constant in the whole observation time.

Under these assumptions, the signal received at SA n in o-polarization, with $o \in \{l, r\}$, is given by

$$y_{n,o}[s_q + s] = \boldsymbol{d}_{n,o}\boldsymbol{P}^{(c)}(q)\boldsymbol{x}[s_q + s] + z_{n,o}[s_q + s], \tag{7.4}$$

where $\boldsymbol{d}_{n,o} = (\boldsymbol{d}_{n,o}^1, \boldsymbol{d}_{n,o}^2, \ldots, \boldsymbol{d}_{n,o}^K)$, s_q is the time offset when the transmission of a pilot sequence for the qth slot starts and $s = 0, \ldots, L-1$ is a time index. The observation signal $\boldsymbol{\mathcal{Y}}_{n,o}(q) = (y_{n,o}[s_q], y_{n,o}[s_q + 1], \ldots, y_{n,o}[s_q + L - 1])$ in the coherence time q at SA n and o-polarization, is given by

$$\boldsymbol{\mathcal{Y}}_{n,o}(q) = \boldsymbol{d}_{n,o}\boldsymbol{P}^{(c)}(q)\boldsymbol{X}_q + \boldsymbol{\mathcal{Z}}_{n,o}(q) \tag{7.5}$$

where $\boldsymbol{X}_q$ is the $2RK \times L$ matrix whose rows are the pilot sequences of the active STs and $\boldsymbol{\mathcal{Z}}_{n,o}(q)$ is the L-dimensional row vector of the noise $\boldsymbol{\mathcal{Z}}_{n,o}(q) = (z_{n,o}[s_q], z_{n,o}[s_q + 1], \ldots, z_{n,o}[s_q + L - 1])$.

7.1.2 Directivity Estimation

In this subsection, we describe our approach to the estimation of the directivity vectors. It consists of two steps. In the first step, we perform a standard linear estimation of the transfer channel matrix based on standard linear least squares estimation (LSE) in each time slot. The second step consists of a nonlinear estimation of the directivity vectors based on a least squares error criterion.

Let $\boldsymbol{h}_{n,r}(q)$ and $\boldsymbol{h}_{n,l}(q)$ be the transfer vectors from all the ST to the n-th SA at q-th time slot in left and right polarization, respectively. They

consist of K blocks $\boldsymbol{h}_{n,r}^{k}(q)$ and $\boldsymbol{h}_{n,l}^{k}(q)$ defined as

$$\begin{aligned}\boldsymbol{h}_{n,r}^{k}(q) &= \left(h_{n,rr}^{k,(1)}(q),\, h_{n,rl}^{k,(1)}(q), \cdots,\, h_{n,rr}^{k,(R)}(q),\, h_{n,rl}^{k,(R)}(q)\right) \\ &= \left(d_{n,rr}^{k} P_{k,r}^{(1)}(q),\, d_{n,rl}^{k} P_{k,l}^{(1)}(q), \cdots,\, d_{n,rr}^{k} P_{k,r}^{(R)}(q),\, d_{n,rl}^{k} P_{k,l}^{(R)}(q)\right)\end{aligned}$$

and

$$\begin{aligned}\boldsymbol{h}_{n,l}^{k}(q) &= \left(h_{n,lr}^{k,(1)}(q),\, h_{n,ll}^{k,(1)}(q), \cdots,\, h_{n,lr}^{k,(R)}(q),\, h_{n,ll}^{k,(R)}(q)\right) \\ &= \left(d_{n,lr}^{k} P_{k,r}^{(1)}(q),\, d_{n,ll}^{k} P_{k,l}^{(1)}(q), \cdots,\, d_{n,lr}^{k} P_{k,r}^{(R)}(q),\, d_{n,ll}^{k} P_{k,l}^{(R)}(q)\right),\end{aligned}$$

respectively. Then, (7.5) reduces to

$$\boldsymbol{\mathcal{Y}}_{n,o}(q) = \boldsymbol{h}_{n,o}(q)\boldsymbol{X}_q + \boldsymbol{\mathcal{Z}}_{n,o}(q). \tag{7.6}$$

By applying standard results on linear LSE (see e.g. [36]), we obtain the LSE estimation of $\boldsymbol{h}_{n,r}(q)$ and $\boldsymbol{h}_{n,l}(q)$ given by

$$\hat{\boldsymbol{h}}_{n,l}(q) = \boldsymbol{\mathcal{Y}}_{n,l}\boldsymbol{X}_q^H(\boldsymbol{X}_q\boldsymbol{X}_q^H)^{-1} \tag{7.7}$$

and

$$\hat{\boldsymbol{h}}_{n,r}(q) = \boldsymbol{\mathcal{Y}}_{n,r}\boldsymbol{X}_q^H(\boldsymbol{X}_q\boldsymbol{X}_q^H)^{-1}, \tag{7.8}$$

respectively.

The estimation error is $\boldsymbol{\varepsilon}_{n,o}(q) = \hat{\boldsymbol{h}}_{no}(q) - \boldsymbol{h}_{no}(q)$, $o = \{r, l\}$. By rearranging the components in $\hat{\boldsymbol{h}}_{n,r}(q)$ and $\hat{\boldsymbol{h}}_{n,l}(q)$ and exploiting the assumptions $d_{n,ll}^{k} = d_{n,rr}^{k}$ and $d_{n,lr}^{k} = d_{n,rl}^{k}$, we obtain the system of equations

$$\left\{\begin{array}{rcl} d_{n,rr}^{k} P_{k,r}^{(1)}(q) &=& \hat{h}_{n,rr}^{k,(1)}(q) + \varepsilon_{n,rr}^{k,(1)}(q) \\ d_{n,rl}^{k} P_{k,r}^{(1)}(q) &=& \hat{h}_{n,lr}^{k,(1)}(q) + \varepsilon_{n,lr}^{k,(1)}(q) \\ d_{n,rr}^{k} P_{k,l}^{(1)}(q) &=& \hat{h}_{n,ll}^{k,(1)}(q) + \varepsilon_{n,ll}^{k,(1)}(q) \\ d_{n,rl}^{k} P_{k,l}^{(1)}(q) &=& \hat{h}_{n,rl}^{k,(1)}(q) + \varepsilon_{n,rl}^{k,(1)}(q), \\ & \vdots & \\ d_{n,rr}^{k} P_{k,l}^{(R)}(q) &=& \hat{h}_{n,ll}^{k,(R)}(q) + \varepsilon_{n,ll}^{k,(R)}(q) \\ d_{n,rl}^{k} P_{k,l}^{(R)}(q) &=& \hat{h}_{n,rl}^{k,(R)}(q) + \varepsilon_{n,rl}^{k,(R)}(q), \end{array}\right. \tag{7.9}$$

where the indices of the components of the estimates and estimation error vectors $\hat{\boldsymbol{h}}_{n,o}^{k}(q)$ and $\boldsymbol{\varepsilon}_{n,o}^{k}(q)$ are defined consistently with the ones of vector $\boldsymbol{h}_{n,o}^{k}(q)$. By making use of (7.2), we express (7.9) in a matrix form as function of the channel parameters α_1^k, α_2^k and α_3^k. Let us define the vectors $\boldsymbol{\alpha}^k = \left(\alpha_1^k, \alpha_2^k, \alpha_3^k\right)^T$, and the matrix

$$\widetilde{\boldsymbol{G}}_n^{\tau,k} = \left(\boldsymbol{g}_{n,r}^{\tau(1),T}, \boldsymbol{g}_{n,r}^{\tau(2),T}, \boldsymbol{g}_{n,r}^{\tau(3),T}\right) \tag{7.10}$$

where $\boldsymbol{g}_{n,r}^{\tau(i)}$ is the first row vector of the block $\boldsymbol{G}_n^{\tau,x(i)}$ of matrix $\boldsymbol{G}$. Then,

$$\boldsymbol{d}_{n,r}^{k,T} = \widetilde{\boldsymbol{G}}_n^k \boldsymbol{\alpha}^k. \tag{7.11}$$

By substituting (7.11) in (7.9), we obtain

$$\begin{cases} P_{k,r}^{(1)}(q)\widetilde{\boldsymbol{G}}_n^{\tau,k}\boldsymbol{\alpha}^k &= \hat{\boldsymbol{h}}_{n,r}^{k,(1)}(q) + \boldsymbol{\varepsilon}_{n,r}^{k,(1)}(q) \\ P_{k,l}^{(1)}(q)\widetilde{\boldsymbol{G}}_n^{\tau,k}\boldsymbol{\alpha}^k &= \hat{\boldsymbol{h}}_{n,l}^{k,(1)}(q) + \boldsymbol{\varepsilon}_{n,l}^{k,(1)}(q) \\ & \vdots \\ P_{k,r}^{(R)}(q)\widetilde{\boldsymbol{G}}_n^{\tau,k}\boldsymbol{\alpha}^k &= \hat{\boldsymbol{h}}_{n,r}^{k,(R)}(q) + \boldsymbol{\varepsilon}_{n,r}^{k,(R)}(q) \\ P_{k,l}^{(R)}(q)\widetilde{\boldsymbol{G}}_n^{\tau,k}\boldsymbol{\alpha}^k &= \hat{\boldsymbol{h}}_{n,l}^{k,(R)}(q) + \boldsymbol{\varepsilon}_{n,l}^{k,(R)}(q) \end{cases} \tag{7.12}$$

where $\widehat{\boldsymbol{h}}_{n,r}^{k,(\ell)}(q) = \left(\widehat{h}_{n,rr}^{k,(\ell)}(q), \widehat{h}_{n,lr}^{k,(\ell)}(q)\right)^T$, $\widehat{\boldsymbol{h}}_{n,l}^{k,(\ell)}(q) = \left(\widehat{h}_{n,ll}^{k,(\ell)}(q), \widehat{h}_{n,rl}^{k,(\ell)}(q)\right)^T$, and $\boldsymbol{\varepsilon}_{n,r}^{k,(\ell)}(q)$ and $\boldsymbol{\varepsilon}_{n,l}^{k,(\ell)}(q)$ are defined similarly.

The directivity estimation reduces to the estimation of the parameters $\boldsymbol{\alpha}$. We estimate these parameters based on a nonlinear least squares error criterion. The optimization problem is formulated as follows,

Problem $\boldsymbol{P_0}$

$$\begin{array}{ll} \textbf{minimize} & \displaystyle\sum_{\substack{\ell=1,\dots R \\ q=0,\dots,Q-1 \\ n=1,\dots,N}} \|\hat{\boldsymbol{h}}_{n,r}^{k,(\ell)}(q) - P_{k,r}^{(\ell)}(q)\widetilde{\boldsymbol{G}}_n^{\tau,k}\boldsymbol{\alpha}\|^2 + \|\hat{\boldsymbol{h}}_{n,l}^{k}(q) - P_{k,l}^{(\ell)}(q)\widetilde{\boldsymbol{G}}_n^{\tau,k}\boldsymbol{\alpha}\|^2 \\ \textbf{subject to} & 0 \le \alpha_i \le 1, \quad i = 1,2,3 \\ & \sum_{i=1}^3 \alpha_i = 1 \end{array}$$

Problem P_0 does not reduce to linear LSE because of the presence of nuisance parameters $P_{k,o}^{(\ell)}(q)$ and it is in general nonconvex. The following theorem establishes the equivalence of P_0 to a generalized symmetric Eigenvalue Complementarity Problem (EiCP) well-studied in optimization theory (see e.g. [37] and references therein).

Theorem 2. *The optimization Problem P_0 is equivalent to the problem* ***Problem $\boldsymbol{P}_1$***

$$\begin{array}{ll} \textbf{\textit{maximize}} & f(\boldsymbol{\alpha}, \tau; \hat{\boldsymbol{h}}_r^k(0), \hat{\boldsymbol{h}}_l^k(0), ..., \hat{\boldsymbol{h}}_l^k(Q-1)) \\ & = \dfrac{\boldsymbol{\alpha}^T \mathfrak{Re}(\boldsymbol{\Theta}(\tau, \hat{\boldsymbol{h}}_r^k(0), ..., \hat{\boldsymbol{h}}_l^k(Q-1)))\boldsymbol{\alpha}}{\boldsymbol{\alpha}^T \mathfrak{Re}(\boldsymbol{\Gamma}(\tau))\boldsymbol{\alpha}} \\ \textbf{\textit{subject to}} & \sum_{i=1}^3 \alpha_i = 1 \quad 0 \le \alpha_i \le 1, \qquad i = 1,2,3 \end{array}$$

being $\boldsymbol{\Theta}(\tau, \hat{\boldsymbol{h}}_r^k(0), ..., \hat{\boldsymbol{h}}_l^k(Q-1))$ *and* $\boldsymbol{\Gamma}(\tau)$ *the* 3×3 *matrices defined as :*

$$\boldsymbol{\Theta}(\tau, \hat{\boldsymbol{h}}_l^k(0), ..., \hat{\boldsymbol{h}}_l^k(Q-1)) = \tag{7.13}$$

$$\widetilde{\boldsymbol{G}}^{\tau,k,H}\left(\sum_{q=0}^{Q-1}\sum_{\ell=1}^{R}\left(\hat{\boldsymbol{h}}_r^{k,(\ell)}(q)\hat{\boldsymbol{h}}_r^{k,(\ell)H}(q) + \hat{\boldsymbol{h}}_l^{k,(\ell)}(q)\hat{\boldsymbol{h}}_l^{k,(\ell)H}(q)\right)\right)\widetilde{\boldsymbol{G}}^{\tau,k}, \tag{7.14}$$

$$\boldsymbol{\Gamma}(\tau) = \widetilde{\boldsymbol{G}}^{\tau,H}\widetilde{\boldsymbol{G}}^{\tau} \tag{7.15}$$

with $\hat{\boldsymbol{h}}_o^{k,(\ell)}(q) = \left(\hat{\boldsymbol{h}}_{1,o}^{k,(\ell)H}(q), ..., \hat{\boldsymbol{h}}_{N,o}^{k,(\ell)H}(q)\right)^H$, $\widetilde{\boldsymbol{G}}^{\tau,k} = \left(\widetilde{\boldsymbol{G}}_1^{\tau,k,H}, ..., \widetilde{\boldsymbol{G}}_N^{\tau,k,H}\right)^H$ *and* $\widetilde{\boldsymbol{G}}_n^{\tau,k,H} = (\boldsymbol{g}_{n,r}^{\tau_1}, \boldsymbol{g}_{n,r}^{\tau_2}, \boldsymbol{g}_{n,r}^{\tau_3})$. *Here* $\boldsymbol{g}_{n,r}^{\tau_i}$ *is the first row of the block* $\boldsymbol{G}_n^{\tau_i}$ *of matrix* $\boldsymbol{G}$, $\hat{\boldsymbol{h}}_{n,r}^{k,(\ell)}(q) = (\hat{h}_{n,rr}^{k,(\ell)}, \hat{h}_{n,lr}^{k,(\ell)})^T$ *and* $\hat{\boldsymbol{h}}_{n,l}^{k,(\ell)}(q) = (\hat{h}_{n,rl}^{k,(\ell)}, \hat{h}_{n,ll}^{k,(\ell)})^T$.

Proof :

By using the definitions of $\hat{\boldsymbol{h}}_o^{k,(\ell)}$ and $\widetilde{\boldsymbol{G}}^{\tau,k}$ in the statement of the theorem, the objective function of Problem P_0 can be rewritten as

$$f(\boldsymbol{\alpha}, \tau, \boldsymbol{P}^k(q)) = \sum_{\ell=1}^{R}\sum_{q=0}^{Q-1} \|\hat{\boldsymbol{h}}_r^{k,(\ell)}(q) - P_{k,r}^{(\ell)}(q)\widetilde{\boldsymbol{G}}^{\tau,k}\boldsymbol{\alpha}\|^2 + \|\hat{\boldsymbol{h}}_l^{k,(\ell)}(q) - P_{k,l}^{(\ell)}(q)\widetilde{\boldsymbol{G}}^{\tau,k}\boldsymbol{\alpha}\|^2$$
$$= \sum_{\ell=1}^{R}\sum_{q=0}^{Q-1} |P_{k,r}^{(\ell)}|^2 \boldsymbol{\alpha}^H \widetilde{\boldsymbol{G}}^{\tau,k,H}\widetilde{\boldsymbol{G}}^{\tau,k}\boldsymbol{\alpha} - \mathfrak{Re}\left(P_{k,r}^{(\ell)}\hat{\boldsymbol{h}}_r^{k,(\ell)H}(q)\widetilde{\boldsymbol{G}}^{\tau,k}\boldsymbol{\alpha}\right) + \hat{\boldsymbol{h}}_r^{k,(\ell)H}(q)\hat{\boldsymbol{h}}_r^{k,(\ell)}(q)$$
$$+ \sum_{\ell=1}^{R}\sum_{q=0}^{Q-1} |P_{k,l}^{(\ell)}|^2 \boldsymbol{\alpha}^H \widetilde{\boldsymbol{G}}^{\tau,k,H}\widetilde{\boldsymbol{G}}^{\tau,k}\boldsymbol{\alpha} - \mathfrak{Re}\left(P_{k,l}^{(\ell)}\hat{\boldsymbol{h}}_l^{k,(\ell)H}(q)\widetilde{\boldsymbol{G}}^{\tau,k}\boldsymbol{\alpha}\right) + \hat{\boldsymbol{h}}_l^{k,(\ell)H}(q)\hat{\boldsymbol{h}}_l^{k,(\ell)}(q) \tag{7.16}$$

The application of the rules of complex gradient operators (see e.g. [38], [39]) yields

$$\frac{\partial f(\boldsymbol{\alpha}, \tau, \boldsymbol{P}^k(q))}{\partial P_{k,o}^{(\ell)}(q)} = 2P_{k,o}^{(\ell)}(q)\boldsymbol{\alpha}^H\widetilde{\boldsymbol{G}}^{\tau,k,H}\widetilde{\boldsymbol{G}}^{\tau,k}\boldsymbol{\alpha} - 2\boldsymbol{\alpha}^H\widetilde{\boldsymbol{G}}^{\tau,k,H}\hat{\boldsymbol{h}}_o^{k,(\ell)}(q). \tag{7.17}$$

Since $f(\boldsymbol{\alpha}, \tau, \boldsymbol{P}^k(q))$ is convex in $P_{k,o}^{(\ell)}(q)$, for any given $\boldsymbol{\alpha}$, it is minimized by the value of $P_{k,o}^{(\ell)}(q)$ where (7.17) vanishes, i.e.

$$P_{k,o}^{(t)}(q) = \frac{\boldsymbol{\alpha}^H\widetilde{\boldsymbol{G}}^{\tau,k,H}\hat{\boldsymbol{h}}_o^{k,(\ell)}(q)}{\boldsymbol{\alpha}^H\widetilde{\boldsymbol{G}}^{\tau,k,H}\widetilde{\boldsymbol{G}}^{\tau,k}\boldsymbol{\alpha}}, \quad o = \{r, l\}. \tag{7.18}$$

By substituting (7.18) in $f(\boldsymbol{\alpha}, \tau, \boldsymbol{P}^k(q))$ and neglecting the constant terms, we obtain the optimization problem

$$\begin{array}{ll} \textbf{minimize} & -\sum_{\ell=1}^{R}\sum_{q=0}^{Q-1}\left(\dfrac{\boldsymbol{\alpha}^H\widetilde{\boldsymbol{G}}^{\tau,k,H}\hat{\boldsymbol{h}}_r^{k,(\ell)}(q)\hat{\boldsymbol{h}}_r^{k,(\ell)H}(q)\widetilde{\boldsymbol{G}}^{\tau,k}\boldsymbol{\alpha}}{\boldsymbol{\alpha}^H\widetilde{\boldsymbol{G}}^{\tau,k,H}\widetilde{\boldsymbol{G}}^{\tau,k}\boldsymbol{\alpha}} + \dfrac{\boldsymbol{\alpha}^H\widetilde{\boldsymbol{G}}^{\tau,k,H}\hat{\boldsymbol{h}}_l^{k,(\ell)}(q)\hat{\boldsymbol{h}}_l^{k,(\ell)H}(q)\widetilde{\boldsymbol{G}}^{\tau,k}\boldsymbol{\alpha}}{\boldsymbol{\alpha}^H\widetilde{\boldsymbol{G}}^{\tau,k,H}\widetilde{\boldsymbol{G}}^{\tau,k}\boldsymbol{\alpha}}\right) \\ \textbf{subject to} & \sum_{i=1}^{3}\alpha_i = 1 \quad 0 \le \alpha_i \le 1, \qquad i = 1, 2, 3 \end{array}$$

which is equivalent to

$$\begin{array}{ll} \textbf{maximize} & f(\boldsymbol{\alpha}, \tau) = \dfrac{\boldsymbol{\alpha}^H\boldsymbol{\Theta}(\tau)\boldsymbol{\alpha}}{\boldsymbol{\alpha}^H\boldsymbol{\Gamma}(\tau)\boldsymbol{\alpha}} \\ \textbf{subject to} & \sum_{i=1}^{3}\alpha_i = 1 \quad 0 \le \alpha_i \le 1, \qquad i = 1, 2, 3. \end{array}$$

By observing that $\boldsymbol{\Theta}(\tau)$ and $\boldsymbol{\Gamma}(\tau)$ are Hermitian, $\boldsymbol{\alpha}$ is a vector of reals, and the quadratic forms are real, the equalities $\boldsymbol{\alpha}^H\boldsymbol{\Theta}(\tau)\boldsymbol{\alpha} = \boldsymbol{\alpha}^H\mathfrak{Re}\left(\boldsymbol{\Theta}(\tau)\right)\boldsymbol{\alpha}$ and $\boldsymbol{\alpha}^H\boldsymbol{\Gamma}(\tau)\boldsymbol{\alpha} = \boldsymbol{\alpha}^H\mathfrak{Re}\left(\boldsymbol{\Gamma}(\tau)\right)\boldsymbol{\alpha}$ hold. This concludes the proof of Theorem 2. ■

The optimal vector $\boldsymbol{\alpha}^*$ provides the desired estimate of the parameter vector $\boldsymbol{\alpha}^k$ and a PLSE of the directivity column block $\boldsymbol{D}^k$ is given by $\widehat{\boldsymbol{D}}^k = \sum_{i=1}^{3} \alpha_i \boldsymbol{G}^{\tau(i)}$.

Interestingly, Problem P_1 does not require an explicit estimation of the nuisance parameters, i.e. the propagation coefficients, with consequent computational complexity and numerical error propagation reduction.

In the rest of this section we discuss how to determine a solution of Problem P_1.

Let us observe that $f(\boldsymbol{\alpha}, \tau)$ assumes the same value on each of the points belonging to the same ray passing through the origin, i.e, $f(\boldsymbol{\alpha}, \tau) = f(\rho\boldsymbol{\alpha}, \tau)$ for any nonzero real ρ. Therefore, given any vector $\boldsymbol{\alpha}^*$ maximizing $f(\boldsymbol{\alpha}, \tau)$, it is straightforward to derive from it a vector that achieves the optimal value $f(\boldsymbol{\alpha}^*, \tau)$ and satisfies the constraint $\sum_i \alpha_i = 1$ by setting

$$\boldsymbol{\alpha}_{opt} = \frac{\boldsymbol{\alpha}^*}{\|\boldsymbol{\alpha}^*\|_1}. \tag{7.19}$$

Based on (7.19), the constraints $\alpha_i \leq 1$ are also satisfied if $\alpha_i \geq 0$. Thus, the problem is very similar to a generalized eigenvalue problem (see e.g. [40]). However, in general $\boldsymbol{\alpha}$, a solution of the generalized eigenvector problem does not satisfy the constraints $\alpha_i \geq 0$. In the following, we discuss the use of the solutions of a generalized eigenvalue problem to find a solution to P_1 which satisfies also the constraints $\alpha_i \geq 0$.

The global minimum of function $f(\boldsymbol{\alpha}, \tau)$ is achieved by the eigenvector corresponding to the maximum generalized eigenvalue of $\mathfrak{Re}(\boldsymbol{\Theta})$ and $\mathfrak{Re}(\boldsymbol{\Gamma}^k)$. The other generalized eigenvectors of $\mathfrak{Re}(\boldsymbol{\Theta})$ and $\mathfrak{Re}(\boldsymbol{\Gamma}^k)$ achieve local maxima, local minima or saddle points [2] of the function $f(\boldsymbol{\alpha}, \tau)$. Moreover, $f(\boldsymbol{\alpha}, \tau)$ is a continuous function of $\boldsymbol{\alpha}$. Therefore, if the generalized eigenvector of $\mathfrak{Re}(\boldsymbol{\Theta})$ and $\mathfrak{Re}(\boldsymbol{\Gamma})$ yielding the global optimum of the unconstrained problem does not have all components of the same sign, i.e. it cannot be normalized to satisfy the constraint $\alpha_i \geq 0$, the solution of P_1 in the nonnegative orthant is achieved by the other generalized eigenvectors of $\mathfrak{Re}(\boldsymbol{\Theta})$ and $\mathfrak{Re}(\boldsymbol{\Gamma})$ or falls on the boundary of the nonnegative orthant. Then, we can compute the solution of P_1 by exhaustive search on the boundary and among the generalized eigenvectors. Among the generalized eigenvectors, we need to analyze the ones that have all the components of the same sign. The value of $f(\boldsymbol{\alpha}, \tau)$ is given by the generalized eigenvalue corresponding to the generalized eigenvector.

For searching the solution of P_1 on the boundary, we need to consider two different cases : (a) Two elements of $\boldsymbol{\alpha}$ are 0; (b) One element of $\boldsymbol{\alpha}$ is 0. In the former case, the value of $f(\boldsymbol{\alpha}, \tau)$ can be easily computed by

$$f(\boldsymbol{\alpha}, \tau) = \left| \frac{\mathfrak{Re}(\boldsymbol{\Theta})_{ii}}{\mathfrak{Re}(\boldsymbol{\Gamma})_{ii}} \right| \tag{7.20}$$

where $\mathfrak{Re}(\boldsymbol{\Theta})_{ii}$ and $\mathfrak{Re}(\boldsymbol{\Gamma})_{ii}$ denotes the ith diagonal element of $\mathfrak{Re}(\boldsymbol{H}^k)$ and $\mathfrak{Re}(\boldsymbol{\Gamma}^k)$, respectively.

---

2. As well known, the optimization of any Rayleigh quotient $\frac{\boldsymbol{x}^T\boldsymbol{A}\boldsymbol{x}}{\boldsymbol{x}^T\boldsymbol{B}\boldsymbol{x}}$, with $\boldsymbol{A}, \boldsymbol{B}$ squared matrices and $\boldsymbol{x}$ vector of consistent dimension, is equivalent to the optimization of $\boldsymbol{x}^T\boldsymbol{A}\boldsymbol{x}$ constrained to $\boldsymbol{x}^T\boldsymbol{B}\boldsymbol{x} = K$. It is straightforward to observe that the gradient of the corresponding Lagrangian vanishes in any $(\lambda, \boldsymbol{v})$, being λ and $\boldsymbol{v}$ respectively a generalized eigenvalue and the corresponding eigenvector of the matrices $\boldsymbol{A}$ and $\boldsymbol{B}$.

In the latter case, we examine the maximum value of $f(\boldsymbol{\alpha}, \tau)$ for $\alpha_i = 0, i = 1, 2, 3$ separately. For $\alpha_i = 0$, $\alpha_j > 0$, $i, j = 1, 2, 3$, $i \neq j$, we have

$$\frac{\boldsymbol{\alpha}^{(\backsim i)H} \mathfrak{Re}(\boldsymbol{\Theta})^{(\backsim i)} \boldsymbol{\alpha}^{(\backsim i)}}{\boldsymbol{\alpha}^{(\backsim i)H} \mathfrak{Re}(\boldsymbol{\Gamma})^{(\backsim i)} \boldsymbol{\alpha}^{(\backsim i)}} \tag{7.21}$$

where $\boldsymbol{\alpha}^{(\backsim i)}$ denotes the vector obtained from $\boldsymbol{\alpha}^*$ by suppressing the i-th component and $\mathfrak{Re}(\boldsymbol{X})^{(\backsim i)}$ denotes the matrix obtained from the matrix $\boldsymbol{X}$ by suppressing the i-th row and column. We retain the generalized eigenvectors of $\mathfrak{Re}(\boldsymbol{\Theta})^{(\backsim i)}$ and $\mathfrak{Re}(\boldsymbol{\Gamma})^{(\backsim i)}$ with components of the same sign.

To summarize, to solve the optimization problem (P_1) we analyze all the generalized eigenvectors of $\mathfrak{Re}(\boldsymbol{\Theta})$ and $\mathfrak{Re}(\boldsymbol{\Gamma})$, the generalized eigenvectors of $\mathfrak{Re}(\boldsymbol{\Theta})$ and $\mathfrak{Re}(\boldsymbol{\Gamma})$, $i = \{1, 2, 3\}$ and the values (7.20). We compare the values of $f(\boldsymbol{\alpha}, \tau)$ in all the possible cases and choose the maximum one. The corresponding $\boldsymbol{\alpha}^*$ yields the desired estimation.

In order to solve the directivity estimation problem for all the active STs over the full coverage area it is relevant to further observe that (a) Problem (P_1) has to be solved for each ST ; (b) In the general case, the three nearest points surrounding the k-th ST are not known. Then, an exhaustive search over the whole possible triplets of adjacent reference points is required and the triplet yielding the least squared error is selected. In a practical system, such exhaustive search is not required also in case of ST's mobility and the search can be limited to triples adjacent to the area covered by the triplet used in the previous estimation.

The PLSE algorithm is detailed in Algorithm 3.

1 Determine $\boldsymbol{\alpha}^{k^*} \equiv (\alpha_1^{k^*}, \alpha_2^{k^*}, \alpha_3^{k^*})$ has the maximizer of the eigenvalue complementarity problem :

$$\begin{aligned} \textbf{maximize} \quad & f(\boldsymbol{\alpha}, \tau; \hat{\boldsymbol{h}}_r^k(0), \hat{\boldsymbol{h}}_l^k(0), ..., \hat{\boldsymbol{h}}_l^k(Q-1)) \\ & = \frac{\boldsymbol{\alpha}^T \mathfrak{Re}(\boldsymbol{\Theta}(\tau, \hat{\boldsymbol{h}}_r^k(0), ..., \hat{\boldsymbol{h}}_l^k(Q-1)))\boldsymbol{\alpha}}{\boldsymbol{\alpha}^T \mathfrak{Re}(\boldsymbol{\Gamma}(\tau))\boldsymbol{\alpha}} \\ \textbf{subject to} \ & \sum_{i=1}^3 \alpha_i = 1 \quad 0 \leq \alpha_i \leq 1, \qquad i = 1,2,3 \quad \textbf{Problem } \mathbf{P}_1 \end{aligned}$$

being $\boldsymbol{\Theta}(\tau, \hat{\boldsymbol{h}}_r^k(0), ..., \hat{\boldsymbol{h}}_l^k(Q-1))$ and $\boldsymbol{\Gamma}(\tau)$ the 3×3 matrices defined as :

$$\begin{aligned} & \boldsymbol{\Theta}(\tau, \hat{\boldsymbol{h}}_r^k(0), ..., \hat{\boldsymbol{h}}_l^k(Q-1)) = \\ & \widetilde{\boldsymbol{G}}^{\tau,k,H} \left(\sum_{q=0}^{Q-1} \sum_{\ell=1}^{R} \left(\hat{\boldsymbol{h}}_r^{k,(\ell)}(q) \hat{\boldsymbol{h}}_r^{k,(\ell)H}(q) + \hat{\boldsymbol{h}}_l^{k,(\ell)}(q) \hat{\boldsymbol{h}}_l^{k,(\ell)H}(q) \right) \right) \widetilde{\boldsymbol{G}}^{\tau,k}, \\ & \boldsymbol{\Gamma}(\tau) = \widetilde{\boldsymbol{G}}^{\tau,k,H} \widetilde{\boldsymbol{G}}^{\tau,k} \end{aligned} \tag{7.22}$$

with $\hat{\boldsymbol{h}}_o^{k,(\ell)}(q) = \left(\hat{\boldsymbol{h}}_{1,o}^{k,(\ell)H}(q), ..., \hat{\boldsymbol{h}}_{N,o}^{k,(\ell)H}(q) \right)^H$, $\widetilde{\boldsymbol{G}}^{\tau,k} = \left(\widetilde{\boldsymbol{G}}_1^{\tau,k,H}, ..., \widetilde{\boldsymbol{G}}_N^{\tau,k,H} \right)^H$ and $\widetilde{\boldsymbol{G}}_n^{\tau,k,T} = (\boldsymbol{g}_{n,r}^{\tau_1}, \boldsymbol{g}_{n,r}^{\tau_2}, \boldsymbol{g}_{n,r}^{\tau_3})$. Here $\boldsymbol{g}_{n,r}^{\tau_i}$ is the first row of the block $\boldsymbol{G}_n^{\tau_i}$ of matrix $\boldsymbol{G}$, $\hat{\boldsymbol{h}}_{n,r}^{k,(\ell)}(q) = (\hat{h}_{n,rr}^{k,(\ell)}, \hat{h}_{n,lr}^{k,(\ell)})^T$ and $\hat{\boldsymbol{h}}_{n,l}^{k,(\ell)}(q) = (\hat{h}_{n,rl}^{k,(\ell)}, \hat{h}_{n,ll}^{k,(\ell)})^T$.

2 Determine

$$\hat{\boldsymbol{D}}^{k^*} = \sum_{i=1}^{3} \alpha_i^{k^*} \boldsymbol{G}^{\tau_i}. \tag{7.23}$$

Algorithm 3: PLSE algorithm for directivity vectors estimation

7.2 PLSE for Connection-oriented Channels

In this section, we discuss the application of the PLSE algorithm to a practical system with connection-oriented communications [3]. First, we illustrate the peculiarities of this system; then, we summarize the steps to apply the proposed PLSE algorithm to it.

In a connection-oriented communication, the gateway has the prior knowledge of the number of active STs and pilot sequences utilized by each ST. Moreover, the gateway is aware of the area where each ST is located from the previous estimation up to some estimation error and mismatches due to the ST mobility. This gateway may update the estimation of the directivity coefficients based on the previous estimation. It searches the k-th ST in a circle $\mathcal{C}_k(\hat{\mathfrak{S}}_k, \mathfrak{R}_k)$, where center $\hat{\mathfrak{S}}_k$ is the estimated position of ST k at the previous step, and $\mathfrak{R}_k$ is the radius. We denote the distance between the actual position of ST k and the center of the circle $\mathcal{C}_k$ as $D_{a,k}$.

An algorithm for connection-oriented communications based on the PLSE estimation is summarized in Algorithm 4

```
for k = 1, ..., K do
    for q = 1, ..., Q do
        Calculate ĥ^k_{n,o}(q), {o} = {r, l} according to (7.7) and (7.8).
    end
end
for k = 1, ..., K do
    Determine all the Π_k adjacent triplets located in C_k(Ŝ_k, R_k)
    for i = 1, ...Π_k do
        Compute the optimal parametric coefficients α by solving the
        optimization problem P_1;
    end
    select triplet and parameter α yielding to the minimum least
    squares.
    Determine the directivity vector of the ST k corresponding to the
    optimum triplet and optimum α by applying (8.15).
end
```

Algorithm 4: Algorithm connection-oriented channel based on PLSE

7.3 Numerical Performance Assessment

In this section, we analyze the performance of the proposed algorithm under two different assumptions, namely, the gateway does not make use of the prior

3. A connection-oriented communication mode is a date communications where the devices at the end points use a protocol to establish an end-to-end logical or physical connection before any data may be sent

knowledge of the area which ST is located in and a whole map exhaustive search is performed or it does utilize previous estimation and a limited-region search is performed.

The simulations are performed for satellite terminals equipped with two antennas, i.e., $R = 2$. The satellite is endowed with 163 SA. For the simulations, we utilize the actual directivity vectors of a geostationary system serving the European area. The propagation coefficients are generated according to the Surrey model in [15]. The power of the transmit signals is set to be 0 dBW. The results are obtained by averaging over 100 system realizations, i.e., 100 different groups of STs are randomly generated and the performance of the system is assessed over each realization. The event when the distance between the actual position and the estimated position of a terminal is greater than 40 kilometers is referred to as "estimation failure." The positions of the STs are generated randomly and uniformly in a rectangular region covering the most of Europe. Throughout the whole section, if not differently specified, the following assumptions are made : (1) Pilot sequence is either 100, 150 or 200 QPSK symbols; (2) In the case of limited-region search, the gateway searches the STs in a circle with a radius of 160 kilometers and the center of the circle is the previous estimated position; (3) In order to initialize the algorithm, the distance D_a between the center of the circle and the actual position of ST is normally distributed with zero mean and variance 20 kilometers^2.

Figure 7.1 shows the estimation error of the PLSE in terms of position errors [4] for increasing levels of noise. In the system there are 30 active STs. The number of coherence time intervals in the simulation is 30. As evidenced by Figure 7.1, when the noise increases, the estimation error of STs' positions increase only slightly in both assumptions since the interference from other STs plays a major role. In general, the algorithm based on prior knowledge (limited-region search) outperforms the algorithm based on the whole map exhaustive search. The performance gap between the two implementations decreases when the pilot sequences length increases.

A similar trend appears in Figure 7.2 where the estimation failure probability of the PLSE algorithm for increasing levels of noise is presented. The exhaustive search approach has an estimation failure probability above 10% for pilot length of 100 symbols, while the estimation failure events vanishes for pilot length of 200 symbols.

Figure 7.1 and Figure 7.2 suggest that the impact of the noise on the performance of PLSE algorithm is not significant. To improve the estimation, it is more effective to mitigate the interference among the STs by increasing the length of pilots.

The impact of the number of active STs in the system on the PLSE estimation is shown in terms of distance estimation error in Figure 7.3 and in terms of estimation failure in Figure 7.4. In this simulation, $Q = 30$, the noise is absent and only co-channel interference is present. When the number of STs is greater than 20, the position's estimation error increases rapidly when the length of the pilot is 100 in both types of estimation, as apparent from Figure 7.3. On the contrary, when the length of the training pilot is 200, the estimation error of the positions of STs

4. The choice to show the performance in terms of error on the distance instead of the error on the directivity vectors is due to the fact that the average error on the directivity vector is not very representative because to the large length of the directivity vectors (163 elements) and their large range of variation. This choice is adopted throughout all this section.

increases very slowly and the PLSE achieves a good estimation of the positions.

A similar trend is shown in Figure 7.4 for the estimation failure probability. It is worth noticing that, when K STs are transmitting, the channels consists of $2RK = 4K$ links and the performance starts degrading significantly when the training length approaches $4K$ or is lower than $4K$.

We also analyze the impact of Q, the number of coherence time intervals, on the PLSE estimation of the STs' positions. In our simulations, $K = 40$. The noise is absent. Figure 7.5 and Figure 7.6 show the impact of the number of coherence time intervals on the estimation errors of the STs' locations and the estimation failure probability, respectively. Even in this case, the algorithm based on the prior information outperforms the exhaustive search. Interestingly, the algorithms performance is not sensitive to the number of coherence time intervals when the pilot length is greater than $2RK$. On the contrary, it has a beneficial impact when the training length is short and does not guarantee good performance.

Additionally, recall that the PLSE algorithm has been derived under the assumption of absence of coupling between co-polarization and absence of cross-polarization, i.e., $a = 0$ and $b = 0$ in the correlation matrix. We evaluate the impact of these correlation coefficients. In the simulations, we assume $a = -15$dB and $b = -22$dB. Figure 7.7 and Figure 7.8 show the impact of the correlation coefficients at the receiver on the estimation errors of the STs' locations and the estimation failure probability, respectively. The figures show that the two coefficients have a minor impact on the algorithm's performance.

In the following, we study the impact of the distance between adjacent STs in the limited-region search approach. We generate the positions of the STs on a square region. Each ST has the same distance to its adjacent ST. In the simulations, the noise is absent and the length of the pilot sequence is 200. The number of coherence time intervals is 30. The gateway utilizes the information from the previous estimation. The gateway searches the ST in a circle with radius of 240 kilometers. The distance between the actual position of the STs and the center of the circle is normally distributed and has a variance of 40 kilometers.

Figure 7.9 shows the impact of the distance between adjacent STs. As expected, when the distance between adjacent STs increases, the PLSE algorithm achieves a better performance. Figure 7.9 also indicates that, for given distance between adjacent STs, as the number of STs increases, the estimation errors of the STs' positions also increases slightly.

Finally, we study the impact of the radius of searching zone $\mathfrak{R}_k$ and the distance between the actual position of the ST and the center of the searching area, $\mathrm{D}_{a,k}$. In our simulations, $K = 40$, the noise is absent and the pilot length is 200. The number of coherence time intervals is 30. The positions of the STs are randomly and uniformly generated. Additionally, we force the minimal distance between two adjacent STs to be not less than 40 kilometers.

Figure 7.10 shows the estimation error of the positions of STs with different radius lengths. When the standard deviation of the distance between the center point of the searching area and the actual position is 96 kilometers, the estimation error of the position is more than 2 kilometers if the searching is only executed in a circle with radius equals to 80 kilometers. As the radius of the searching area increases, the estimation error of the positions decreases dramatically to approximately 0.3 kilometers when the searching is performed in a circle having a radius equals to 144 kilometers. When the variance of the distance between the center point of the

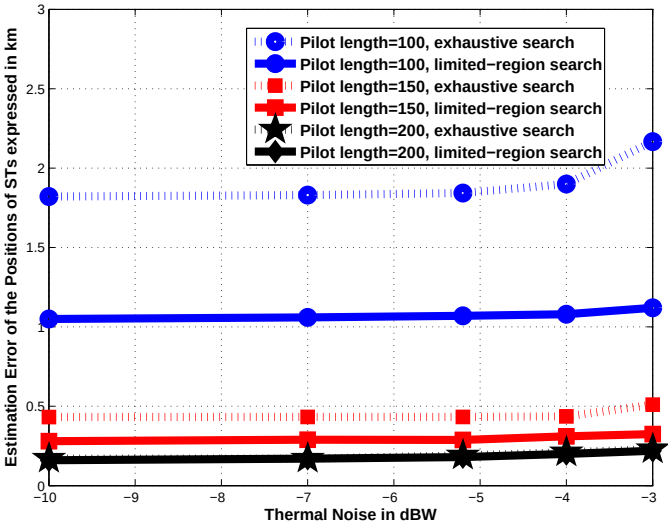

FIGURE 7.1 – Estimation error of STs positions in km versus different levels of noise with different pilot lengths and searching area. System settings : $K = 30$, $Q = 30$

searching area and actual position is 24 kilometers, searching the ST in a circle with radius 80 kilometers is sufficient, i.e., as the radius increases, the performance of the PLSE algorithm does not improve further.

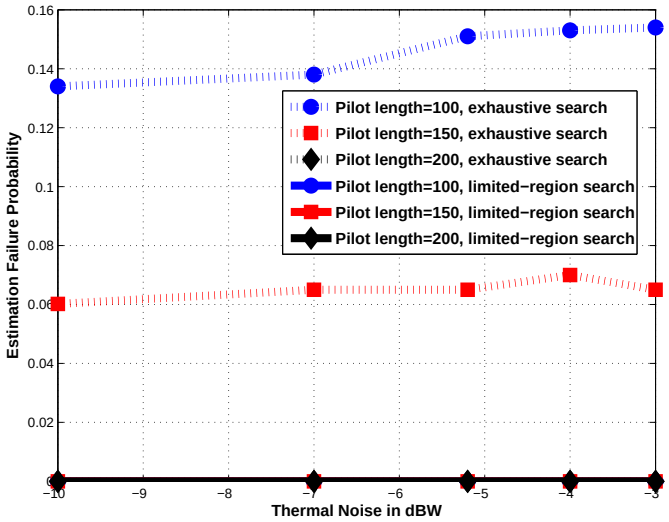

FIGURE 7.2 – Estimation failure probability versus different levels of noise with different pilot lengths and searching area. System settings : $K = 30$, $Q = 30$

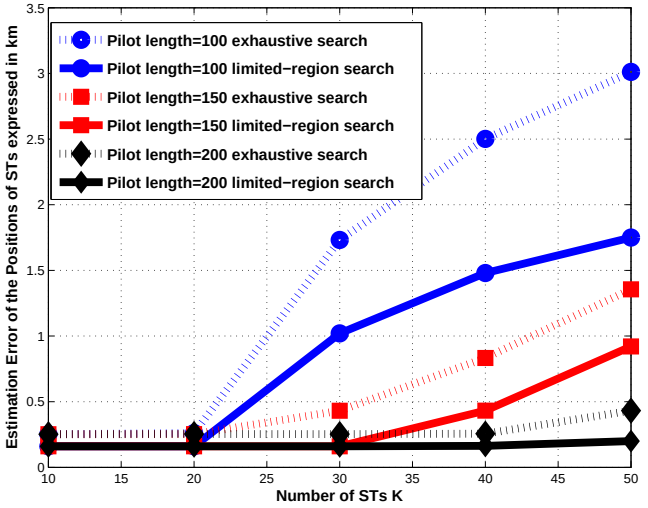

FIGURE 7.3 – Estimation error of the positions of STs versus number of STs with different pilot lengths and searching area. System settings : $Q = 30$, Noise$= -\infty$dBW

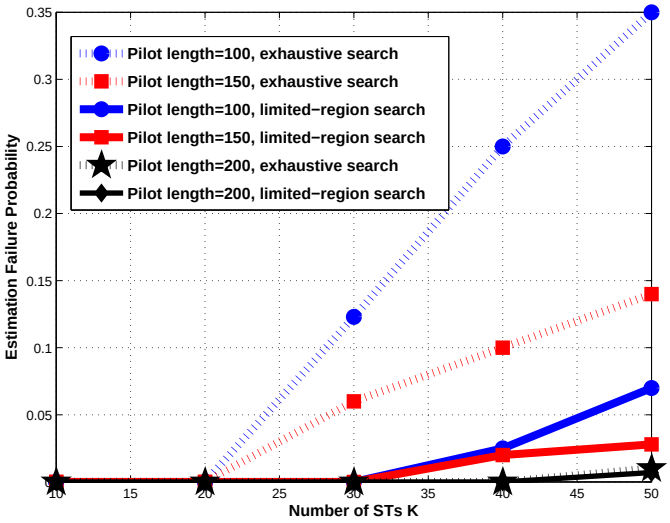

FIGURE 7.4 – Estimation failure probability versus number of STs with different pilot lengths and searching area. System settings : $Q = 30$, Noise= $-\infty$dBW

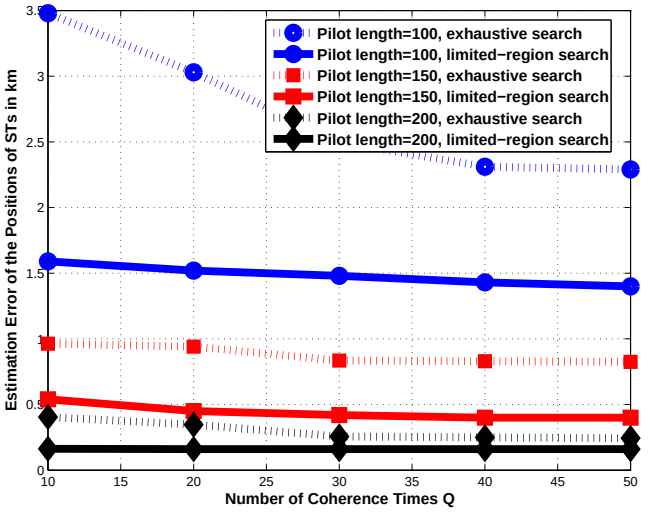

FIGURE 7.5 – Estimation error of the positions of STs versus number of coherence time intervals with different pilot lengths and searching area. System settings : $K = 40$, Noise= $-\infty$dBW

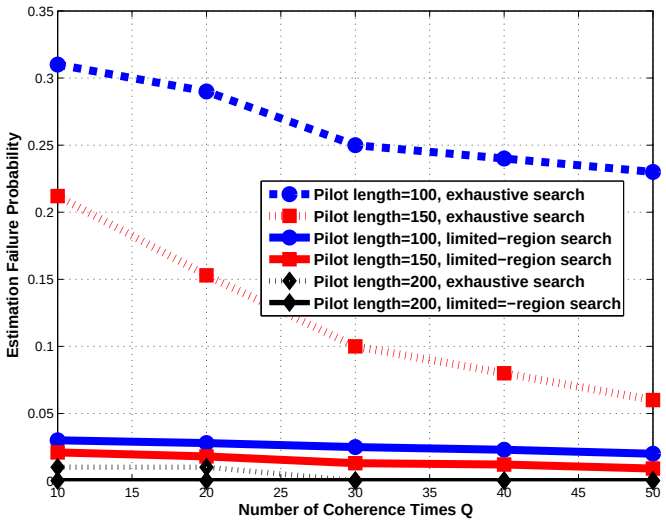

FIGURE 7.6 – Estimation failure probability versus number of coherence time intervals with different pilot lengths and searching area. System settings : $K = 40$, Noise= $-\infty$dBW

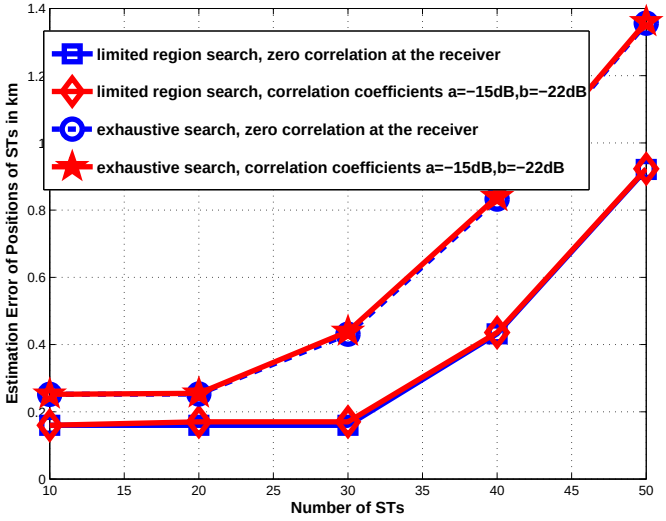

FIGURE 7.7 – Estimation error of the positions of STs expressed in km versus number of STs for different correlation coefficients at the receiver with different pilot lengths and searching area. System settings : Noise= $-\infty$dBW, $Q = 30$, pilot length=150

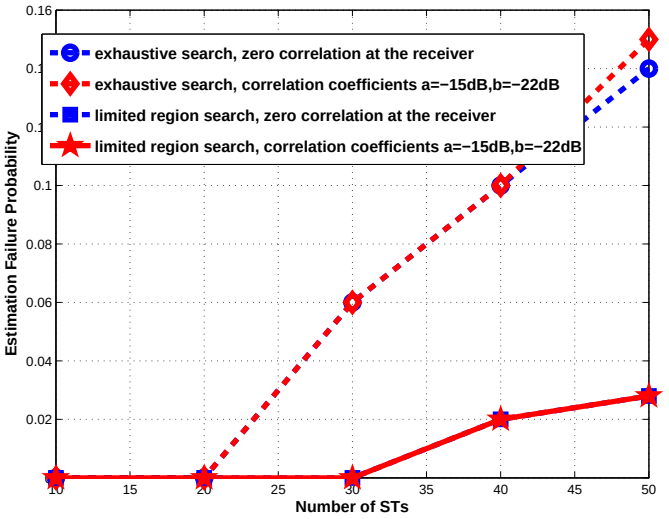

FIGURE 7.8 – Estimation failure probability versus number of STs for different correlation coefficients at the receiver with different pilot lengths and searching area. System settings : Noise= $-\infty$dBW, $Q = 30$, pilot length=150

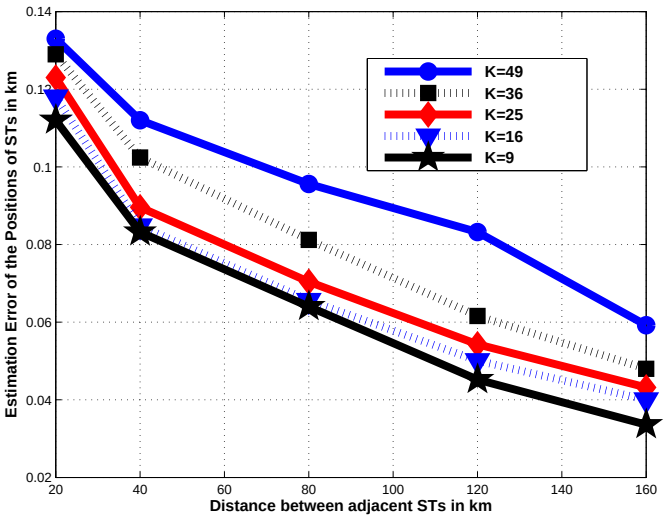

FIGURE 7.9 – Estimation error of the positions of STs expressed in km versus the distance between adjacent STs. System settings : $Q = 30$, Noise= $-\infty$dBW, pilot length=200, region-limited search

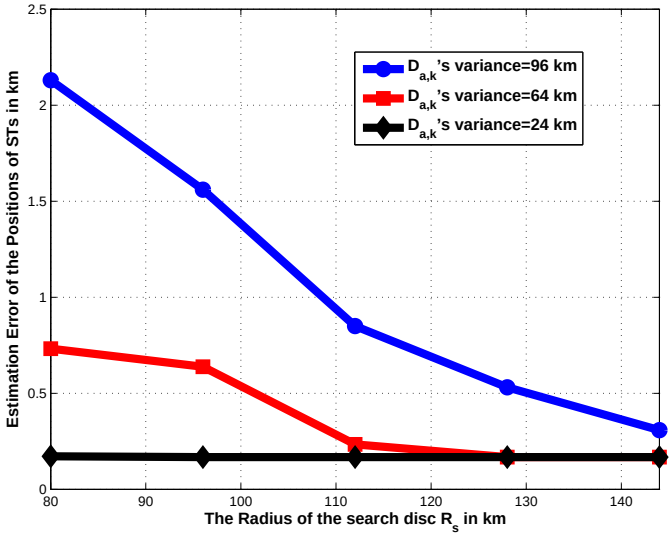

FIGURE 7.10 – Estimation error of the positions of STs expressed in km versus the length of the radius of the searching zone. System settings : $K = 40$,$Q = 30$, Noise= $-\infty$dBW, pilot length=200, region-limited search

7.4 Conclusions

In this chapter, we propose an algorithm, dubbled PLSE algorithm, to estimate the directivity vectors on the basis of a least squares error criterion. our algorithm does not require the estimation of nuisance parameters. Therefore, the complexity of this algorithm remains low.

We assess the performance of the proposed algorithm under two different assumptions : 1) the gateway does not use the prior knowledge of the area where ST is located and a whole map exhaustive search is required ; 2) the gateway uses the previous estimation and a limited-region search is performed. Numerical results show that for both cases, the proposed PLSE algorithm achieves good estimation of the positions and directivity vectors of STs. Moreover, limited-region search always outperforms the exhaustive search. Simulation results also suggest that in order to improve the performance of PLSE, we should increase the training length rather than increasing the number of coherence time intervals.

Chapter 8

Contention Resolution and Channel Estimation in Satellite Random Access Channels

The ST initiate their communications by sending a request of service to the gateway through a random access channel (RACH). In this chapter, we study the random access channel of a multi-beam SS with the twofold objectives of improving the throughput of the RACH and obtaining an initial estimation of the directivity vector of each new ST entering in the system. This latter estimation is relevant at a system level to provide essential information for the frequency allocation and to initialize the directivity estimation algorithm discussed in Chapter 7 for connection-oriented communications. More specifically, in this chapter, we extend the application of the PLSE algorithm proposed in Chapter 7 to a RACH scenario. In contrast to the scenario of a connection-oriented communication, in a RACH scenario, the gateway is not aware a prior of the number of STs sending a request of service, the training sequences they are using, and their approximative locations. Successive estimation of directivity vectors based on the PLSE algorithm will be used to discriminate STs adopting the same training sequences but located sufficiently far apart.

In this chapter, we assume universal frequency reuse and utilize the spatial diversity and strong directivity patterns of multi-antenna satellite to discriminate among colliding STs. In other words, diversity and directivity of the SA provide an unique "signature" to each ST that is exploited for multiuser detection, i.e. contention resolution. A fundamental step of this technique is the estimation of the unique signature of the directivity vector for each ST.

We propose two algorithms for the detection of transmitting STs, possible resolution of collisions and channel estimation, namely, Grid Reduction (GR) approach and Successive Channel Cancelation (SCC) approach. By using the strong directionality of the SA, the knowledge of the radiation diagram, we can estimate the

directivity vectors of the active STs. Then, based on this intermediate estimation and diversity in space, we estimate the instantaneous CSI. In the Grid Reduction approach, we estimate the STs sequentially. At each iteration, the estimation of the directivity vector for the ST of interest enables to narrow the searching area of the remaining undetected active STs. In the SCC approach, we estimate the channel realizations iteratively and remove the interference caused by the ST estimated in the current iteration. We evaluate the performance of the two approaches through numerical simulations. Compared to the conventional RACH system, both approaches provide significant improvements. Furthermore, SCC approach always outperforms the GR approach. The performance of the RACH are also compared to the one of connection oriented channel studied in [41].

This chapter is structured as follows. In Section 8.1, we present the state of the art and the existing contention-resolution methods in the RACH of a satellite system. In Section 8.2, we describe the system model adopted in this chapter. In Section 8.3, we describe our approaches to detect the active STs and estimate their instantaneous CSI. In Section 8.4, the performance of the proposed methods are assessed by numerical simulations. In Section 8.5, we make the conclusions.

8.1 State of the Art

The enhancement of the satellite random access channel is going to play a crucial role in the development and success of a modern Mobile Satellite System (SS). Already in current standards for interactive broadband networks, the RACH finds a wider utilization thanks to mechanisms that enable the transmission of short bursts and support capacity reservation for transmission of longer packets in the RACH. Additionally, in modern mobile SS, with interactive consumer-type STs, traffic aggregation at STs will be greatly reduced and the utilization of RACH will become even more frequent.

Nowadays, by exploiting some random access protocols, such as Slotted Aloha (S-Aloha) [6], [7] and its enhanced version Diversity Slotted Aloha, (DS-Aloha) [8], the current satellite standards for satellite communication network, namely, Digital Video Broadcasting Return Channel via Satellite (DVB-RCD) [42] and the Telecommunication Industry Association (TIA) IP over Satellite (IPoS) [43] enable the transmission of small packets through a S-Aloha random access contention channel.

Aloha was originally analyzed and implemented in the AlohaNet at the University of Hawaii in 1970. Slotted Aloha (S-Aloha) [6], [7] is a variant of Aloha, appeared later. It is currently widely utilized for TDMA satellite networks.

In the pure Aloha system, each terminal requires to transmit short packets at a random time. They transmit their packets bursts in a completely unsynchronized manner. However, as the number of terminals sharing the same channel increases, the probability of losing packets because of collisions also increase. Figure 8.1 shows an Aloha random access channel with two overlapping packets.

In order to improve the throughput of the Aloha random access channel, a synchronized time based scheme called Slotted Aloha was introduced later. In S-Aloha system, a sequence of slots are defined, each slot has the same duration as a packet transmission time. Each terminal can start transmission at the beginning of a slot. In S-Aloha system, if several packets overlap, they overlap completely with each other. S-Aloha scheme has a larger throughput compared with the pure Aloha

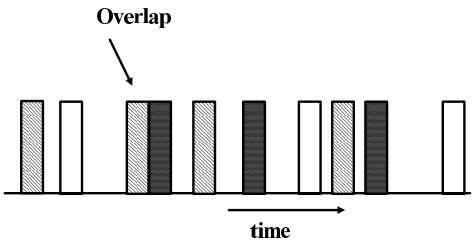

FIGURE 8.1 – Packets from several STs on an Aloha Channel

scheme under the same offered traffic. In both schemes, if a packet collides with the others, it has to be retransmitted again. This causes large transmission delay and decreases the system throughput.

Diversity Slotted Aloha is proposed in [8]. In this scheme, a terminal transmits multiple copies of the same packet. If one copy of a packet is correctly received, the receiver rejects all the other replicas. DS-Aloha outperforms S-Aloha in terms of delay performance when the traffic is light. DS-Aloha can be categorized into two types, namely, frequency DS-Aloha and time DS-Aloha. In frequency DS-Aloha scheme, multiple copies of the same packet are simultaneously transmitted on different frequency bands. In time DS-Aloha scheme, they are transmitted on a single high-speed channel but spaced apart by random time intervals. The interesting readers can refer to [8] for more details.

Although S-Aloha and DS-Aloha have been widely implemented in the current satellite networks, however, they offer quite poor throughput performance. This motivates the study of more efficient Aloha protocols. Recently, an improved version of S-Aloha and DS-Aloha dubbed Contention Resolution Diversity Slotted Aloha (CRDSA) was proposed in [44]. By utilizing CRDSA protocol, most of the packets contentions and burst collisions can be cleared up by iterative interference cancelation techniques. It outperforms greatly the classical S-Aloha and DS-Aloha in term of throughput. Furthermore, it also decreases the packet loss ratio and reduces the delay of packet transmission versus the traffic of the channel.

Similar with DS-Aloha, the CRDSA protocol generates two replicas for the same packet. The two identical packets are referred as "twin" bursts. The twin bursts carry the same preamble and payload information, they are sent in two randomly selected slots within the same time frame. The preamble contains information about the slot position of the corresponding twin burst. Additionally, each burst signalling information points to its twin location.

The basic idea of CRDSA is that, if a packet is successfully transmitted, then the information signalling carried by it can be exploited and cancel the interference that is caused by its twin burst in another slot. Therefore, the packets transmitted by other STs can be recovered. This interference cancelation is performed iteratively until most of the frame packets that were originally lost because of collisions are recoverd.

Both simulated and analytical results show that the CRDSA provides great improvements compared to S-Aloha and DS-Aloha in terms of throughput and packet loss ratio. In [45], the performance of CRDSA scheme is analyzed and optimized.

Additionally, some satellite protocols, for example, Demand Assignment Multiple Access (DAMA) [46] provides a capacity reservation mechanism for longer

packets transmission. However, they cannot be implemented for the transmission of short bursts since the response time for DAMA is too long.

In a terrestrial RACH, Carrier Sense Multiple Access (CSMA) [47] protocols can be performed to avoid contentions. Unfortunately, they can not be implemented in satellite networks since the channel sensing is not feasible. Therefore, the carrier sensing mechanism does not fit in the frame of this work.

All the above mentioned techniques improve the performance of the RACH by modifying the multiple access channel (MAC) layer. We are not aware of the previous work that exploits the properties of the physical layer to improve the RACH throughput.

In this Chapter, we attack this problem. In the following sections, we present the techniques that can be implemented in the physical layer to improve the RACH throughput. The techniques applied at the physical layer are also complementary to the mentioned techniques at MAC layer and could coexist.

8.2 System Model

In this work, we consider a satellite system consisting of a gateway, a bent-pipe satellite equipped with N SAs, and STs endowed with R antennas. All the antennas transmit in left and right polarizations. We focus on a random access channel. An ALOHA protocol with synchronized transmissions is assumed. The STs that want to transmit, initiate the transmission at the beginning of a certain slot and the signals are received synchronously at the gateway. During each slot, each ST transmits Q packets frames. In general, the duration of a slot transmission is longer than the coherence time of the channel while a packet duration is shorter. The gateway is oblivious of the number K of STs actually transmitting. Furthermore, the gateway is oblivious of the area where the transmitting STs are located.

The STs share a training sequence set $\mathbb{X}$. The set $\mathbb{X}$ is partitioned into U groups. Each group consists of $2R$ different training sequences and the partition is known to the gateway. ST k selects randomly one group and transmit $2R$ training sequences, one for each antenna and polarization. The gateway is also oblivious of the specific training sequences chosen by the STs.

In this chapter, we adopt the same channel model and notation adopted in Chapter 7. For the sake of completeness, we define it again here. Further discussions on the underlying assumptions for the system model can be found in Chapter 7.

The discrete-time baseband received signal at the gateway at time t during the transmission of frame q is given by

$$\boldsymbol{y}[t] = \boldsymbol{D}\boldsymbol{P}^{(c)}(q)\boldsymbol{x}[t] + \boldsymbol{z}[t]. \tag{8.1}$$

The definition of $\boldsymbol{y}[t]$, $\boldsymbol{D}$, $\boldsymbol{x}[t]$ and $\boldsymbol{z}[t]$ is already given in Chapter 7. $\boldsymbol{P}^{(c)}(q)$ accounts for the propagation matrix and correlation matrix, it is constant in frame q.

Matrix $\boldsymbol{P}^{(c)}(q)$ is a block diagonal matrix with K independent blocks $\boldsymbol{P}^{k}(q)$ of size $2 \times 2R$ and form

$$\boldsymbol{P}^{k}(q) = \begin{pmatrix} P_{k,r}^{(1)}(q) & 0 & \cdots & P_{k,r}^{(R)}(q) & 0 \\ 0 & P_{k,l}^{(1)}(q) & \cdots & 0 & P_{k,l}^{(R)}(q) \end{pmatrix},$$

Directivity matrix $\boldsymbol{D}$ can conveniently be structured in KN blocks $\boldsymbol{D}^{k}$ already

defined in Section 7.1. Furthermore, the directivity column block $\boldsymbol{D}^k$ of ST k is given by convex combination of the directivity column vectors with identical coefficients

$$\boldsymbol{D}^k = \alpha_1^k \boldsymbol{G}^{\tau(1)} + \alpha_2^k \boldsymbol{G}^{\tau(2)} + \alpha_3^k \boldsymbol{G}^{\tau(3)}, \tag{8.2}$$

where $0 \leq \alpha_i^k \leq 1$, and $\sum \alpha_i^k = 1$. The definition of $\boldsymbol{G}$ and α_i follows the definition given in Section 7.1.

The STs' detection and corresponding channel estimation are based on the synchronous transmissions of training sequences of length L by all active STs. The signal received at the n-th SA in o-polarization, with $\{o\} \in \{l, r\}$, is given by

$$y_{n,o}[s_q + s] = \boldsymbol{d}_{n,o} \boldsymbol{P}(q) \boldsymbol{x}[s_q + s] + z_{n,o}[s_q + s], \tag{8.3}$$

where s_q is the time offset when the transmission of a training sequences for the q-th frame starts and $s = 0, \ldots, L-1$ is a time index. The received signal $\mathbb{y}_{n,o}(q) = (y_{n,o}[s_q], y_{n,o}[s_q + 1], \ldots, y_{n,o}[s_q + L - 1])$ corresponding to training sequences of the q-th frame at the n-th SA and o-polarization is given by

$$\mathbb{y}_{n,o}(q) = \boldsymbol{d}_{n,o} \boldsymbol{P}(q) \boldsymbol{X}_q + \mathbb{z}_{n,o}(q) \tag{8.4}$$

where $\boldsymbol{X}_q$ is the $2RK \times L$ matrix whose rows are the training sequences of the active STs and $\mathbb{z}_{n,o}(q)$ is the L-dimensional row vector of the noise $\mathbb{z}_{n,o}(q) = (z_{n,o}[s_q], z_{n,o}[s_q + 1], \ldots, z_{n,o}[s_q + L - 1])$.

8.3 Detection of active STS and Multi-STs Channel Estimation

In this section, we describe our approaches to detect the active STs and estimate their instantaneous CSI. They consist of three steps. In the first step, we detect the training sequence groups that have been used by the STs. In the second step, we estimate the sum of the channel coefficients of all the STs employing the same training sequence group. The final step resolves contention among different STs using the same training sequence by estimating the channel coefficients of some or all the colliding STs.

8.3.1 Training Sequences Detection

The approach adopted to detect the training sequences is based on the correlation between the received signal at the gateway and the U groups of training sequences. The algorithm is summarized in Algorithm 5.

We denote the number of groups of training sequence transmitted at least by one ST as W. Furthermore, we denote the number of STs that use the w-th detected group as K_w and by $\mathfrak{X}_w$ the $2R \times L$ matrix whose rows are the training sequences of group w. In the proposed algorithm, the group w is detected as transmitted if the correlation of $\mathfrak{X}_w$ with the received signal is above a certain threshold. It is worth noticing that after the detection of training sequences, the gateway is still oblivious of K_w, the number of STs transmitting group w.

```
Set threshold ζ
for u = 1, ..., U do
    for q = 1, ..., Q do
        for n = 1, ..., N do
            Calculate c_{u,q,n} = ‖ 𝔛_u 𝔶_n(q)^H ‖^2
        end
        c_{u,q} = max_n c_{u,q,n}
    end
    if Σ_{q=1}^{Q} c_{u,q} > ζ then
        𝔛_u is utilized by at least one ST
    end
end
```

Algorithm 5: Estimation of utilized trainings

8.3.2 LSE Estimation of Transfer Matrix

Let us introduce $\boldsymbol{h}^k_{n,r}(q)$ and $\boldsymbol{h}^k_{n,l}(q)$. They are the transfer vectors in left and right polarizations from the k-th ST to the n-th SA. They are defined as

$$\begin{aligned}\boldsymbol{h}^k_{n,r}(q) &= \left(h^{k,(1)}_{n,rr}(q),\, h^{k,(1)}_{n,rl}(q), \cdots,\, h^{k,(R)}_{n,rr}(q),\, h^{k,(R)}_{n,rl}(q)\right)\\ &= \left(d^k_{n,rr}P^{(1)}_{k,r}(q),\, d^k_{n,rl}P^{(1)}_{k,l}(q), \cdots,\, d^k_{n,rr}P^{(R)}_{k,r}(q),\, d^k_{n,rl}P^{(R)}_{k,l}(q)\right)\end{aligned} \tag{8.5}$$

and

$$\begin{aligned}\boldsymbol{h}^k_{n,l}(q) &= \left(h^{k,(1)}_{n,lr}(q),\, h^{k,(1)}_{n,ll}(q), \cdots,\, h^{k,(R)}_{n,lr}(q),\, h^{k,(R)}_{n,ll}(q)\right)\\ &= \left(d^k_{n,lr}P^{(1)}_{k,r}(q),\, d^k_{n,ll}P^{(1)}_{k,l}(q), \cdots,\, d^k_{n,lr}P^{(R)}_{k,r}(q),\, d^k_{n,ll}P^{(R)}_{k,l}(q)\right).\end{aligned} \tag{8.6}$$

Let

$$\mathfrak{h}^w_{n,o} = \sum_{k\in\Pi_w} \boldsymbol{h}^k_{n,o}(q) \qquad \{o\} \in \{r,l\},$$

where Π_w denotes the set of indices corresponding to STs transmitting the training sequence group w. Then, the received signal corresponding to training sequence transmitted in the q-th frame can be written as

$$\mathfrak{y}_{n,o}(q) = \sum_{w=1}^{W} \mathfrak{h}^w_{n,o}(q)\mathfrak{X}_w + \mathfrak{Z}_{n,o}(q). \tag{8.7}$$

By applying standard results on linear LSE (see e.g. [36]), we obtain the LSE estimation of $\mathfrak{h}^w_{n,o}(q)$ given by

$$\hat{\mathfrak{h}}^w_{n,o}(q) = \mathfrak{y}_{n,o}\mathfrak{X}^H_w(\boldsymbol{X}_q\boldsymbol{X}^H_q)^{-1}, \qquad \{o\} \in \{r,l\}. \tag{8.8}$$

The corresponding estimation error is $\boldsymbol{\varepsilon}_{n,o}(q) = \hat{\mathfrak{h}}^w_{n,o}(q) - \mathfrak{h}^w_{n,o}(q)$, $\{o\} \in \{r,l\}$.

8.3.3 Contention resolution and multiuser channel estimation

Our multi-ST channel estimation is based on the following system of equations obtained from (8.5) and (8.6), the definition of the estimation error, and by utilizing the assumptions $d^k_{n,ll} = d^k_{n,rr}$ and $d^k_{n,lr} = d^k_{n,rl}$

$$\begin{cases} \sum_{k\in\Pi_w} d^k_{n,rr} P^{(1)}_{k,r}(q) &= \hat{\mathfrak{h}}^{w,(1)}_{n,rr}(q) + \varepsilon^{w,(1)}_{n,rr}(q) \\ \sum_{k\in\Pi_w} d^k_{n,lr} P^{(1)}_{k,r}(q) &= \hat{\mathfrak{h}}^{w,(1)}_{n,lr}(q) + \varepsilon^{w,(1)}_{n,lr}(q) \\ \sum_{k\in\Pi_w} d^k_{n,rr} P^{(1)}_{k,l}(q) &= \hat{\mathfrak{h}}^{w,(1)}_{n,ll}(q) + \varepsilon^{w,(1)}_{n,ll}(q) \\ \sum_{k\in\Pi_w} d^k_{n,rl} P^{(1)}_{k,l}(q) &= \hat{\mathfrak{h}}^{w,(1)}_{n,rl}(q) + \varepsilon^{w,(1)}_{n,rl}(q) \\ &\vdots \\ \sum_{k\in\Pi_w} d^k_{n,rr} P^{(R)}_{k,l}(q) &= \hat{\mathfrak{h}}^{w,(R)}_{n,ll}(q) + \varepsilon^{w,(R)}_{n,ll}(q) \\ \sum_{k\in\Pi_w} d^k_{n,rl} P^{(R)}_{k,l}(q) &= \hat{\mathfrak{h}}^{w,(R)}_{n,rl}(q) + \varepsilon^{w,(R)}_{n,rl}(q) \end{cases} \tag{8.9}$$

where the indices of the components of the estimation $\hat{\mathfrak{h}}^{w}_{n,o}(q)$ and the estimation error vector $\boldsymbol{\varepsilon}^{w}_{n,o}(q)$ are defined consistently with the ones of vector $\boldsymbol{h}^k_{n,o}(q)$ in (8.5) and (8.6). If we had known the directivity vectors of the active STs, the channel estimation would have reduced to a standard linear multiuser channel estimation. However, the gateway does not know neither the directivity vectors nor the number of colliding STs.

Let us denote by $\mathcal{T}$ the set of all adjacent triplets τ on the reference grid and let τ_i denotes the index of the directivity block column of the i-th element of τ in the matrix $\boldsymbol{G}$. If the active ST k^* is located in the triangle identified by the triplet of points τ^*, we can obtain an estimation of $\boldsymbol{D}^{k^*}$ and $\boldsymbol{P}^{k^*}$ by minimum norm-two fitting. This problem has been investigated in the case when the set Π_w is a singleton in Chapter 7 and its application to this problem is straightforward if we consider the remaining ST channels as noise.

In the case of a singleton Π_w, we can perform channel estimation by exhaustive search over $\mathcal{T}$ and selects the triplet for which $f(\boldsymbol{\alpha}, \tau; \hat{\mathfrak{h}}^{w}_{r}(0), ..., \hat{\mathfrak{h}}^{w}_{l}(Q-1))$ defined in Algorithm 3 is maximum. In the case of multiple elements Π_w, we are interested in determining all the local maxima of the piecewise function $f(\boldsymbol{\alpha}, \tau; \hat{\mathfrak{h}}^{w}_{r}(0), ..., \hat{\mathfrak{h}}^{w}_{l}(Q-1))$ obtained by considering all possible triplets in $\mathcal{T}$. In order to solve this problem, we benefit from the additive nature of the transmitted signals and the strong directionality of the SAs to propose two heuristic approaches.

Successive Channel Cancelation (SCC) Approach : The rational behind SCC approach is to iterate over the channel estimation and the subsequent cancelation of the corresponding signal contribution from the received signal.

Let $\mathfrak{y}^{(0)}_{n,o}(q) = \mathfrak{y}_{n,o}(q)$. At iteration j, we estimate the sum of the channels of the colliding STs that have not been detected yet by applying

$$\hat{\mathfrak{h}}^{w}_{n,o}(q; j) = \mathfrak{y}^{(j-1)}_{n,o} \mathcal{X}^H_w (\boldsymbol{X}_q \boldsymbol{X}^H_q)^{(-1)}, \quad \{o\} \in \{r, l\}. \tag{8.10}$$

Then, we determine the triplet $\tau \in \mathcal{T}$ and the vector $\boldsymbol{\alpha}$ solving the optimization problem

$$\begin{aligned} \textbf{maximize} \quad & f^{(j)}(\boldsymbol{\alpha}, \tau; \hat{\mathfrak{h}}_r^{w}(0;j), \hat{\mathfrak{h}}_l^{w}(0;j), ..., \hat{\mathfrak{h}}_l^{w}(Q-1;j)) \\ & = \frac{\boldsymbol{\alpha}^T \mathfrak{Re}(\boldsymbol{\Theta}(\tau, \hat{\mathfrak{h}}_r^{w}(0;j), ..., \hat{\mathfrak{h}}_l^{w}(Q-1;j)))\boldsymbol{\alpha}}{\boldsymbol{\alpha}^T \mathfrak{Re}(\boldsymbol{\Gamma}(\tau))\boldsymbol{\alpha}} \\ \textbf{subject to} \ & \textstyle\sum_{i=1}^{3} \alpha_i = 1 \quad 0 \leq \alpha_i \leq 1, \qquad i = 1,2,3 \quad \textbf{Problem } \mathbf{P}_2 \end{aligned}$$

where $\boldsymbol{\Theta}(\tau, \hat{\mathfrak{h}}_r^{w}(0;j), ..., \hat{\mathfrak{h}}_l^{w}(Q-1;j))$ and $\boldsymbol{\Gamma}(\tau)$ are 3×3 matrices defined as :

$$\begin{aligned} & \boldsymbol{\Theta}(\tau^j, \hat{\mathfrak{h}}_r^{w}(0;j), ..., \hat{\mathfrak{h}}_l^{w}(Q-1;j)) \\ & = \widetilde{\boldsymbol{G}}^{\tau,k,H} \Big(\sum_{q=0}^{Q-1} \sum_{\ell=1}^{R} (\hat{\mathfrak{h}}_r^{w,(\ell)}(q;j) \hat{\mathfrak{h}}_r^{w,(\ell)H}(q;j) + \hat{\mathfrak{h}}_l^{w,(\ell)}(q;j) \hat{\mathfrak{h}}_l^{w,(\ell)H}(q;j))) \widetilde{\boldsymbol{G}}^{\tau,k}, \end{aligned} \tag{8.11}$$

$$\boldsymbol{\Gamma}(\tau) = \widetilde{\boldsymbol{G}}^{\tau,k,H} \widetilde{\boldsymbol{G}}^{\tau,k}, \tag{8.12}$$

$\widetilde{\boldsymbol{G}}^{\tau,k}$ is as in Algorithm 3. The optimum values of τ and $\boldsymbol{\alpha}$ enable the estimation of the channel along the same lines as in Algorithm 3, equations (8.14), (8.15) and (8.16). Let us denote by $\hat{\mathfrak{h}}_{n,o}^{w,(j)}$, $o \in \{r, l\}$, the estimation of the channel at step j. SCC approach removes from the signal $\mathfrak{y}_{n,o}^{(j-1)}(q)$ the contribution from the detected ST to obtain

$$\mathfrak{y}_{n,o}^{(j)}(q) = \mathfrak{y}_{n,o}^{(j-1)}(q) - \hat{\mathfrak{h}}_{n,o}^{w,(j)} \mathfrak{X}_w. \tag{8.13}$$

The algorithm terminates if the channel estimate $\hat{\mathfrak{h}}_{n,o}^{w,(j)}$ does not yield to a correct decoding of the transmitted information.

SCC approach is detailed in Algorithm 6.

Grid Reduction (GR) Approach : As in Chapter 7, we compare the maximum of $f(\boldsymbol{\alpha}, \tau; \hat{\mathfrak{h}}_r^{w}(0), ..., \hat{\mathfrak{h}}_l^{w}(Q-1))$ over all triplets τ in $\mathcal{T}$ and then select the triplet yielding the maximum $f(\boldsymbol{\alpha}, \tau; \hat{\mathfrak{h}}_r^{w}(0), ..., \hat{\mathfrak{h}}_l^{w}(Q-1))$. The maximizer of $f(\boldsymbol{\alpha}, \tau; \hat{\mathfrak{h}}_r^{w}(0), ..., \hat{\mathfrak{h}}_l^{w}(Q-1))$ determines the estimation of the ST channel. If the channel estimation enables a successful decoding of the detected ST, we remove from $\mathcal{T}$ all the triplets containing reference points whose directivity vector have high correlation with the estimated directivity vector and we obtain a reduced set $\mathcal{T}^{(1)}$. In the following steps, we iterative along similar lines but we adopt more and more reduced sets $\mathcal{T}^{(j)}$. The algorithm terminates when the obtained channel estimation does not allow a successful decoding. GR approach is detailed in Algorithm 7.

Set w.
Set threshold η.
Set $j = 0$.
for $q = 1, ..., Q$ **do**
    Calculate $\hat{\mathfrak{h}}^{w}_{n,o}(q)$, $\{o\} \in \{r, l\}$ according to (8.8).
    Set $\hat{\mathfrak{h}}^{w}_{n,o}(q;0) = \hat{\mathfrak{h}}^{w}_{n,o}(q)$.
end
Solve Problem P_2 and determine the maximizer $(\boldsymbol{\alpha}_0^*, \tau_0^*)$,
Determine directivity vector $\boldsymbol{D}^{k^*}$ of the given ST corresponding to the optimum triplet τ_0^* and optimum $\boldsymbol{\alpha}_0^*$ by applying (8.15) ;
Calculate $\hat{P}^{(\ell)}_{k,o}(q;0)$ according to (8.14) ;
Calculate $\hat{\boldsymbol{H}}^{k^*}$ according to (8.16) ;
Calculate $\mathfrak{y}^{(j)}_{n,o}(q)$ according to (8.13) ;
Check if ST k^* can be successfully decoded ;
$j = j + 1$.
while *ST is successfully decoded* **do**
    Solve Problem P_2 and determine the maximizer $(\boldsymbol{\alpha}_j^*, \tau_j^*)$,
    Determine directivity vector $\boldsymbol{D}^{k^*}$ of a ST corresponding to the optimum triplet τ_j^* and optimum $\boldsymbol{\alpha}_j^*$ by applying (8.15) ;
    Calculate $\hat{P}^{(\ell)}_{k,o}(q;j)$ according to (8.14) ;
    Calculate $\hat{\boldsymbol{H}}^{k^*}$ according to (8.16) ;
    Calculate $\mathfrak{y}^{(j)}_{n,o}(q)$ according to (8.13) ;
    Check if ST k^* can be successfully decoded ;
    $j = j + 1$.
end

Algorithm 6: SCC estimation for contention resolution and multiuser channel estimation

Set w.
Set threshold η.
Set threshold ϕ.
Set $j = 0$.
Set $\mathcal{T}^{(0)} = \mathcal{T}$.
for $q = 1, ..., Q$ **do**
  Calculate $\hat{\mathfrak{h}}^{w}_{n,o}(q)$, $\{o\} \in \{r, l\}$ according to (8.8).
end
Solve Problem P_2 over the set $\mathcal{T}^{(0)}$ and determine the maximizer $(\boldsymbol{\alpha}^*_0, \tau^*_0)$,
Determine

$$\hat{P}^{(\ell)}_{k^*,o}(q) = \frac{\boldsymbol{\alpha}^{k^*T} \widetilde{\boldsymbol{G}}^{\tau,k,H} \hat{\mathfrak{h}}^{w,(\ell)}_{o}(q)}{\boldsymbol{\alpha}^{k^*T} \widetilde{\boldsymbol{G}}^{\tau,k,H} \widetilde{\boldsymbol{G}}^{\tau,k} \boldsymbol{\alpha}^{k^*}}, \quad \{o\} \in \{r, l\} \quad \text{and} \quad \forall q = 0, .., Q-1. \tag{8.14}$$

Determine the directivity vector $\boldsymbol{D}^{k^*}$ by applying

$$\hat{\boldsymbol{D}}^{k^*} = \sum_{i=1}^{3} \alpha^{k^*}_i \boldsymbol{G}^{\tau_i}. \tag{8.15}$$

Determine the channel estimation $\boldsymbol{H}^{k^*}$ by applying

$$\hat{\boldsymbol{H}}^{k^*} = \hat{\boldsymbol{D}}^{k^*} \hat{\boldsymbol{P}}^{k^*}(q), \tag{8.16}$$

with

$$\hat{\boldsymbol{P}}^{k^*}(q) = \begin{pmatrix} \hat{P}^{(1)}_{k^*,r}(q) & 0 & \cdots & \hat{P}^{(R)}_{k^*,r}(q) & 0 \\ 0 & \hat{P}^{(1)}_{k^*,l}(q) & \cdots & 0 & \hat{P}^{(R)}_{k^*,l}(q) \end{pmatrix}.$$

Check if ST k^* can be successfully decoded.
while *ST k^* is successfully decoded* **do**
  Remove from $\mathcal{T}^j$ all the triplets τ such that the directivity vector of a reference point τ_i has the correlation with the directivity vector $\boldsymbol{D}^{k^*}$ higher than ϕ to obtain $\mathcal{T}^{(j+1)}$;
  Solve Problem P_2 over the set $\mathcal{T}^{(j+1)}$ and determine the maximizer $(\boldsymbol{\alpha}^*_j, \tau^*_j)$,
  Determine the directivity vector $\boldsymbol{D}^{k^*}$ by applying (8.15).
  Determine the channel estimation $\boldsymbol{H}^{k^*}$ by applying (8.16).
  Check if ST k^* can be successfully decoded.
  $j = j + 1$.
end

Algorithm 7: GR Approach for contention resolution and multiuser channel estimation

8.4 Numerical Results

In this section, we analyze the performance of the two proposed approaches through numerical simulations. The simulations are performed for STs equipped with two antennas ($R = 2$). The satellite is endowed with $N = 163$ SAs. The power of the transmit signals is set to 0dBW. We assume the thermal noise is absent and only co-channel interference is present. The number of transmitted frames Q is 50. The positions of the STs are generated randomly and uniformly in a rectangular region covering most of Europe. The results are obtained by averaging over 20 system realizations, i.e., 20 different groups of STs randomly generated. The pilot sequence length is either 160 or 200. We consider two types of training sequences in the simulations : 1) random QPSK training sequences. In this case, the training sequences set is always partitioned into 50 groups ; 2) orthogonal training sequences. In this case, the training sequence set is partitioned into 40 and 50 groups for training lengths 160 and 200, respectively.

The perspective of this work is substantially different from other works [44] [6] [7] [8] [9] [10] that improve the throughput of the RACH by proper design of the MAC layer. The proposed approaches modify the physical layer but are independent from the MAC layer. Then, to keep the analysis independent of a specific MAC protocol, the performance metrics that we use are necessarily different from the standard metrics utilized for the analysis of MAC protocols : throughput and offered channel traffic. Additionally, the comparison of the proposed approaches with standard MAC protocols for MAC is further exacerbated by the fact that we consider here a network and exploit its spatial and user diversity while the methods in [6], [7], [8], [9], [10], [45] consider a single receiver.

The relevant metrics in this work are the estimation failure probability and the normalized estimation error. The event that the gateway fails to detect an active ST is referred to as 'estimation failure'. As metric to assess the performance of the instantaneous CSI estimation, we adopt the average ratio between the norm of the estimation error and the norm of the exact channel, i.e, $\xi = \mathbb{E}_k \left(\frac{\|\boldsymbol{\varepsilon}_{\boldsymbol{H}_k}\|^2}{\|\boldsymbol{H}_k\|^2} \right)$, where $\boldsymbol{\varepsilon}_{\boldsymbol{H}_k} = \boldsymbol{H}_k - \hat{\boldsymbol{H}}_k$.

As benchmark system, we consider a conventional RACH system with fixed beamforming. In the conventional RACH system, we assume that four frequency bands are available. Each band supports 40 fixed beams isolated by frequency reuse.

The impact of the number of active STs on the proposed estimation approaches is shown in terms of estimation failure probability in Figure 8.2, in terms of estimation error in positions in Figure 8.3 and in terms of estimation error in instantaneous CSI in Figure 8.4. The estimation failure probability of the two proposed approaches is much lower than the conventional benchmark with obvious gain in serving a higher number of STs. Figure 8.2 also indicates that for each type of training sequences, the SCC approach always outperforms the GR approach. As expected, the use of orthogonal training sequences is beneficial when compared to the use of randomly generated training sequences [1].

1. The use of orthogonal training implies an ideal system completely synchronized, since asynchronism destroy orthogonality. On the contrary, random generated training sequences do not suffer from this effect and offer a bound to the performance loss due to lack of synchronism/orthogonality. Techniques to limit the performance degradation due to asynchronism are known. However, the analysis of this aspect exceeds the scope of this work.

Figure 8.4 and Figure 8.3 show a trend similar to the one in Figure 8.2. Furthermore, the performance of the RACH is compared to the one of the connection oriented channel studied in Section 7.2. From Figure 8.2, the performance loss due to collisions in the RACH is apparent.

The impact of assuming that the correlation coefficients a, b are negligible are also studied. We compare the case when a and b are both zero to the case where $a = -15$dB, and $b = -22$dB. We evaluate the system performance in terms of estimation failure probability in Figure 8.5 and in terms of estimation error of positions in Figure 8.6. Figure 8.5 shows that for the two cases, the estimation failure probability coincides and Figure 8.6 indicates that of a and b are different from zeros, the estimation error increases slightly. However, the difference is very limited. Therefore, we can conclude that the effect of neglecting coupling among antennas and cross-polarization is very minor.

The impact of different training sequences and training length on the SCC approach is analyzed in Figure 8.7, Figure 8.8, and 8.9. It is worth noticing that when K STs are transmitting, the channel consists of $2RK = 4K$ links and all of them have to be estimated. Figure 8.7 shows that, if random QPSK training is adopted, the estimation failure probability grows rapidly as the number of STs increases and approaches the number of different training groups. On the contrary, if we adopt orthogonal training sequences, the SCC approach still can provide good estimation performance in similar conditions. A similar trend is also shown in Figure 8.9.

Finally, we study the impact of the distance between adjacent STs on the SCC approach. We generate the STs' positions on a square grid. Each ST has the same distance from its adjacent ST. Figure 8.10 shows the impact of the distance between adjacent STs in terms of the norm of instantaneous CSI estimation error. As expected, when the distance between adjacent STs increases, SCC approach achieves better performance and the norm of instantaneous CSI estimation error decreases. Note that Figure 8.10 cannot be compared with the simulation results obtained in Figure 8.4, since the positions of the STs are generated in a much smaller area and the interference among the active STs is larger.

8.5 Conclusions

In this chapter, we proposed two algorithms, namely, the SCC and GR algorithms, for detection of transmitting STs, resolution of collisions, and channel estimation. We show that both approaches outperform greatly the conventional fixed beamforming system in terms of estimation failure probability. Therefore, they can increase significantly the system capacity in term of serving number of STs. Additionally, both algorithms can achieve very good performance of detecting active STs and channel estimation. The numerical simulations show that SCC algorithm always outperforms the GR algorithm. Moreover, they indicate that, in order to improve the accuracy of channel estimation, we can adopt orthogonal signals (however, they imply strict constraints for synchronization) or we can increase the training length.

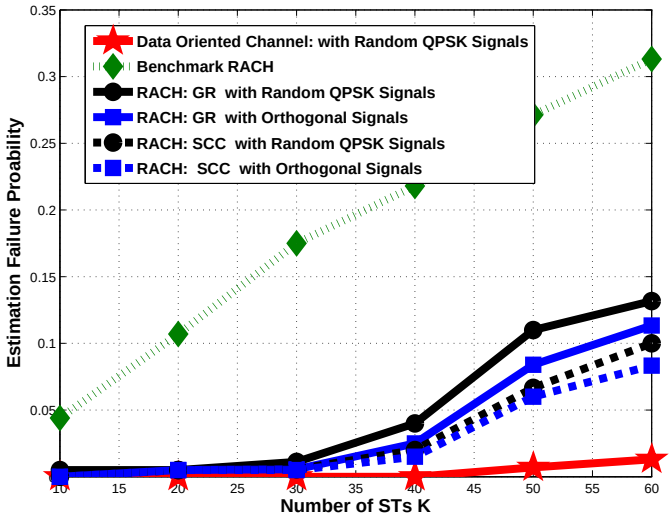

FIGURE 8.2 – Estimation failure probability versus varying number of STs with different types of training sequences. System settings : $Q = 50$, Noise=$-\infty$dBW, training length= 200, $U = 50$

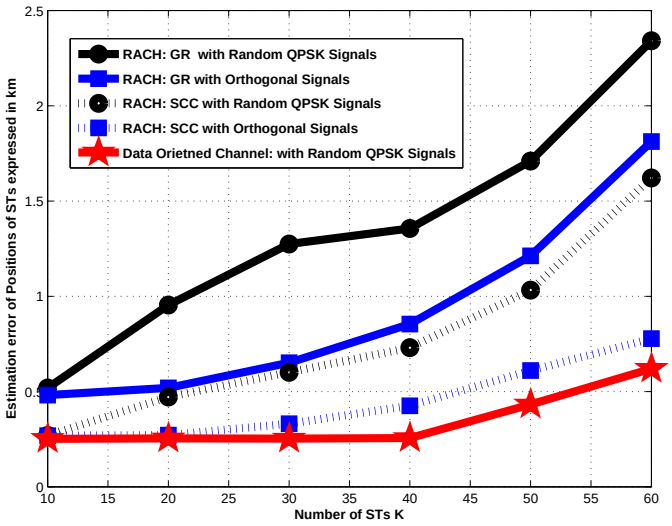

FIGURE 8.3 – Estimation error of ST's positions versus varying number of STs with different types of training sequences. System settings : $Q = 50$, Noise=$-\infty$dBW, training length= 200, $U = 50$

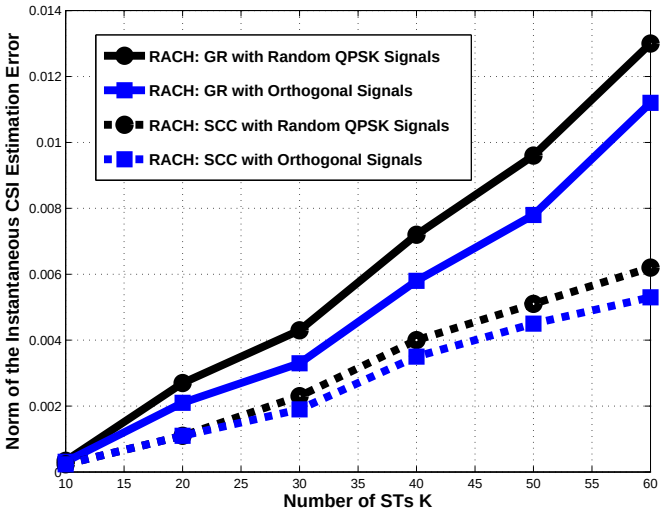

FIGURE 8.4 – Estimation error norm of instantaneous CSI versus varying number of STs with different types of training sequences. System settings : Q=50, Noise=$-\infty$dBW, training length= 200, U=50

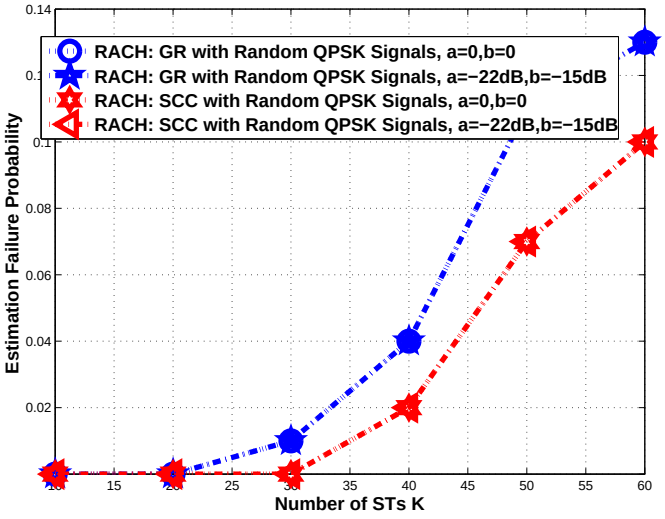

FIGURE 8.5 – Estimation failure probability versus varying number of STs with different values of correlation coefficients a and b. System settings : $Q = 50$, Noise=$-\infty$dBW, training length= 200, $U = 50$

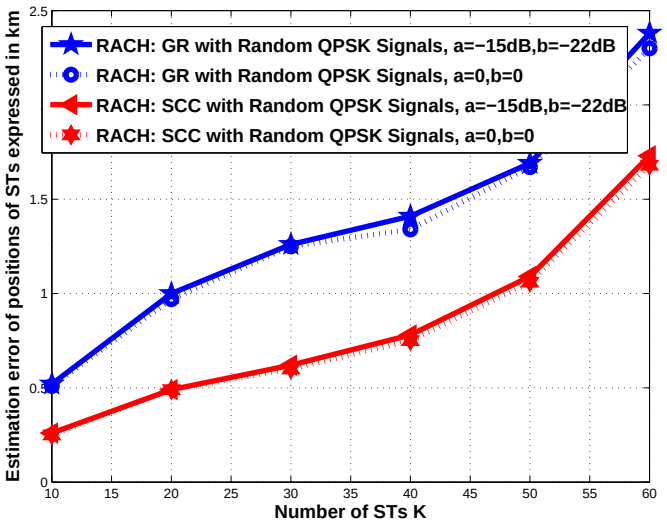

FIGURE 8.6 – Estimation error of ST's positions versus varying number of STs with different values of correlation coefficients a and b. System settings : $Q = 50$, Noise=$-\infty$dBW, training length= 200, $U = 50$

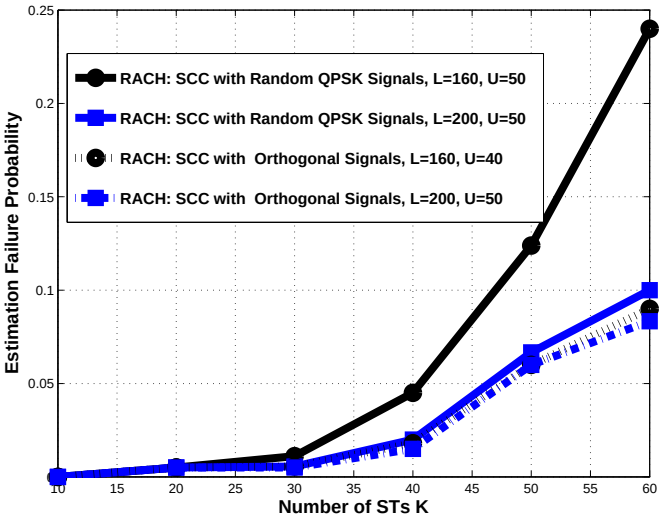

FIGURE 8.7 – Estimation failure probability versus varying number of STs with different types of training sequences for SCC approach. System settings : $Q = 50$, Noise=$-\infty$dBW

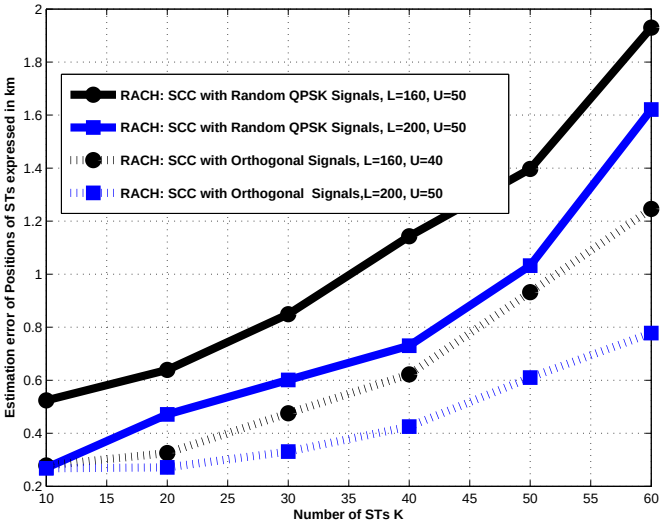

FIGURE 8.8 – Estimation error of ST's positions versus varying number of STs with different types of training sequences for SCC approach. System settings : $Q = 50$, Noise$=-\infty$dBW

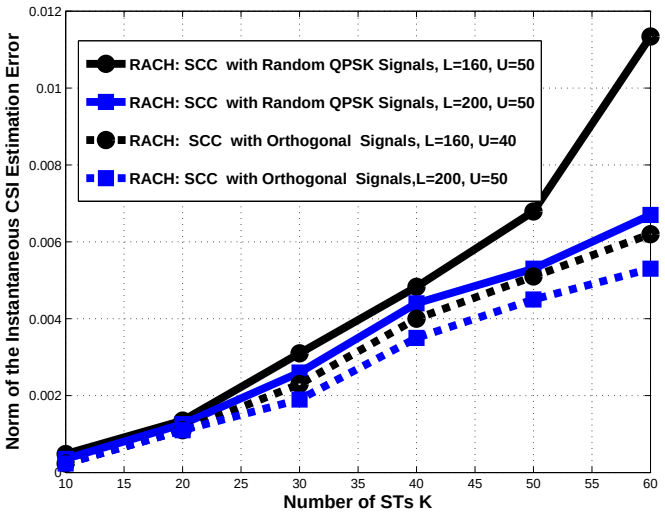

FIGURE 8.9 – Estimation error of instantaneous CSI versus varying number of STs with different types of training sequences for SCC approach. System settings : $Q = 50$, Noise$=-\infty$dBW

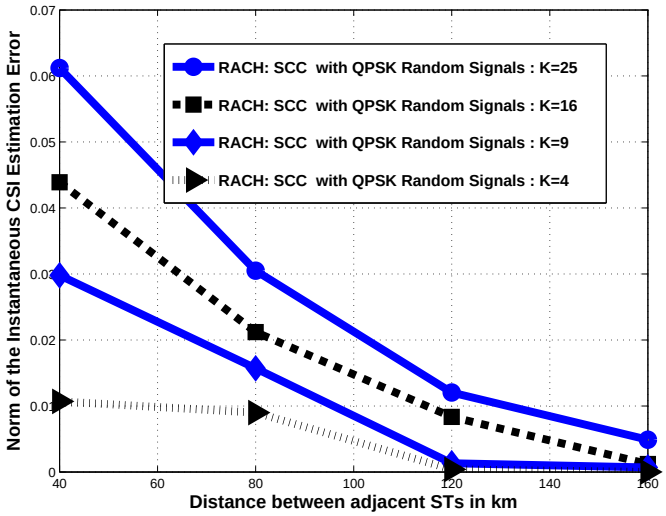

FIGURE 8.10 – Estimation error norm of instantaneous CSI versus distance between adjacent STs in km for SCC approach. System settings : training length= 200, $U = 50$, Noise=$-\infty$dBW, $Q = 50$

Chapter 9

Resource Allocation in an SDMA Satellite System

Nowadays, Space Division Multiple Access (SDMA) based on adaptive beamforming at the access point is considered as an efficient mean to increase system capacity and support rate-demanding services. However, the promised improvements require a careful assignment of the users to the available frequency bands. In this chapter, we focus on frequency allocation at the MAC in an SS with adaptive beamforming. We propose two low-complexity algorithms to assign an available frequency bands to the STs, namely, Min-Max directivity correlation algorithm and Min-Average directivity correlation algorithm. We compare the performance of the two algorithms with random frequency allocation.

This chapter is structured as follows : In Section 9.1, we present the starte of art on frequency band allocation in SDMA systems. In Section 9.2, we describe our algorithms. In Section 9.3, we assess the performance of the two algorithms and compare it with a random allocation. In Section 9.4, we draw some conclusions.

9.1 State of Art

Many efforts have been devoted to the allocation of resources (frequencies, bands, time slots) problem in SDMA systems. In [48], the authors consider a TDD narrow band system. They study the problem of allocation of dynamic slots in packet-switched indoor systems. A critical assumption in dynamic slot allocation is that the channel remains constant from the time where the measurement is made until SDMA/TDMA frame is transmitted. The gateway measures the spatial channel characteristic when it transmits in the uplink direction, exploits the obtained information and constructs SDMA/TDMA frames. The authors show that the problem performing optimal dynamic slot allocation under a minimum-SINR constraint is NP-complex. In [48], several heuristic schemes for the slot allocation are proposed and analyzed by numerical simulations. The simulation indicates that

these algorithms can provide significant improvements in terms of system capacity compared with random slot allocation. It is well known that SDMA with smart antennas enables intra-cell reuse by multiplexing spatial separable users and therefore, increases the channel capacity. In [48], resource allocation in multiple access schemes ignores completely the intra-cell user spatial separation. Different users in the same cell are assigned to different channels, the intra-cell resource reuse is inefficient.

In [49], the authors assume an SDMA system with OFDM signaling. If several users share a subcarrier and their SIR requirements are satisfied, they are called *spatially separable*. Spatial separability between users are determined by their spatial covariance matrices. It depends on the following factors such as angular and multi-path characteristics of users. Additionally, it also depends on the transmission rate of the users and their SIR requirements. In [49], the authors propose a heuristic greedy algorithm to allocate spatially separable users in the same subcarriers, and to adjust the beamformer of users appropriately, without taking into account of power constrain. The algorithm is a greedy algorithm based on the assumption of sequential insertion of spatially separable users in subcarriers. User reassignment is not taken into consideration for the sake of complexity.

The basic idea of this greedy algorithm can be evaluated as follows : When a user arrives in the system, it is assigned to an appropriate subcarrier, such that it increases the total rate of the subcarriers. Co-channel users of a subcarrier must be spatially separable and the SIR at the corresponding receivers must be also guaranteed. The assignment process is repeated until no further user assignment to the subcarriers can increase the total throughput or until the cardinality of the cochannel users assigned to all subcarriers reaches the number of available antennas available at the base station. The algorithm is also assessed by some numerical simulations. Simulations show that the subcarrier allocation yields significant benefits in throughput compared with nonadaptive allocation by exploiting the ST spatial separation.

In [49], the authors also consider the same scenario with a power constraint. Another algorithm which maximizes the total rate with a total power constraint is proposed. However, this algorithm requires that only one ST is assigned to each subcarrier.

In [50], the authors consider an SDMA/OFDM-based system in downlink with a base station is equipped with multiple antennas while each user is equipped with a single receiving antenna. An optimal resource allocation scheme is studied in order to maximize the transmission rate under the total power constraint and each user QoS requirement (e.g., bit and symbol error rate requirement). In [50], the authors show that the rate maximization problem can be transferred into a convex optimization problem. They also propose a complexity-reduced algorithm that can converge with 5 iterations. Different from the work in [49], this algorithms allows different combinations of users in different subcarriers. It is also shown that for the high power constraint case, the proposed algorithm outperforms greatly the algorithms proposed in [49] in terms of average rate per subcarrier by numerical simulations.

Another adaptive resource allocation approach for SDMA/OFDM system, which jointly allocates subcarriers, power and bits according to the instantaneous channel state information is studied in [51]. The objective of this algorithm is to minimize the overall transmit power and guarantee each ST's QoS requirements simultaneously.

The presences of co-channel interference and QoS requirements make the problem extremely complicated due to its inherent characteristics of non-linear and non-convex. Thus, an algorithm with reduced-complexity is proposed for practical implementation. Users are allocated into different subcarriers according to their spatial signature's correlations. Only users whose mutual correlation is sufficiently low are allowed to transmit in the same carrier and severe co-channel interference can be avoided. Therefore, the original joint subcarrier, bit and power allocation problem boils down into single-user optimization problems and the complexity is greatly reduced. Numerical simulations indicate that the proposed algorithm provides great improvements in terms of power gain compared with the non-adaptive systems. However, this algorithm requires high quality of channel state information, and it is applicable when the assumption that the channel state remains static between successive time slots can hold.

In this thesis, we consider an SDMA-based SS with fast fading propagation coefficients. Thus, the algorithm proposed in [48] cannot be applied since its dynamic slot allocation requires the satellite channel to be constant from the time when the channel measurement is made until the time when a SDMA/TDMA frame is transmitted. The algorithm in [51] cannot be applied since it requires a high quality of CSI. The satellite channel varies extremely rapidly and also due to the long propagation delay, it is impossible to capture the instantaneous CSI. The algorithm [49] could match our system assumption. However, the complexity of the greedy resource allocation algorithm is very high, its computational complexity is $O(UKN^4)$, where U represents the number of available subcarriers, K represents the number of STs and N represents the number of antennas equipped at the gateway. Therefore, for practical implementation, we propose algorithms with lower complexity.

9.2 Resource Allocation Algorithm

In this chapter, we assume that U distinct carriers are available. Each ST is assigned to one of the U orthogonal carrier. In this section, we propose two low-complexity allocation schemes to assign the STs to the available carrier.

The basic idea of our approaches is to form large sets of STs. Each ST is assigned to a different carrier based on the properties of the directivity coefficients.

For the sake of simplicity, we assume that the STs are sequentially inserted in the system and carrier reassignments are not performed, i.e, the STs already assigned to a carrier cannot be reallocated. On the contrary, beamforming adjustment is allowed, i.e. the beamformers for all the STs in a carrier can be optimized to account for the presence of additional interfering STs. Note that this choice to avoid carrier reallocation is consistent with the need to minimize the number of hand-overs between carriers. In fact, this impacts on signaling load and implies an involvement of the STs. On the contrary, the update of a beamformer is completely transparent to STs and can be performed by the gateway at any time.

A sequential algorithm can be easily adapted to the allocation of a group of new incoming STs, reallocation of STs with degraded quality of service (QoS) because of mobility, etc. In the sequential approach, at each step of the algorithm, a given user is assigned to a carrier and the beamforming vectors of the other users are adjusted, in a way that the target SINRs are ensured.

We propose two algorithms dubbed "*Min-Max directivity correlation algorithm*" (shortly Min-Max) and '*Min-Average directivity correlation algorithm*" (shortly

Min-Average) to allocate the STs.

These algorithms exploit the (eventually estimated) directivity coefficients.

Let us denote by $\boldsymbol{d}^e$ the directivity vector of the e-th ST entering in the system and with $\boldsymbol{D}^{(u)}$ the directivity matrix whose columns are the directivity vectors of the STs already allocated in carrier u.

In the Min-Max directivity correlation algorithm, a carrier u^* is allocated to the new terminal e if its directivity matrix $\boldsymbol{D}^{(u^*)}$ minimizes the maximum of the correlation with the directivity vector $\boldsymbol{d}^e$. In other words,

$$u^*_{minmax} = \underset{u=1,\ldots,U}{\operatorname{argmin}} (\max \boldsymbol{D}^{(c)H} \boldsymbol{d}^e). \tag{9.1}$$

In a Min-Average directivity correlation algorithm, a carrier u^* is allocated to an incoming ST e if the average absolute correlation is minimized, i.e.

$$u^*_{av} = \underset{u=1,\ldots,U}{\operatorname{argmin}} \|\boldsymbol{D}^{(c)H} \boldsymbol{d}^e\|_1. \tag{9.2}$$

The design of these two algorithms can be motivated as follows :

- If two STs have directivity matrices with high correlation, they cause high interference to each other. Then, when we adopt the target SINR beamforming, a huge amount of power will be devoted to achieve the SINR targets or the beamforming will not be feasible. Therefore, it is necessary to allocate STs with highly correlated directivity vectors to different carriers.
- The covariance of the intermodulation noise is determined by the total transmit power. Then, a reduction of the transmit power will also reduce the intermodulation noise in the system.
- This algorithm is based only on calculating the correlation of the directivity matrices of the terminals. Thus, it has a low computation complexity.

9.2.1 Min-Max Directivity Correlation Algorithm

In the Min-Max directivity correlation algorithm, we adopt an exhaustive search over all available carriers for each ST and select the one for which the maximum correlation is minimized.

In the following we detail the algorithm assuming that the system is initially empty. Thus, first we insert U STs randomly chosen into the U distinct carriers. Afterward, each subsequent ST is processed and the carrier u^* satisfying the optimization (9.1) is assigned to this ST. Once a carrier is allocated to the ST, the directivity matrix of such a carrier $\boldsymbol{D}^{u^*}$ is updated to include the directivity vector of the incoming ST. Finally, an updated beamformer is designed. The ST will be refused by the system if the power required by the updated beamformer exceeds the carrier power constraint otherwise it is included in the system. The Min-Max algorithm is detailed in Algorithm 8.

9.2.2 Min-Average Directivity Correlation Algorithm

The Min-Average directivity correlation algorithm is very similar to the Min-Max directivity correlation algorithm and considerations similar to the ones illustrated in Section 9.2 hold. The Min-Average algorithm is detailed in Algorithm 9.

$\mathcal{S}$ is the set of STs.
for $k = 1, ..., U$ **do**
  Carrier k is allocated to ST k in $\mathcal{S}$;
end
for $k = U + 1, ..., |\mathcal{S}|$ **do**
  for $m = 1, ..., U$ **do**
    calculate $\boldsymbol{d}^{(k)}\boldsymbol{D}^{(m)H}$;
    Choose the maximum entry of the vector $\boldsymbol{d}^{(k)}\boldsymbol{D}^{(m)H}$ and assign it to ψ_m, i.e.
    $\psi_m = \max \boldsymbol{d}^{(k)}\boldsymbol{D}^{(m)H}$.
  end
  Select the carrier u^* for which ψ_m is maximum, i.e.
  $c^* \leftarrow \underset{m=1,...,U}{\text{argmax}} \psi_m$
  Update the beamforming matrix $\boldsymbol{D}^{u^*}$ for a given target SINR. ;
  if *power required by updated beamformer exceeds carrier power constraint* **then**
    ST k is excluded from the system;
    else
      Allocate u^* to ST k ;
    end
  end
end

Algorithm 8: Min-Max Directivity Correlation Algorithm

$\mathcal{S}$ is the set of STs.
for $k = 1, ..., U$ **do**
  Carrier k is allocated to ST k in $\mathcal{S}$;
end
for $k = U + 1, ..., |\mathcal{S}|$ **do**
  for $m = 1, ..., U$ **do**
    calculate $\boldsymbol{d}^{(k)}\boldsymbol{D}^{(m)H}$;
    Choose the maximum entry of the vector $\boldsymbol{d}^{(k)}\boldsymbol{D}^{(m)H}$ and assign it to ψ_m, i.e.
    $\chi_m = \|\boldsymbol{d}^{(k)}\boldsymbol{D}^{(m)H}\|_1$.
  end
  Select the carrier u^* for which χ_m is maximum, i.e.
  $u^* \leftarrow \underset{m=1,...,U}{\text{argmax}} \chi_m$. ;
  Update the beamforming matrix $\boldsymbol{D}^{u^*}$ for a given target SINR.;
  if *power required by updated beamformer exceeds carrier power constraint* **then**
    ST k is excluded from the system;
    else
      Allocate u^* to ST k;
    end
  end
end

Algorithm 9: Min-Average Directivity Correlation Algorithm

9.3 Numerical Performance Assessment

In this section, we assess the performance of the two carrier allocation algorithms, (Min-Max and Min-Average algorithms), in terms of achieved SINR, power efficiency (ratio between the transmit power per ST and achieved SINR, this merit is defined in Section 6.4) and outage probability [1]. We also compare the performance of the two algorithms to random allocation.

In the simulations, we assume that 4 orthogonal carriers are available. The number of STs is either 200 or 400. The position of STs are randomly generated in the coverage area of Europe. The variance of the thermal noise introduced at the STs is -10dBW. The ratio between the variance of the intermodulation noise and the transmit power is -15dB. The maximum available power for each carrier at the gateway is 15dBW. The beamformer at the gateway is designed according to Approach B introduced in Section 6.2. In this section, we do not take into consideration the impacts of the directivity estimation in the reverse link and the transfer channel estimation at the STs. Therefore, in this section, we assume that a perfect knowledge of the channel is both available at the gateway and the STs.

The simulation results are obtained by averaging over 40 different simulations, i.e., 40 different groups of ST's positions are randomly generated and the performance is obtained by averaging over the performance in the 40 different scenarios.

Figure 9.1 and 9.2 compare the three different allocation approaches in terms of achieved SINR at the STs' receivers when $K = 200$ and $K = 400$, respectively. For the same target SINR, the Min-Max allocation algorithm outperforms the other two. For the same target SINR, the Min-Max algorithm achieves a SINR approximately 0.5dB higher than the Min-Average algorithm and Min-Average achieves 0.5dB higher SINR than random allocation when $K = 400$.

Figure 9.3 and 9.4 shows the ratio between transmit power per ST and the achieved SINR when the three different carrier allocation algorithms are applied. By implementing the Min-Max algorithm, the transmit power at the gateway decreases significantly compared to the other two allocation strategies. Consequently, also the variance of the intermodulation noise decreases.

Figure 9.5 and 9.6 compare the outage probability of the three allocation algorithms. The results are consistent with the previous ones. In fact, the outage probability reduces significantly when the Min-Max algorithm is applied compared to the application of random algorithm and the Min-Average algorithm. When the Min-Max algorithm is applied, the system achieves 6dB target-SINR without suffering from outage events. On the contrary, the outage probability is almost as high as 80% and 60% when the random allocation algorithm and the Min-Average algorithm, respectively, are applied.

1. in this chapter, outage probability is defined as the probability a ST to be rejected by the satellite system

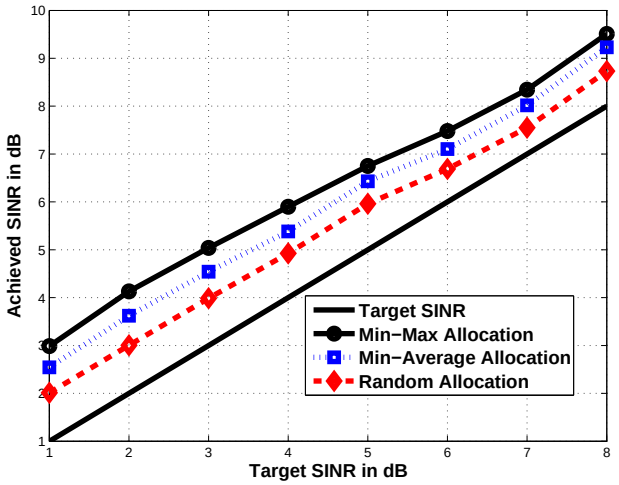

FIGURE 9.1 – Achieved SINR in dB versus target SINR in dB, when different carrier allocation algorithms are applied. System settings : $K = 200$, $\sigma_n^2 = -10$dBW, CIM= -15dB.

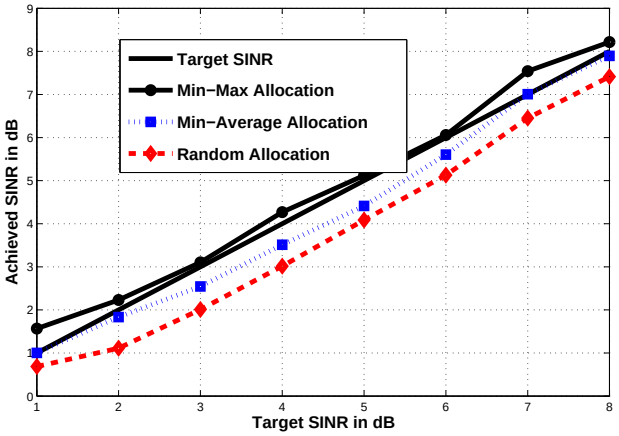

FIGURE 9.2 – Achieved SINR in dB versus target SINR in dB, when different carrier allocation algorithms are applied. System settings : $K = 400$,$\sigma_n^2 = -10$dBW, CIM= -15dB.

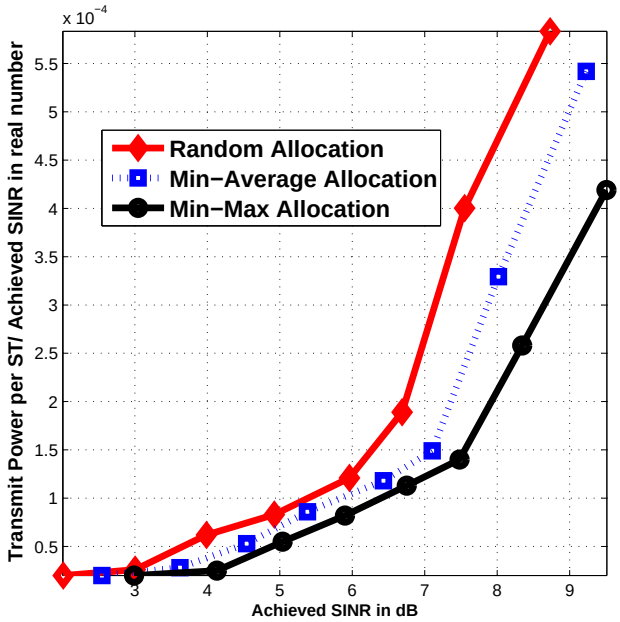

FIGURE 9.3 – Power efficiency versus achieved SINR in dB at the STs' receivers, when different carrier allocation algorithms are applied. System settings : $K = 200$, $\sigma_n^2 = -10$dBW, CIM$= -15$dB.

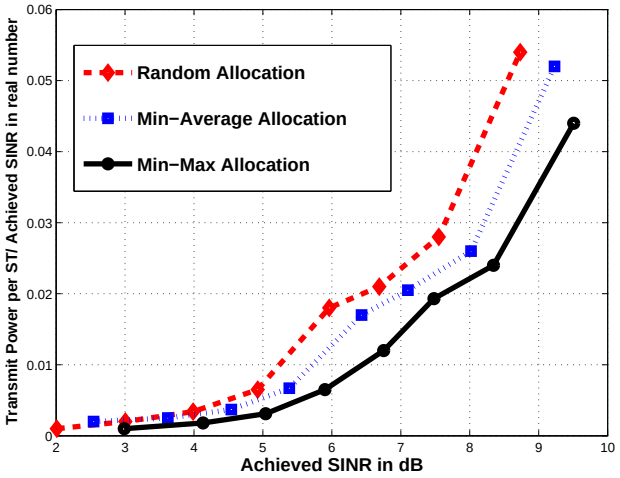

FIGURE 9.4 – Power efficiency versus achieved SINR in dB at the STs'receivers, when different carrier allocation algorithms are applied. System settings : $K = 400$, $\sigma_n^2 = -10$dBW, CIM$= -15$dB.

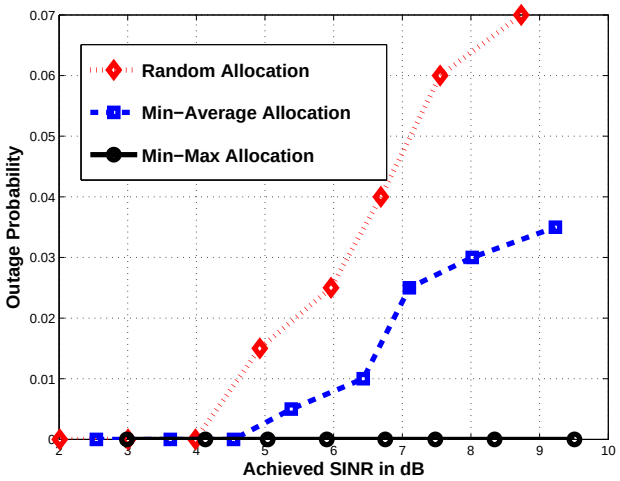

FIGURE 9.5 – Outage probability versus achieved SINR in dB , when different carrier allocation algorithms are applied. System settings : $K = 200$, $\sigma_n^2 = -10$dBW, CIM= -15dB.

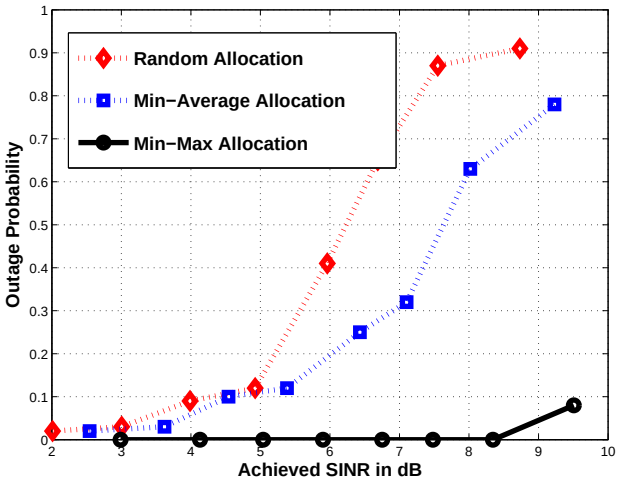

FIGURE 9.6 – Outage probability versus achieved SINR in dB, when different carrier allocation algorithms are applied. System settings : $K = 400$, $\sigma_n^2 = -10$dBW, CIM= -15dB

9.4 Conclusions

In this chapter, we propose two low-complexity algorithms for frequency allocation in a SDMA based SS, namely, Min-Max and Min-Average algorithms. Numerical simulations show that both algorithms achieve a very good tradeoff between complexity and performance. Compared with the random allocation approach, both algorithms have much higher power efficiency and achieve a higher SINR. Additionally, Min-Max algorithm always outperforms the Min-Average algorithm. Especially, Min-Max algorithm suffers from very little outage events even when the number of STs is very large.

Chapter 10

Complete System Performance Assessment

In this chapter, we assess the capacity of the SS with adaptive beamforming when the beamforming matrix is designed on the basis of the estimation of the directivity matrix from the measurements of the reverse link. Additionally, we compare the adaptive beamforming system to a conventional satellite system with inter-beam frequency reuse. The focus of the study is on the physical layer and an adequate implementation of the physical layer is required. A meaningful comparison of the two different physical layers is on the basis of the use of the signal-to-interference plus noise ratio (SINR) at the output of detectors at physical layer. The capacity of the system is defined as the maximum number of STs that can be supported by the system with a given average target SINR and a given probability of outage events, i.e, event that a ST, whose request of service is correctly detected, cannot be accepted.

In order to evaluate the system performance, we built a simulator consisting of two independent parts, a first part that simulates a random access channel and a second part, the main body of the simulator, this simulates the connection oriented channel in the forward link and in the reverse link. The latter includes (1) the reverse link simulator for the estimation of the forward link directivity matrix, (2) the forward link based on the basis of adaptive beamforming, (3) units for controlling functions like frequency carrier allocation.

A simulation requires first to run the random access channel simulator. Thus, the outputs of the random access simulator are provided as input to the main body of the simulator.

It is worth noting that the assumption to implement the random access channel as completely independent of the simulator for the connection oriented channel is suitable for a system with a large number of satellite terminals, theoretically infinite, as in the case of the system we are considering. In fact, in this case, the arrival rate of the STs in the system is independent of the STs in the system.

The global structure of the simulator is shown in Figure 10.1. This chapter is organized as follows : Section 10.1 describes the random access simulator. Section 10.2 illustrates the simulator for the connection-oriented channel. Section 10.3 evaluates the system performance by numerical simulations. Section 10.4 draws the conclusions.

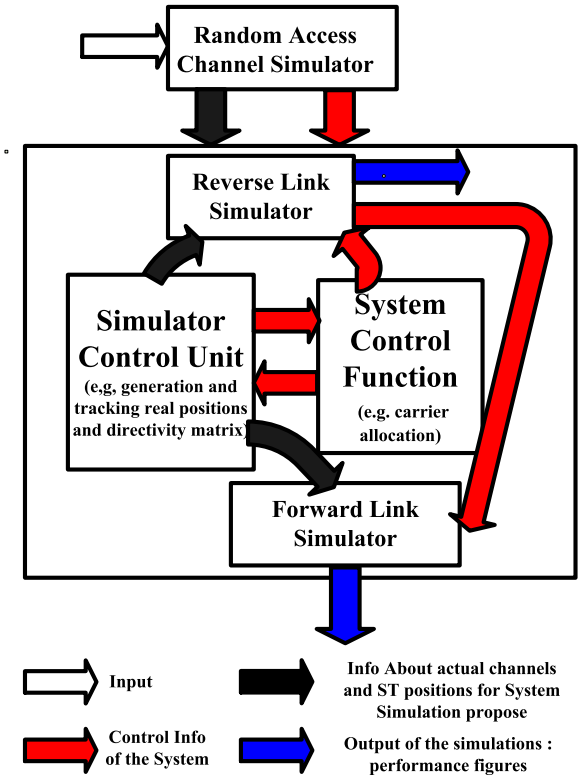

FIGURE 10.1 – Simulator : Global Structure

10.1 Random Access Simulator

In this section, we introduce the general structure of the random access channel module. This general structure is shown in Figure 10.2.

We assume that all the STs access to the random access channel in a slotted time interval and they are perfectly synchronized. The random access simulator performs detection of requests of service and estimation of directivity coefficients. The output is provided to the main body of the simulator.

The information at the input of the random access simulator includes : (1) the arrival rate of the STs ; (2) the time interval of the simulation in the form of number of time slots ; and (3) the area where the STs are randomly generated. The output of the simulator consists of the following information : (1) the total number of requests accepted by the system ; (2) the actual positions and directivity coefficients of the satellite terminals ; (3) the estimated directivity coefficients of the detected STs.

It is worth noticing that the actual directivity coefficients are not used for channel detection and estimation, nor for adaptive beamforming design. They are used to simulate the reverse and forward link.

The estimated directivity coefficients are provided as output to the system control unit to perform carrier allocation and eventually the design of the adaptive beamformer.

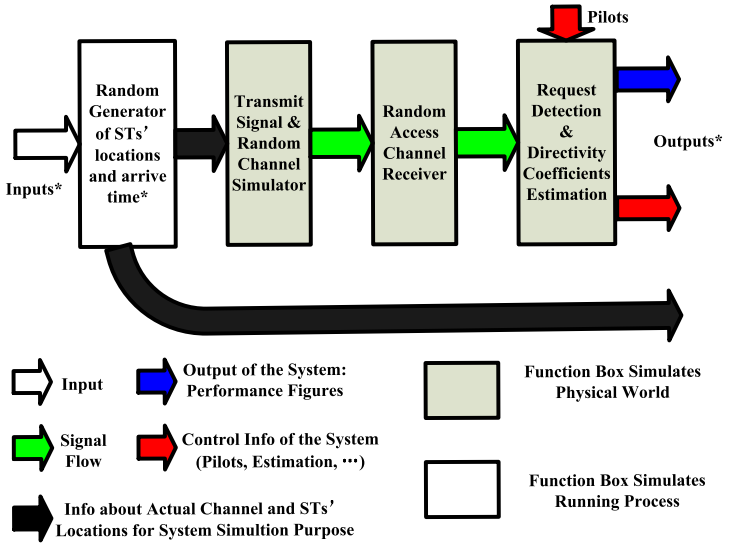

FIGURE 10.2 – Simulator of the Random Access Channel

The structure of the random access channel simulator is shown in Figure 10.2. It consists of four parts, namely :

- Random Generator of STs' location and arrival time ;
- Transmit Signal & Random Channel Simulator ;
- Random Access Channel Receiver ;
- Request Detection & Directivity Coefficients Eestimation.

In the simulation, the ST locations are generated randomly and uniformly in a certain area inside Europe. The new terminals arrive in the system according to a Poisson process [16] with a given arrival rate. The transmit signals are QPSK signals. Furthermore, the reverse link channel is built according to the model in Section 5.2. By using the actual positions of the active STs, we obtain the directivity coefficients of the STs, the propagation matrix and correlation matrix are also generated. The QPSK signals are transmitted through the reverse link channel, interpaired by intermodulation noise and thermal noise, and received by the gateway. Then, by observing the received signal at the gateway, the fourth part of the simulator performs contention resolution and channel estimation. In the simulation, we employ the SCC approach proposed in Chapter 8.

The output of the random access simulator is fed to the main simulator to perform carrier allocation and eventually adaptive beamforming. Channel estimation on the random access channel is similar to the joint multi-terminal channel esti-

mation performed in the main body of the simulator. However, in contrast to the channel estimation unit in the main body where carrier allocation guarantees that the STs are distinguishable, in the random access channel, collisions may happen. In this case, the colliding service requests that are not detected, are not accepted. In a real system, the requests would be submitted again in a different time slot. The simulator does not include this aspect since it is relevant to assess the performance of a random access protocols, but it does not affect the assessment of the performance of the detection capabilities of multiple STs due to the multiuser channel estimator, which is the focus of this work. With this choice, the system simulator is kept independent of the selected random access protocol.

In a real system, a poor channel estimation would imply a high BER at the receiver. This could be detected by error detection codes at the physical layer or at higher layers. Since no decoding operation will be implemented in the simulator, the SINR of each communication flow at the output of the symbol detector will be computed and compared to a given threshold. If the computed SINR is higher than a given threshold, the service request is considered to be successfully detected, otherwise, it is not detected and the ST is not accepted in the system.

10.2 Main Simulator : Forward Link and Reverse Link

In this section, we illustrate the main body of the simulator. The main body consists of 5 main parts, namely, the simulator control unit, the system control function unit, the reverse link chain, the beamforming design unit and the forward link chain.

The general structure of the satellite simulator main body is shown in Figure 10.3. It contains 12 function boxes. As shown in the Figure, the function boxes that simulate the physical world are colored in gray, while the function boxes that simulate the running processes in the system are not colored, and the performance evaluation boxes are drawn in dash.

In the following subsections, we explain the general idea of the simulations performed by the main body.

10.2.1 Simulator Control Unit

In the simulator control unit, there are three blocks, namely :

- Initial random generator of ST positions ;
- Tracker of the actual ST's positions and carrier allocation storage ;
- Mobility simulator & Call stop ;

In the simulation, we start from a cruise condition with a given number of STs already allocated in the system. Therefore, this unit (1) generates randomly the positions of the STs in the area defined as input and (2) provides a noisy version of directivity matrix coefficients to the carrier allocation.

Furthermore, we also evaluate the impact of the mobility of the STs on system performance. In the simulatior, all the satellite terminals are moving towards a random generated direction at a random generated speed inside a certain area. Moreover, the STs quit the system according to a Possion death process with a given departure rate. The simulation is performed over a given number of time

slots. When the total number of time slots spanned by the simulation is reached, the simulation is terminated.

10.2.2 System Control Unit

The system control function unit includes the function box of carrier allocation for reverse/forward link. We assume that the spectrum is organized in pairs of carriers : all the STs allocated into a carrier for the forward link are allocated to the corresponding paired carrier for the reverse link.

An SDMA system requires a careful carrier allocation in order to achieve good system performance. In the simulation, we employ the "min-max" approach proposed in Section 9.2 to perform the carrier allocation.

When a ST arrives in the system, it is allocated to the carrier where the estimated directivity matrix of the ST minimizes the maximum of the correlation with the directivity vectors of the STs already assigned to that carrier. It is worth noticing that the resource allocation is not on the basis of the actual directivity vectors of the STs : only the estimated directivity vectors can be used in carrier allocation.

Due to the mobility of the STs, the performance of the beamformer might degrade. In this case, the STs already in the system have to be reallocated. When the "beamforming design" unit fails to achieve the target SINR, a warning message will be sent to the carrier allocation box.

10.2.3 Reverse Link Unit

The reverse link unit simulates the transmission of the signals in the reverse link and the funcion at the gateway including the directivity matrix estimation. There are three blocks in the structure of the reverse link :

- ST's transmitter bank simulator ;
- Reverse link multi-carrier channel simulator ;
- Joint channel estimator.

In the simulation, the reverse link channel is simulated according to the model described in Section 5.2. We generate the directivity coefficients according to their actual positions, and the propagation matrix is generated according to the Surrey model in [15]. The transmitted QPSK signals pass through the reverse link channel, accompanied by the thermal noise and intermodulation noise, at the gateway and the satellite, respectively.

By observing the received signal, the gateway performs the directivity estimation on each carrier independently. The estimation is performed by using the PLSE algorithm proposed in Chapter 7. Additionally, the gateway has a prior knowledge of the estimated positions of the active STs in the previous frame. The gateway is aware of the area where each ST is located from the previous estimation up to estimation errors and mismatches due to the ST's mobility. Therefore, the gateway may update the estimation of the directivity coefficients based on the previous estimation. It needs only to estimate the directivity coefficients in a given area. Therefore, Algorithm 4 proposed in Section 7.2 is implemented in the simulator.

10.2.4 Beamforming Design Unit

The beamforming design unit is used to design beamforming coefficients in a way that the STs in the system can achieve a certain target SINR. This function

box connects the reverse link to the forward link. In the simulator, we implement the algorithm proposed in Section 6.2 to design the adaptive beamformer for each carrier. If the target SINR cannot be met by implementing the algorithm, a warning message will be sent to the carrier allocation box in order to indicate that under the current carrier allocation, the target cannot be met and requires a reallocation.

10.2.5 Forward Link Unit

The forward link unit contains four different parts, namely :

- Transmit signal simulator, consisting of a bank of signal generators followed by a beamformer ;
- Forward link channel simulator ;
- Receiver simulator for a given carrier ;
- Performance evaluation with time evolution.

In the transmit signal simulator, the transmitted signals are QPSK signals. They are modulated by the beamforming matrix before transmission.

The forward link channel simulator follows the model described in Section 5.1. The directivty coefficients of each carrier are computed based on the actual positions of the STs. The modulated transmitted signals pass through the forward link, accompanied by intermodulation noise induced on board and thermal noise at the receiver.

In the receiver simulator, each ST is equipped with multi-stream detector (MSD). At each ST, the forward link channel is estimated independently and the MSD is designed accordingly in order to detect the transmit signal. Channel estimation and multi-stream detection are performed. The output is then fed to the performance evaluation box.

In the performance evaluation box, the whole system performance is assessed continuously. The actual achieved SINR of each ST in each time frame at the input and output of the multi-stream detector is calculated. Different kinds of system performance are available according to different possibilities to average the achieved SINR.

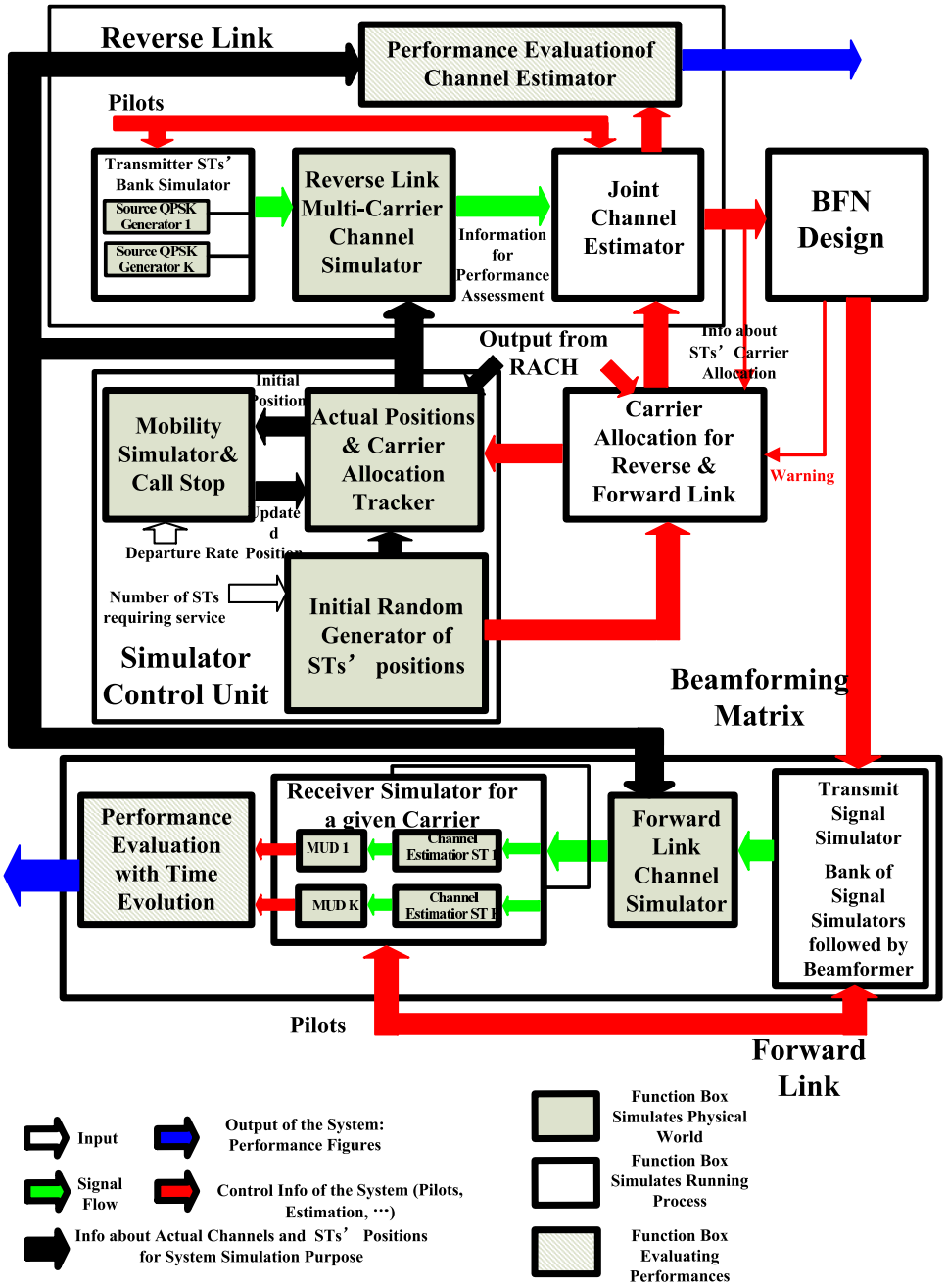

FIGURE 10.3 – Simulator

10.3 Numerical Performance Assessment

In this section, we analyze the performance of the complete SS assessed by numerical simulations. The simulations are performed for STs equipped with two antennas, ($R = 2$). The satellite is endowed with $N = 163$SAs. We randomly generate the positions of the STs on the map of Europe. The propagation coefficients are generated according to the Surrey model [15]. In subsection 10.3.1, we analyze the system performance in the random access channel. In subsection 10.3.2, we analyze the system performance in the connection oriented channel based on adaptive beamforming. The complete SS performance is compared with a conventional fixed beamforming system with frequency reuse.

10.3.1 Random Access Channel Performance Assessment

In this subsection, we consider the RACH in a real SS. We adopt the SCC approach described in Section 8.3 to detect the transmitting STs, possibly resolve of collisions and estimate channel and the directivity vectors. The relevant metrics in this subsection are the estimation failure probability i.e., when the gateway fails to detect an active ST, the normalized estimation error i.e., the average ratio between the norm of the estimation error of the instantaneous channel and the exact instantaneous channel and the estimation error of positions i.e., the average distance between the estimate positions and the actual positions.

If it is not differently stated, throughout this subsection, we make the following assumptions : 1) the correlation coefficients at the receiver are $a = -15$dB and $b = -22$dB, 2) the STs that want to initiate a transmission arrive in the system according to a Poisson process with a certain given rate, 3) random QPSK training sequences are adopted and the training length is either 200 or 400, the training set is partitioned into 50 or 100 groups, respectively, 4) the training sequence transmission power is 0dBW, 5) the thermal noise at the gateway is Gaussian distributed with covariance $\sigma_n^2 = -10$dBW, 6) the ratio between the intermodulation noise and the receive power at the gateway is -15dB, 7) the positions of the STs are generated randomly and uniformly in the region ([-10, 40],[-10 60],[20, 40],[20, 60]) in Figure 5.2, 8) the simulation results are obtained by averaging over 100 system realizations, i.e, 100 different groups of STs randomly generated.

As a benchmark, we consider the same conventional RACH system with beamforming (seen in Section 8.4). In this conventional RACH system, four frequency bands are available. Each band supports 40 fixed beams isolated by frequency reuse.

The impact of the arrival rate of new STs entering a system based on the SCC approach is shown in terms of estimation failure probability in Figure 10.4, normalized estimation error in Figure 10.5 and error of positions estimation in Figure 10.6, respectively. The number of coherence time intervals in the simulation is 50. As apparent in Figure 10.6, when the arrival rate of the STs increases, the estimation error in terms of positions also increases. It also appears that, by increasing the training length, the estimation error of STs' positions can be considerably reduced . When the arrival rate is 80, with the training length equals to 200, the estimation error of positions is 3.8 km, while with training length equals to 400, the estimation error of positions reduces to 2 km. Similar trend is also shown in Figure 10.4. By increasing the training length from 200 to 400, also the estimation failure probability can be significantly reduced. When the arrival rate is less than

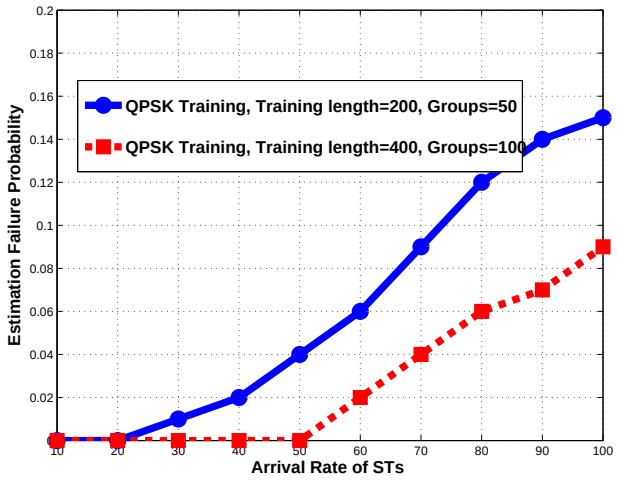

FIGURE 10.4 – SCC approach, estimation failure probability versus varying arrival rate of STs with different training group cardinalities. System settings : $\sigma_n^2 = -10$dBW, CIM= -15dB, $Q = 50$

50, by adopting training length of 400, the estimation failure probability remains at a very low level, approximately zero.

The impact of noise and intermodulation noise in the estimation is shown in Figure 10.7 and Figure 10.8 in terms of estimation failure probability and estimation error of positions, respectively. In the simulations, the number of coherence time intervals is 50, the training length is 400 and the training set is partitioned into 100 groups. Figure 10.7 and Figure 10.8 suggest that the impact of the presence of thermal noise is minor. The presence of intermodulation noise degrades the system performance slightly.

10.3.2 Connection Oriented Channel Performance Assessment

In this subsection, we assess the SS performance in the connection-oriented channel. We consider both the reverse link and forward link.

In the reverse link, we perform the directivity vectors estimation. We adopt the Parametric Least Square Error (PLSE) algorithm introduced in Section 7.1. The metrics that we adopt in the connection-oriented channel's reverse link are the estimation failure probability [1], and the error of positions estimation of STs'.

In the forward link, based on the directivity vector estimations, we allocate the STs to different frequencies based on Min-Max algorithm proposed in Section 9.2. Then, we design the adaptive beamforming in each frequency band. In this subsection, we adopt the Approach B proposed in Section 6.2 to design the beamformer. The metrics that we adopt for the forward link are the achieved average SINR, the outage probability [2], the power efficiency, i.e., the transmit power per ST and per

1. We recall here that an estimation failure occurs when the distance between the actual and estimated position of a ST is greater than 40 km.

2. An event of outage occurs when a ST cannot be served by the gateway.

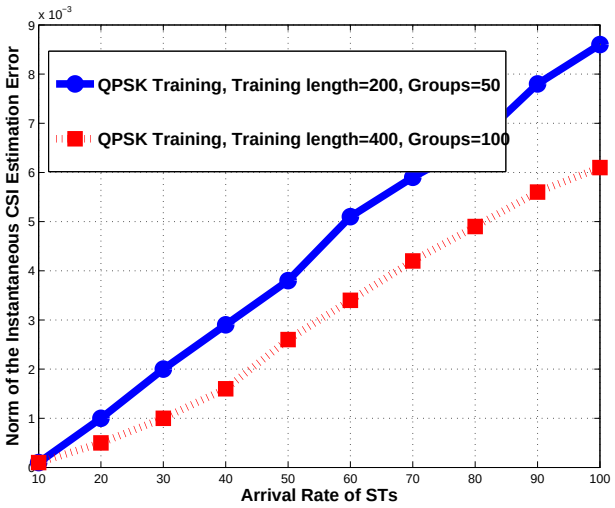

FIGURE 10.5 – SCC approach, norm of the instantaneous CSI estimation error versus arrival rate of STs with different training group cardinality. System settings : $\sigma_n^2 = -10$dBW, CIM$= -15$dB, $Q = 50$

the achieved SINR.

If it is not specially indicated, throughout this subsection, we make the following assumptions : 1) the correlation coefficients at the receiver are $a = -15$dB and $b = -22$dB 2) the signals transmitted by the gateway and STs are QPSK signals, 3) the thermal noise at the STs' and gateway receivers is Gaussian distributed with covariance $\sigma_n^2 = -10$dBW, 4) the ratio between the intermodulation noise and the receive power at the gateway is -15dB, 5) four orthogonal frequencies are available in the SS.

10.3.3 Reverse Link Numerical Performance Assessment

Firstly, we analyze the system performance of the connection-oriented channel in the reverse link. We utilize the output from the RACH channel. The STs detected by the RACH are transmitting in the connection-oriented channel. In the reverse link, the gateway performs the directivity vectors estimation and searches the transmitting STs in a circle with a certain radius. In the simulation, we assume the radius is 160 kilometers, and the center of the circle is the estimated position obtained in the RACH. In the connection-oriented channel, QPSK pilots sequences adopted by the STs are known by the gateway. The training length is either 200 or 400. The power of training signal is set to be 0dBW.

Figure 10.9 shows the estimation error of STs' positions of the PLSE algorithm with different number of active STs. In the simulation, we assume the number of coherence time intervals is $Q = 50$. When the number of STs is greater than 60, the estimation error of positions increases rapidly when the pilot length is 200. On the contrary, when the length of the training pilot is 400, the error of position estimation increases very slowly and the PLSE achieves a very good estimation of the positions in the connection-oriented channel. Figure 10.10 shows the estimation failure probability for different numbers of active STs. It shows that in the

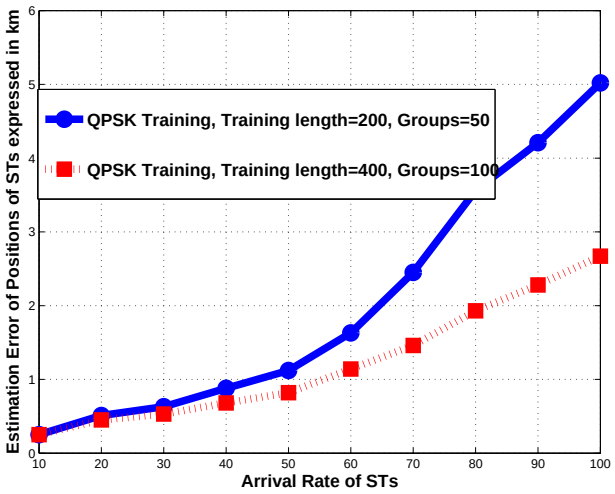

FIGURE 10.6 – SCC approach, error of ST's positions estimation versus varying arrival rate of STs with different training groups. System settings : $\sigma_n^2 = -10$dBW, CIM= -15dB, $Q = 50$

connection-oriented channel, the estimation failure probability remains at a very low level. When $K = 100$, if we adopt a training length equals to 200, the outage probability is 0.03, and if we adopt a training length equals to 400, the outage probability remains zero if the number of STs K is less than 70.

We also analyze the impact of the thermal noise and the intermodulation noise in Figure 10.11 and 10.12. Figure 10.12 indicates that for typical values of both thermal noise and intermodulation noise, do not impact the estimation failure probability. In Figure 10.11, it is interesting to notice that, as the number of STs increases, with different levels of thermal noise and intermodulation noise, the errors of ST's position estimation almost coincide. This is due to the fact that the interference among STs plays a more relevant role than directivity vectors estimates of the STs.

10.3.4 Performance Assessment of the Forward Link Numerical

In the forward link, based on the directivity estimation, we perform frequency allocation and beamforming design at the gateway. Moreover, each ST is equipped with MSD. At each ST, the forward link channel is estimated independently and the MSD is designed accordingly in order to detect the transmit signal. Channel estimation and multi-stream detection are performed. In the simulation, we assume in the forward link, total available power at the gateway is 10dBW. The training length to perform MSD equals to 200.

Simulation Results for Min-Max Frequency Allocation Approaches

First of all, we evaluate the Min-Max frequency allocation strategy when the adaptive beamformer is designed based on the estimated directivity vectors. In the

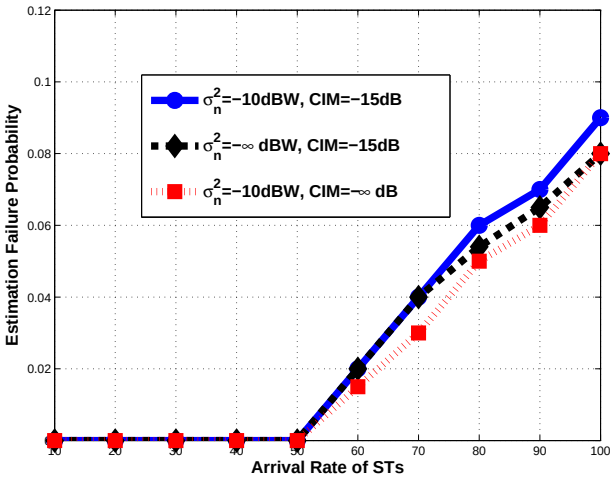

FIGURE 10.7 – SCC approach, estimation failure probability versus varying arrival rate of STs with different levels of noise. System settings : $Q = 50$, training length= 400, $U = 100$

simulations, the number of STs is 400. Figure 10.13 compares the Min-Max frequency allocation and random allocation in term of achieved SINR at the STs' receivers. It shows that the Min-Max algorithm allows to increase the SINR by approximately 1dB compared to random allocation. Figure 10.14 shows the transmit power per ST normalized to the achieved SINR when different allocation approaches are adopted. By implementing the Min-Max allocation strategy, the transmit power required to achieve the same SINR decreases significantly compared to random allocation. Figure 10.15 compares the outage probability of the two allocation strategies. When the achieved SINR is higher than 4dB, the outage failure probability increases sharply if we adopt random allocation. On the contrary, if the Min-Max frequency allocation is adopted, the outage probability remains at a very low level even when the achieved SINR is as high as 7dB.

Figure 10.13, 10.14 and 10.15 show that, when the beamformer is designed on the basis of the estimate of directivity vectors, by adopting the Min-Max frequency allocation algorithm, the system performance can be improved significantly compared with random allocation.

Simulation results for static terminals

We analyze system performance when the STs are static. We adopt the Min-Max frequency allocation strategy. We assume the total number of STs is either 200 or 400. Since all the carriers are identical, we examine only one of the four carriers.

We assess the degradation of the SS performance due to the mismatch between the estimated and actual directivity vectors. In the simulations, the number of STs is 200 or 400. Figure 10.16 compares the achieved SINR when the beamforming is designed on the basis of the estimated and actual directivity vectors. It is obvious that the beamformer based on actual directivity vectors outperforms the one based on estimated directivity vectors. However, the performance degradation is

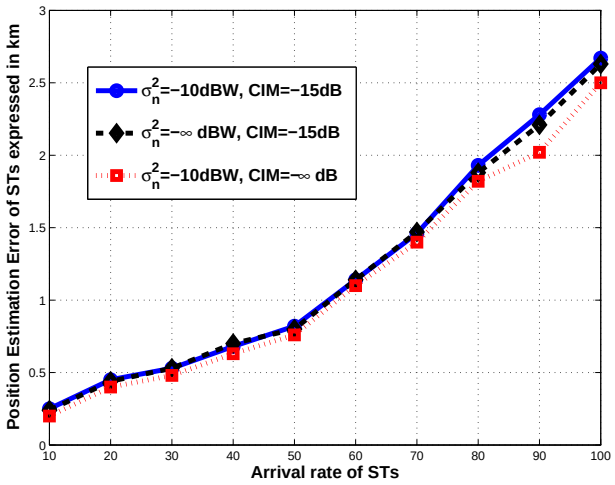

FIGURE 10.8 – SCC approach, Estimation error of ST's positions versus varying arrival rate of STs with different levels of noise. System settings : $Q = 50$, training length= 400, $U = 100$

not significant. The gap is always below 0.1dB. A similar trend is also shown in Figure 10.17. The system performance in terms of power efficiency for the two kinds of beamformers is very close. Figure 10.18 shows the outage probability when the beamforming is designed based on estimated and actual directivity vectors. It is worth mentioning that for $K = 400$, when the achieved SINR is high as 6.5dB, the outage probability still remains as zero.

Additionally, we evaluate the SS performance with a different number of active STs. Figure 10.19 and 10.20 show the system performance in terms of achieved SINR and power efficiency with different number of active STs. In the simulations, the target SINR is 2dB or 5dB. As apparent from Figure 10.19, as the number of STs increases, the achieved SINR decreases significantly. When the number of STs is equal to 400, the average achieved SINR almost equal to the target SINR. Figure 10.20 shows the power efficiency for a different number of STs when the target SINR is 2dB. When the number of STs is larger than 200, the required power to meet the target SINR per ST boosts greatly.

Simulation results for mobile terminals

In this subsubsection, we analyze system performance when the STs are moving. Each terminal is moving inside the map at a random generated speed and in a random generated direction. Due to the mobility of STs, the directivity vectors of the STs changes. However, since the system updates the positions of the satellite terminals and computes again the beamforming matrix at regular intervals, the beamforming matrix remains static for one minute. Moreover, we assume that the mobile terminals have the ability to adjust their own multistream detector instantaneously. We analyze the robustness of the beamformer to mobility and the system performance degradation due to the delay in updating the beamformer.

We assess the system performance when the number of STs is 400. The speed

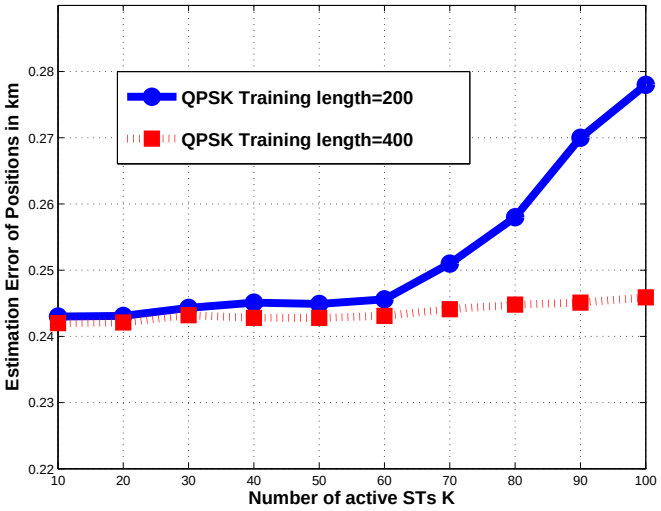

FIGURE 10.9 – PLSE algorithm, error of ST's positions estimation versus different number of active STs, with different levels of training length. System settings : $\sigma_n^2 = -10$dBW, CIM= -15dB, $Q = 50$

of each ST is uniformly distributed in the range from 80km/h and 140km/h. The moving direction of each terminal is uniformly distributed between 0 and 2π.

Figure 10.21 compares the achieved SINR in one minute. We can see from the figure that the degradation of achieved SINR due to the mobility is less than 0.1dB in one minute. This degradation is still acceptable. Figure 10.22 shows the power efficiency in one minute. The power efficiency almost does not degrade in one minute.

Simulation Results for Adaptive Beamforming versus Conventional Beamforming

We compare the performance of the adaptive beamforming and conventional beamforming systems. We assume that in both systems, 4 orthogonal carriers are available. In the adaptive beamformer, the STs are allocated to the carrier by the Min-Max strategy. For the conventional beamformer strategy, each beam remains constant, and points to a position in the coverage area. Adjacent beams use different frequencies. One beam cannot serve more than one ST at a time. Both schemes aim to ensure that the lowest level of achieved SINR is above a certain level. Additionally, each terminal designs its own multi-stream detector according to the acquired knowledge about the channel.

The simulations are performed for various number of STs K, namely, $K = 80$, $K = 200$ and $K = 400$. We set the maximal total power at the gateway for the conventional beamformer to be 15dBW, while the maximal power for the adaptive beamformer is the actual power required by the conventional beamformer. Both schemes ensure that the lowest achieved SINR among all the STs should meet a given target.

Figure 10.23 shows the outage probability of the two schemes. For the conven-

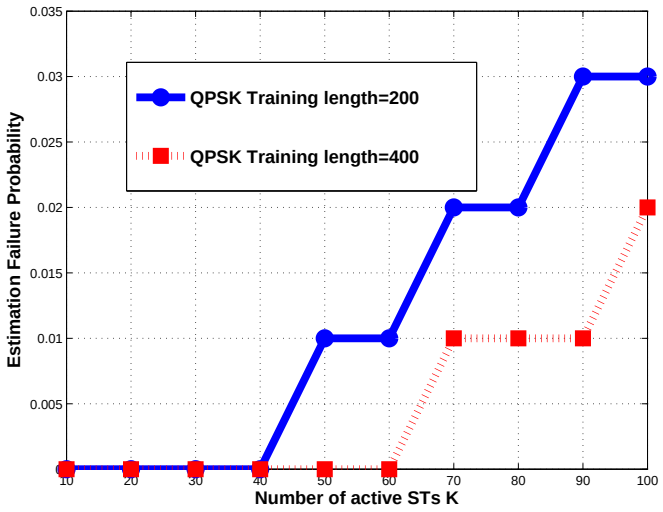

FIGURE 10.10 – PLSE algorithm, estimation failure probability versus different number of active STs, with different levels of training length. System settings : $\sigma_n^2 = -10$dBW, CIM= -15dB, $Q = 50$

tional beamforming, the outage probability is not correlated to the target SINR. Once the constant beamforming for a given target SINR is achieved, the outage events depends on the geographic distributions of the STs. For the conventional beamforming system, when $K = 80$, the outage probability is approximately 10%, when $K = 400$, the outage probability is approximately 37.5%. For the adaptive beamforming system, if the target SINR is 2dB or 4dB, when $K = 400$, the outage probability remains zero. When target SINR is 8dB, the outage probability for $K = 400$ is about 7%. Figure 10.23 shows that the adaptive beamforming system substantially outperforms the conventional beamforming system in terms of outage probability.

Figure 10.24 compares the power efficiency of adaptive and conventional beamforming when $K = 200$ and the target SINR is 2, 3 and 4dB. The conventional system achieves higher SINR. However, the power per ST per achieved SINR is much higher than the adaptive beamformer. Conventional beamformer is not optimized to minimize the transmit power and therefore could waste transmit power. On the contrary, the adaptive beamformer consumes much less power to ensure the target SINR.

Figure 10.25 and 10.26 show the histogram of the achieved SINR when the target SINR is 2dB or 3dB for both types of beamformings with $K = 200$. It can be seen that conventional beamforming always achieve a higher SINR than adaptive beamforming. The achieved SINR of adaptive beamforming is always higher than the target, but approximately 2dB lower than conventional beamformings. Thus, the adaptive beamforming is more efficient than conventional beamforming since it is tailored on the STs' positions. The distribution of the conventional beamforming is also much more sparse than that of adaptive beamforming. The support of conventional beamforming is 6.7dB when the target SINR is 3dB. On the contrary, for adaptive beamforming, the support is merely 2.1dB. In the conventional beam-

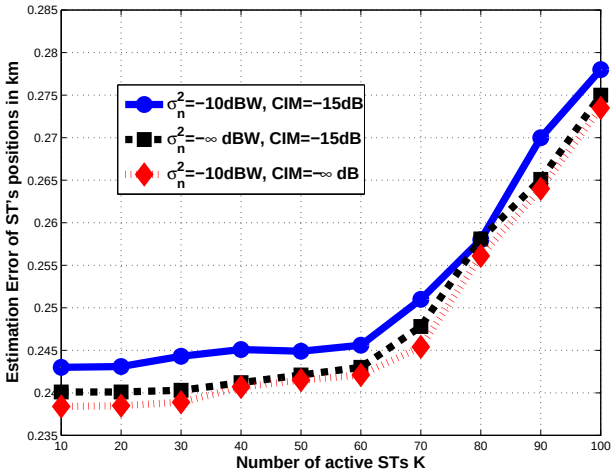

FIGURE 10.11 – PLSE algorithm, error of ST's positions estimation versus different number of STs , with different levels of noise. System settings : training length= 200, $Q = 50$

forming system, if a ST is located on the edge of coverage area of a beam, the achieved SINR is much lower than if had been located in the center of the beam. On the contrary, the adaptive beamformer tailors on STs, therefore, in the adaptive beamforming system, STs achieve closer performance.

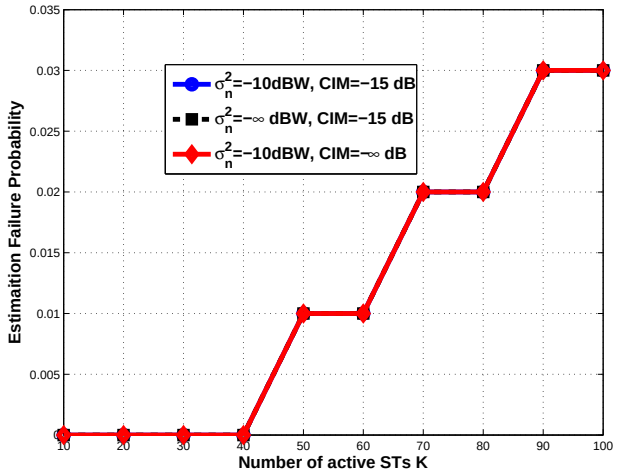

FIGURE 10.12 – PLSE algorithm, estimation failure probability versus different number of STs , with different levels of noise. System settings : training length= 200, $Q = 50$

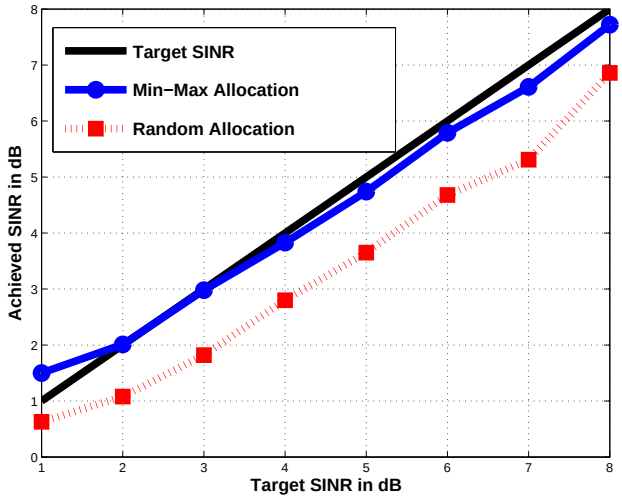

FIGURE 10.13 – Achieved SINR in dB versus target SINR in dB when applying different carrier allocation algorithms. System settings : $K = 400$, $\sigma_n^2 = -10$dBW, CIM= -15dB, training length= 200

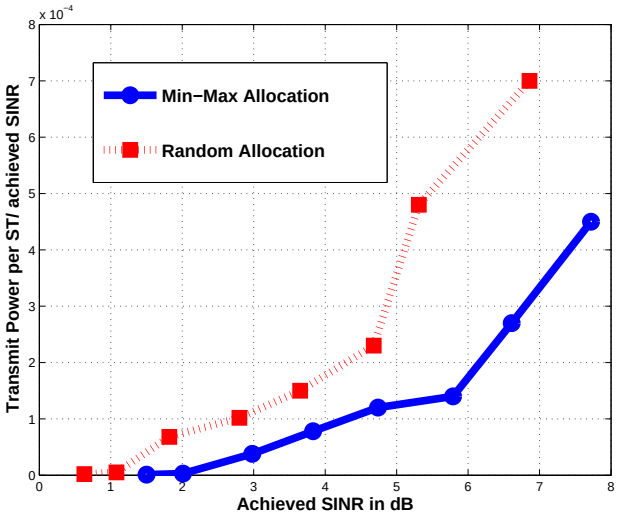

FIGURE 10.14 – Power efficiency versus achieved SINR in dB when applying different carrier allocation algorithms. System settings : $K = 400$, $\sigma_n^2 = -10$dBW, CIM= -15dB, training length= 200

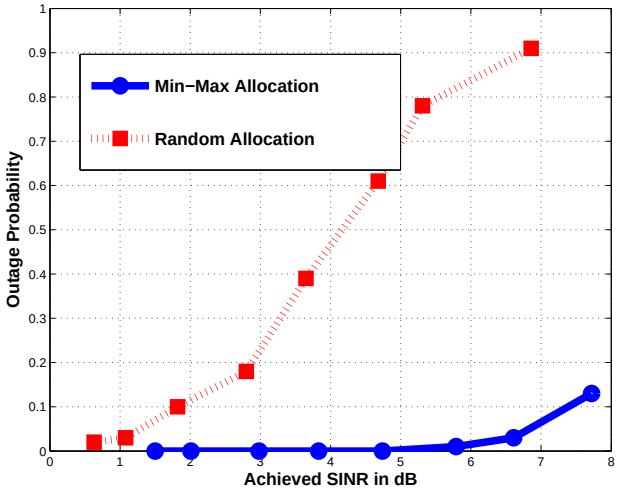

FIGURE 10.15 – Outage probability versus achieved SINR in dB when applying different carrier allocation algorithms. System settings : $K = 400$, $\sigma_n^2 = -10$dBW, CIM= -15dB, training length= 200

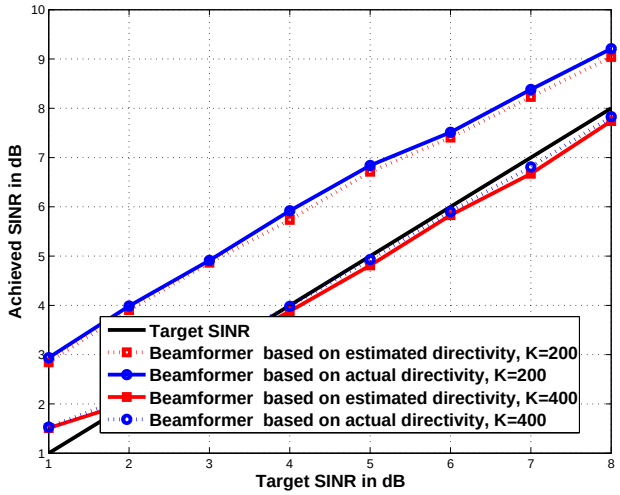

FIGURE 10.16 – Achieved SINR in dB versus target SINR in dB when the beamformer is designed based on estimated and actual directivity vectors. System settings : $K = 200$ or 400, $\sigma_n^2 = -10$dBW, CIM=15dB, training length= 200

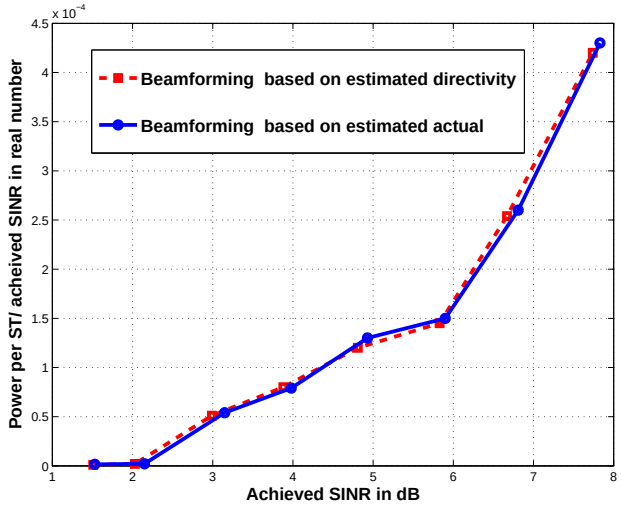

FIGURE 10.17 – Power efficiency versus achieved SINR in dB when the beamformer is designed based on estimated and actual directivity vectors. System settings : $K = 400$, $\sigma_n^2 = -10$dBW, CIM=15dB, training length= 200

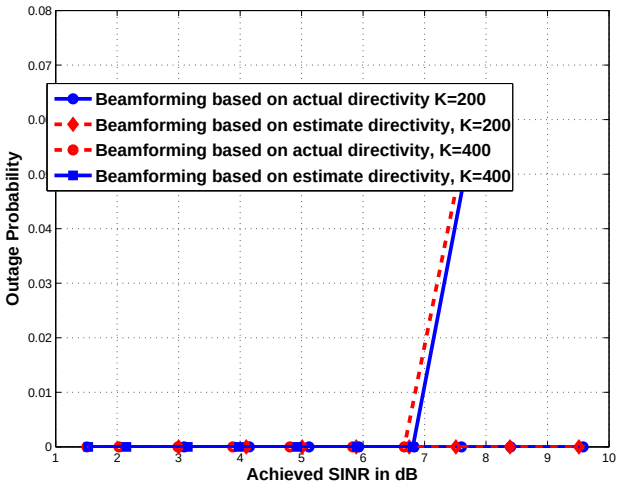

FIGURE 10.18 – Outage probability versus achieved SINR in dB when the beamformer is designed based on estimated and actual directivity vectors. System settings : $\sigma_n^2 = -10$dBW, CIM=15dB, training length= 200

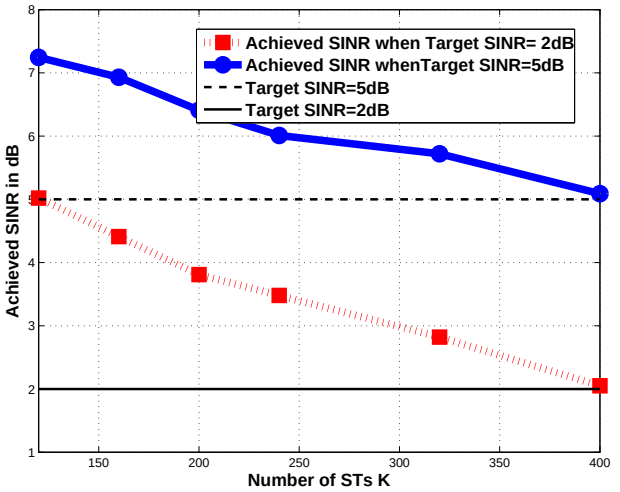

FIGURE 10.19 – Achieved SINR in dB versus number of STs K. System settings : $\sigma_n^2 = -10$dBW, CIM=15dB, training length= 400

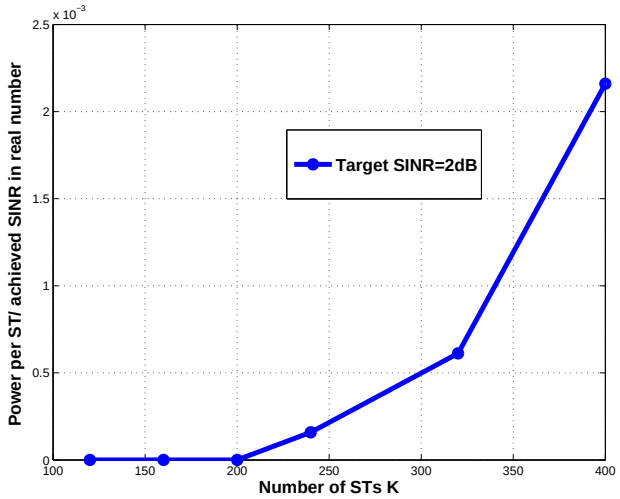

FIGURE 10.20 – Power efficiency versus Number of STs K. System settings : target SINR = 2dB, $\sigma_n^2 = -10$dBW, CIM=15dB, training length= 200

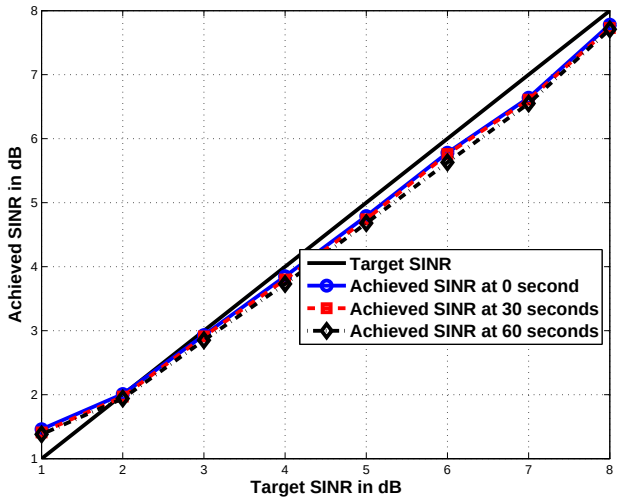

FIGURE 10.21 – Achieved SINR in dB versus target SINR in dB for mobile STs in one minute. System settings : $K = 400$, $\sigma_n^2 = -10$dBW, CIM=15dB, training length= 200

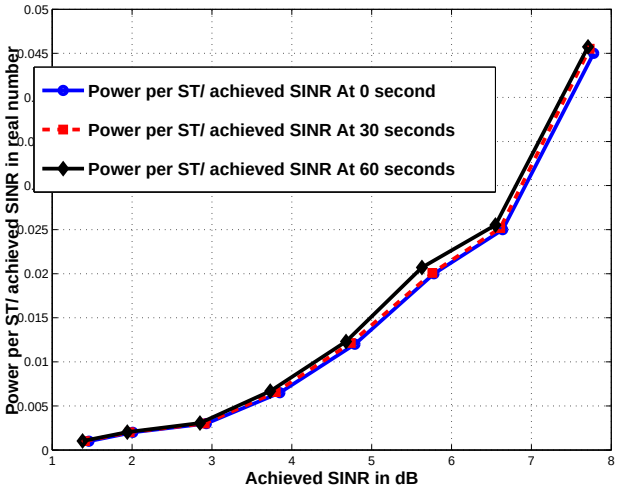

FIGURE 10.22 – Power efficiency versus achieved SINR in dB for mobile STs in one minute. System settings : $K = 400$, $\sigma_n^2 = -10$dBW, CIM=15dB, training length= 200

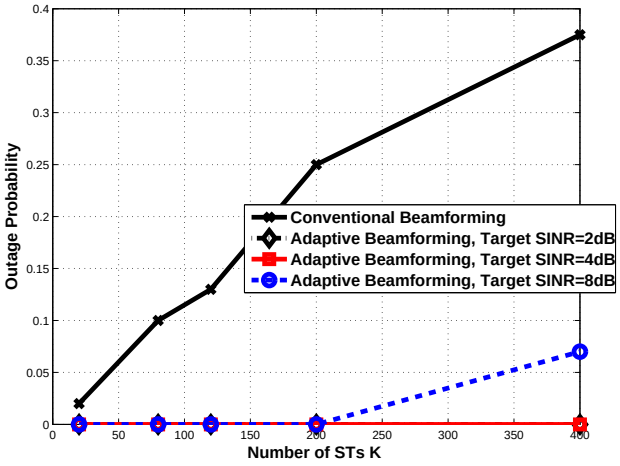

FIGURE 10.23 – Outage probability versus number of STs for adaptive and fixed beamforming design schemes. System settings : the maximal available power for conventional beamformer is 15dBW, $\sigma_n^2 = -10$dBW, CIM=-15dB, training length= 200

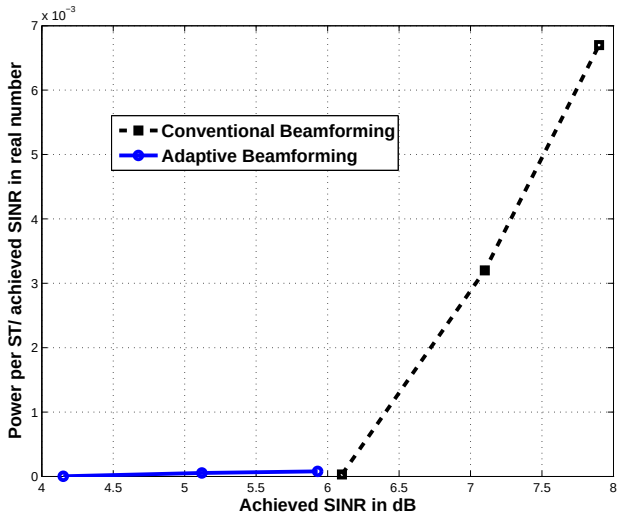

FIGURE 10.24 – Power efficiency versus achieved SINR in dB for adaptive and conventional beamforming design schemes. System settings : the maximal available power for fixed beamforming is 15dBW $K = 200$, Target SINR$=2, 3$ or 4dB, $\sigma_n^2 = -10$dBW, CIM$=-15$dB, training length$= 200$

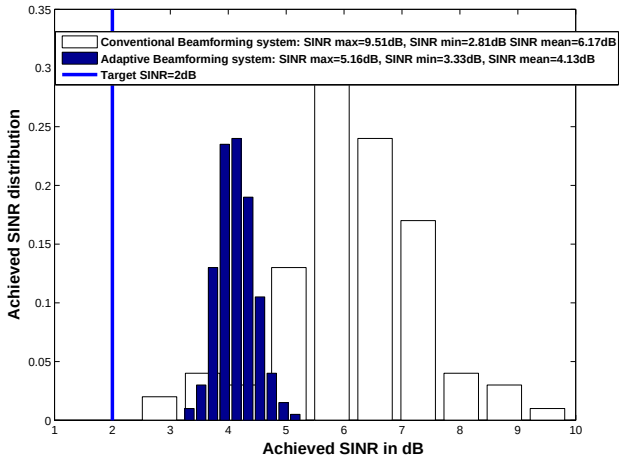

FIGURE 10.25 – Histogram of achieved SINR for adaptive and fixed beamforming design schemes. System settings : the maximal available power is 15dBW, $K = 200$, SINR target$=2$dB, $\sigma_n^2 = -10$dBW, CIM$=-15$dB, training length$= 200$

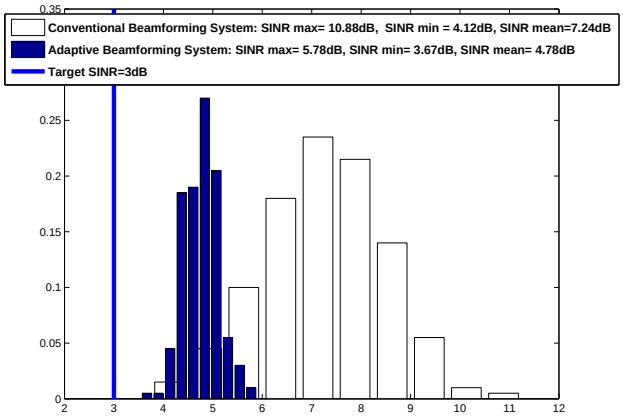

FIGURE 10.26 – Histogram of achieved SINR for adaptive and fixed beamforming design schemes. System settings : the maximal available power is 15dBW, $K = 200$, SINR target=3dB, $\sigma_n^2 = -10$dBW, CIM=-15dB, training length= 200

10.4 Conclusions

The analysis carried out in the previous section shows that adaptive beamforming is an excellent candidate for next generation satellite systems. In fact, when compared to conventional beamformering, it provides a very high gain in capacity, i.e. it increases the number of users that can be supported by the system with a given guaranteed QoS. Additionally, the adaptive beamformer reduces the variance of the achieved SINR and effectively utilizes the available power.

One critical aspect in this study is the estimation of the directivity vectors. Simulation results show that in the RACH, the proposed SCC approach can achieve a very good estimation of the directivity vectors in the presence of thermal noise and intermodulation noise. The estimation failure probability can be greatly reduced compared with a conventional fixed beamforming system. Therefore, the throughput increases and transmission delay is reduced. Similarly, in the connection-oriented channel, the PLSE approach also provides very good estimation of directivity vectors. By increasing the training length, the estimated positions of STs can be very close to the actual positions of STs.

In the connection-oriented channel, we compare the low-complexity Min-Max allocation approach with random allocation based on the estimated direcitivity vectors. The simulations show that the capacity of a SS can be significantly improved by using the Min-Max approach. The proposed approach achieves a higher SINR than random allocation. More importantly, by adopting the Min-Max approach, outage events can be greatly reduced. Thus, the capacity of the system is enhanced.

Another critical aspect in this study is the robustness of the system against mismatches between the actual directivity vectors and the estimated directivity vectors for beamforming design. This issue has also been object of analysis in this part of thesis. We investigate the effects of the mismatch. Simulations suggest that system performance degradation due to the directivity vectors estimation error is very limited. Therefore, the estimated directivity vectors can be used for the beamforming design. Additionally, the effects of the intermodulation noise and thermal noise have been also object of investigation. Numerical results suggest that when frequency allocation is employed, the impacts of thermal noise and intermodulation noise are very minor.

Deuxième partie

Resource Allocation in Slow Fading Interfering Channels with Partial Knowledge of the Channels

Chapter 11

Allocation de ressources dans un canal ?variation lente avec connaissance partielle du canal

Dans la deuxième partie de cette thèse, on étudie un canal à interférence avec évanouissements par blocs et avec connaissance de l'état du canal des liens directs (pas de connaissance statistique sur les liens interférents). Les liens interférents sont modélisés comme des canaux ayant une distribution de Rayleigh. Avec cette hypothèse, la fiabilité des communications ne sont pas assurée et un certain niveau de niveau de probabilité de coupure doit être toléré. On considère une allocation de ressources optimisée pour des fonctions d'utilités basées sur débit réel prenant en compte les événements d'interruption. On propose des algorithmes d'allocation des ressources basés d'un coté sur les deux jeux bayésiens et par ailleurs sur l'optimisation. Dans le contexte des jeux bayésiens, nous étudions les deux cas de l'allocation de *puissance* pour des *débits de transmission prédéfinis* et allocation emph conjointe des puissances et taux de transmission.

Ce chapitre est structuré comme suit. Dans la section 12.1, l'état de l'art sur l'allocation des ressources pour les canaux à interférence sont présentés. La section 12.2 est consacrée à l'examen de certain concepts fondamentaux de la théorie des jeux. Dans la section 12.3, le modèle du système est décrit ; Dans la section 12.4, le problème de la répartition de puissance et des dabits est formulé comme un problème d'optimisation de jeu bayésienne ; Dans la section 12.5, le cas pratique de débits fixes est considéré [1] où chaque source doit déterminer la puissance qui maximise son utilité. Dans la section 12.6, on considére le cas général où chaque source doit choisir sa stratégie conjointement en termes de puissance et le débit de transmission. Dans la section 12.7 on considère la démarche d'optimisation dans les

1. dans les systèmes pratiques les débits sont généralement attribués à la couche supérieure et définis dans un ensemble discret, éventuellement un singleton.

deux régimes asymptotiques des systèmes limités par l'interférence et ceux limités par le bruit. Des expressions approchée pour l'allocation des ressources sont établies. Dans la section 12.8, on présente, quelques résultats numériques. Finalement, dans la section 12.9, les conclusions de la partie II sont résumés.

11.1 Etat de l'art

L'important gain en efficacité spectrale obtenue par un partage du spectre des fréquences disponible rend inéluctable l'investigation des canaux à interférence et alimente une activité de recherche intense sur ce sujet. Le canal à interférence est intrinsèquement caractérisé par un niveau limité de la coopération entre les entités de communication qui sont plus en concurrence pour les mêmes ressources et par une gestion décentralisée de ces dernières. Ces interactions complexes peuvent être modélisées avec succès du point de vue de la théorie des jeux. Cette orientation reçoit actuellement une attention considérable (voir par exemple [52–56]). La majorité de ces contributions se concentrent sur le cas de connaissance parfaite des canaux de transmission au niveau de l'émetteur. Des algorithmes itératifs ont été proposés, sauf que leur convergence vers un point d'équilibre est basée sur les retours des divers récepteurs. Un exemple bien connu et largement étudié dans cette classe d'algorithmes est l'algorithme itératif waterfilling qui convient bien aux canaux sélectifs à interférences (voir [54] et références incluses). Chaque récepteur contribue à la densité spectrale de puissance globale (PSD) de l'interférence plus bruit au niveau de l'émetteur d'intérêt, et l'émetteur adapte la PSD de sa transmission en conséquence. Les vitesses de convergence de ces algorithmes limitent leur applicabilité. En outre, les retours d'information nécessaires réduit l'efficacité spectrale du système. Dans [53] des canaux à évanouissements lents sont considérés avec des informations d'état partielles. En utilisant l'approche des jeux répétés, des informations sur le canal et les interactions sont acquises. Lorsque les contraintes d'un système de communication ne permettent pas la convergence des algorithmes itératifs ou lorsque les algorithmes itératifs ne prennent pas en charge les retours d'informations intensifs requis, les jeux bayésiens fournissent un cadre théorique commode. L'allocation des ressources basée sur les jeux bayésiens sont adoptées dans [57–59]. Les travaux présentés dans [57,58] mettent l'accent sur des canaux à évanouissement rapide alors que le jeu bayésien dans [59] est appliqué à des canaux à évanouissements lents à accès multiples mettant en oeuvre un multiplexage par répartition de fréquences orthogonales (OFDM). Il est intéressant de noter que [59] montre qu'en termes de débit réalisable, l'allocation des ressources basée sur les jeux bayésiens conduit à des performances comparables à une allocation de ressources basée sur une optimisation qui assume l'entière connaissance du canal à l'émetteur.

11.2 Jeu Stratégique, Equilibre de Nash et Jeu Bayesien

11.2.1 Jeu Stratégique

Un jeu stratégique est composé de trois éléments :

1. Un ensemble fini $\mathcal{S}$ of K de joueurs.

2. Un ensemble de stratégies $\mathcal{P} = \mathcal{P}_1 \times \mathcal{P}_2 ... \times \mathcal{P}_K$ non vide, où $\mathcal{P}_k$ dénote l'ensemble de stratégies du joueur $k \in \mathcal{S}$.
3. un ensemble de fonctions d'utilités $\mathcal{U} = (\mathcal{U}_1(x), ..., \mathcal{U}_K(x))$, d'actions $x \in \mathcal{P}$ où chaque joueur k choisit une action x_k qui induit un profil d'action $x = (x_1, ..., x_K)$ suite à quoi le joueur k obtient son utilité notée $\mathcal{U}_k(x)$.

11.2.2 Equilibre de Nash

On suppose que tous les joueurs prennent des décisions simultanément et rationnellement. Si le résultat dépend des stratégies adoptées par les autres joueurs, on ne peut pas prédire l'issue des acteurs multiples par une simple analyse d'un des joueurs isolé. On doit tenir compte de tous les joueurs. L'équilibre de Nash (NE) est un résultat possible pour le cas de la non prise de décision.

NE est nommé d'après le mathématicien américain John Nash, qui a introduit ce concept en 1950 [60]. Il s'agit d'un concept fondamental de la théorie des jeux. Ce concept peut être simplement exprimé comme un ensemble d'actions, de sorte qu'aucun joueur ne peut obtenir une plus grande utilité en déviant unilatéralement sa propre action, tandis que les autres joueurs gardent leurs actions inchangée.

Définition de l'équilibre de Nash [61] : L'équilibre de Nash est un profil d'actions $x^* \in \mathcal{P}$ avec la propriété que pour chaque joueur $k \in \mathcal{S}$, on a :

$$\forall x_k \in \mathcal{P}_k, \quad x_k \neq x_k^* : \mathcal{U}_k(x_k^*, x_{\sim k}^*) \geq \mathcal{U}_k(x_k, x_{\sim k}^*) \tag{11.1}$$

Si l'inégalité de l'équation 12.1 est stricte, alors l'équilibre obtenu est un stricte NE, autrement dit, si un joueur peut modifier son action unilatérale sans être laisé, la NE est appelé un faible NE.

Un jeu où un joueur peut choisir une seule action à la fois est défini comme un jeu de pure stratégie. Dans les jeux de stratégie pure, le NE est nommé comme NE de pure stratégie. Dans certains cas, au lieu de simplement choisir une action, les joueurs sont en mesure de sélectionner plus q'une série d'actions avec certaines distributions de probabilité. Ce type de jeu est appelé stratégies mixtes. Le NE des stratégies mixtes est alors un profil d'action mixte avec la propriété qu'aucun joueur ne peut obtenir une plus grande utilité espérée par des changements unilatéraux de son propre profil d'action, alors que les autres laissent leurs profils propres inchangés.

Les caractéristiques des jeux sont analysées en termes d'existence, de multiplicité et de stabilité des NEs. Dans [62], les auteurs donnent un aperçu de ces problèmes.

Une condition qui assure l'existence d'au moins un NE est donnée dans le théorème suivant,

Théorème [62] : Un équilibre existe pour tout jeu concave de K joueurs.

En outre, dans [62], la multiplicité des NEs est analysée. Les auteurs montrent que pour chaque jeu strictement concave, le NE est unique.

11.2.3 Jeu bayésien

Dans un jeu stratégique de base, tous les joueurs ont une parfaite connaissance de la structure du jeu, c'est à dire, les profils d'action disponibles pour les autres joueurs et les fonctions d'utilité des autres joueurs. Il s'agit d'une hypothèse assez

forte. Dans de nombreux cas, les joueurs ne sont pas certains sur les caractéristiques des autres joueurs. Ces jeux à information incomplète sont appelées *Jeux bayésiens*.

La notion de *type* est introduite par John Harsayi [63] pour modéliser les jeux bayésiens. Les joueurs sont caractérisées par des informations privées, comme les utilités, les préférences et les croyances au sujet d'autres joueurs avant que le jeu ne commence. "'Type"' contient toutes les informations pertinentes sur les caractéristiques privés de certains joueurs. En outre, le type d'un joueur est seulement connu par lui-même.

Définition de jeu bayésien [64] [65] : Jeu bayésien est un jeu sous forme stratégique avec des informations incomplètes. Il se compose des éléments suivants :

- Un ensemble fini $\mathcal{S} = \{1, ..., K\}$ de K joueurs.
- Un ensemble de stratégies non vide, $\mathcal{P} = (\mathcal{P}_1 \times ... \times \mathcal{P}_K)$ pour tous les joueurs, où $\mathcal{P}_k$ représente l'ensemble de stratégies disponibles pourle joueur $k \in \mathcal{S}$
- Un ensemble de types Θ, $\Theta = \Theta_1 \times ... \times \Theta_K$, où Θ_k est l'ensemble de types pour le joueur k.
- Une distribution de probabilité sur les types $p_k(\theta_k)$ (des coyances à priori communes sur les types des joueurs) pour tout $k \in \mathcal{S}$ et $\theta_k \in \Theta_k$
- Une fonction d'utilité pour chaque joueur $k \in \mathcal{S}$ $u_k : \mathcal{P}_1 \times ... \times \mathcal{P}_K \times \Theta_1 \times ... \times \Theta_K$.

Remarques :

- Le joueur k utilise une probabilité conditionnelle $p(\theta_{\sim k} \mid \theta_k)$ pour prendre ces décisions et mettre à jour les croyances sur les distributions des types des autres joueurs.
- Une stratégie peut affecter différentes actions à différents types. Les stratégies sont données par correspondances entre l'espace des types vers l'espace des actions, $x_k : \Theta_k \to \mathcal{P}_k$ with elements $x_k(\theta_k)$

Si le joueur k adopte une stratégie x_k, les autres joueurs utilisent des stratégies de $x_{\sim}k$ et le type de joueur k est θ_k, déterminé en moyennant sur tous les types et leurs croyances conditionnelles sur les autres types, la fonction d'utilité obtenue est donnée par :

$$\mathbb{E}u_k(x_k \mid x_{\sim k}, \theta_k) = \sum_{\theta_{\sim k} \in \Theta_{\sim k}} u_k(x_k, x_{\sim k}(\theta_{\sim k}), \theta_k, \theta_{\sim k}) p(\theta_{\sim k} \mid \theta_k) \tag{11.2}$$

Un équilibre de Nash bayésien est similaire à la notion de NE dans un jeu stratégique de base, avec la seule différence que les joueurs doivent prendre en compte les attentes sur les types d'autres joueurs.

Definition de équilibre Nash pour jeu bayésien [65] Un profil d'action $x^*(\theta) = (x_1^*(\theta_1), x_2^*(\theta_2), ..., x_K^*(\theta_K))$ est un équilibre de Nash bayésien si :

$$\mathbb{E}u_k(x_k^* \mid x_{\sim k}, \theta_k) \geq \mathbb{E}u_k(x_k^{'} \mid x_{-k}, \theta_k)$$

pour tout $x_k^{'}(\theta_k) \in X_k$ et tous les types θ_k.

Il est également connu que chaque jeu bayésien fini a un équilibre de Nash bayésien [63].

Chapter 12

Resource Allocation in Slow Fading Interfering Channels with Partial Knowledge of the Channels

In Part II of this thesis, we investigate a block fading interference channel with knowledge of the state of the direct links but only statistical knowledge on the interfering links. The interfering links are modeled as Rayleigh distributed. With this assumption, reliable communications are not possible and a certain level of outage has to be tolerated. We consider the resource allocation for utility functions based on the real throughput accounting for outage events. We propose resource allocation algorithms based on both Bayesian games and optimization. In the context of Bayesian games, we investigate the two cases of *power* allocation *for predefined transmission rates* and *joint power and rate* allocation.

This chapter is structured as follows. In Section 12.1, we present the state of art of resource allocation in interfering channels. In Section 12.2 is devoted to a review of some fundamental concepts of game theory. In Section 12.3, we describe the system model; In Section 12.4, we formulate the rate and power allocation problem as Bayesian game and optimization problem; In Section 12.5, we consider the practical case in which rate is fixed [1] and each source has to determine the power which maximizes its utility. In Section 12.6, we consider the general case where each source has to select its strategy defined in terms of power and transmitting rate, jointly. In Section 12.7 we consider the optimization approach in the two asymptotic regimes of interference limited and noise limited systems. Closed form expressions for the resource allocation are provided. In Section 12.8, some numerical results are

1. In practical systems rates are typically allocated at higher layer and defined in a discrete set, eventually, singleton.

shown. Finally, in Section 12.9, the conclusions of Part II are drawn.

12.1 State of the Art

The large gain in spectral efficiency achievable by sharing the complete frequency spectrum makes ineludible the investigation of the interference channels and is fueling intense research activities on this topic. The interference channel is intrinsically characterized by a limited level of cooperation among communication entities which are rather competing for the same resources and by a decentralized resource management. These complex interactions can be modeled successfully in a game theoretical framework. This direction of investigation is currently receiving considerable attention (e.g., see [52–56]). Many contributions focus on the channels with complete CSI at transmitters. Alternatively, iterative algorithms are proposed whose convergence to an equilibrium point is based on the feedbacks from receivers. A well known and thoroughly studied example of this class of algorithms is the iterative waterfilling algorithm suitable for frequency selective interference channels (see [54] and references therein). Each receiver feeds the overall power spectral density (PSD) of the interference plus noise back to the transmitter of interest, and the transmitter adapts its transmit PSD consequently. The convergence speed of these algorithms limits their applicability. Additionally, the required feedback reduce the system spectral efficiency. In [53] slow fading channels are considered with initial partial CSI. By using the approach of repeated games, information about the channel and the interactions is acquired. When the constraints of a communication system do not allow for the convergence of iterative algorithms or do not support the intensive feedbacks required by iterative algorithms, Bayesian games provide a convenient theoretical framework. Resource allocation based on Bayesian games are adopted in [57–59]. The works in [57, 58] focus on fast fading channels while the Bayesian game in [59] is applied to slow fading multiple access channels based on orthogonal frequency division multiplexing (OFDM). Interestingly, [59] shows that, in terms of achievable throughput, the resource allocation based on Bayesian games has performance comparable to a resource allocation based on an optimization which assumes full channel state information at the transmitter.

12.2 Strategic Game, Nash Equilibrium and Bayesian Game

12.2.1 Strategic Game

A strategic game consists of three elements : 1) a finite set $\mathcal{S}$ of K players, 2) a nonempty strategy set $\mathcal{P} = \mathcal{P}_1 \times \mathcal{P}_2 ... \times \mathcal{P}_K$, where $\mathcal{P}_k$ denotes the strategy set for player $k \in \mathcal{S}$, 3) a set of utility functions $\mathcal{U} = (\mathcal{U}_1(x), ..., \mathcal{U}_K(x))$ of action $x \in \mathcal{P}$, where each player k chooses action x_k, leading to the joint action profile $x = (x_1, ..., x_K)$, and player k obtains its utility as $\mathcal{U}_k(x)$.

12.2.2 Nash Equilibrium

We assume that all the players are making decisions simultaneously and rationally. If the outcome depends on the strategies adopted by other players, we cannot

predict the outcome of the multiple players by simply analyzing a single player independently. We must consider all the players. Then, Nash Equilibrium (NE) is a possible outcome of a interactive decision-making kind of game.

NE is named after the American mathematician John Nash, who introduced this concept in 1950 [60]. It is a fundamental concept in game theory. This concept can simply be expressed as a set of actions, such that no single player can obtain a higher utility by deviating unilaterally its own action while the other players keep their actions unchanged.

Definition of Nash Equilibrium [61] : A Nash Equilibrium is an action profile $x^* \in \mathcal{P}$ with the property that for every player $k \in \mathcal{S}$, we have

$$\forall x_k \in \mathcal{P}_k, \quad x_k \neq x_k^* : \mathcal{U}_k(x_k^*, x_{\sim k}^*) \geq \mathcal{U}_k(x_k, x_{\sim k}^*) \tag{12.1}$$

If the inequality of equation 12.1 holds strictly, then the equilibrium is a strict NE, otherwise, if some player can change its action unilaterally without hurting itself, the NE is called a weak NE.

A game where a player can choose a single action at a time, the game is defined as pure-strategy game. The NE in the pure-strategy game is referred as pure-strategy NE. In some cases, instead of simply choosing an action, players are able to select over a set of actions with some probability distributions. This kind of game is called mixed strategies. The mixed strategy NE is then a mixed action profile with the property that no single player can obtain higher expected utility by change unilaterally from its own action profile, while the others keep unchanged their own action profiles.

The characteristics of games are analyzed in terms of existence, multiplicity, and stability of NEs. In [62], the authors provide some insights of the these issues.

A condition that ensures the existence of at least one NE is given in the following theorem,

Theorem [62] : An equilibrium exists for every concave K-player game.

Furthermore, in [62], the multiplicity of the NEs is analyzed. The authors show that for every strictly concave game, the NE is unique. Interesting readers can refer to [62] for the more information.

12.2.3 Bayesian Game

In a basic strategic game, all the players have perfect knowledge of the structure of the game, i.e., the action profiles available to other players and the utility functions of other players. This is a rather strong assumption. In many cases, players are not certain about the characteristics of other players. These games with incomplete information are called *Bayesian Games*.

The concept of *type* is introduced by John Harsayi [63] to model Bayesian games. Players are characterized by private information, such as utilities, preferences and beliefs about other players before the game starts. "Type" contains all the relevant information about certain player's private characteristics. Furthermore, the type of a player is only known by itself.

Definition of Bayesian Game [64] [65] : A Bayesian game is a strategic form game with incomplete information. It consists of the following elements :

- a finite set $\mathcal{S} = \{1, ..., K\}$ of K players
- a nonempty strategy set, $\mathcal{P} = (\mathcal{P}_1 \times ... \times \mathcal{P}_K)$ for all the players, where $\mathcal{P}_k$ denotes the strategy set available for player $k \in \mathcal{S}$

- a type set Θ, $\Theta = \Theta_1 \times ... \times \Theta_K$, where Θ_k is the set of types of player k.
- a probability distribution over types $p_k(\theta_k)$ (common prior beliefs about the player's types) for all $k \in \mathcal{S}$ and $\theta_k \in \Theta_k$
- an utility function for each $k \in \mathcal{S}$ $u_k : \mathcal{P}_1 \times ... \times \mathcal{P}_K \times \Theta_1 \times ... \times \Theta_K$.

Remarks :

- Player k uses the conditional probability $p(\theta_{\sim k} \mid \theta_k)$ to make decisions and update its beliefs about the distribution of other players' types.
- A strategy may assign different actions to different types. Strategies are given by a mapping from the type space to the action space, $x_k : \Theta_k \rightarrow \mathcal{P}_k$ with elements $x_k(\theta_k)$

If player k adopts strategy x_k, other players use the strategies $x_{\sim k}$ and the type of player k is θ_k, by taking expectations over all types and its conditional beliefs about others' type, the expected utility function is given by

$$\mathbb{E}u_k(x_k \mid x_{\sim k}, \theta_k) = \sum_{\theta_{\sim k} \in \Theta_{\sim k}} u_k(x_k, x_{\sim k}(\theta_{\sim k}), \theta_k, \theta_{\sim k}) p(\theta_{\sim k} \mid \theta_k) \tag{12.2}$$

A Bayesian Nash Equilibrium is similar to the concept of NE in a basic strategic game, with the only difference that the players need to take into account the expectations over other players' types.

Definition of Bayesian Game Nash Equilibrium [65] An action profile $x^*(\theta) = (x_1^*(\theta_1), x_2^*(\theta_2), ..., x_K^*(\theta_K))$ is a Bayesian Nash Equilibrium if

$$\mathbb{E}u_k(x_k^* \mid x_{\sim k}, \theta_k) \geq \mathbb{E}u_k(x_k^{'} \mid x_{-k}, \theta_k)$$

for all $x_k^{'}(\theta_k) \in X_k$ and for all the types θ_k.

It is also known that every finite Bayesian Game has a Bayesian Nash Equilibrium [63].

12.3 System Model

Let us consider an interference channel with two sources $\mathcal{S}_1, \mathcal{S}_2$ and two destinations $\mathcal{D}_1, \mathcal{D}_2$. The two sources transmit independent information and source $\mathcal{S}_i$ aims at communicating with destination $\mathcal{D}_i$, for $i = 1, 2$. We assume that the channel is block fading, i.e. the channel gains of all the links are constant in the time-frame of a codeword but are independent and identically distributed from codeword to codeword. Note that these channels are often referred to as quasistatic channels or as channels with delay-limited capacity [66]. We denote by g_i, $i = 1, 2$ the channel power gains of the direct links $\mathcal{S}_1 - \mathcal{D}_1$ and $\mathcal{S}_2 - \mathcal{D}_2$ and by h_{12} and h_{21} the channel power gains of the interfering links $\mathcal{S}_1 - \mathcal{D}_2$ and $\mathcal{S}_2 - \mathcal{D}_1$. All the channel gains fade independently such that the channel power gain statistics are completely determined by marginal distributions. Each source transmits only private information that can be decoded only by its targeted destination, or equivalently, each receiver performs single user decoding. Additionally, each source knows the realizations of both direct links g_1 and g_2 but not the realizations of the power gains h_{12} and h_{21} for the interfering links. This corresponds to a typical situation (e.g. in cellular systems) where the receivers estimate only the channel gains of the direct links and feed them back to the transmitter, but neglect interfering links. Throughout this work we make the additional assumption that the power gains of the interfering links are Rayleigh distributed, i.e. their probability density function is given by

$\gamma_{H_{ij}}(h_{ij}) = \frac{1}{\sigma_{ij}^2} \mathrm{e}^{-\frac{h_{ij}}{\sigma_{ij}^2}}$. Furthermore, these statistics are known to both sources. At the receiver the channel is impaired by additive Gaussian noise with variance N_0.

12.4 Problem Statement

Because of the partial knowledge of the channel by the sources and the assumption of block fading, reliable communications, i.e. with error probability arbitrarily small, are not feasible (e.g., see [67]) and outage events may happen. If the source i transmits at a certain rate, expressed in nat/sec, with constant transmitted power P_i, an outage event happens if[2]

$$R_i > \log\left(1 + \frac{P_i g_i}{N_0 + P_j h_{ji}}\right), \qquad i, j = 1, 2 \text{ with } i \neq j, \tag{12.3}$$

and the outage probability of source i depends on the choice of R_i, P_i and P_j. We define the throughput as the *average information correctly received by the destination*. Then, the throughput is given by

$$T_i(P_i, R_i, P_j) = R_i \Pr\left\{R_i \leq \log\left(1 + \frac{P_i g_i}{N_0 + P_j h_{ji}}\right)\right\} \tag{12.4}$$

where $i, j = 1, 2$ with $i \neq j$, and $\Pr\{\mathcal{E}\}$ denotes the probability of the event $\mathcal{E}$.

The two sources need to determine autonomously and in a decentralized manner the transmitting power P_i and, eventually also the rate R_i. A natural criterion is to allocate such resources in order to maximize the throughput while keeping power consumption moderate. Then, we define the objective function for source $\mathcal{S}_i$ as

$$u_i((P_i, R_i), (P_j, R_j)) = T_i(P_i, R_i, P_j) - C_i P_i \tag{12.5}$$

where C_i is the cost for unit power.

By making use of the assumption on the power gain distributions of the interfering links, the utility of $\mathcal{S}_i$ is given by

$$\begin{aligned}
&u_i((R_i, P_i), (R_j, P_j)) \\
&= R_i \Pr\left\{R_i \leq \log\left(1 + \frac{P_i g_i}{N_0 + P_j h_{ji}}\right)\right\} - C_i P_i \\
&= \begin{cases}
R_i\left(1 - \exp\left(-\frac{t_i}{P_j \sigma_{ij}^2}\right)\right) - C_i P_i, & \{P_j > 0,\ P_i, R_i \geq 0\}; \\
0, & \{P_j > 0,\ P_i = R_i = 0\}; \\
R_i - C_i P_i, & \{P_j = 0, R_i \geq 0, P_i \geq \frac{(\mathrm{e}^{R_i} - 1) N_0}{g_i}\}; \\
-C_i P_i, & \{P_j = 0, R_i, P_i \geq 0, P_i \leq \frac{(\mathrm{e}^{R_i} - 1) N_0}{g_i}\};
\end{cases} \\
&= \begin{cases}
R_i F_i(t_i) - C_i P_i, & \{P_j > 0,\ R_i \geq 0\} \setminus \{P_i = R_i = 0\}; \\
0, & \{P_j > 0,\ P_i = R_i = 0\}; \\
R_i - C_i P_i, & \{P_j = 0, R_i \geq 0, P_i \geq \frac{(\mathrm{e}^{R_i} - 1) N_0}{g_i}\}; \\
-C_i P_i, & \{P_j = 0, R_i, P_i \geq 0, P_i \leq \frac{(\mathrm{e}^{R_i} - 1) N_0}{g_i}\};
\end{cases}
\end{aligned} \tag{12.6}$$

2. We adopt the notation log for natural logarithms and rates are expressed in nat/sec.

where $t_i = \frac{P_i g_i}{\mathrm{e}^{R_i}-1} - N_0$ and $F_i(t_i) = 1 - \exp\left(-\frac{t_i}{P_j \sigma_{ij}^2}\right)$ and C_i is the cost of unit power by user i.

We study the resource allocation problem by two different criteria. In the optimization approach, the transmitters cooperate to maximize a global utility function accounting for the total throughput and the costs due to transmissions :

$$u(P_1, R_1, P_2, R_2) = u_1((P_1, R_1), (P_2, R_2)) + u_2((P_2, R_2), (P_1, R_1)). \tag{12.7}$$

Note that in this case the costs C_1 and C_2 can be interpreted as the Lagrangian multipliers of constraints on the average transmitted powers P_1 and P_2. Then, the utility function (12.7) corresponds to the dual function (e.g. see [40]) of a constrained optimization problem with objective function

$$T(P_1, R_1, P_2, R_2) = T_1(P_1, R_1, P_2) + T_2(P_2, R_2, P_1). \tag{12.8}$$

Alternatively, we investigate the case as the sources $\mathcal{S}_1$ and $\mathcal{S}_2$ are rational and selfish and allocate their powers and, eventually, their rates to maximize their own utility functions. In this case the problem falls naturally into the framework of competitive games. The objective of source $\mathcal{S}_i$ is to determine the transmit power P_i, and eventually the rate R_i, that selfishly maximizes its utility function $u_i((P_i, R_i), (P_j, R_j))$ under the assumption that a similar strategy is adopted by the other source.

12.5 Interference Game for Power Allocation

In this section we assume that the rates R_1 and R_2 are assigned to the source and define the power allocation problem as a strategic game $\mathcal{G}_\mathcal{P}$ defined by the triplet $\left\{\mathrm{S}, \mathcal{P}, (u_i)_{i\in\mathrm{S}}\right\}$, where $\mathrm{S} = \{\mathcal{S}_1, \mathcal{S}_2\}$ is the set of players or sources, $\mathcal{P}$ represents the set of strategies, and u_i is the utility function of source $\mathcal{S}_i$. The set of strategies is $\mathcal{P} = \mathbb{R}^+ \times \mathbb{R}^+$, where $\mathbb{R}^+$ is the set of nonnegative real numbers. Note that in this case R_i and R_j need be interpreted as parameters of the utility function (12.5) rather than as variables. Furthermore, we assume that $R_i \neq 0$ for $i = 1, 2$ otherwise the game becomes trivial. The definition of the game depends on the costs C_1 and C_2 via the utilities in (12.5). When convenient, for the sake of comprehension we express this dependency explicitly via the notation $\mathcal{G}_\mathcal{P}(C_1, C_2)$.

We shall look for a Nash equilibrium, that is, a strategy $(P_1^*, P_2^*) \in \mathcal{P}$ such that for any $(P_1, P_2) \in \mathcal{P}$,

$$\begin{aligned} u_1((R_1, P_1), (R_2, P_2^*)) &\leq u_1((R_1, P_1^*), (R_2, P_2^*)), \\ u_2((R_2, P_2), (R_1, P_1^*)) &\leq u_2((R_2, P_2^*), (R_1, P_1^*)). \end{aligned}$$

The existence of Nash equilibria for game $\mathcal{G}_P$ is established in the following proposition.

Proposition 1. *A Nash equilibrium of the game $\mathcal{G}_P$ exists in any closed interval and it is a fixed point of the equation*

$$\rho((P_1^*, P_2^*), (P_1^*, P_2^*); R_1, R_2) = \max_{(\pi_1, \pi_2)\in\mathcal{P}} \rho((P_1^*, P_2^*), (\pi_1, \pi_2); R_1, R_2) \tag{12.9}$$

being

$$\rho((P_1,P_2),(\pi_1,\pi_2);R_1,R_2) = \\ u_1((R_1,\pi_1),(R_2,P_2)) + u_2((R_2,\pi_2),(R_1,P_1)). \quad (12.10)$$

Proof : By noting that

$$\frac{\partial^2 u_i}{\partial P_i^2} = -\frac{R_i g_i^2}{P_j^2 \sigma_{ji}^4 (\mathrm{e}^{R_i}-1)^2} \exp\left(-\frac{t_i}{P_j \sigma_{ji}^2}\right) \quad (12.11)$$

is negative everywhere in $\mathcal{P}$, in any closed and convex set of $\mathcal{P}$ the above defined game is an N-concave game as defined in [62]. Then, Theorem 1 in [62] guarantees the existence of a Nash equilibrium in any closed and convex set of $\mathcal{P}$. ■

The Nash equilibria of the game $\mathcal{G}_{\mathcal{P}}$ need to satisfy the system of equations

$$\frac{\partial u_i}{\partial P_i} = -\frac{R_i}{P_j \sigma_{ji}^2} F'(t_i) - C_i = 0 \qquad i,j \in \{1,2\},\ i \neq j. \quad (12.12)$$

From (12.12) it is straightforward to express P_i as a function of P_j, the strategy of the other competing node $\mathcal{S}_j$,

$$P_i = p_i(P_j) \overset{def}{=} \frac{(\mathrm{e}^{R_i}-1)}{g_i}\left(N_0 - \sigma_{ji}^2 P_j \log\left(\frac{C_i(\mathrm{e}^{R_i}-1)\sigma_{ji}^2 P_j}{R_i g_i}\right)\right) \quad (12.13)$$

with $i,j = 1,2$ and $i \neq j$. This function $p_i(P_j)$ provides the best strategy that node $\mathcal{S}_i$ can apply when node $\mathcal{S}_j$ adopts the strategy P_j, and it is shortly referred to as best response of node $\mathcal{S}_i$ to node $\mathcal{S}_j$. The plot of these curves on the plane $P_1 - P_2$ admits interesting interpretation. The points where the two curves intersect correspond to Nash equilibria. Additionally, it provides information on the convergence of a best response algorithm.

The analysis of the best response algorithm yields to the following proposition characterizing the set of Nash equilibria.

Proposition 2. *The strategic game $\mathcal{G}_{\mathcal{P}}$ might have at most three Nash equilibria in the interval $[0,P_1^{\blacktriangle}] \times [0,P_2^{\blacktriangle}]$, being $P_i^{\blacktriangle} = \frac{N_0}{g_i}(\mathrm{e}^{R_i}-1) + \frac{R_i}{C_i \mathrm{e}}$.*

Proof : Note that the best response P_i in (12.13) is defined for $P_j = [0,\overline{P}_j)$ where $\overline{P}_j$ is the point the best response (12.13) of $\mathcal{S}_i$ to P_j crosses $P_i = 0$, i.e., it is the solution to

$$\sigma_{ji}^2 P_j \log\left(\frac{C_i(\mathrm{e}^{R_i}-1)\sigma_{ji}^2 P_j}{R_i g_i}\right) = N_0.$$

Source $\mathcal{S}_i$ responds with the power allocation $P_i^{\square} = \frac{\mathrm{e}^{R_i}-1}{g_i} N_0$ to the strategy $P_j = 0$ of source j and with $P_i = 0$ to $P_j = \overline{P}_j$. It is increasing in the interval $[0,P_j) = \left[0, \frac{R_i g_i \mathrm{e}^{-1}}{C_i \sigma_{ji}^2 (\mathrm{e}^{R_i}-1)}\right)$, with maximum $P_i^{\blacktriangle} = \frac{N_0}{g_i}(\mathrm{e}^{R_i}-1) + \frac{R_i}{C_i \mathrm{e}}$, decreasing elsewhere, and concave everywhere. Based on this analysis these games might have at most three Nash equilibria as apparent from Figure 12.1. ■

Figures 12.1.(a), 12.1.(b), 12.1.(c) show the best responses (12.13) for the sources in the (P_1,P_2)-plane in the cases of three, two, and one Nash equilibria, respectively.

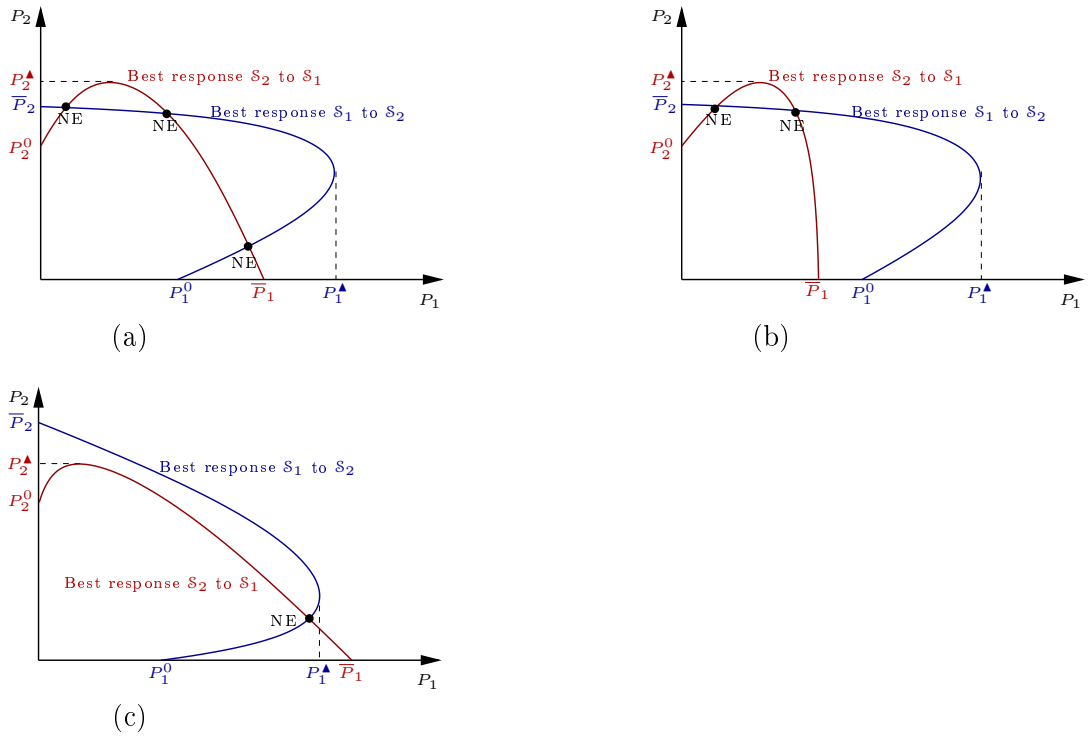

FIGURE 12.1 – Possible Nash equilibrium set for game $\mathcal{G}_{\mathcal{P}}$

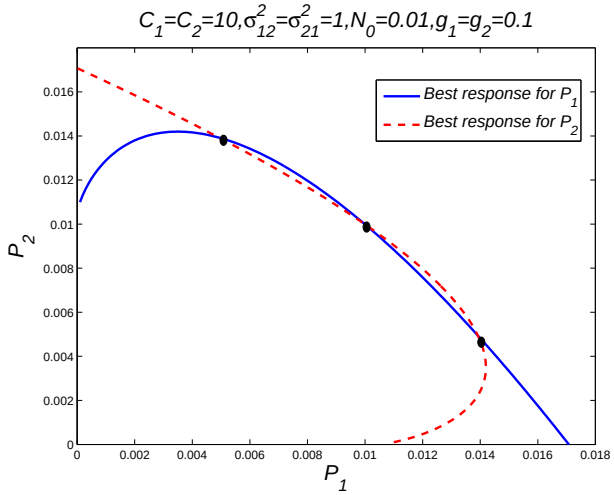

FIGURE 12.2 – Example of a system with three Nash equilibria

Figure 12.2 shows the best responses of a system with more than a Nash equilibrium and the following setting : $R_1 = 0.1$, $R_2 = 0.1$, $C_1 = 10$ $C_2 = 10$, $g_1 = 0.1$, $g_2 = 0.1$, $\sigma_{12}^2 = 1$, $\sigma_{21}^2 = 1$, and $N_0 = 0.01$.

From Figure 12.2 we can identify the following points which are easy to determine and have some interesting features :

- The minimum transmitted power $\overline{P}_1/\overline{P}_2$ from node $\mathcal{S}_1/\mathcal{S}_2$ such that the best response from source $\mathcal{S}_2/\mathcal{S}_1$ corresponds to absence of transmission, i.e. $p_2(\overline{P}_1) = 0$ $/p_1(\overline{P}_2) = 0$. Such points $(\overline{P}_1, 0)$ and $(0, \overline{P}_2)$ are obtained as solution to the equations

$$\sigma_{12}^2 \overline{P}_1 \log\left(\frac{C_2(\mathrm{e}^{R_2}-1)\sigma_{12}^2\overline{P}_1}{g_2 R_2}\right) = N_0 \tag{12.14}$$

and

$$\sigma_{21}^2 \overline{P}_2 \log\left(\frac{C_1(\mathrm{e}^{R_1}-1)\sigma_{21}^2\overline{P}_2}{g_1 R_1}\right) = N_0 \tag{12.15}$$

respectively.

- The points corresponding to the maxima of the best responses $p_1(P_2)$ and $p_2(P_1)$, i.e.

$$(P_1^{\blacktriangle}, P_2^{o}) = \left(\frac{N_0}{g_1}(\mathrm{e}^{R_1}-1) + \frac{R_1}{C_1\mathrm{e}},\ \frac{g_1 R_1}{C_1 \mathrm{e}\sigma_{21}^2(\mathrm{e}^{R_1}-1)}\right) \tag{12.16}$$

and

$$(P_1^{o}, P_2^{\blacktriangle},) = \left(\frac{g_2 R_2}{C_2 \mathrm{e}\sigma_{12}^2(\mathrm{e}^{R_2}-1),\ \frac{N_0}{g_2}(\mathrm{e}^{R_2}-1) + \frac{R_2}{C_2\mathrm{e}}}\right), \tag{12.17}$$

respectively.

The characteristics of the Nash equilibrium set are of primary relevance to predict the output of a game. The uniqueness of a Nash equilibrium is an appealing property for an uncoordinated system. In the following proposition we provide sufficient conditions for the uniqueness of the Nash equilibrium.

Proposition 3. *Let $P_i = p_i(P_j)$ denote the best response of $\mathcal{S}_i$ to power allocation P_j of $\mathcal{S}_j$ as defined in (12.13). Let $\overline{P}_1/\overline{P}_2$ be solutions to (12.14)/(12.15), respectively, and $P_1^{\blacktriangle}/P_2^{\blacktriangle}$ be defined as in (12.16)/(12.17). If*

$$P_i^{\blacktriangle} \leq \overline{P}_i, \qquad\qquad i = 1, 2$$

and

$$\frac{P_2^{\blacktriangle}}{\gamma_2} + \overline{P}_1 \leq p_1(P_2^{\blacktriangle}) \qquad or \qquad \frac{P_1^{\blacktriangle}}{\gamma_1} + \overline{P}_2 \leq p_2(P_1^{\blacktriangle})$$

being $\gamma_i = \frac{\mathrm{d}p_i}{\mathrm{d}P_j}\Big|_{P_j=\overline{P}_j}$, then $\mathcal{G}_{\mathcal{P}}$ has a unique Nash equilibrium.

Proof : Let us consider Figure 12.1.(c). We focus on the best response $p_2(P_1)$ of node $\mathcal{S}_2$ to $\mathcal{S}_1$ and observe that the curve $p_2(P_1)$ lies below the tangent to $p_2(P_1)$ in $\overline{P}_1$ because of the concavity of $p_2(P_1)$. Such a tangent is given by

$$P_2 = \gamma_2(P_1 - \overline{P}_1) \tag{12.18}$$

where $\gamma_i = \left.\frac{\mathrm{d}p_i}{\mathrm{d}P_j}\right|_{P_j=\overline{P}_j}$. Additionally, assume that $P_1^{\blacktriangle} \leq \overline{P}_1$ and $P_2^{\blacktriangle} \leq \overline{P}_2$. Then, all the Nash equilibria lie below the tangent (12.18) and tangent (12.18) crosses $p_1(P_2)$, at most, in two points. If one of the two points has coordinates $(\widetilde{P}_1, \widetilde{P}_2)$ with $\widetilde{P}_2 \geq P_2^{\blacktriangle}$, then the two curves $p_1(P_2)$ and $p_2(P_1)$ cross only in one point and the Nash equilibrium is unique. Note that, from 12.18 the condition $\widetilde{P}_2 \geq P_2^{\blacktriangle}$ is equivalent to the condition that $P_1 = \frac{P_2^{\blacktriangle}}{\gamma_2} + \overline{P}_1 \leq p_1(P_2^{\blacktriangle})$. Exchanging the role of node $\mathcal{S}_1$ and $\mathcal{S}_2$ a similar condition should also hold. This complete the proof of Proposition 3. ■

In the rest of this section we modify the game $\mathcal{G}_{\mathcal{P}}$ to account for the relevant practical issue of power constraints. The constrained game $\mathcal{G}_{\mathcal{P}}^c$ is defined by $\mathcal{G}_{\mathcal{P}}^c = \{\mathcal{S}, \mathcal{P}_c, (T_i)_{i\in\mathcal{S}}\}$, where $\mathcal{S}$ is as for the game $\mathcal{G}_{\mathcal{P}}$, $T_i \equiv T_i(P_i, R_i, P_j)$ is the throughput defined in (12.4), and the strategy set $\mathcal{P}_c = [0, P_1^{\mathrm{MAX}}] \times [0, P_2^{\mathrm{MAX}}]$, being P_1^{MAX} and P_2^{MAX} the maximum transmit powers. Games $\mathcal{G}_{\mathcal{P}}$ and $\mathcal{G}_{\mathcal{P}}^c$ are closely related as illustrated in the following proposition.

Proposition 4. *The Nash equilibria of the game $\mathcal{G}_{\mathcal{P}}^c$ exist and correspond to the Nash equilibria (P_1^*, P_2^*) of games $\mathcal{G}_{\mathcal{P}}(C_1, C_2)$ such that $C_1(P_1^{\mathrm{MAX}} - P_1^*) = C_2(P_2^{\mathrm{MAX}} - P_2^*) = 0$ for $C_1, C_2 \geq 0$.*

Proof : As for Proposition 1, it is straightforward to verify that $\frac{\partial^2 T_i}{\partial P_i^2} \geq 0$, $i = 1, 2$. Additionally, the strategy set is convex. Thus, Theorem 1 in [62] holds. A Nash equilibrium exists and it is the fixed point (P_1^*, P_2^*) satisfying the equation

$$\rho^c((P_1^*, P_2^*), (P_1^*, P_2^*); R_1, R_2) = \max_{(\pi_1,\pi_2)\in\mathcal{P}_c} \rho^c((P_1^*, P_2^*), (\pi_1, \pi_2); R_1, R_2) \quad (12.19)$$

being $\rho^c((P_1, P_2), (\pi_1, \pi_2); R_1, R_2) = T_1(\pi_1, R_1, P_2) + T_2(\pi_2, R_2, P_1)$. By applying the Karush-Kuhn-Tucker (KKT) conditions (e.g. see [40]), it is straightforward to recognize that the Nash equilibria of $\mathcal{G}_{\mathcal{P}}^c$ coincide with the Nash equilibria (P_1^*, P_2^*) of game $\mathcal{G}_{\mathcal{P}}(C_1, C_2)$ such that $C_1(P_1^{\mathrm{MAX}} - P_1^*) = C_2(P_2^{\mathrm{MAX}} - P_2^*) = 0$. ■

12.6 Interference Games for Joint Power and Rate Allocation

In this section we consider a communication system where the transmitters need to allocate both power and rate jointly with the aim of maximizing their own utility functions (12.5). The problem is defined as a strategic game $\mathcal{G} = \left\{\mathcal{S}, \overline{\mathcal{P}}, \{u_i\}_{i\in\{1,2\}}\right\}$, where $\mathcal{S}$ is the set of players, i.e., the two transmitters, $\mathcal{P}$ is the strategy set defined by $\overline{\mathcal{P}} \equiv \{((P_1, R_1), (P_2, R_2)) | P_1, P_2, R_1, R_2 \geq 0\}$, and u_i is the utility function defined in (12.5). Power and rate allocation is obtained as an equilibrium point of the system. When both transmitters aim at maximizing their utility function, a Nash equilibrium is the allocation strategy $(P_1^*, R_1^*, P_2^*, R_2^*)$ such that

$$u_1(P_1^*, R_1^*, P_2^*, R_2^*) \geq u_1(P_1, R_1, P_2^*, R_2^*) \quad \text{for} \quad \forall P_1, R_1 \in \mathbb{R}_+$$

$$u_2(P_1^*, R_1^*, P_2^*, R_2^*) \geq u_2(P_1^*, R_1^*, P_2, R_2) \quad \text{for} \quad \forall P_2, R_2 \in \mathbb{R}_+.$$

It is straightforward to verify that the utility function is not concave in R_i. Then, the classical results on N-concave games in [62] cannot be applied. The analysis

of the general case results very complex. A preliminary characterization of Nash equilibria for game $\mathcal{G}$ is provided in the following proposition. This proposition provides closed form expressions of the Nash equilibria at the boundary of the strategy set jointly with explicit conditions for the points to be Nash equilibria. Possible Nash equilibria internal to the strategy set are provided in an implicit form and they will be further analyzed in additional propositions.

Proposition 5. *A boundary point of the strategy set $\overline{\mathcal{P}}$ is a Nash equilibrium if and only if*

$$P_i = R_i = 0 \tag{12.20}$$

$$P_j = \frac{1}{C_i} - \frac{N_0}{g_j} \qquad R_j = \log\left(\frac{g_j}{N_0 C_j}\right) \tag{12.21}$$

and the following conditions are satisfied

$$g_j - N_0 C_j \geq 0 \tag{12.22}$$

$$\frac{g_i \alpha_j}{C_i \sigma_{ji}^2} \exp\left(-\frac{g_i \alpha_j}{C_i \sigma_{ji}^2} + \frac{1}{N_0 \alpha_j} + 1\right) \geq 1, \tag{12.23}$$

being $i, j \in \{1, 2\}$, $i \neq j$, and $\alpha_j = \frac{C_j g_j}{g_j - N_0 C_j}$.

An internal point of the strategy set $\overline{\mathcal{P}}$ is a Nash equilibrium if and only if it is solution of the system of equations

$$\frac{1}{P_j \sigma_{ji}^2} \exp\left(-\frac{t_i}{P_j \sigma_{ji}^2}\right) = \frac{C_i(\mathrm{e}^{R_i} - 1)}{R_i g_i} \qquad i, j = 1, 2. \tag{12.24}$$

where $t_i = \frac{P_i g_i}{\mathrm{e}^{R_i} - 1} - N_0$ and P_1 and P_2 are given as functions of R_1 and R_2 by

$$\begin{bmatrix} P_1 \\ P_2 \end{bmatrix} = \begin{bmatrix} C_1 \frac{\mathrm{e}^{R_1}}{\mathrm{e}^{R_1} - 1} & \frac{C_1 \sigma_{21}^2}{R_1 g_1}(\mathrm{e}^{R_1} - 1) \\ \frac{C_2 \sigma_{12}^2}{R_2 g_2}(\mathrm{e}^{R_2} - 1) & C_2 \frac{\mathrm{e}^{R_2}}{\mathrm{e}^{R_2} - 1} \end{bmatrix}^{-1} \begin{bmatrix} 1 \\ 1 \end{bmatrix} \tag{12.25}$$

and it satisfies the following inequalities

$$1 + R_i + \frac{g_i R_i}{C_i P_j \sigma_{ji}^2 (\mathrm{e}^{R_i} - 1)} - \frac{2 R_i \mathrm{e}^{R_i}}{\mathrm{e}^{R_i} - 1} > 0 \tag{12.26}$$

$$\frac{R_i^2 g_i}{C_i P_j \sigma_{ji}^2 (\mathrm{e}^{R_i} - 1)} - R_i - \left(1 - \frac{R_i \mathrm{e}^{R_i}}{\mathrm{e}^{R_i} - 1}\right)^2 > 0. \tag{12.27}$$

Proof : Let us consider first a Nash equilibrium internal to the strategy set $\overline{\mathcal{P}}$. For the joint allocation of the powers and rates the Nash equilibria necessarily satisfy the following system of equations

$$\begin{aligned} \frac{\partial u_i}{\partial P_i} &= \frac{R_i g_i}{\mathrm{e}^{R_i} - 1} F_i'(t_i) - C_i = 0 && i = 1, 2 \\ \frac{\partial u_i}{\partial R_i} &= F_i(t_i) - \frac{R_i P_i g_i \mathrm{e}^{R_i}}{(\mathrm{e}^{R_i} - 1)^2} F_i'(t_i) = 0 && i = 1, 2 \end{aligned} \tag{12.28}$$

or, equivalently, the system

$$1-\exp\left(-\frac{t_i}{P_j\sigma_{ji}^2}\right)=P_iC_i\frac{\mathrm{e}^{R_i}}{\mathrm{e}^{R_i}-1} \qquad i=1,2 \tag{12.29}$$

$$\frac{1}{P_j\sigma_{ji}^2}\exp\left(-\frac{t_i}{P_j\sigma_{ji}^2}\right)=\frac{C_i(\mathrm{e}^{R_i}-1)}{R_ig_i} \qquad i,j=1,2. \tag{12.30}$$

By linearly combining (12.29) and (12.30) with coefficients 1 and $P_j\sigma_{ji}^2$, respectively, we obtain

$$C_i\frac{\mathrm{e}^{R_i}}{\mathrm{e}^{R_i}-1}P_i+C_i\frac{\mathrm{e}^{R_i}-1}{g_iR_i}P_j\sigma_{ij}^2=1 \qquad i,j=1,2. \tag{12.31}$$

From the system of 2-equations (12.31) it is straightforward to obtain (12.25).

A solution of the the system of 4-equations (12.29)-(12.30) is a Nash equilibrium if it satisfies the conditions

$$\frac{\partial^2u_i}{\partial R_i^2}<0,\ \frac{\partial^2u_i}{\partial P_i^2}<0,\ H=\frac{\partial^2u_i}{\partial R_i^2}\frac{\partial^2u_i}{\partial P_i^2}-\left(\frac{\partial^2u_i}{\partial P_i\partial R_i}\right)^2>0. \tag{12.32}$$

Note that

$$\frac{\partial^2u_i}{\partial R_i^2}=-\frac{P_ig_i\mathrm{e}^{R_i}}{P_j\sigma_{ji}^2(\mathrm{e}^{R_i}-1)^2}\exp\left(-\frac{t_i}{P_j\sigma_{ji}^2}\right)\left(2-\frac{2R_i\mathrm{e}^{R_i}}{\mathrm{e}^{R_i}-1}+R_i+\frac{g_iR_iP_i\mathrm{e}^{R_i}}{P_j\sigma_{ji}^2(\mathrm{e}^{R_i}-1)^2}\right) \tag{12.33}$$

$$\frac{\partial^2u_i}{\partial P_i^2}=-\frac{R_ig_i^2}{P_j^2\sigma_{ji}^4(\mathrm{e}^{R_i}-1)^2}\exp\left(-\frac{t_i}{P_j\sigma_{ji}^2}\right) \tag{12.34}$$

and the Hessian

$$H=\frac{g_i^2\exp\left(-\frac{2t_i}{P_j\sigma_{ji}^2}\right)}{P_j^2\sigma_{ji}^4(\mathrm{e}^{R_i}-1)^2}\left(\frac{R_i^2g_iP_i\mathrm{e}^{R_i}}{P_j\sigma_{ji}^2(\mathrm{e}^{R_i}-1)^2}-\left(1-\frac{R_i\mathrm{e}^{R_i}}{\mathrm{e}^{R_i}-1}\right)^2\right). \tag{12.35}$$

Thus, conditions (12.32) reduce to the conditions that the second factors in the r.h.s of (12.33) and (12.35) are positive, i.e.,

$$2-\frac{2R_i\mathrm{e}^{R_i}}{\mathrm{e}^{R_i}-1}+R_i+\frac{g_iR_iP_i\mathrm{e}^{R_i}}{P_j\sigma_{ji}^2(\mathrm{e}^{R_i}-1)^2}>0 \tag{12.36}$$

$$\frac{R_i^2g_iP_i\mathrm{e}^{R_i}}{P_j\sigma_{ji}^2(\mathrm{e}^{R_i}-1)^2}-\left(1-\frac{R_i\mathrm{e}^{R_i}}{\mathrm{e}^{R_i}-1}\right)^2>0. \tag{12.37}$$

By observing from (12.31), that,

$$P_i=\left(1-\frac{C_i\sigma_{ji}^2P_j}{g_iR_i}(\mathrm{e}^{R_i}-1)\right)\frac{(\mathrm{e}^{R_i}-1)}{C_i\mathrm{e}^{R_i}}, \tag{12.38}$$

and by substituting them in (12.36) and (12.37), we obtain (12.26)-(12.27).

Let us turn to the case of a Nash equilibrium at the boundary of the strategy set. Without loss of generality we assume that $P_i = R_i = 0$. Then, the best response of user j to a strategy $P_i = R_i = 0$ is obtained by transmitting at the maximum rate $R_j^o = \log\left(1 + \frac{P_j g_j}{N_0}\right)$ with a power maximizing the payoff $u_j = \log\left(1 + \frac{P_j g_j}{N_0}\right) - C_j P_j$. It is apparent that the payoff is maximized for $P_j^{\square} = \frac{1}{C_j} - \frac{N_0}{g_j}$ and the strategy (R_j, P_j) is feasible if and only if $g_j - N_0 C_j \geq 0$. Policy (12.20) is a Nash equilibrium if and only if $P_i = R_i = 0$ is the best response of player i when player j transmits with power $P_j^{\square} = \frac{1}{C_j} - \frac{N_0}{g_j}$. This is verified if and only if $u_i((R_i, P_i), (R_j^{\square}, P_j^{\square}))$ does not have local maxima in the positive quadrant such that $u_i((R_i, P_i), (R_j, P_j)) > 0$. A local maximum (R_i, P_i) satisfies (12.30) and (12.38) for $(R_j, P_j) = (R_j^{\square}, P_j^{\square})$. Substituting (12.38) in (12.30) yields

$$1 - \frac{x_i R_i}{\mathrm{e}^{R_i} - 1} \exp\left(-\frac{x_i}{\mathrm{e}^{R_i}} + \frac{\mathrm{e}^{R_i} - 1}{R_i \mathrm{e}^{R_i}} + n_i\right) = 0 \tag{12.39}$$

with $x_i = \frac{g_i g_j C_j}{C_i \sigma_{ji}^2 (g_j - N_0 C_j)}$ and $n_i = \frac{g_j - N_0 C_j}{C_j N_0 g_j}$. It is possible to show that (12.39) admits a single positive root which is the best response in terms of rate to the strategy $(R_j^{\square}, P_j^{\square})$ of user j if and only if $1 - x_i \exp(-x_i + 1 + n_i) > 0$. The proof of this condition is a special case of the proof of Proposition 10 proven in a subsequent appendix. Then, a local maximum in the positive quadrant does not exit if and only if $1 - x_i \exp(-x_i + 1 + n_i) \leq 0$. For $\alpha_j = \frac{C_j g_j}{g_j - N_0 C_j}$ we obtain (12.22). This concludes the proof of Proposition 5. ■

In order to get additional insights into the system behavior and in particular into the Nash equilibria internal to the strategy set $\overline{\mathcal{P}}$, we consider first of all the following extreme cases before discussing the general case : (1) the noise tends to zero, (*interference limited regime*), (2) the noise is much higher than the transmitted power (*high noise regime*).

12.6.1 Interference Limited Regime

When the noise variance N_0 is negligible compared to the interference power level, the payoff function is efficiently approximated by (12.6), with $t_i = \frac{P_i g_i}{\mathrm{e}^{R_i} - 1}$. Note that in the interference limited regime, the payoff (12.6) of node $\mathcal{S}_i$ is defined for $0 \leq N_0 \ll P_j$, i.e. $P_j > 0$. In the following proposition equilibria of game $\mathcal{G}$ are obtained as equilibria of an equivalent game in a single decision variable x_i for source $\mathcal{S}_i$.

Proposition 6. *When the the noise variance tends to zero, a Nash equilibrium of game $\mathcal{G}$ and internal to $\overline{\mathcal{P}}$ satisfy the system of equations*

$$\begin{aligned} x_1 &= \kappa_2 f(x_2) \\ x_2 &= \kappa_1 f(x_1) \end{aligned} \tag{12.40}$$

where $x_i = \frac{g_i}{C_i P_j \sigma_{ji}^2}$, $\kappa_i = \frac{C_i g_j}{C_j \sigma_{ij}^2}$, $i, j \in 1, 2$, $i \neq j$ and

$$f(x) = \left(1 - \frac{\mathrm{e}^{R(x)} - 1}{xR(x)}\right)^{-1} \left(1 - \mathrm{e}^{-R(x)}\right)^{-1} \tag{12.41}$$

for $1 < x < \infty$. *In (12.41),* $R(x)$ *is the unique* ***positive*** *solution of the equation*

$$1 - \frac{xR}{\mathrm{e}^R - 1}\exp\left(-\frac{x}{\mathrm{e}^R} + \frac{\mathrm{e}^R - 1}{R\mathrm{e}^R}\right) = 0 \tag{12.42}$$

such that

$$-x + \frac{\mathrm{e}^R - 1}{R} \neq 0. \tag{12.43}$$

Let (x_1^0, x_2^0) *be solutions of system (12.40). The corresponding Nash equilibrium is given by*

$$P_1 = \frac{g_2}{C_2 x_2^0 \sigma_{12}^2}, \quad R_1 = R(x_1^0),$$
$$P_2 = \frac{g_1}{C_1 x_1^0 \sigma_{21}^2}, \quad R_2 = R(x_2^0).$$

Proof : From (12.28), (12.31), and $t_i = \frac{P_i g_i}{\mathrm{e}^R - 1}$, a Nash equilibrium satisfies the following equation

$$\frac{\partial u_i}{\partial R_i} = 1 - \frac{x_i R_i}{\mathrm{e}^{R_i} - 1}\exp\left(-\frac{x_i}{\mathrm{e}^{R_i}} + \frac{\mathrm{e}^{R_i} - 1}{R_i \mathrm{e}^{R_i}}\right) = 0 \tag{12.44}$$

with $x_i = \frac{g_i}{C_i P_j \sigma_{ji}^2}$. It is apparent that the point $R_i \neq 0$ satisfying

$$-1 - x_i R_i + \mathrm{e}^{R_i} = 0 \tag{12.45}$$

is also a solution of (12.44). It is worth to observe that (12.45) admits a positive solution only for $x_i > 1$ and for $x_i > 1$, (12.44) admits two zeros. The greatest zero is the positive root of (12.45) while the smallest, denoted by $R_i = R_i^*(x_i)$, has an intermediate values between zero and the root of (12.44). It can be determined numerically. Additionally, $\frac{\partial u_i}{\partial R_i}$ is positive in the interval $(0, R_i^*(x_i))$ and then alternates its sign. Then, $R_i^*(x_i)$ corresponds to a maximizer and is the best response of user i in terms of rate to the the policy of user j. By substituting $R_i = R^*(x_i)$, $x_i = \frac{g_i}{P_j \sigma_{ji}^2 C_i}$ and $P_i = \frac{g_j}{\sigma_{ij}^2 C_i x_j}$ in (12.31), x_j can be expressed as a function of x_i

$$x_j = \frac{C_i g_j}{C_j \sigma_{ij}^2}\left(1 - \frac{\mathrm{e}^{R^*(x_i)} - 1}{x_i R^*(x_i)}\right)^{-1}\left(1 - \mathrm{e}^{-R^*(x_i)}\right)^{-1} \tag{12.46}$$

Thanks to the selection of the root to (12.44), the selected x_j is a maximum. It can be verified numerically that conditions (12.26) and (12.27) are always satisfied by $R_i = R^*(x_i)$ for any interference channel in the interference limited regime thanks to the fact they depend on the system parameters only via x_i. ■

Remarks

- The solution $R(x_j)$ to (12.42) is the rate which maximizes the utility function corresponding to the transmit power of the other transmitter $P_i = \frac{g_j}{C_j x_j \sigma_{ij}^2}$. It lies in the interval $\left(0, \overline{R}(x_j)\right)$ and we refer to it as the *best response in terms of rate* of player j to strategy P_i of player i. Similarly, $\kappa_j f(x_j)$ is inverse proportional to the *best response in terms of power* of user j to the strategy P_i of its opponent.
- Interestingly, the solution (x_1^0, x_2^0) to system (12.40) depends on the system parameters only through the constants κ_1 and κ_2.

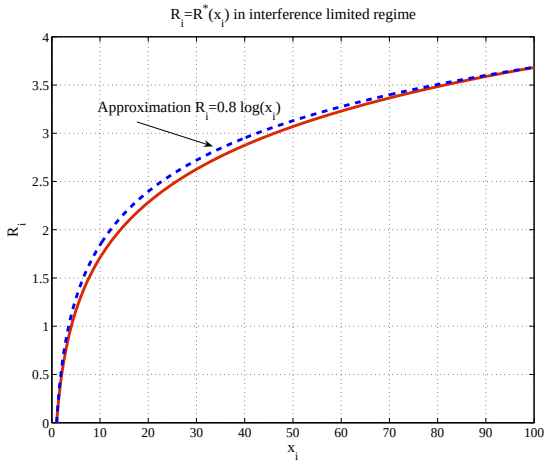

FIGURE 12.3 – Best response $R^*(x_i)$ of user i to the transmitted power $P_j = \frac{g_i}{x_i \sigma_{ji} C_i}$ in solid line and its approximation $0.8\log x_i$ in dashed line.

- The existence and uniqueness of a Nash equilibrium for the class of systems considered in Proposition 6 reduces to the analysis of the solution of system (12.40) and depends on the system via κ_1 and κ_2.
- The solution to (12.42) can be effectively approximated by $R(x) \approx 0.8\log(x)$. Then, the function $f(x)$ is approximated by

$$\widetilde{f}(x) = \left(1 - \frac{\mathrm{e}^{0.8\log(x)} - 1}{x 0.8\log(x)}\right)^{-1} \left(1 - \mathrm{e}^{-0.8\log(x)}\right)^{-1}. \tag{12.47}$$

  In Figure 12.4, $f(x)$ is plotted and compared to its approximation $\widetilde{f}(x)$. The approximation $\widetilde{f}(x)$ matches almost perfectly $f(x)$ in a way that it can be utilized efficiently for practical and analytical objectives.

The following proposition provides sufficient conditions for the existence of a Nash equilibrium.

Proposition 7. *When the noise variance is negligible compared to the interference, a Nash equilibrium of the game $\mathcal{G}$ exists if*

$$(\kappa_1 - 1)(\kappa_2 - 1) > 0 \tag{12.48}$$

with κ_i defined in Proposition 6.

Proof : Let us observe that the curve $x_2 = \kappa_1 f(x_1)$ has two asymptotes in $x_1 = 1$ and $x_2 = \kappa_1$ and $x_1 = \kappa_2 f(x_2)$ has two asymptotes in $x_2 = 1$ and $x_1 = \kappa_2$. If $\kappa_1 > 1$ ($\kappa_1 < 1$) the curve $x_2 = \kappa_1 f(x_1)$ lies on the right (left) of other curve as $x_1 \to +\infty$. Similarly, if $\kappa_2 > 1$ ($\kappa_2 < 1$) the curve $x_1 = \kappa_2 f(x_2)$ lies on the left (right) of other curve as $x_2 \to +\infty$. Then, because of the continuity of the two curves, they have to cross at least in one point. Thus, two curves cross if $\kappa_1 < 1$ and $\kappa_2 < 1$ or if $\kappa_1 > 1$ and $\kappa_2 > 1$. These conditions are implied by (12.48). This concludes the proof of Proposition 7. ■

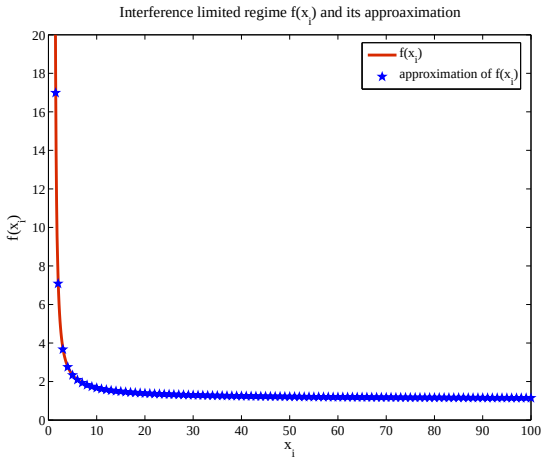

FIGURE 12.4 – $f(x_i)$ in solid line and its approximation $\widetilde{f}(x_i)$

General conditions for the uniqueness of the Nash equilibrium are difficult to determine analytically. Let us observe that, in generally speaking, a system in the interference limited regime may have more than one Nash equilibrium. Let us consider a system with $\kappa_1 = \kappa_2$. The two curves $x_j = \kappa_i f(x_i)$, $i, j \in \{1, 2\}, i \neq j$, cross each other in $x_1 = x_2$. Furthermore, the curve $x_2 = \kappa_1 f(x_1)$ ($x_1 = \kappa_2 f(x_2)$) has two asymptotes in $x_1 = 1$ and $x_2 = \kappa_1$ ($x_2 = 1$ and $x_1 = \kappa_2$). Then, for $\kappa_1 = \kappa_2 = 1$, the two curves cross again in $(1, +\infty)$ and $(+\infty, 1)$. Let us observe now Figure 12.5 where the best responses of the two systems corresponding to the two pairs of coefficients $\kappa_1^{(1)} = \kappa_2^{(1)} = 1.05$ and $\kappa_1^{(2)} = \kappa_2^{(2)} = 2$ are plotted. It becomes apparent that the curves with $\kappa_1^{(1)} = \kappa_2^{(1)} = 1.05$ will cross again for large x_1 and x_2 values since $x_2 = \kappa_1^{(1)} f(x_1)$ has two asymptotes in $x_1 = 1$ and $x_2 = 1.05$, while $x_1 = \kappa_2^{(1)} f(x_2)$ has two asymptotes in $x_2 = 1$ and $x_1 = 1.05$. These crossing points correspond to NEs. In contrast, the curves with $\kappa_1^{(1)} = \kappa_2^{(1)} = 2$ will diverge from each other. It is worth noticing that for $x_1 \gg 1$, $x_2 \approx 1$ and for $x_2 \gg 1$, $x_1 \approx 1$. From a telecommunication point of view, it is necessary to question whether the model for $N_0 \ll P_j g_j$ is still applicable. In fact, in such a case, $P_i \ll \frac{g_i}{C_i \sigma_{ij}^2}$, but also $P_i \gg N_0$ has to be satisfied because of the system model assumptions. Typically, the additional NEs with some $x_i \approx 1$ are not interesting from a physical point of view since the system model assumptions are not satisfied. Thus, additional NEs are artifacts introduced by the asymptotic model.

By numerical simulations, we could observe that games with multiple Nash equilibria exist for a very restricted range of system parameters, more specifically for $1 \leq \kappa_i \leq 1.1$.

Proposition 6 suggests also an iterative algorithm for computing a Nash equilibrium based on the best response. Choose an arbitrary point $x_1^{(0)}$ and compute the corresponding value $x_2^{(0)} = \kappa_1 f(x_1^{(0)})$. From a practical point of view, this is equivalent to choose arbitrarily the transmitted power $P_2^{(0)} = \frac{g_1}{\sigma_{21}^2 x_1^{(0)} C_1}$ for transmitter 2 and determine the power allocation for source $\mathcal{S}_1$ which maximizes its utility function. The optimum power allocation for node $\mathcal{S}_1$ is $P_1^{(0)} = \frac{g_2}{\sigma_{12}^2 x_2^{(0)} C_2}$. We shortly

refer to $P_1^{(0)}$ as the best response of node $\mathcal{S}_1$ to node $\mathcal{S}_2$. Then, by using $x_2^{(0)}$ it is possible to compute $x_1^{(1)} = \kappa_2 f\left(x_2^{(0)}\right)$, the best response of node $\mathcal{S}_2$ to source $\mathcal{S}_1$. By iterating the computation of the best responses of node $\mathcal{S}_1$ and node $\mathcal{S}_2$, we can obtain resource allocations closer and closer to the Nash equilibrium and converge to the Nash equilibrium. We refer to this algorithm as the best response algorithm.

The best response algorithm is very appealing for its simplicity. Nevertheless, its convergence is not guaranteed. This issue is illustrated in Figure 12.5. Let us consider the interference channel with $\kappa_1 = \kappa_2 = 1.05$ and the corresponding solid and dashed curves $x_2 = \kappa_1 f(x_1)$ and $x_1 = \kappa_2 f(x_2)$. The Nash equilibrium exists and is unique, but the best response algorithm diverges from the Nash equilibrium even for choices of the initial point arbitrarily close to the Nash equilibrium but different from it. Numerical results show that, if κ_1 and κ_2 are both greater than 1.1, the best response algorithm always converges to a Nash equilibrium.

Proposition 8. *For sufficiently large κ_1 and κ_2, the fixed point iterations*

$$\begin{cases} x_1^{(k+1)} = \kappa_2 f(x_2^{(k)}), \\ x_2^{(k+1)} = \kappa_1 f(x_1^{(k)}), \end{cases} \tag{12.49}$$

converge.

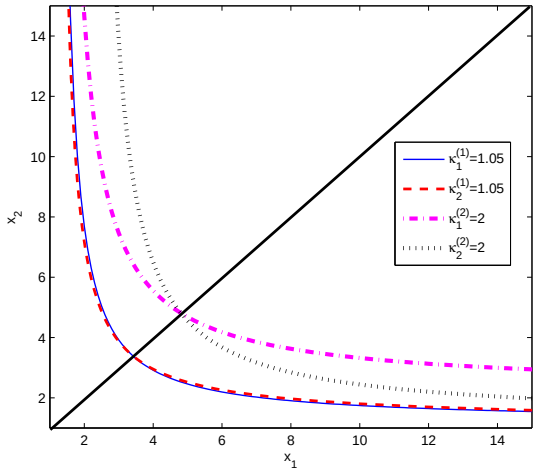

FIGURE 12.5 – Graphical investigation of convergence of the best response algorithm in the interference limited regime

In fact, large values of κ_1 and κ_2 correspond to practical situations where the channel gain of the direct link is higher than the variance of the interfering link.

Proof : Let $R(x)$ and $f(x)$ be defined as in (12.42) and (12.41), respectively. From the theory of contraction mapping, we know that the fixed point iterations (12.49) converge if the eigenvalues of the matrix

$$\begin{bmatrix} 0 & \kappa_1 f'(x_2^*) \\ \kappa_2 f'(x_1^*) & 0 \end{bmatrix}$$

are in absolute value lower than one. The fixed point (x_1^*, x_2^*) is a solution of the system

$$\begin{cases} x_1^* = \kappa_1 f(x_2^*), \\ x_2^* = \kappa_2 f(x_1^*). \end{cases}$$

The above matrix condition is equivalent to

$$\kappa_1 f'(x_1^*)\kappa_2 f'(x_2^*) < 1 \tag{12.50}$$

Since the function $f(x)$ has a horizontal asymptote $y = 1$, we conclude that

$$x_1^* \sim \kappa_1, \quad x_2^* \sim \kappa_2, \quad \kappa_1, \kappa_2 \to \infty.$$

And hence the condition (12.50) becomes

$$\kappa_1 f'(\kappa_1)\kappa_2 f'(\kappa_2) < 1$$

Thus, the above condition is satisfied if the rate of decrease of the derivative $f'(\kappa_1)$ is faster than $1/\kappa_1$. First, let us estimate the rate of growth of $R(x)$. For large x, the equation (12.42) can be written in the form

$$\frac{e^R}{xR} = \exp\left(-\frac{x}{e^R} + \frac{e^R - 1}{Re^R}\right) + o(1),$$

or, by taking logarithm, in the form

$$R = \log(x) + \log(R) - \frac{x}{e^R} + o(1),$$

The above equation implies that the asymptotic rate of growth of $R(x)$ is at least $\log(x)$. In turn, this implies that the derivative of $f(x)$ decreases asymptotically as $1/(x\log(x))$ or faster. Consequently, the condition (12.50) is satisfied for large enough κ_1 and κ_2. ■

12.6.2 High Noise Regime

Let us turn to the case when noise is much higher than the useful received power, $P_i g_i \ll N_0$. The throughput can be approximated by

$$\begin{aligned} \overline{T}_i\left(P_i, R_i, P_j, P_j\right) &= R_i \Pr\left\{R_i \le \tfrac{P_i g_i}{N_0 + P_j h_{ji}}\right\} \\ &= R_i \Pr\left\{h_{ji} \le \tfrac{1}{P_j}\left(P_i \tfrac{g_i}{R_i} - N_0\right)\right\} \end{aligned} \tag{12.51}$$

Interestingly, the throughput in (12.51) is nonzero for $\frac{P_k}{R_k} > \frac{N_0}{g_k}$. Since Proposition 5 defines completely the Nash equilibria on the boundary of the strategy set in the general case, in this section we focus only on internal points of $\overline{\mathcal{P}}$. Then, the utility function is given by

$$v_i(P_i, R_i, P_j, R_j) = R_i\left(1 - \exp\left(-\frac{\left(P_i \frac{g_i}{R_i} - N_0\right)}{P_j \sigma_{ji}^2}\right)\right) - C_i P_i \tag{12.52}$$

for $i = 1, 2$. Correspondingly, we consider the game $\overline{\mathcal{G}} = \left\{\mathcal{S}, \overset{o}{\overline{\mathcal{P}}}, \mathcal{V}\right\}$, where the set of players coincides with the corresponding set in $\mathcal{G}$ while the utility function set $\mathcal{V}$ consists of the functions (12.52) and $\overset{o}{\overline{\mathcal{P}}}$ is the open interval obtained from $\overline{\mathcal{P}}$. The joint rate and power allocation is given by a Nash equilibrium of game $\overline{\mathcal{G}}$.

The following proposition states the conditions for the existence and uniqueness of a Nash equilibrium in the strategy set and provides the equilibrium point.

Proposition 9. *Game $\overline{\mathcal{G}}$ admits a Nash equilibrium if and only if*

$$\frac{g_i}{C_i} > N_0, \quad i = 1, 2.$$

If the above conditions are satisfied, $\overline{\mathcal{G}}$ has a unique equilibrium $\left((R_i^*, P_i^*), (R_j^*, P_j^*)\right)$ where P_i^* and P_j^* are the unique roots of the equations

$$\left(1 - \ln\left(\frac{C_j P_i \sigma_{ij}^2}{g_j}\right)\right) P_i \sigma_{ij}^2 = \frac{g_j}{C_j} - N_0 \tag{12.53}$$

and

$$\left(1 - \ln\left(\frac{C_i P_j \sigma_{ji}^2}{g_i}\right)\right) P_j \sigma_{ji}^2 = \frac{g_i}{C_i} - N_0 \tag{12.54}$$

in the intervals $\left(0, \frac{g_j}{C_j \sigma_{ij}^2}\right)$ and $(0, \frac{g_i}{C_i \sigma_{ji}^2})$ respectively. Also,

$$R_i = \frac{P_i g_i C_i}{g_i - P_j \sigma_{ji}^2 C_i} \quad \textit{and} \quad R_j = \frac{P_j g_j C_j}{g_j - P_i \sigma_{ij}^2 C_j}.$$

Proof : In this case the system of equations satisfied by Nash equilibria is given by

$$\frac{\partial v_i}{\partial P_i} = \frac{g_i}{P_j \sigma_{ji}^2} \exp\left(-\frac{1}{P_j \sigma_{ji}^2}\left(P_i \frac{g_i}{R_i} - N_0\right)\right) - C_i$$

and

$$\frac{\partial v_i}{\partial R_i} = 1 - \left(1 + \frac{P_i g_i}{\sigma_{ji}^2 P_j R_i}\right) \exp\left(-\frac{1}{\sigma_{ji}^2 P_j}\left(P_i \frac{g_i}{R_i} - N_0\right)\right)$$

with $i, j = 1, 2$, and $i \neq j$.

Also,

$$\frac{\partial v_2}{\partial P_2} = \frac{g_2}{P_1 \sigma_{12}^2} \exp\left(-\frac{1}{P_1 \sigma_{12}^2}\left(P_2 \frac{g_2}{R_2} - N^0\right)\right) - C_2$$

and

$$\frac{\partial v_2}{\partial R_2} = 1 - \left(1 + \frac{P_2 g_2}{\sigma_{12}^2 P_1 R_2}\right) \exp\left(-\frac{1}{P_1 \sigma_{12}^2}\left(P_2 \frac{g_2}{R_2} - N_0\right)\right).$$

Furthermore

$$\frac{\partial^2 v_i}{\partial P_i^2} = -\frac{g_i^2}{\sigma_{ji}^4 P_j^2 R_i} \exp\left(-\frac{1}{P_j \sigma_{ji}^2}\left(P_i \frac{g_i}{R_i} - N_0\right)\right) < 0,$$

and

$$\frac{\partial^2 v_i}{\partial R_i^2} = -\frac{g_i^2 P_1^i}{P_j^2 R_i^3 \sigma_{ji}^4} \exp\left(-\frac{1}{P_j \sigma_{ji}^2}\left(P_i \frac{g_i}{R_i} - N_0\right)\right) < 0.$$

Thus, the roots of the equations

$$\frac{\partial v_i}{\partial P_i} = 0 \qquad \text{and} \qquad \frac{\partial v_i}{\partial R_i} = 0 \qquad i, j = 1, 2,\ i \neq j \tag{12.55}$$

supply us with the best response strategies for source $\mathcal{S}_i$.

Note that the first equation in (12.55) is equivalent to the following one :

$$\frac{P_i g_i}{R_i} = N_0 - \ln\left(\frac{C_i P_j \sigma_{ji}^2}{g_i}\right) P_j \sigma_{ji}^2. \tag{12.56}$$

Similarly the second is equivalent to

$$\left(1 + \frac{P_i g_i}{R_i} \frac{1}{P_j \sigma_{ji}^2}\right) \exp\left(-\frac{1}{P_j \sigma_{ji}^2}\left(\frac{P_i g_i}{R_i} - N_0\right)\right) = 1 \tag{12.57}$$

By substituting (12.56) into (12.57) we obtain

$$\left(1 - \ln\left(\frac{C_i P_j \sigma_{ji}^2}{g_i}\right)\right) P_j \sigma_{ji}^2 = \frac{g_i}{C_i} - N_0. \tag{12.58}$$

Let $f_i(P_j) = \left(1 - \ln\left(\frac{C_i P_j \sigma_{ji}^2}{g_i}\right)\right) P_j \sigma_{ji}^2$, then,

$$\frac{d\, f_i(P_j)}{d\, P_j} = -\sigma_{ji}^2 \ln\left(\frac{C_i P_j \sigma_{ji}^2}{g_i}\right).$$

Thus, $f_i(P_j)$ is increasing for $P_j \in \left(0, \frac{g_i}{C_i \sigma_{ji}^2}\right)$ and decreasing for $P_j \in \left(\frac{g_i}{C_i \sigma_{ji}^2}, \infty\right)$. Thus,

$$f_i\left(\frac{g_i}{C_i \sigma_{ji}^2}\right) = \max_{P_j} f_i(P_j)$$

It is clear that

$$f_i\left(\frac{g_i}{C_i \sigma_{ji}^2}\right) = g_i/C_i > g_i/C_i - N_0.$$

Thus, (12.58) has two roots P_{j1*} and P_{j2*} such that $P_{j1*} < \frac{g_i}{C_i \sigma_{ji}^2}$ and $P_{j2*} > \frac{g_i}{C_i \sigma_{ji}^2}$.

By (12.58),

$$-\ln\left(\frac{C_i P_j \sigma_{ji}^2}{g_i}\right) P_j \sigma_{ji}^2 = \frac{g_i}{C_i} - N_0 - P_j \sigma_{ji}^2.$$

which implies, by (12.56),

$$\frac{P_i g_i}{R_i} = \frac{g_i}{C_i} - P_j \sigma_{ji}^2.$$

Since $P_i g_i / R_i > 0$ we have that P_j has to be such that $P_j < g_i/(C_i \sigma_{ji}^2)$. This completes the proof of Proposition 9. ■

Interestingly, the power allocation of node $\mathcal{S}_i$ decouples from the one of node $\mathcal{S}_j$ and P_i depends on its opponent only via the system parameter ratio $\frac{C_j}{g_j}$.

12.6.3 General Case

Let us consider now the general case, when the noise, the powers of interferences and the transmitted powers are of the same order of magnitude. A Nash equilibrium necessarily satisfies the system of equations (12.24) and (12.25). Substituting (12.25) in (12.24) yields

$$1 - \frac{x_i R_i}{\mathrm{e}^{R_i} - 1} \exp\left(-\frac{x_i}{\mathrm{e}^{R_i}} + \frac{\mathrm{e}^{R_i} - 1}{R_i \mathrm{e}^{R_i}} + n_i \right) = 0 \quad i = 1, 2 \tag{12.59}$$

with $n_i = \frac{N_0}{P_j \sigma_{ji}^2}$. Equations (12.25) and (12.59) provide an equivalent system to be satisfied by a Nash equilibrium. In order to determine a Nash equilibrium, we can proceed as in the case of the interference limited regime. Observe that, in this case, (12.59) depends on the system parameters and the other player strategy not only via x_i but also via n_i. Then, the general analysis feasible for any communication system in the interference limited regime is no longer possible and the existence and multiplicity of Nash equilibria should be studied independently for each communication system. Nevertheless, we can follow an approach similar to the one adopted for the interference limited regime. In the following, we detail guidelines for this analysis.

From (12.59), it is possible to determine the best response in terms of rate of transmitter i to policy P_j of transmitter j. Conditions for the existence of such best response are detailed in the following statement.

Proposition 10. *If $x_i > 1$, (12.59) admits positive roots if and only if*

$$1 - x_i \mathrm{e}^{-x_i + 1 + n_i} > 0. \tag{12.60}$$

If (12.60) is satisfied, (12.59) admits a single positive root in the interval $(0, \log x_i)$, which corresponds to the best response in terms of rate to policy P_j of source $\mathcal{S}_j$.

Proof : Let us consider the function of the variable R parametric in x and ζ

$$\mathcal{F}(R; x, \zeta) = -\zeta \exp\left(-\frac{x}{\mathrm{e}^R} + \frac{\mathrm{e}^R - 1}{R\mathrm{e}^R} \right) + \frac{\mathrm{e}^R - 1}{xR}. \tag{12.61}$$

Note that the equation $\mathcal{F}(R; x, \zeta) = 0$ is equivalent to (12.42) and (12.59) for $\zeta = 1$ and $\zeta = \mathrm{e}^{n_i}$, respectively. We analyze the behaviour of $\mathcal{F}(R; x, \zeta)$ in order to characterize its zeros for $\zeta \in [1, +\infty)$. The analysis for $\zeta = 1$ was already carried out in the proof of Proposition 6.

The following limits hold

$$\lim_{R \to 0^+} \mathcal{F}(R; x, \zeta) = \mathcal{F}(0, x, \zeta) = -\zeta \exp(-x + 1) + \frac{1}{x}$$
$$\lim_{R \to +\infty} \mathcal{F}(R; x, \zeta) = +\infty.$$

Let us consider the two functions of the variable R

$$h(R; x) = -\exp\left(-\frac{x}{\mathrm{e}^R} + \frac{\mathrm{e}^R - 1}{R\mathrm{e}^R} \right)$$

and

$$k(R; x) = \frac{\mathrm{e}^R - 1}{xR}.$$

The first function values $-\exp(-x+1)$ in $R=0$ and -1 for $R \to +\infty$. It decreases up to a minimum and then increases again. The function $k(R;x)$ is increasing for any positive value of R. Then, the function $\digamma(R;x,\zeta)$ may decrease in an interval around $R=0$ if the slope (derivative) of the product $\zeta h(R;x)$ is lower and the derivative of $k(R;x)$. For large R it definitively increases. If $\digamma(R;x,\zeta)|_{R=0} < 0$ then, there is an $R = R^{\diamondsuit}$ such that $\digamma(R;x,\zeta) < 0$ for $R \in (0, R^{\diamondsuit})$ and $\digamma(R;x,\zeta) > 0$ for $R \in (R^{\diamondsuit}, +\infty)$. Then, the point $R = R^{\diamondsuit}$ is a minimizer of the utility function of game $\mathcal{G}$. There is no maximizer internal to the strategy set, i.e. the best response to x is $R=0$. If $\digamma(R;x,\zeta)|_{R=0} > 0$, then $\digamma(R;x,\zeta)$ could have two zeros. The first (with lower value) zero corresponds to a maximizer of the utility function. On the contrary, the second corresponds to a minimizer. Thus, a necessary condition for having a nonzero best response is that

$$\digamma(0;x,\zeta) = -\zeta \exp(-x+1) + \frac{1}{x},$$

which coincides with (12.60) for $x > 0$ and $\zeta = \mathrm{e}^n$. Let us denote by $R^{(a)}(x,\zeta)$ and $R^{(b)}(x,\zeta)$ the zeros of $\digamma(R;x,\zeta)$ corresponding to the maximizer and minimizer of the utility function. Since $h(R;x)$ is negative for any $R > 0$ and $x > 1$, for $\zeta \geq 1$ it results

$$\digamma(R;x,\zeta) \leq \digamma(R;x,1).$$

This implies that $R^{(a)}(x,\zeta) \leq R^{(a)}(x,1)$ and $R^{(b)}(x,\zeta) \geq R^{(b)}(x,1)$.

We observe that for $x > 1$

$$\digamma(\log(x);x,1) \leq 0$$

and recall that $\digamma(R;x,1) < 0$ only in the interval $(R^{(a)}(x,1), R^{(b)}(x,1))$. Thus, $R = \log(x)$ separates the zeros of $\digamma(\log(x);x,1)$, i.e. $R^{(a)}(x,1) \leq \log(x) \leq R^{(b)}(x,1)$. Since

$$R^{(a)}(x,\zeta) \leq R^{(a)}(x,1) \leq \log(x) \leq R^{(b)}(x,1) \leq R^{(b)}(x,\zeta),$$

$R = \log(x)$ also separate the two eventual roots of $\digamma(R;x,\zeta)$. This concludes the proof of Proposition 10. ■

From the best responses in terms of rate, it is straightforward to determine the best response in terms of powers for the two players.

12.7 Optimum Joint Rate and Power Allocation

In this section, we study the joint rate and power allocation when both transmitting nodes cooperate to maximize the utility function in the same strategy set $\overline{\mathcal{P}}$ of game $\mathcal{G}$ (see Section 12.6).

The objective function is defined as

$$u(P_1,P_2,R_1,R_2) = \sum_{i=1,i\neq j}^{2} \left(T_i(P_i,R_i,P_j,R_j) - C_iP_i\right) \tag{12.62}$$

$$= \sum_{i=1}^{2} \left(R_iF_i(t_i) - C_iP_i\right). \tag{12.63}$$

We consider again the two extreme regimes when the noise is very high and when it is negligible compared to the interference power level. In both cases we

show that the optimum resource allocation privileges a single user transmission. The following two propositions state the results.

Proposition 11. *Let us assume that the noise is very high compared to the power transmitted by the transmitter, or equivalently,* $\frac{g_i}{C_i} > N_0$ *and* $\frac{g_i}{C_i} \approx N_0$, $i = 1, 2$. *Then, if*

$$\log \frac{g_i}{C_i N_0} > \log \frac{g_j}{C_j N_0} \quad i, j = 1, 2 \quad i \neq j \tag{12.64}$$

transmitter $\mathcal{S}_i$ *transmits at power* $P_i = \frac{1}{g_i}\left(\frac{g_i}{C_i} - N_0\right)$ *and rate* $R_i = \log\left(\frac{g_i}{C_i N_0}\right) \approx \frac{g_i}{C_i N_0}$, *and the transmitter* j *is silent, i.e.* $P_j = R_j = 0$.

Similarly, when the noise is negligible compared to the interference from the other user the following result holds.

Proposition 12. *Let us assume that the noise variance is very low while the potential interference from the source could be substantially higher, i.e,* $N_0 \to 0$ *and* $\frac{\sigma_{21}^2}{C_2} \gg 0$ *for transmitter 1 and* $N_0 \to 0$ *and* $\frac{\sigma_{12}^2}{C_1} \gg 0$ *for transmitter 2. There does not exist an optimum allocation strategy for both* $P_1, P_2 > 0$. *If (12.64) is satisfied, transmitter* i *transmits at power and rate*

$$P_i = \frac{1}{g_i}\left(\frac{g_i}{C_i} - N_0\right) \approx \frac{1}{C_i} \text{ and } R_i = \log\left(\frac{g_i}{C_i N_0},\right)$$

respectively, while transmitter j *stays silent.*

Proof : In order to prove Proposition 11 we first show that, for $C_1, C_2 > 0$ there is no optimum corresponding to resource allocation implying both nodes in the interference limited region. Then, we show that an optimum implying that one of the sources causes an interference much higher than the noise level of the other communication cannot be internal to $\overline{\mathcal{P}}$ but it could lie on its boundary. More specifically, it is a working point where the source causing high interference is the only one that transmits. The applicability of the model for the interference limited regime for the other communication provides the conditions in Proposition 11 for the optimality of the point at the boundary of $\overline{\mathcal{P}}$.

Let us assume that there exist an optimum corresponding to the a condition where both communications occur in the interference limited region. We show by contradiction that such a situation does not happen. Let us consider the utility function in (12.7). Its derivatives with respect to P_i and R_i are given by

$$\frac{\partial u}{\partial P_i} = \frac{R_i g_i}{P_j \sigma_{ij}^2 (\mathrm{e}^{R_i} - 1)} \exp\left(-\frac{t_i}{P_j \sigma_{ij}^2}\right) - \frac{R_j t_j}{\sigma_{ji}^2 P_i^2} \exp\left(-\frac{t_j}{P_i \sigma_{ij}^2}\right) - C_i \tag{12.65}$$

and

$$\frac{\partial u}{\partial R_i} = 1 - \exp\left(-\frac{t_i}{P_j \sigma_{ij}^2}\right) - \frac{R_i P_i g_i \mathrm{e}^{R_i}}{P_j \sigma_{ij}^2 (\mathrm{e}^{R_i} - 1)^2} \exp\left(-\frac{t_i}{P_j \sigma_{ij}^2}\right), \tag{12.66}$$

respectively. An extreme (maximizer or minimizer) of (12.7) internal to $\overline{\mathcal{P}}$ should satisfy the system of equations

$$\frac{\partial u}{\partial P_i} = \frac{\partial u}{\partial R_i} = 0, \tag{12.67}$$

i.e.,

$$\frac{R_i g_i}{\sigma_{ij}^2 P_j (\mathrm{e}^{R_i}-1)} \exp\left(-\frac{t_i}{P_j}\right) - \frac{R_j t_j}{\sigma_{ji}^2 P_i^2} \exp\left(-\frac{t_j}{\sigma_{ji}^2 P_i}\right) = C_i, \quad i,j \in \{1,2\}, i \neq j \tag{12.68}$$

and

$$1 - \exp\left(-\frac{t_i}{P_j \sigma_{ij}^2}\right) = \frac{P_i R_i g_i \mathrm{e}^{R_i}}{(\mathrm{e}^{R_j}-1)^2 P_j \sigma_{ij}^2} \exp(-\frac{t_i}{P_j \sigma_{ij}^2}), \quad i,j \in \{1,2\}, i \neq j. \tag{12.69}$$

From (12.69) we obtain

$$\exp\left(-\frac{t_i}{\sigma_{ij}^2 P_j}\right) = \frac{\sigma_{ij}^2 P_j (\mathrm{e}^{R_i}-1)^2}{\sigma_{ij}^2 (\mathrm{e}^{R_i}-1)^2 P_j + R_i g_i \mathrm{e}^{R_i} P_i}, \quad i,j \in \{1,2\}, i \neq j. \tag{12.70}$$

In the interference limited region, $t_i = \frac{P_i g_i}{\mathrm{e}^{R_i}-1}$, as already discussed in Section 12.6. Then, substituting (12.70) into (12.68) yields

$$\frac{R_i g_i (\mathrm{e}^{R_i}-1)}{(\mathrm{e}^{R_i}-1)^2 P_j + R_i g_i \mathrm{e}^{R_i} P_i} - \frac{P_j R_j g_j (\mathrm{e}^{R_j}-1)}{P_i \left[(\mathrm{e}^{R_j}-1)^2 P_i + R_j g_j \mathrm{e}^{R_j} P_j\right]} = C_i \quad i,j \in \{1,2\}, i \neq j. \tag{12.71}$$

We show that the system of equations (12.71) does not admit any solution such that $P_i > 0$ and $R_i > 0$. Let us define

$$S_i = \frac{R_i g_i (\mathrm{e}^{R_i}-1)}{\sigma_{ij}^2 (\mathrm{e}^{R_i}-1)^2 P_j + R_i g_i \mathrm{e}^{R_i} P_i} \tag{12.72}$$

and observe that $S_i > 0$ for $P_i > 0$ and $R_i > 0$. Then, (12.71) can be rewritten as

$$\begin{bmatrix} 1 & -\frac{P_2}{P_1} \\ -\frac{P_1}{P_2} & 1 \end{bmatrix} \begin{bmatrix} S_1 \\ S_2 \end{bmatrix} = \begin{bmatrix} C_1 \\ C_2 \end{bmatrix}. \tag{12.73}$$

Since the matrix in the l.h.s. (left hand side) has rank 1, the system would admit infinite solutions if and only if

$$\frac{C_2}{C_1} = -\frac{P_1}{P_2}.$$

However, $C_1, C_2 > 0$, thus the system (12.71) does not admit any positive solution.

Let us consider now the possibility to have an optimum point such that one node is working in the interference limited region. Without loss of generality we can assume that $\mathcal{S}_1$ is such a source and $0 \leq N_0 \leq P_2$. Then, (12.65), (12.66), (12.68), and (12.69) hold for

$$t_1 = \frac{P_1 g_1}{\mathrm{e}^{R_1}-1} \tag{12.74}$$

and

$$t_2 = \frac{P_2 g_2}{\mathrm{e}^{R_2}-1} - N_0. \tag{12.75}$$

Then, following the same approach as in the case when both communications occur in the interference limited regime we obtain

$$\begin{bmatrix} 1 & -\left(\frac{P_2}{P_1} - \frac{R_2(\mathrm{e}^{R_2}-1)}{P_1 g_2} N_0\right) \\ -\frac{P_1}{P_2} & 1 \end{bmatrix} \begin{bmatrix} S_1 \\ S_2 \end{bmatrix} = \begin{bmatrix} C_1 \\ C_2 \end{bmatrix}. \tag{12.76}$$

Since the matrix in the l.h.s. has rank 2, the system admits a unique solution with

$$S_2 = \frac{\left(C_1 + \frac{P_2}{P_1} C_2\right) P_1 g_2}{(\mathrm{e}^{R_2} - 1) N_0 R_2}. \tag{12.77}$$

The previous equation (12.77) and the definition in (12.72) yield

$$\frac{\left(C_1 + \frac{P_2}{P_1} C_2\right) P_1 g_2}{(\mathrm{e}^{R_2} - 1) N_0 R_2} = \frac{R_2 g_2 (\mathrm{e}^{R_2} - 1)}{\sigma_{21}^2 (\mathrm{e}^{R_2} - 1)^2 P_1 + R_2 g_2 \mathrm{e}^{R_2} P_2}. \tag{12.78}$$

By making use of the assumption that $P_2, R_2 > 0$, we can rewrite (12.78) as

$$(C_1 P_1 + C_2 P_2) \left[\frac{P_1}{R_2^2 P_2 g_2} + \frac{g_2 \mathrm{e}^{R_2}}{\sigma_{21}^2 (\mathrm{e}^{R_2} - 1)^2 R_2} \right] = \frac{N_0}{P_2 \sigma_{21}^2}. \tag{12.79}$$

Since we assume that $N_0 \ll P_2$, thus, $\frac{N_0}{P_2 \sigma_{21}^2} \to 0$ when $\mathcal{S}_1$ is in the interference limited regime. This observation implies again that

$$C_1 P_1 + C_2 P_2 \approx 0.$$

Therefore, there is no optimum internal to $\overline{\mathcal{P}}$ in the interference limited region of Source 1. ■

Closed form resource allocation strategies for the general case are not available and numerical constrained optimization is necessary.

12.8 Numerical Results

In this section, we assess the performance of the proposed algorithms and compare them. The resource allocation has a complex dependency on several system parameters, e.g. noise, channel gains, costs. We have seen from the proposed best response algorithm that, in reasonable cases, the algorithm converges to the Nash equilibrium in internal points of the interval, not on its boundary. This has a two-fold benefit. Firstly, this implies that a centralized communication is unnecessary. Secondly, for the Nash equilibrium in the interval, both users are transmitting and this guarantees the fairness of the system. In this section, we mainly consider Nash equilibrium internal to the strategy set. We first investigate the performance of the game based resource allocation on the system parameters. We consider a system with parameters $\sigma_{12}^2 = \sigma_{21}^2 = 0.1$ and $g_1 = g_2 = 1$. Figure 12.6 shows the throughput attained by the algorithm for joint power and rate allocation based on Bayesian games for increasing costs $C_i = C_j$. As expected, in the general case, an increase of the costs implies a decrease of the achievable throughput. The solid line in Figure 12.6 shows the throughput in the interference limited regime. In this case the system performance is completely independent of the channel cost. At first glance, this behavior could appear surprising. However, it is a straightforward consequence of Proposition 6 when we observe that the best responses depend on the costs only via the ratio C_1/C_2. The dependency of the throughput on the costs becomes more and more relevant when the noise increases. This is apparent from the dot curve and the dashed curve in Figure 12.6. The dashed-dotted line in Figure 12.6 shows the degradation in terms of throughput, when the presence of noise is neglected in

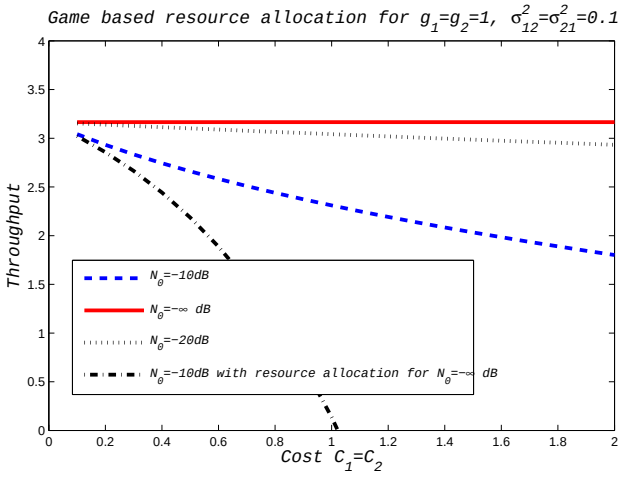

FIGURE 12.6 – Throughput attained at the Nash equilibrium versus costs $C_1 = C_2$ for different values of the noise.

the resource allocation but $N_0 = -10dB$. Figure 12.7 illustrates the dependency of the throughput on the channel attenuation g_2 of node $\mathcal{S}_2$ for the following set of parameters : $\sigma_{12}^2 = \sigma_{21}^2 = 0.1$, $N_0 = -10dB$, $C_1 = C_2 = 1$. For increasing values of g_2, the total throughput increases. In contrast, the throughput of node $\mathcal{S}_1$ decreases because of the increased interference of $\mathcal{S}_2$ on $\mathcal{S}_1$. Note that for game based resource allocation the nodes access simultaneously to the channel while the optimum resource allocation privileges a *time sharing* policy.

Figure 12.8 compares the game based resource allocation to frequency sharing. Assumed that each user has a certain power constraint, and in the frequency sharing case, each user transmits separately with its own maximum available power half of the total transmitting time. For a low power constraint, the throughput of the game-based resource allocation outperforms the frequency sharing strategy. However, when the available transmitting power gets large, the frequency sharing strategy gains larger throughputs than the game-based resource allocation.

Figure 12.9 and 12.10 compare the game-based resource allocation to the optimum one. They show the throughput and the power, respectively, as function of the costs. For very low values of N_0 and low costs, the optimum resource allocation outperforms significantly the game based approach at the expenses of fairness. In fact, the former assigns the spectrum to a single user. The performance loss at the Nash equilibrium decreases as the costs increases. The gap between the the throughput attained by optimum resource allocation and Nash equilibrium shown in Figure 12.10 is usually referred as price of anarchy in literature.

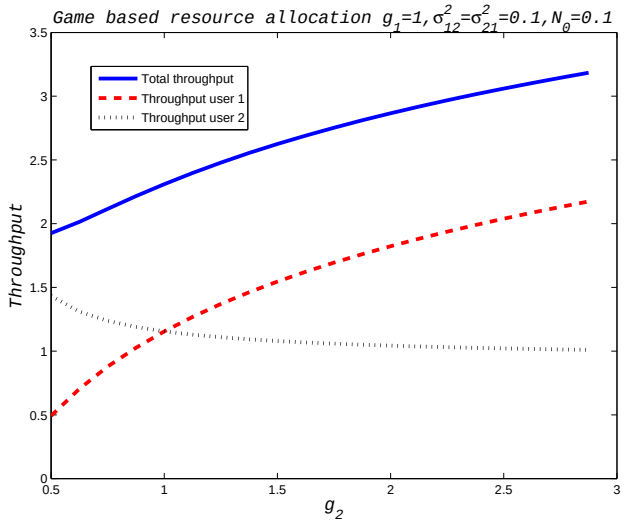

FIGURE 12.7 – Throughput of the two communications and total throughput attained at the Nash equilibrium versus the channel attenuation g_2 of node $\mathcal{S}_2$.

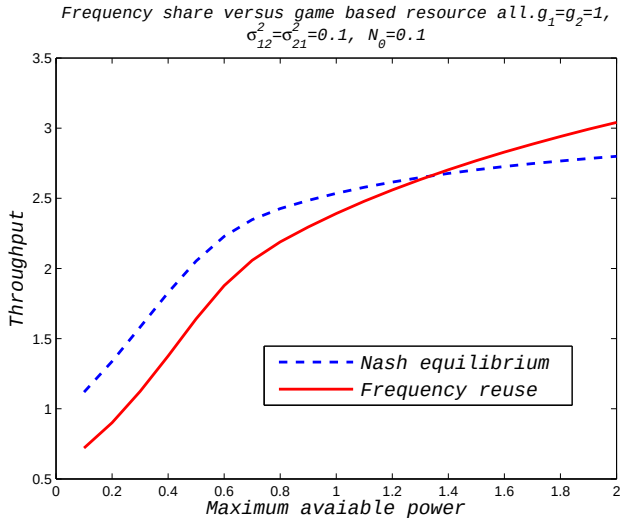

FIGURE 12.8 – Throughput versus maximum available power attained at Nash equilibria and by frequency sharing.

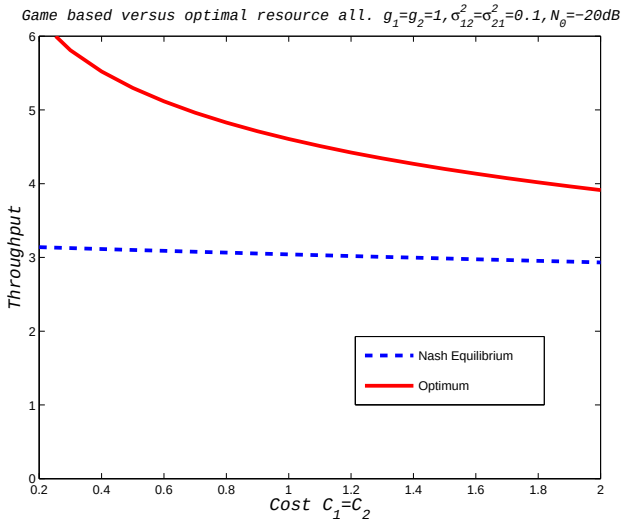

FIGURE 12.9 – Throughput versus costs $C_1 = C_2$. Comparison between the throughput attained by Bayesian games or by optimum resource allocation.

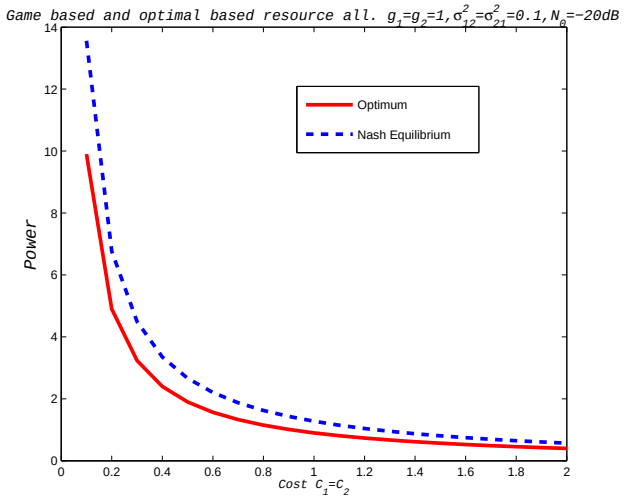

FIGURE 12.10 – Transmitted power versus costs $C_1 = C_2$. Comparison between the resources allocated by Nash equilibria or by optimum resource allocation.

12.9 Conclusions

In Part II, we investigate the behavior of a wireless communication system when the transmitting sources have only partial knowledge of the channel. We consider a block fading interference channel with knowledge of the state of the direct links but only statistical knowledge about the interfering links. We consider the resource allocation for utility functions based on the real throughput accounting for outage events. We propose resource allocation algorithms based on both Bayesian games and optimization.

In the context of Bayesian games, we investigate the two cases of *power* allocation *for predefined transmission rates* and *joint power and rate* allocation. We show that the first game boils down to a concave game. Thus, Nash equilibrium always exist and we show that they are at most three. Some sufficient conditions for the uniqueness of the Nash equilibria are also provided. On the contrary, the second group of games is not concave and its analysis is performed by introducing an equivalent game. The characteristics of the game theoretical approaches are analyzed in terms of existence, multiplicity, and stability of the Nash equilibria. Special attention is devoted to the asymptotic regimes of high noise and to the interference limited regime. In the former case, a closed form expression for the Nash equilibrium is provided. In the latter case, criteria for the convergence of best response algorithms are discussed. The optimization approach is also analyzed in the two above mentioned regimes and closed form expressions for the resource allocation are provided. Interestingly, in the asymptotic regimes, the optimum allocation implies a condition of starvation for one communication, while the resource allocation based on Baysian games is fairer.

Chapter 13

Conclusions and Perspectives

In this chapter, we conclude the two parts of this thesis and discuss shortly some possible perspectives and extensions of future works.

13.1 Conclusions

In the thesis, we consider two different communication systems where complete CSI is not available.

In Part I of this thesis, we consider a SS based on adaptive beamforming with mobile ST. In the satellite channel, the propagation delay is very long compared to the coherence time. Therefore, instantaneous CSI becomes stale very quickly and cannot be used for the design of adaptive beamforming. We propose an approach, namely, the PLSE algorithm to estimate the slow-varying component, more specifically, the directivity vectors of the channel. Then, we use this partial CSI to design the adaptive beamformer. We also consider the detection of active STs, possible resolve of collision in the random access channel. Numerical results show that the adaptive beamformer designed based on the estimated directivity vectors outperforms significantly a conventional fixed beamforming system in terms of served STs and power efficiency.

In Part II of this thesis, we consider a block fading interfering channel with two transmitter/receiver pairs. For both transmitters, CSI of direct links are perfectly known. However, they only have the statistical knowledge of the interfering links. We study the problem of transmission and power allocation in an autonomous and decentralized manner in the absence of perfect CSI. We propose resource allocation algorithms based on Bayesian games and optimization. In the context of Bayesian games, we analyze the existence, the multiplicity and stability of Nash equilibria. Special attention is devoted to the asymptotic regimes of high noise and to the interference limited regime. The optimization approach is also analyzed in the above two regimes and closed form expressions for the resource allocation are provided.

13.2 Perspectives of Part I

The possible future developments of Part I could be as the following ones :

- *Design of Adaptive Beamforming based on directivity vectors :* In Chapter 6, we propose two practical heuristics algorithms for the beamforming design. The complexity of the proposed algorithms remains low, and they can be implemented in the practical systems easily. However, it would be interesting to study the design of an almost optimal transceiver (beamformer and receivers) based on limited CSI. This could be done, while keeping complexity low by making use of Random Matrix theory. The design of a robust beamformers could be a further more advanced step.
- *Estimation of directivity vectors in the reverse link :* In Chapter 7, we propose a parametric model of the channels where the directivity vector is parametrically represented by a linear combination of given known directivity vectors. We assumed perfect knowledge of the directivity vectors, i.e., of the joint radiation patterns of SAs. However, this implies perfect calibration and realization of SAs. A directivity vector estimation robust to perturbation of the reference values is an appealing extension of the proposed work. Additionally, if the directivity vectors of the reference points are not available, new approaches to estimate the directivity vectors only based on the observation of received signals at the gateway have to be developed.
- *Contention Resolutions in random access channel :* In Chapter 8, we have shown that when we adopt QPSK signals as training sequences, as the number of STs increases, the requirements of training length and group cardinality become quite demanding with consequent loss in spectral efficiency. Orthogonal training sequences allow for much higher performance compared to random training. However, they impose strict synchronization requirements. A careful design of the training sequences, e.g. Gold codes provides a good tradeoff between the synchronization requirements and good performance.

13.3 Perspectives of Part II

- In Part II of this thesis, we consider two pairs of transmitters/receivers. In the future work, we could investigate the scenario where K pairs of transmitters/receivers are communicating.
- For the optimization joint rate and power allocation problem, closed form resource allocation strategies are given in the interference limited regime and high noise regime. However, a rigorous optimization technique for the general case is not available. Further efforts could be devoted to the analysis of this problem.

Bibliography

[1] M. Sharif and B. Hassibi, "On the capacity of mimo broadcast channels with partial side information," *Information Theory, IEEE Transactions on*, vol. 51, no. 2, pp. 506 – 522, feb. 2005.

[2] L. C. Godara, *Handbook of Antennas in Wireless Communications.* CPC press LLC, 2002.

[3] G. Maral and M. Bousquet, *Satellite Communications Systems.* Jon Wiley Sons Ltd, 1993.

[4] A. S. Ivica Stevanovic and J. R. Mosig, "Smart antenna systems for mobile communications," Lausanne, Suisse, Tech. Rep., 2003.

[5] G. Caire, L. Cottatelluci, M. Debbah, G. Lechner, and R. Muller, "Interference Mitigation Techniques for Satellite Systems," *Novel Intra-System Interference Mitigation Techniques & Technologies for Next Generations Broadband Satellite Systems*, april 2005.

[6] L. G. Roberts, "ALOHA packet systems with and without slots and capture," in *APPANET Systen Note 8 (NIC11290)*, jun 1972.

[7] N. Abramson, "The throughput of packet broadcasting channels," *Communications, IEEE Transactions on*, vol. 25, no. 1, pp. 117 – 128, jan 1977.

[8] G. Choudhury and S. Rappaport, "Diversity ALOHA–a random access scheme for satellite communications," *Communications, IEEE Transactions on*, vol. 31, no. 3, pp. 450 – 457, mar 1983.

[9] D. Raychaudhuri, "ALOHA with multipacket messages and ARQ-type retransmission protocols–throughput analysis," *Communications, IEEE Transactions on*, vol. 32, no. 2, pp. 148 – 154, feb 1984.

[10] Raychaudhuri, "Stability, throughput, and delay of asynchronous selective reject ALOHA," *Communications, IEEE Transactions on*, vol. 35, no. 7, pp. 767 – 772, jul 1987.

[11] H. V. Poor, *An Introduction to Signal Detection and Estimation.* Springer-Verlag, 1996.

[12] T. L. Marzetta, "Blast Training : Estimating Channel Characteristics for High Capacity Space-Time Wireless," in *Proc. 37th Annual Allerton Conference on Communications, Control, and Computing*, 1999, pp. 958–966.

[13] J. Baltersee, G. Fock, and H. Meyr, "Achievable rate of MIMO channels with data-aided channel estimation and perfect interleaving," *Selected Areas in Communications, IEEE Journal on*, vol. 19, no. 12, pp. 2358 –2368, dec 2001.

[14] D. Samardzija and N. Mandayam, "Pilot-assisted estimation of MIMO fading channel response and achievable data rates," *Signal Processing, IEEE Transactions on*, vol. 51, no. 11, pp. 2882 – 2890, nov 2003.

[15] P. R. King, "Modelling and Measurement of the Land Mobile Satellite MIMO Radio Propagation Channel," *PhD Thesis*, 2007.

[16] G. Grimmett and D. Stirzaker, *Probability and Random Processes* . Oxford University Press, 1992.

[17] B. R. Elbert, *Introduction to Satellite Communication.* Artech-House, 2008.

[18] P. Fortescue, L. Mottershead, G. Swinerd, and J. Stark, *Spacecraft Systems Engineering.* John Wiley and Sons, 2003.

[19] M.Costa, "Writing on dirty paper," *IEEE Trans. Information Theory*, vol. 29, no. 1, pp. 439–441, may 1983.

[20] G. Caire and S. S. Shamai, *Writing on dirty tape with LDPC codes.* Multiantenna Channels : Capacity, Coding and Signal Processing, Editors : Gerard J. Foschini and Sergio VerdÃ?, American Mathematical Society, ISBN : 082183407X ,DIMACS Series in Discrete Mathematics and Theoretical Computer Science, Volume 62, November 1, 2003, 11 2003. [Online]. Available : http ://www.eurecom.fr/publication/1338

[21] M. Tomlinson, "New automatic equaliser employing modulo arithmetic," *Electronics Letters*, vol. 7, no. 5, pp. 138 –139, 25 1971.

[22] H. Harashima and H. Miyakawa, "Matched-transmission technique for channels with intersymbol interference," *Communications, IEEE Transactions on*, vol. 20, no. 4, pp. 774 – 780, aug 1972.

[23] Q. Spencer, A. Swindlehurst, and M. Haardt, "Zero-forcing methods for downlink spatial multiplexing in multiuser mimo channels," *Signal Processing, IEEE Transactions on*, vol. 52, no. 2, pp. 461 – 471, feb. 2004.

[24] R. Fischer, *Precoding and Signal Shaping for Digital Transmission.* John Wiley and Sons Inc., New York,, 2002.

[25] S. Shi, M. Schubert, and H. Boche, "Downlink MMSE Transceiver Optimization for Multiuser MIMO Systems : Duality and Sum-MSE Minimization," *Signal Processing, IEEE Transactions on*, vol. 55, no. 11, pp. 5436 –5446, nov. 2007.

[26] M. Schubert and H. Boche, "Solution of the multiuser downlink beamforming problem with individual SINR constraints," *Vehicular Technology, IEEE Transactions on*, vol. 53, no. 1, pp. 18 – 28, jan. 2004.

[27] N. Vucic, H. Boche, and S. Shi, "Robust Transceiver Optimization in Downlink Multiuser MIMO Systems," *Signal Processing, IEEE Transactions*, vol. 57, no. 9, pp. 3576 –3587, sep 2009.

[28] N. Vucic and H. Boche, "Robust qos-constrained optimization of downlink multiuser miso systems," *Signal Processing, IEEE Transactions on*, vol. 57, no. 2, pp. 714 –725, feb. 2009.

[29] S. Christensen, R. Agarwal, E. Carvalho, and J. Cioffi, "Weighted sum-rate maximization using weighted mmse for mimo-bc beamforming design," *Wireless Communications, IEEE Transactions on*, vol. 7, no. 12, pp. 4792 –4799, december 2008.

[30] M. Shenouda and T. Davidson, "Nonlinear and linear broadcasting with qos requirements : Tractable approaches for bounded channel uncertainties," *Signal Processing, IEEE Transactions on*, vol. 57, no. 5, pp. 1936 –1947, may 2009.

[31] ——, "On the design of linear transceivers for multiuser systems with channel uncertainty," *Selected Areas in Communications, IEEE Journal on*, vol. 26, no. 6, pp. 1015 –1024, august 2008.

[32] T. Bogale, B. Chalise, and L. Vandendorpe, "Robust transceiver optimization for downlink multiuser mimo systems," *Signal Processing, IEEE Transactions on*, vol. 59, no. 1, pp. 446 –453, jan. 2011.

[33] D. Tse, R. Yates, and Z. Li, "Fading Broadcast Channels with State Information at the Receivers," in *Communication, Control, and Computing, 2008 46th Annual Allerton Conference on*, sept. 2008, pp. 221 –227.

[34] G. Zheng, K.-K. Wong, and T.-S. Ng, "Robust linear mimo in the downlink : a worst-case optimization with ellipsoidal uncertainty regions," *EURASIP J. Adv. Signal Process*, vol. 2008, pp. 154 :1–154 :15, Jan. 2008.

[35] S. Ulukus and R. D. Yates, "Adaptive Power Control and MMSE Interference Suppression," in *Baltzer/ACM Wireless Networks*, vol. 4, no. 6, 1998.

[36] S. M. Kay, "Fundamentals of Statistical Signal Processing, Volume 1 : Estimation Theory," in *Prentice Hall Signal Processing Series*, vol. 1. Prentice Hall, 1993.

[37] M. Queiroz, J. Judice, and C. Humes, "The Symmetric Eigenvalue Complementarity Problem," in *Mathematics of Computation*, vol. 73, no. 248, aug 2003, pp. 1849–1863.

[38] S. Boyd and L. Vandenberghe, *Convex Optimization*. version 20081118 [Online], Available : http ://www2.imm.dtu.dk/pubdb/p.php ?3274, 2008.

[39] D. Brandwood, "A complex gradient operator and its application in adaptive array theory," *Communications, Radar and Signal Processing, IEE Proceedings F*, vol. 130, no. 1, pp. 11 –16, feb 1983.

[40] K. B. Petersen and M. S. Pedersen, *The matrix cookbook*. Convex Optimization, 2007.

[41] L. Xiao and L. Cottatellucci, " Parametric least squares estimation for nonlinear satellite channels," sep 2012, to appear in IEEE Trans. Vehicular Technology, fall.

[42] U. Reimers, *Digital Video Broadcasting (DVB) ; Interaction Channel for Satellite Distribution Systems*. European Telecommunication Standardisation Institute (ETSI) EN 301 790 V.141, september 2005.

[43] H. Network, *IP Over Satellite*. Telecommunication Industry Association TIA-1008, october 2003.

[44] E. Casini, R. De Gaudenzi, and O. Herrero, "Contention resolution diversity slotted ALOHA (CRDSA) : An enhanced random access schemefor satellite access packet networks," *Wireless Communications, IEEE Transactions on*, vol. 6, no. 4, pp. 1408 –1419, april 2007.

[45] G. Liva, "Graph-based analysis and optimization of contention resolution diversity slotted aloha," *Communications, IEEE Transactions on*, vol. 59, no. 2, pp. 477 –487, february 2011.

[46] T. Le-Ngoc and J. Mohammed, "Combined free/demand assignment multiple access (cfdama) protocols for packet satellite communications," in *Universal Personal Communications, 1993. Personal Communications : Gateway to the 21st Century. Conference Record., 2nd International Conference on*, vol. 2, oct 1993, pp. 824 –828.

[47] S. S. Lam, "A carrier sense multiple access protocol for local networks," 1979.

[48] F. Shad, T. Todd, V. Kezys, and J. Litva, "Dynamic slot allocation (DSA) in indoor SDMA/TDMA using a smart antenna basestation," *Networking, IEEE/ACM Transactions on*, vol. 9, no. 1, pp. 69 –81, feb 2001.

[49] I. Koutsopoulos and L. Tassiulas, "Adaptive resource allocation in SDMA-based wireless broadband networks with OFDM signaling," in *INFOCOM 2002. Twenty-First Annual Joint Conference of the IEEE Computer and Communications Societies. Proceedings. IEEE*, vol. 3, 2002, pp. 1376 – 1385 vol.3.

[50] Y. M. Tsang and R. Cheng, "Optimal resource allocation in SDMA/multiinput-single-output/OFDM systems under QoS and power constraints," in *Wireless Communications and Networking Conference, 2004. WCNC. 2004 IEEE*, vol. 3, march 2004, pp. 1595 – 1600.

[51] Y. J. Zhang and K. Letaief, "An efficient resource-allocation scheme for spatial multiuser access in MIMO/OFDM systems," *Communications, IEEE Transactions on*, vol. 53, no. 1, pp. 107 – 116, jan. 2005.

[52] R. A. Berry and D. N. C. Tse, "Information Theory Meets Game Theory on The Interference Channel," *Proc. of IEEE Information Theory Workshop (ITW)*, pp. 140 –144, June 2009.

[53] R. Etkin, A. Parekh, and D. Tse, "Spectrum sharing for unlicensed bands," *Selected Areas in Communications, IEEE Journal on*, vol. 25, no. 3, pp. 517 –528, april 2007.

[54] G. Scutari, D. Palomar, and S. Barbarossa, "Asynchronous iterative water-filling for gaussian frequency-selective interference channels," *Information Theory, IEEE Transactions on*, vol. 54, no. 7, pp. 2868 –2878, july 2008.

[55] ——, "Mimo cognitive radio : A game theoretical approach," in *Signal Processing Advances in Wireless Communications, 2008. SPAWC 2008. IEEE 9th Workshop on*, july 2008, pp. 426 –430.

[56] E. Jorswieck, E. Larsson, and D. Danev, "Complete characterization of the pareto boundary for the miso interference channel," *Signal Processing, IEEE Transactions on*, vol. 56, no. 10, pp. 5292 –5296, oct. 2008.

[57] S. Adlakha, R. Johari, and A. J. Goldsmith, "Competition in wireless systems via bayesian interference games," *CoRR*, vol. abs/0709.0516, 2007.

[58] G. He, L. Cottatellucci, and M. Debbah, "The waterfilling game - theoretical framework for distributed wireless network information flow," *"EURASIP Journal on Wireless Communications and Networking", Special issue on Game theory, Volume 2010 (2010), Article ID 482975*, 10 2009. [Online]. Available : http ://www.eurecom.fr/publication/2959

[59] S. Akbarzadeh, L. Cottatellucci, and C. Bonnet, "Bayesian equilibria in slow fading ofdm systems with partial channel state information," in *Future Network and Mobile Summit, 2010*, june 2010, pp. 1 –16.

[60] J. F. N. Jr., "Equilibrium points in n-person games," *Proceedings of the National Academy of Sciences of the United States of America*, vol. 36, pp. 48–49, January 1950.

[61] M. J. Osborne and A. Rubinstein, *A Course in Game Theory.* The MIT Press ; First edition, 1994.

[62] J. Rosen, "Existence and uniqueness of equilibrium points for concave n-person games," *The Econometric Society*, vol. 33, no. 3, pp. 520 –534, July 1965.

[63] J. C. Harsanyi, "Games with incomplete information played by "bayesian" players, i-iii," *Manage. Sci.*, vol. 50, pp. 1804–1817, Dec. 2004.

[64] L. Kockesen, *Bayesian Games.*

[65] G. Ordonez, *Notes on Bayesian Games.* UCLA, 2006.

[66] S. V. Hanly and D. N. C. Tse, "Multi-access fading channels - part ii : Delay-limited capacities," *IEEE Trans. Inform. Theory*, vol. 44, pp. 2816–2831, 1998.

[67] D. Tse and P. Viswanath, *Fundamentals of Wireless Communications.* Cambrige MA : Cambridge University Press, 2005.